UNIVERSITY OF SOUTHAMPTON

FACULTY OF ENGINEERING, SCIENCE & MATHEMATICS

SCHOOL OF CHEMISTRY

THE STUDY OF ALUMINIUM ANODES FOR HIGH POWER DENSITY AL-AIR BATTERIES WITH BRINE ELECTROLYTES

By

Maria Nestoridi

Thesis for the degree of Doctor of Philosophy

To my father Antonios, my mother Zenia and my grandmother Konstantia

UNIVERSITY OF SOUTHAMPTON

ABSTRACT

FACULTY OF ENGINEERING, SCIENCE & MATHEMATICS

SCHOOL OF CHEMISTRY

Doctor of Philosophy

THE STUDY OF ALUMINIUM ANODES FOR HIGH POWER DENSITY AL-AIR BATTERIES WITH BRINE ELECTROLYTES

by Maria Nestoridi

In this thesis aluminium alloys containing small additions of both tin (~ 0.1 wt %) and gallium (~ 0.05 wt %) are shown to dissolve anodically at high rates in sodium chloride media at room temperatures; current densities > 0.2 A cm^{-2} can be obtained at potentials close to the open circuit potential, ~ -1.5 V *vs* SCE. Alloys that do not contain both tin and gallium were shown not to dissolve at such a negative potential. The tin exists in the alloys as a second phase, typically as ~ 1 μm inclusions (precipitates) distributed throughout the aluminium structure, and anodic dissolution occurs to form rounded pits around the tin inclusions. The pits were different in structure from the crystallographic pits commonly observed with Al and other alloys. The change in pit structure and the negative shift in dissolution potential indicate that the AlMgSnGa alloys dissolve by a different mechanism. Although the distribution of the gallium in the alloy could not be established, it is also shown to be critical in the formation of these pits as well as maintaining their activity. The stability of the alloys to open circuit corrosion and the overpotential for high rate dissolution, both critical to battery performance, is shown to depend on factors in addition to elemental composition; both heat treatment and mechanical working influence the performance of the alloy. The correlation between alloy performance and their microstructure has been investigated.

Imaging of the surface with a resolution of 10 – 20 μm was used for the direct observation of the anodic dissolution of aluminium alloys containing Sn and Ga. The resolution allows confirmation that hydrogen evolution occurs from the Sn inclusions. Using microelectrodes with only a few Sn inclusions in their surface, it is shown that the evolution of H_2 is not continuous and this may be correlated with a potential shift to significantly less negative potentials.

After proving experimentally that the performance of an Al-air battery in 2 M NaCl is limited both by the O_2 cathode and the extent of dissolution of Al alloy, experiments were carried out to define the factors ultimately limiting the extent of the anodic alloy dissolution reaction. Using a cell with a low electrolyte volume to surface area ratio, it was shown that in many conditions dissolution stopped after the passage of 1000 C cm^{-2} due to a high impedance, thick film of $Al(OH)_3/Al_2O_3$ crystals clinging to the surface. Removal of this film allowed the dissolution to recommence. The charge limitation probably depends on cell design but a high charge density would be difficult to achieve with a low electrolyte volume.

Table of Contents

List of Figures

Figure 4.3: *The surface of samples of AB50V alloy under the backscatter detector of the SEM* ***a)*** *before and* ***b)*** *after 50 mA* cm^{-2} *were applied for 10 seconds at the alloy.*

Figure 4.4: *Applying a constant anodic current of 50 mA* cm^{-2} *at AB50V alloy for 10 minutes in a) 0.2 M NaCl, b) 2 M NaCl and c) saturated NaCl. . The experiments were repeated more than twenty times and the "steady state" potential was reproducible to* ± *5 mV.*

Figure 4.5: *Potential vs time response for the alloy AB50V in 2 M NaCl in an experiment where the alloy surface was initially activated by passing a current density of 50 mA* cm^{-2} *for 600 seconds and then current densities of 1, 2, 10, 50, 100, 200 and 500 mA* cm^{-2} *at 600 seconds intervals were imposed. The inset shows the steady state current density potential relationship. At all current densities below 100 mA* cm^{-2} *the potentials are reproducible to ± 10 mV. At higher current densities, IR drop, hydrogen evolution and loss of material led to poorer reproducibility and current oscillation.*

Figure 4.6: *The influence of the current density during the activation period (600 seconds) on the voltammetry for the anodic dissolution of Al.*

Figure 4.7: *Current/potential characteristics for the alloys AB50V, B0 and I0 of the control-current experiments where current density was progressively increased after activation at 50 mA* cm^{-2} *in 2 M NaCl.*

Figure 4.8: *Experiment where different current densities where applied for 600 seconds in untreated I0 and AB50V alloys and I0 alloy heat treated at various temperatures for 2 hours in 2 M NaCl. Below 100 mA* cm^{-2}*, the reproducibility was ±10 mV. At higher current densities, IR drop, hydrogen evolution and loss of material led to poorer reproducibility and current oscillation*

Figure 4.9: *Potential for 120 mA* cm^{-2}*vs heat treatment temperature from control current experiments with heat treated I0 alloys in 2 M NaCl. Replicate experiments were reproducible to ±10 mV as indicated by error bars.*

Figure 4.10: *Experiment where different current densities where applied for 600 seconds in untreated I0 alloy in various solutions. These were 2 M NaCl + 0.01 M NaOH (black line), 2 M NaCl + 0.1 M NaOH (red line), 2 M NaCl + 1 M NaOH (green line) and 2 M NaCl + 0.001 M HCl (blue line). Below 100 mA* cm^{-2}*, the reproducibility was ±10 mV. At higher current densities, IR drop, hydrogen evolution and loss of material led to poorer reproducibility and current oscillation.*

Figure 4.11: *SEM images of the alloys (a) AB50V, (b) B0 and (c) I0 under the backscatter detector of the SEM.*

Figure 4.12: *TEM images of the alloys (a) AB50V, (b) B0 and (c) I0.*

Figure 4.13: *Surface of the AB50V alloy, after 10 seconds chemical etching in Kellers reagent, observed under the secondary electron detector of the SEM.*

Figure 4.14.: *SEM and EDX analysis of AB50V alloy after a chemical etching for 10 seconds in Kellers reagent; rounded pits around Sn and SnMg inclusions can be observed.*

Figure 4.15: *SEM analysis of AB50V after a) 10 s and b) 30 s etching with Keller's reagent.*

Figure 4.16: *SEM image of 99.999% pure Al after 10 seconds chemical etching in Kellers reagent. Pits or any other surface damage cannot be observed.*

Figure 4.17: *SEM images of a) B0 and b) I0 alloys after 10 seconds etching in Kellers reagent under the backscatter electron detector. Pitting occurs around Sn and SnMg inclusions.*

Figure 4.18: ***a)*** *AB50V etched with Kellers reagent that does not include HF (only* HNO_3*, HCl,* H_2O*),* ***b)*** *Kellers where HF was diluted times 4 and* ***c)*** *HF in* H_2O *with the same concentration (0.24 M) as in Kellers.*

Figure 4.19: *SEM images of B1 alloy after 10 seconds etching in Kellers reagent showing* ***a)*** *the alloy surface under the backscatter electron detector at low resolution and* ***b)*** *the selected area in the red circle of Figure 4.19 a) under the secondary electron detector at high resolution.*

Figure 4.20: *SEM images of the surface of the alloy AB50V after a passage of a current density of 50 mA* cm^{-2} *for 10 seconds. a) low magnification image, b) medium magnification image, c) high magnification image with EDX analysis at various points. The EDX analyses are shown as atomic % reporting only the metal components.*

Figure 4.21: *AB50V anodically etched by 50 mA* cm^{-2} *in 2 M NaCl for a) 1, b) 10 and c) 60 seconds \and AB50V anodically etched by 1 mA* cm^{-2} *in 2 M NaCl for d) 10, e) 60 and f) 125 seconds respectively.*

Figure 4.22: *SEM images of the surface of the alloy B1 (Sn no Ga) after it has been imposed to 50 mA* cm^{-2} *for 10 seconds using a) secondary electron detector and b) backscatter detector and EDX analysis at selected points. The EDX analysis are shown as atomic % in which only the metal components are included.*

Figure 4.23: *EBSD analysis results including: a), b) and c) Grain boundary maps for AB50V, B0 and I0 alloys and d), e) and f) orientation maps of AB50V, B0 and I0 alloys respectively – note different scales.*

Figure 4.24: *Pole Figures from the stereographic analysis software corresponding to grain maps (Figure 4.21).*

Figure 4.25: *EBSD maps of the I0 alloy a) electropolished and b) electropolished and heat treated at 573 K for 2 hours.*

Figure 4.26: *EBSD orientation boundary maps (in black and white) and grain boundary maps (colour) for AB50V alloy heat treated at 573,a) and b), and 873 K c) and d), respectively.*

Figure 4.27: *Pole Figures of AB50V alloy after heat treatment at a) 573 K and b)*

Figure 5.12: *Cell voltage vs time response to the imposition of anodic current densities of 50 (green line), 170 (black line) and 200 mA cm^{-2}(red line), to the anode Al alloy I0 vs stainless steel 904L.*

Figure 5.13: *I0 electrode and Al oxide / hydroxide on it at the end of the experiment.*

Figure 5.14: *Impedance measurements at several stages before during and after a chronopotentiometric experiment where 170 mA cm^{-2} were applied to I0 in 2 M NaCl at room temperature. The parameters R_{ct},, C_{dl} and R_s have been noted in one of the Bode plots..*

Figure 5.15: *The first 300 seconds chronopotentiometric response where a current density of 170 mA cm^{-2} was applied to I0 alloy in 2 M NaCl when stainless steel 904 L is used as the counter electrode.*

Figure 5.16: *SEM images captured from different parts of the surface of I0 alloy after 300 seconds of a chronopotentiometric experiment where a current density of 170 mA cm^{-2} was applied to it in 2 M NaCl:* ***(a)*** *and* ***(b)*** *are SEI images and* ***(c)*** *and* ***(d)*** *are BEC images.*

Figure 5.17: *SEM images to investigate pit* ***(a)*** *formed after 300 s of applying 170 mA cm^{-2} to I0 in 2 M NaCl:* ***(b)*** *High resolution image from an edge of the pit showing the white thick oxide layer surrounding the pit;* ***(c)*** *and* ***(d)*** *are images from different areas of the inside part of the pit showing that Al surface is "muddy" and "wavy". Image* ***(e)*** *shows the formation of a small pit of 20 µm diameter inside the big pit of ~ 200 µm diameter; higher resolution image* ***(f)*** *with the BEC detector and EDX analysis it was clearly showed that the pit is formed around a Sn centre.*

Figure 5.18: *Chronopotentiometric response of I0 alloy in 2 M NaCl when stainless steel 904 L is used as the counter electrode for the first 3000 seconds.*

Figure 5.19: *SEM images captured from different parts of the surface of I0 alloy after a current density of 170 mA cm^{-2} was applied to it for 3000 seconds in 2 M NaCl. Images* ***(a)*** *and* ***(b)*** *are low resolution SEI image of different parts of the surface, showing big*

*pits (~200 µm diameter).Image **(c)** shows the inside part of one of those pits that is consisted of a solid form of Al (III) oxide. Image **(d)** shows Sn particles inside a pit that is accompanied by the EDX analysis presented in Figure 5.24. Images **(e)** and **(f)** are BEC images of the surface captured to show the surface without the charging of the any oxide. Images **(g)** and **(h)** show the "edge effect" of the current where the alloy seems to dissolve more at the edges of the sample.*

Figure 5.20: *EDX analyses for red spotted areas of Figure 5.19 d.*

Figure 5.21: *Chronopotentiometric response of I0 alloy in 2 M NaCl when an anodic current of 170 mA cm^{-2} was applied for 6500 seconds.*

Figure 5.22: *SEM images captured from different parts of the surface of I0 alloy after a current density of 170 mA cm^{-2} was applied to it for 6500 seconds. Image **(a)** is a low resolution image showing the appearance of the surface after this experiment. Image **(b)** shows the edge of the sample. Image **(c)** is a high resolution image of the surface .Image **(d)** is a higher resolution image of image **(c).***

Figure 5.23: *High magnification (x 4500- scale bar 5µm-enlargement of Figure 5.11 (h)) image of a surface of I0 after the alloy had been imposed at a current density of 170mA cm^{-2} for 6500 seconds in 2 M NaCl.*

Figure 5.24: *Crossection SEM images of I0 alloy at different times after the imposition of 170 mA cm^{-2} in 2 M NaCl.*

Figure 5.25: *EDX mapping for oxygen and aluminium of crossections of I0 alloy at different times after the imposition of 170 mA cm^{-2} in 2 M NaCl. Aluminium is shown in pink colour, oxygen is yellow.*

Figure 5.26: *Chronopotentiometric response of I0 alloy when it was subjected to a current density of 170 mA cm^{-2} in 2 M NaCl. The blue curve shows the response in a small perspex cell; the black and red curves are replicate experiments carried out in a 100 ml beaker.*

Figure 5.27: *Chronopotentiometric response of AB50V alloy when it was subjected at a current density of 170 mA cm^{-2} in 2 M NaCl at various temperatures.*

Figure 5.28: *Voltammetry of oxidation of* ***(a)*** *AB50V in 2 M NaCl and* ***(b)*** *pure Al in 2 M NaOH at room temperature and oxygen reduction on Pt/C gas diffusion air electrodes in* ***(c)*** *2 M NaCl and* ***(d)*** *2 M NaOH at 353 K. Oxygen flow rate was 200 cm^3/min. By the purple arrows on the graphs the voltage of a battery in the respective medium is shown at a current density of 150 mA cm^{-2}.*

Figure 6.1: *Configuration of Al electrode, cell optical window and lens during camera experiments.*

Figure 6.2: ***(a)*** *SEM image of a polished AB50V sample before the experiment showing in the red circles the two areas of the alloy where Sn centres were located by EDX,* ***(b)*** *Camera picture of the AB50V dry sample before the experiment,* ***(c)*** *bubbles on two spots only from the surface of AB50V alloy being at OCP in 2 M NaCl,* ***(d)*** *AB50V alloy after a few minutes on OCP showing two pits (inside the red circles) on the areas of the surfaces where from the bubbles where evolved.*

Figure 6.3: ***(a)*** *SEM image of a polished I0 sample before the experiment showing in a red circle where a Sn centre was located by EDX,* ***(b)*** *Camera picture of the I0 dry sample before the experiment,* ***(c)*** *bubbles on a few spots only from the surface of I0 alloy being at OCP in 2 M NaCl,* ***(d)*** *Camera picture of I0 alloy after a few minutes on OCP showing few pits (inside the red circles) on the areas of the surfaces where from the bubbles where evolved.*

Figure 6.4: *SEM image of a polished sample of I0 alloy. Sn centres have been detected by EDX and marked in the red circles of the image.*

Figure 6.5: ***(a)*** *Camera picture of I0 in 2 M NaCl just before the experiment started. Camera pictures at the* ***(b)*** *1^{st} second of the experiment;* ***(c)*** *2^{nd} second of the experiment* ***(d)*** *3^{rd} second of the experiment where 50 mA cm^{-2} were applied to I0 in 2 M NaCl.*

Figure 6.6: *Chronopotentiometric response of I0 alloy (area ~ 0.00125 cm^2) when a current density of 1 mA cm^{-2} was applied to it in 2 M NaCl.*

Figure 6.7: ***(a)*** *Camera picture of the I0 alloy in 2 M NaCl while on OCP where some pits have already formed on the surface.* ***(b)*** *to* ***(g)*** *Camera pictures of the I0 alloy when a current density of 1 mA cm^{-2} was applied to it. Hydrogen evolution occurs from the pits that were formed during the OCP time.* ***(h)*** *SEM image of the alloy I0 after the experiment. Red circles indicate the origin of hydrogen bubbles.*

Figure 6.8: *Chronopotentiometric response of AB50V alloy (area ~ 0.00125 cm^2) when a current density of 1 mA cm^{-2} was applied to it in 2 M NaCl.*

Figure 6.9: *SEM image of AB50V alloy after 1 mA cm^{-2} current density was applied to it in 2 M NaCl for 240 seconds. In the red circle a pit is marked where Sn particles were located with EDX before the experiment.*

Figure 6.10. *Voltammograms for AB50V in 2 M NaCl before and after activation with an anodic current density of 50 mA cm^{-2} for 600 s.*

List of Tables

Author's Declaration

Except where specific reference is made to other sources, the work presented within this thesis is the original work of the author. It has not been submitted, in whole or part, for any other degree.

.....

Maria Nestoridi

Acknowledgements

First of all, I would like to express my gratitude and deepest thanks to my supervisor, Professor Derek Pletcher who guided me through my PhD work. Derek prompted me into developing bold arguments and helped me improve my stream of thought. His talent to teach, patience, experience and scientific excellence make him an irreplaceable person to work with. Derek thank you once again for everything you have taught me and all the support you have given me throughout this work! After these three years I am quite sad for having to stop going to Derek's office asking him: Are you busy?:) But I hope that I have gained a friend and that we will always keep contact regardless of how far we might be from each other.

I would also like to thank my supervisor Professor Robert Wood for the valuable advice and succinct comments that he provided me when needed, for which I am indebted and wish to convey my warmest wishes for the future. I would also like to express my appreciation to Richard Jones, Keith Stoke and Ian Wilcock from dstl for reading my reports and making useful comments about my work, and giving advice and help when it was needed.

I would also like to thank Dr Julian Wharton for helping me with the impedance experiments and for the nice discussions related to my work.

Professor Andrea Russell I would like to thank you for the useful discussions and suggestions during my research. I would also like to thank you for reading my reports and giving me always concise comments on my work.

Dr Peter Birkin thank you very much for looking at these hydrogen bubbles coming from the precious Sn centres on my alloys. Thank you for making the time working with you so enjoyable.

I would also like to thank Dr Shuncai Wang for the training at the SEM and also for his help with the Electron Backscatter Diffraction Analysis and interpretation of it. I would also like to thank Dr Barbara Cressey and Alistair Clark for her technical comments on the SEM results when that was needed.

One of the most important factors influencing your mood during the PhD work is probably the people that you work with in the lab. They can "make your day" just by

smiling to you and being kind. Therefore I would like to say a big THANK YOU GUYS to Miss Clelia (Dr now but always Miss as well for me ☺), Miss Alicja, Jacek, HanTao ,Remigiusz, Jyo, Yusairie that have been in Derek's group and worked with me in the lab.

I would also like to thank my friends, Matthew, Hannah, Nefeli, Alexandros, Katie, and Phil, for being good friends the last three years. Guys even if I change continent I wish that we will never lose contact.

Professor George Attard, Chris and Marcus thanks for being always nice with me. Keep smiling ;)

I would also like to thank Professor Phil Bartlett for offering me a post doc that kept me relaxed towards the end of the writing of my PhD thesis.

A big thank you to dstl for funding this work and giving me the chance to work on something so interesting for these last three years.

I would also like to express my thanks to my family, in particular my parents Antonios and Zaharenia who have always been there for me even if they were far away from Southampton. A big thank you to my brother Konstantinos for listening to me talking for hours about my work all these three years even if he is an aerospace engineer and did not understand a thing about electrochemistry☺ I would also like to thank Leuterh for being supportive and listening to me all these years. Now I know that you never know what to except while waiting at a bus stop ;).

Primarily I came to Southampton just by lack and later I stayed for a reason. Southampton has been a second home for me and this is because of the nice people I have met and worked with. Somebody has to be happy in order to be good in whatever he/she is doing. So the content of the pages of this thesis is directly related to the nice environment and amazing people I have met here in Southampton. I am not sure where I am going next but Southampton and the friends and colleagues I have made here will always be in my heart. THANK YOU ALL for everything!

List of symbols

E_{CELL}	$E_C - E_A$ (V or mV)
E_e	equilibrium (or reversible) potential (V or mV)
η	overpotential, $E - E_e$ (V or mV)
I	current (A, mA or µA)
R_{CELL}	cell resistance (Ω)
m	number of moles of reactant consumed or product formed
n	number of electrons required to convert reactant to product
F	Faraday constant (96485 coulombs $mole^{-1}$)
j	current density (A m^{-2}, mA m^{-2}, µA m^{-2})
j_o	exchange current density (A m^{-2}, mA m^{-2}, µA m^{-2})
α	transfer coefficient (dimensionless)
E	potential *vs* a reference electrode (V or mV)
R	gas constant (J $K^{-1}mol^{-1}$)
T	temperature (K)
Rct	Charge transfer resistance (Ohm)
Rs	Solution resistance (Ohm)
C_{dl}	Capacitance of double layer (F cm^{-2})

CHAPTER 1 Introduction

1.1. Objectives

In the current project, the feasibility of using an aluminium air battery to power an ultralight, unmanned micro-aircraft was investigated. Al batteries in saline, alkaline and, less extensively, acidic electrolytes have been studied over the past 30 years and several battery systems have been tested.[1-3] In the application envisaged, however, the requirement is to minimise the weight and volume of a battery employing a saline electrolyte while achieving a high power output. A satisfactory weight can only be achieved by minimising the amount of aluminium and the volume of electrolyte in the battery. The weight of aluminium determines the energy stored in the battery while the volume of electrolyte is determined by the need to maintain the Al (III) product from aluminium dissolution in a form that does not degrade the battery performance. Preliminary calculations showed that the electrolyte is the major weight in the battery.

Hence, the project had two main components:

(i) To define Al alloys that are stable to corrosion at open circuit but dissolve anodically at a high rate in a NaCl - based electrolyte and to understand the role of the minor elements in accelerating the Al dissolution.

(ii) To determine the factors which limit aluminium dissolution by investigating the nature of the products formed in the dissolution of the Al anode (i.e. soluble products, solid aluminium oxide/hydroxide, form of the solid) as a function of the electrolyte composition and discharge rate.

1.2. Battery characteristics

It is important to understand how the characteristics of a battery depend on its electrode reactions and on the cell design in general.

The terminal voltage of a battery will depend on the free energy change in the overall cell reaction and, hence, the choice of electrode reactions, the kinetics of the electrode reactions and the cell resistance, i.e.

$$E_{CELL} = E_e^C - E_e^A - |\eta_A| - |\eta_C| - IR_{CELL} \quad \text{(E.1)}$$

The voltage of the battery will decrease as the current drawn from the battery is increased, since the η_A, η_C and the IR_{CELL} terms will all increase with current density.

At this point, two basic terms that are usually used in order to characterise battery performance should be defined:[4]

- Power Density (or specific power): The ratio of the power available at any instant from a battery to weight (W/kg).

$$Power\ Density = \frac{Current\ \times \text{Battery}\ Voltage}{weig\,ht} \quad \text{(E.2)}$$

- Energy Density (or Specific Energy): The ratio of the total energy available from a battery to weight (Wh/kg):

$$Energy\ Density = \frac{Current\ \times Battery\ Voltage \times Discharge\ time}{weig\,ht} \quad \text{(E.3)}$$

These will both be a function of discharge rate, i.e. current density.

When discussing the electrochemistry of a single electrode, it is often convenient to discuss power in terms of unit area of electrode, i.e.

$$\text{Power} = current\ density \times battery\ volatage \quad \text{(E4)}$$

Similarly for a single electrode:

$$Energy\ storage = current\ density \times battery\ voltage \times discharge\ time \quad \text{(E5)}$$

In Figure 1.1 a schematic diagram of reactions occurring during the discharge of a battery is shown using theoretical linear sweep voltammetry curves. The cell voltage, excluding the IR_{CELL} of the battery could be estimated from the I-E data for oxidation and reduction processes.

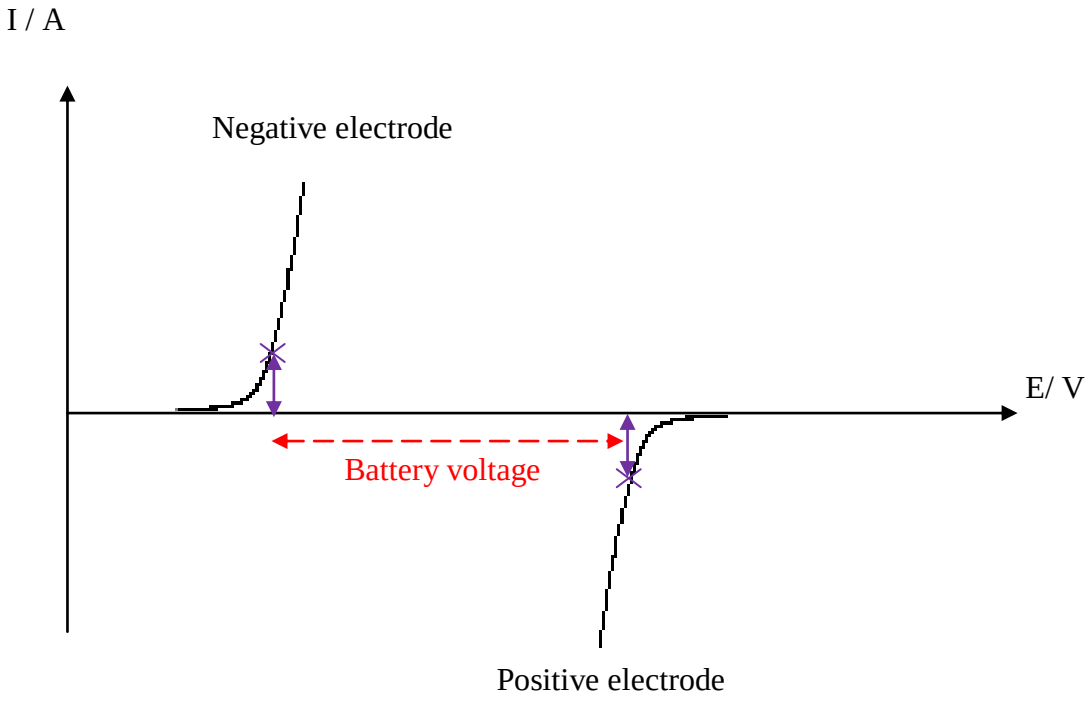

Figure 1.1: *Schematic diagram of electrochemistry reactions in a battery system*

In all batteries, the current achievable is limited by the electrode giving the lower current.

1.3. Al air batteries: The concept – Electrochemistry

Aluminium is of interest as a battery anode for a number of reasons. Firstly due to its ability to transfer three electrons per atom, secondly due to its low atomic mass and thirdly due to its high negative standard potential. These characteristics lead to a high theoretical energy density of 8.1 Wh g^{-1}. In addition the large natural abundance and the low production cost of aluminium make it extremely appealing for use in battery

systems. In an Al air battery all the fuel (Al) is stored in the anode and oxygen is usually taken from the surrounding air.[5]

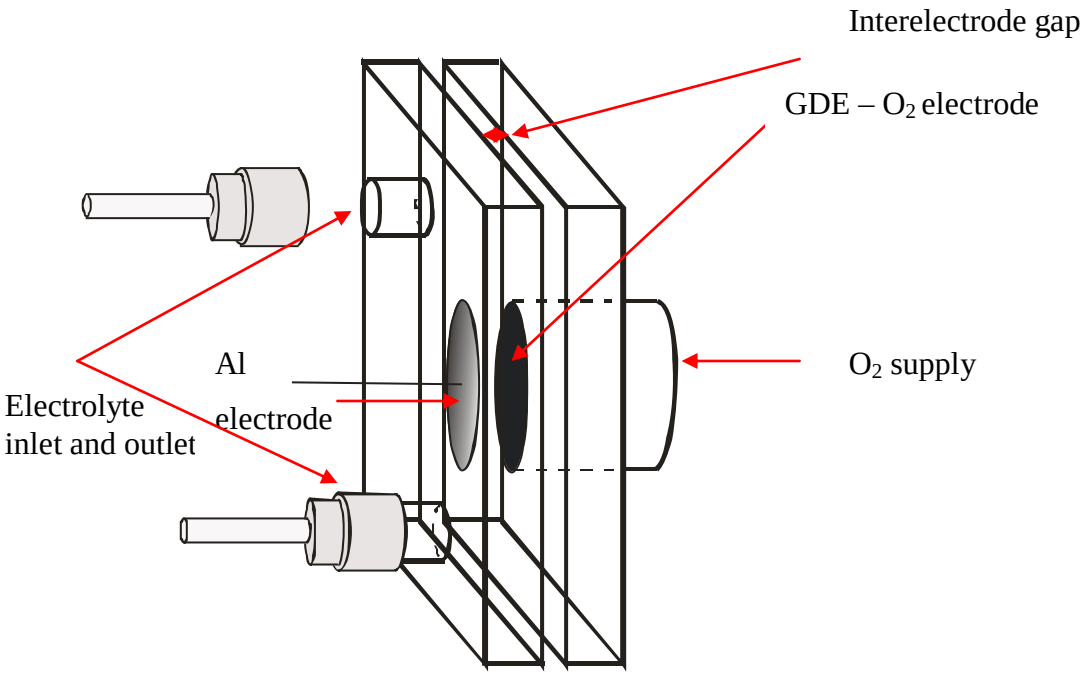

Figure 1.2: *A schematic of a laboratory Al-air battery.*

The discharge reactions for the Al-air cell are.[6]

$$Anode\ Al \rightarrow Al(III) + 3e^- \quad \text{(R.1)}$$

$$Cathode\ O_2 + 2H_2O + 4e^- \rightarrow 4OH^- \quad \text{(R.2)}$$

$$Overall\ 4Al + 3O_2 + 6H_2O \rightarrow 4Al(III) + 12OH^- \quad \text{(R.3)}$$

Unlike the aluminium electrode in alkaline solutions where the product of anodic dissolution is largely the soluble anion $Al(OH)_4^-$ (see reaction R.4)[7]

$$Al + 4OH^- - 3e^- \rightarrow Al(OH)_4^- \quad \text{(R.4)}$$

the speciation in sodium chloride electrolyte of the Al (III) is unclear. The Al (III) may be present as Al^{3+}, Al_2O_3, $Al(OH)_3$, or partly hydrated or chlorinated complexes and the distribution may depend on kinetics as well as thermodynamics. In addition, it is

likely to change with either the Al (III) concentration and/or pH, i.e. the extent of battery discharge. Hence, in this thesis, the term "Al (III)" is intended to cover this variable mix and no attempt is made to balance equations in brine media involving Al (III).

It is important to make clear at this point that at potentials where Al dissolution occurs H_2 evolution is thermodynamically favorable. Hence, H_2 may evolve during battery operation and the corrosion reaction (R.5) is always thermodynamically favorable.

$$Al + H_2O \rightarrow Al(III) + H_2 \quad \text{(R.5)}$$

Due to reaction (R.5) corrosion of aluminium occurs along with anodic dissolution and the aluminium mass loss is more than the Faraday law predicts:

$$Q = \int Idt = mnF \quad \text{(E.6)}$$

To overcome such limitations it is important to understand the role of Al anode and its characteristics as well as treatments of the anode material that could lead to a better battery performance. The target in a real battery must include a potential for the Al anode close to the thermodynamic potential even at high discharge rates and a low corrosion rate at open circuit (for battery storage) and during discharge (for Faradaic efficiency).

Aluminium or its alloys, as has been briefly mentioned earlier in this thesis, can be discharged in saline (neutral), alkaline and acidic electrolytes. Alkaline Al-air systems have an advantage over saline systems due to the higher conductivity of alkaline electrolytes and the higher solubility of Al (III).[6] However, aluminum suffers substantial corrosion in alkaline solution, which results in coulombic losses on discharge and fuel loss during standby.[7] Due to the wishes of the company providing financial support for this work, the studies in this project are limited to NaCl based electrolytes and this increases the problem of obtaining high current densities and cell voltage.

Thermodynamically, an aluminium anode should exhibit a potential of -1.66 V in saline and -2.35 V *vs* SCE in alkaline electrolytes. [5] Also it should display high specific energy. However in such aqueous media, the H_2 evolution reaction is possible and this has a detrimental effect in the performance of an aluminium air-battery.

As it was noted earlier in this section, GDEs are used as the positive electrodes in Al-air systems where the oxygen reduction reaction (ORR) occurs. Such electrode configuration is necessary to overcome the low solubility of oxygen in aqueous electrolytes and hence to achieve meaningful current densities. The principle function of a porous gas diffusion electrode is to provide a large area reaction zone with a minimum of mass transport hindrances for the access of the gaseous reactants and the removal of products. This allows a substantial scaling of the current density based on the geometric area.[8] Indeed, at plate electrode in aqueous solution, the maximum current density is ~1 mA cm^{-2} while in favourable media a GDE can be operated at current densities higher than 1 A cm^{-2}.

The applications of oxygen reduction are strongly dependent on the products involved, either OH^- or HO_2^-.[9] Oxygen reduction is considered to occur mainly through two pathways:[10] (i) a $4e^-$ reduction reaction without the intermediate formation of hydrogen peroxide; (ii) an initial reduction reaction producing H_2O_2 which is possibly then further reduced to OH^-.

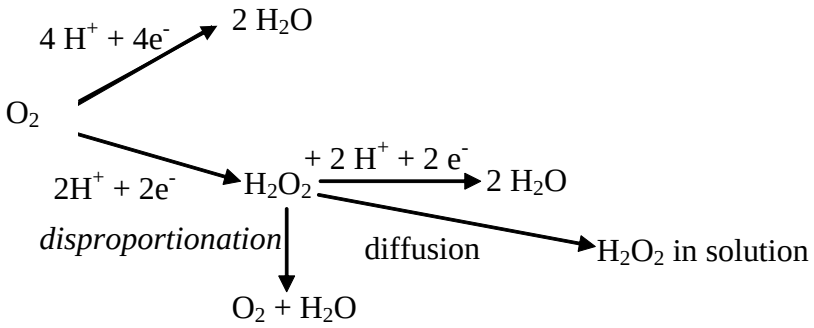

Figure 1.3: *A schematic illustration of ORR possible pathways*

The actual pathway of oxygen reduction depends on the electrode materials and the electrolyte medium.[11] It is important to mention here that in a neutral electrolyte such as

NaCl, O_2 reduction leads to the formation of $OH^-$and an increase in pH. This is particularly important within the pores of a GDE. This causes an adverse negative shift in the O_2 reduction potential.

1.4. Pourbaix diagram for aluminium

In order to summarize the thermodynamic data for the reactions of pure aluminium with water in non-complexing solutions it is common to use a Pourbaix diagram, a diagram showing the potential of a metal couple as a function of pH.[12] Such a diagram shows the zones where a metal would corrode and zones were it would be passive or immune to corrosion (where the corrosion reaction would not be thermodynamically favourable) in an aqueous electrochemical system.[12] In Figure 1.4 the Pourbaix diagram for aluminium in aqueous environment is shown. By looking at Figure 1.4 three regions are distinct. A corrosion, a passivation and an immunity region.

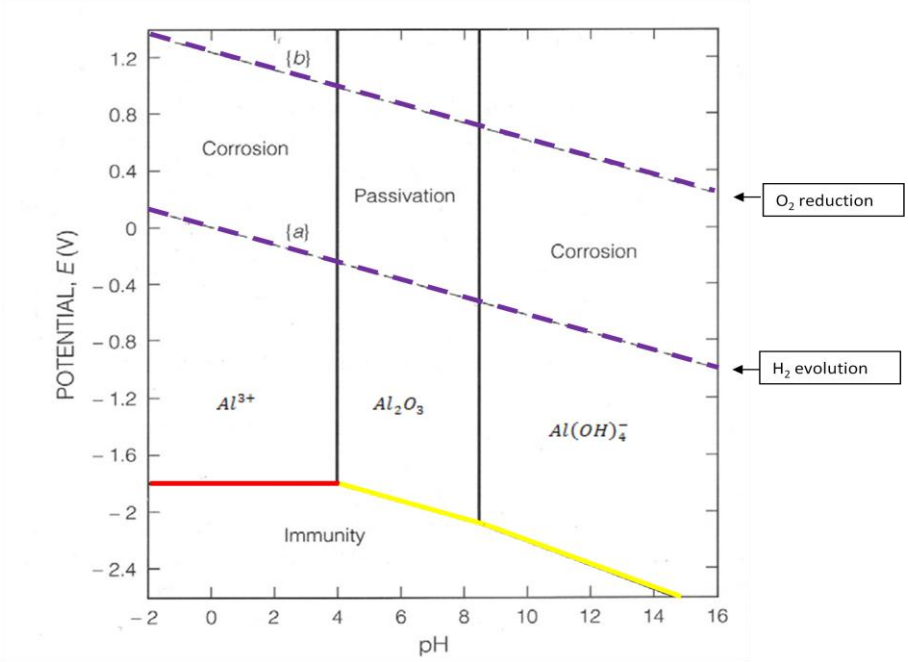

Figure 1.4: *The Pourbaix diagram for aluminium in aqueous environment.*[13]

It has to be noted here that because the dashed lines for hydrogen evolution and oxygen reduction are always above the Al/Al (III) line, (red color line), the Pourbaix diagram predicts that the corrosion of aluminium metal is always thermodynamically favourable on open circuit.

But the thermodynamically predicted products are different: Al^{3+} in acid, Al_2O_3 in neutral and $Al(OH)_4^-$ in alkaline media.

It is important to make clear several issues at this point. Firstly, the Pourbaix diagram considers only the thermodynamics and does not take into account kinetics in any way. Hence, it does not predict the behavior of the metal in practical situations. Furthermore the diagram is for pure aluminium and not alloys and does not consider complexing agents such as Cl^-.

1.5. Kinetics of corrosion

When many metals are in contact with air or an electrolyte solution they will corrode. In solution its surface will take up a potential, the corrosion potential, where no current flows.[12] At the corrosion potential, the current for the oxidation of the metal must be balanced by the current for the reduction reaction, e.g.

$$M - ne \rightarrow M^{n+} \quad \text{(R.6)}$$

$$2H_2O + 2e^- \rightarrow H_2 + 2OH^- \quad \text{(R.7)}$$

Commonly the kinetics of electron transfer reactions are discussed through the Tafel equation:

$$\log j = \log j_o + \frac{\alpha_A nFE}{2.3RT} \quad \text{(E.7)}$$

The corrosion current (I_{cor}) of any metal is given by:

$$-I_{cathodic} = I_{anodic} = I_{cor} \quad \text{(E.8)}$$

In theory the corrosion current could be determined by measurement of the steady state current for hydrogen evolution (or/and oxygen reduction) and metal oxidation as a function of potential and extrapolation of the currents to the corrosion potential.[12] The extrapolation could be easily carried out by plotting log I *vs* E and the data for each electrode reaction should give a linear plot which is the Tafel plot. Such a hypothetical diagram for Al-water system is shown in Figure 1.5. It should be recognized that the corrosion potential and corrosion current are determined by the equilibrium potentials, exchange current densities and Tafel slopes for both the aluminium oxidation and

hydrogen evolution. The corrosion potential (it is a mixed potential) and the corrosion current for aluminium oxidation would depend on the thermodynamics and kinetics of both the Al/Al (III) and H_2O/H_2 (or O_2/OH^-).

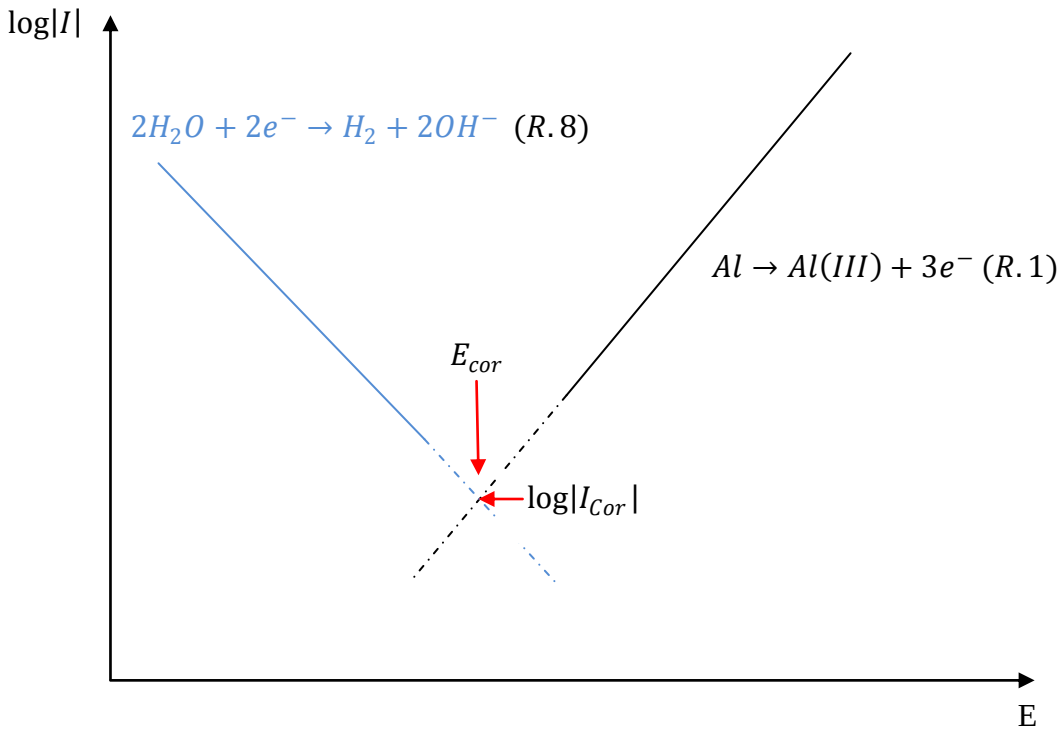

Figure 1.5: *Hypothetical log I vs E diagram for aluminium metal in deoxygenated aqueous electrolyte. The diagram shows the extrapolation to give the corrosion potential and the corrosion current.*[12]

This diagram is, however, unrealistic for Al as if it does not consider the influence of oxide/hydroxide layers on the Al surface.

1.6. Passivation and factors that influence the oxide layer on aluminium

Passivation of aluminium is defined as the formation of a thin layer of a corrosion product (e.g. aluminium oxide) on the aluminium metal surface which acts as a barrier to further oxidation (corrosion) of the metal.[12] The passivating film on aluminium metal and its alloys can be formed by contact with air or an aqueous solution. This oxide/hydroxide layer causes Al to have a more positive potential than its theoretical value.[5] In addition, the oxide film causes the phenomenon so called "delayed action", meaning the time lag before the cell reaches its maximum operating voltage when the

circuit is closed, i.e. breakdown or pitting of the existing passive layer is necessary before high rate Al dissolution is possible. Since Al dissolution occurs while the battery discharges, leading to an enrichment of the electrolyte in soluble aluminate species in alkaline media, it has been suggested that the electrolyte should be continuously treated by the means of a crystallizer coupled to the battery;[7] in the case of saline batteries due to the precipitation of Al^{3+}, periodic replacement of the electrolyte could be made.[14]

The oxide layer formed on aluminium essentially passivates aluminium as has already mentioned in this section.[15] Factors like temperature, the environment and the alloying elements would determine the thickness of the oxide layer. On pure aluminium, the oxide layer formed may be ~ 2-3 nm thick. Heat treatments up to 425^{o}C could result in oxide films up to 20 nm.[16] Upon damage of the oxide layer e.g. by a scratch, a fresh oxide layer will be formed instantly on the metal.[17] Due to the oxide layer aluminium is often protected from corrosion.

The stability of this protective oxide layer can be disturbed by several factors and thereby corrosion would be caused. Once pits or other special sites are formed, an acidic (pH<4) or an alkaline (pH>9) environment could destabilize the native oxide layer of aluminium.[15, 18] In Figure 1.6. a schematic diagram for local pH changes within crevices or pits or beneath blisters where there are net anodic reactions during aluminium corrosion is shown.

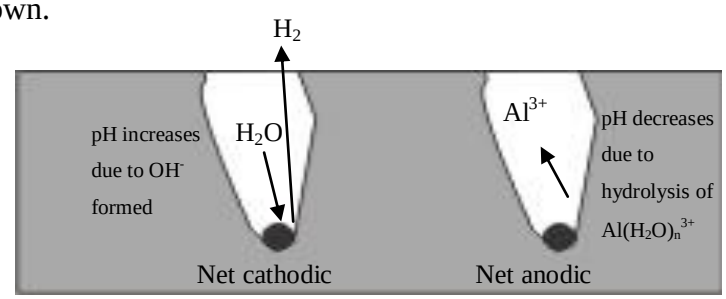

Figure 1.6: *Illustration of net anodic and cathodic reactions and the resulted pH in aluminium pits containing intermetallics.*

In addition ions like chloride could attack the oxide film locally and promote pitting.[18,19] Work has been carried out using X-ray photoelectron spectroscopy (XPS) and X-ray absorption spectroscopy (XAS) that clearly showed that chloride was detected in the

passive film of aluminium at potentials positive to the pitting potential.[20] More recently corrosion pit initiation on aluminium was described by an electrode kinetic model which allows that penetration of chloride ions can occur by migration through oxygen vacancies or by oxide film dissolution. According to the authors pit initiation occurs by chloride assisted localised dissolution at the oxide/metal interface. The propagation stage of pitting on aluminium involves formation of blisters beneath the oxide film due to continuing localized reactions which lead to an acidic localised environment. The blisters subsequently ruptured due to the formation of hydrogen. Finally a mathematical expression of the model showed that the critical pitting potential is a linear function of the logarithm of the chloride concentration (at constant pH), in agreement with experiment (over a pH range of 4 to 8.5).[21] It is important to mention at that point that in commercial alloys, pit initiation usually occurs at second phase particles. And since this is of particular relevance to the project objective, the rest of the thesis will be particularly focused on pit nucleation at second phase particles and local disruption of the oxide layer.

Pb intermetallics with a size of the order of 10 nm were detected in the oxide metal interface of an AlPb alloy. It was suggested that the consequent electrochemical activation was related to reduced passivity of the overlying oxide by Pb enrichment as a result of heat treatment. This led to further segregation of metallic lead as a result of selective oxidation of the more active aluminium matrix during anodic polarization in aqueous chloride environment.[22] Moreover due to the need to develop sacrificial anode materials it has been shown that the formation and distribution of fine intermetallic phases of Mg and Zn in the aluminium matrix have been a key factor in achieving an activation of the anode in chloride solution.[23] Finally, ten elements, Hg, Ga, In, Sn, Bi, Cd, Pb, Zn and Sb, have been identified to induce activation when alloyed with aluminium.[24]

As has been stated by Nisancioglu, (1992), corrosion of aluminium alloys that contain intermetallic phases is essentially a microgalvanic process between the intermetallic particles and the matrix alloy.[25] This author gave the example of phases that act as local cathodes to the aluminium matrix (anode) because of their Fe content. The aluminium

in such a case would undergo a localised attack.[25, 26] According to the above authors an active phase may corrode preferentially in an aluminium alloy or it may act as a sacrificial anode and provide cathodic protection to the surrounding material. In addition due to the electrochemical reactions at the corroding sites, the composition and pH of the electrolyte next to the reaction sites could vary from that of the bulk solution. Finally intermetallic phases of the alloy could corrode selectively, in other words dealloying could occur, that would result in different corrosion characteristics.[25, 26]

1.7. Visual and microscopic observation of Al corrosion

In 1977 an attempt to observe current pulses during pit growth together with the use of a light microscope for visual observation of hydrogen evolution to compare with their current pulses and loudspeaker output was carried out.[27] The aluminium used (electrode area 0.3 cm^2) had been pre-treated (by electropolishing and then anodizing) and then pitted potentiostatically at -0.1 V *vs* SCE. Bursts of H_2 bubbles were correlated with current spikes. Authors observed very large pits of 0.5 mm dimensions under the SEM following the experiment. The authors suggested that during pit growth the oxide substance blocks the pit from the bulk electrolyte. Thus it also impeded the bubbles from leaving the pit immediately. Hence the bubble grows under the oxide until it can escape. In so doing it reduces the area available for ionic conductivity significantly. This explains the relatively large amplitude for the current oscillations.

However several comments have to be made here. First of all, the sample size is quite big for the required observation. Secondly by looking at the SEM image that was taken after 15-20 min (according to authors), the “one pit” that the authors referred to, really looks like many pits that have overlapped and formed a bigger one. The diameter of the pit is approximately half a millimetre! Probably, the authors checked the sample under the SEM long after the first pit was formed. As a result, their work shows that there is a potential to correlate current pulses with gas egress but they do not actually present any optical microscopy images (since probably at that time they could not record from the light microscope) that correlates with electrochemistry characteristics (E-t or I-t curve) at a specific time. In contrast they just presented a partial reproduction of their I-t record

(they do not specify from which time period of the experiment was obtained) for slow bubbles and a portion of their record for smaller and faster bubbles.

More recently Volkov et al., (2004) investigated the local hydrodynamics around a single pit with in situ atomic force microscopy (AFM).[28] The technique was demonstrated on 15 mm diameter aluminium (7% Cu) disk in NaCl solution. The gradient of the density of H_2 bubbles in the vicinity of a corrosion pit brings about hydrodynamic oscillations caused by bubble nucleation and collapse. The amount of evolved hydrogen and the velocity of a bubble growth inside the pit were obtained from the measurements of water displacement transients. Corrosion was initiated by passing an anodic current and further corrosion occurred when the current was switched off but slowly. Since no transient associated with bubble collapse was detected, the authors attributed the transients observed on the Al sample to hydrogen bubble nucleation.

Ambat et al., (2004) observed corrosion reactions of a rolled Al-Fe-Si-Mn alloy in NaCl using a macrosystem ZEISS optical microscope. They performed in situ observations of corrosion and hydrogen evolution at variable depths of aluminium craters ranging from 0.3 to 5 μm.[29] The surface of the corroded sample after the experiment was characterized by SEM. The authors concluded that Fe, Mn and Si intermetallic particles are catalytic sites for cathodic reactions. From the SEM images, the intermetallic particles seem to be smaller than 10 μm in all depths examined. The authors also proved that the high density of particles and solute depletion in the surface gives a much higher pitting susceptibility in the surface than the bulk of the alloy.

Goncharov and Andreev (2006) employed a DCM-130 video camera (with a resolution of 1.3 Mpix) to observe corrosion of an Al-1% Sn alloy in Na_2SO_4 solution.[30] SEM imaging followed the corrosion experiments to identify the inclusions of pure Sn. The authors concluded from their video observation that the cathodic evolution of hydrogen is concentrated only on the inclusions, while the anodic dissolution of aluminium proceeds through its oxide film on the remaining surface. Zhao and Frankel (2007) studied the corrosion process of Al-Zn-Cu-Mg alloys as a function of the potential.[31]

For that purpose, a special cell was attached to the optical microscope. The combination of the surface image and polarization curve allowed easy identification of the surface corrosion processes as a function of potential. From the visual observations the authors reported that the attack was a form of localised corrosion involving local passive film breakdown and accelerated dissolution. The attack grew downward through the surface layer and quickly penetrated the full thickness of the surface layer. Upon reaching the bulk alloy, the attack stopped its downward progress because the conditions were not severe enough to dissolve the matrix. Instead of penetrating into the bulk matrix, the attack propagated outward, away from the initiation site. This dissolution mechanism is similar to the 2D pitting observed for thin metallic films deposited onto an inert substrate.[32]

The authors suggested that the attack of the surface layer may initiate at the Zn-rich grain boundaries in the form of intergranular corrosion. The dissolution at grain boundaries creates a very aggressive environment including low pH and high chloride content. The attack at grain boundaries therefore triggers the dissolution of nanograins but stops at the bulk matrix which is less susceptible. In addition, hydrogen bubbles were generated at the perimeter of the expanding dissolution zone of the surface; some bubbles were released into solution and others remained attached to the surface as the dissolution front passed by.

Furthermore Pidaparti et al., (2008) investigated the pH induced fluorescence both spatially and temporally during corrosion of the aircraft aluminium alloy AA 2024-T3 (Al-Cu-Mg-Zn alloy-containing usually Si, Mn, Cr), in NaCl.[33] The authors accomplished fluorescence imaging by which the metal sample was monitored when a UV light was shed on the metal sample containing the dye. A series of images corresponding to pH changes at various regions of the sample were captured with a CCD camera. Bryant and Greenfield (2006) also used a simple fluorescent method using a hand held UV inspection lamp to detect underfilm aluminium corrosion.[34] The technique used the fluorescence of the Al (III) complex with 8-hydroxyquinoline-5-sulphonic acid (8-HQS).

Microscopic studies on AlMgSnGa alloys were carried out in situ in NaCl by Tuck (1992).[35] He concluded that most of voltage increase occurred in the period when the maximum pit nucleation rate was achieved (during the first 35-40s of a polarisation experiment at 100 mA cm^{-2}). The author interestingly observed that before activation of the alloy (at the very start of the polarisation experiment), evolution of H_2 from the surface was accompanied by the nucleation of crystallographic pits of approximately 120 μm diameter; whereas after activation single rounded pits were seen to nucleate and almost immediately the hydrogen evolution pattern changed. Instead of uniform evolution of gas, most of it seemed to evolve from the nucleation pits.

1.8. Al-air battery: A historical background

It was not until the early 1960s that real work began on the Aluminium-Air cell.[1] Trevethan et al., (1963) found that although the aluminium surface is covered by a passive oxide layer, it was possible to observe a higher voltage than in zinc-air systems.[36] Studies up to 2002 on Al air batteries have been reviewed by several authors.[37, 6] In 2003, Souza and Vielstich published a review on Al air batteries in seawater.[38] Despic et al., (1976) were the first to extensively investigate Al-air batteries using a saline electrolyte (1 M NaCl).[39] Saline battery use has been considered throughout the years in marine applications where seawater (c.a. 3% NaCl) can be the electrolyte. Such batteries are characterized by high specific energies and if their construction allows for refill of the aluminium plates they can be considered as (solid fuel) fuel cells or mechanically rechargeable batteries.[38] One really positive aspect of this kind of saline cells is that they are non-toxic and non-hazardous and that they are friendly to the environment. Another important advantage of saline batteries is the infinite shelf-life in the inactive dry state with easy activation by the addition of seawater.[38] Budevski et al., developed an aluminium air battery operated with 2 M NaCl electrolyte with a power output of (24W) and supplying the energy requirements of a medium-size yacht designed for long periods at sea.[14] Alupower, which was a subsidiary of Alcan, provided the Al alloy (containing Al–Ga-Sn-Mg but the weight % of the elements was not given) anodes for this particular project. From polarization characteristics and corrosion rate measured in 2 M NaCl for the alloy used, it was observed by Budevski et al, (1989) that the alloy exhibits very low corrosion at open

circuit and a relatively low negative difference effect (i.e. the increase in the rate of hydrogen evolution with increasing anodic current density), promising a material efficiency in anodic discharge of 89%.[14] By 1991 research in Al batteries was so developed that patents started to be filed.[40] However most of these Al-air systems were in alkaline electrolytes (high concentrations of NaOH or KOH), and as a result rapid hydrogen evolution could accompany aluminium anode dissolution. In addition, successful Al-air batteries that were developed at that time in such caustic solutions, even though they could achieve high current densities (up to 1000 mA cm^{-2}), they weighed more than 100 kg;[40] due to these reasons these power sources would be inappropriate to use in a lightweight UAV system.

Since 1990's elements such as Hg, Ga, In, Tl and Sn have been known as dopant elements. Alloying aluminium with such metals induces more active behaviour and a more negative potential could be achieved.[24] Hunter et al., investigated Al-Sn binary alloys of varied compositions of Sn in solid solution in the aluminium matrix as candidate anode materials for Al-air batteries that would be used as power sources for a wide range of land based generator and sub-sea propulsion applications.[24] Evidence from linear scan voltammetry experiments in 4 M NaOH showed that the active behaviour of the aluminium anodes is influenced by the presence of Sn in solid solution. The OCP of these Al-Sn alloys was -1.415 V *vs* SCE. From the polarisation curves presented, the most active behaviour of the alloy occurred at about -0.3 V *vs* SCE achieving high current densities (up to 400 mA cm^{-2}), but with a large overpotential. Even though the best Al-Sn anode (0.45 wt% Sn) from that study achieves a high current density it dissolves only at very high overpotentials; the latter in addition to the fact that dramatic H_2 evolution accompanies Al dissolution implies that such anode materials would be inappropriate for an application in lightweight UAVs. In the same year Hamlen et al., (1991) made a short review of advances and applications to new products, as well of the implications of Al-air battery for electric vehicles.[6] As was stated by Rao et al., (1992), Alupower developed a number of saline and alkaline batteries for military applications.[13] Such batteries can be transported as lightweight, collapsable batteries filled with water at the site of the operation. According to these authors, the alkaline Al-air is advantageous when a high power (>50-100W/kg) is desired. The Al-air batteries with saline electrolyte are appropriate for moderate power

(mW/cm^2) demand and when multiple use is required by emptying and rinsing the battery between uses. In addition Rao et al., (1992) demonstrated (they designed and tested it) a module for portable applications (using 8 M KOH) that had an energy density of 435 Wh/kg with a lowest operating temperature of - 40^oC.[13] Also in the 18^{th} International Power Sources Symposium in 1993, Creber and O'Callaghan presented their study on developing a computer model to understand the electrode chemistry and the electrolyte chemical changes which occur in the cell during a battery discharge and simulate the behaviour of both aluminium-air and aluminium–oxygen batteries over a wide range of discharge conditions;[41] the authors claim that the programme accurately predicts battery performance. The anode used for all their work was an Al-Mg-Sn alloy supplied by Alupower.

The growing interest in sub-sea production and exploration of oil and gas wells has created the need to develop long life and high energy density batteries.[42] AB50V alloy (contained 0.63% Mg, 0.14% Sn, 0.04% Ga and 0.0018% Fe) from Alcan was selected by Shen et al., (1994), due to the alloys' low self discharge rate. They developed a battery that had multi-cathodes (comprised of Co_3O_4/C oxygen reduction cathodes) on either side of the anode. The authors showed that such a battery (with 2 M sodium chloride electrolyte) has an energy density of 1008 Wh kg^{-1} over an operating period of one year, significantly higher than all the conventional primary batteries considered for use in sub-sea environments.[42] Again, however, the discharge rate is very low.

Later in the same year, Rudd and Gibbons (1994) started the development of a prototype unmanned, undersea vehicle (UUV) for the US Navy, focusing upon low corrosion Al alloys (alloyed with In-Mn-Mg) and an electrolyte (KOH) management system for processing the by-products of the energy producing reactions.[43] As the authors stated, these developments led to the integration of a single, full size aluminium/oxygen cell with a filter precipitator unit to give over 5000 Ah of operation, with an overall energy density of 3.9 kWh/ kg. More recently Yang and Knickle (2002) reported that the Al-air battery system can generate enough energy and power for driving ranges and acceleration similar to gasoline powered cars.[44] After analysis using a mathematic model for an Al anode in 4 M NaOH and a comparison of their economics with the nickel metal hydride, lead-acid and Al-air batteries, Yang and Knickle (2002)

concluded that the Al-air electric vehicles are the most promising candidates compared to internal combustion engine vehicles in terms of travel range, purchase price, fuel cost and life cycle cost.[44] In addition, a mathematical model by the same authors provided detailed information about cell performance for a wide range of operating and design parameters.[45] The model suggests that higher electrolyte flow rates, smaller cell gaps, higher conductivities, lower parasitic current densities and operation at moderate current density give better cell performance and that in an Al-air cell only the activation and ohmic overpotentials are important.

Later in 2004 Zhang et al. did some further research on the operation and control of an electric vehicle Al-air battery system by creating a method to size battery subsystems in order to optimize battery performance.[46] The purpose of the sub-systems was to regulate the output power of the Al-air battery system and prolong the lifetime of the whole battery system by making the sub-batteries work in shifts. Pure Al is used and an example of a 100 horsepower electric vehicle is given. However the weight of the battery was calculated to be half a ton! The current battery will require replacement of the electrolyte after about 400 km depending upon driving patterns.

A very interesting research study by Zhuk et al., (2006) considered the process of parasitic corrosion as a method for hydrogen production.[47] Hydrogen produced in an aluminium air-battery in this way may be further employed in a hydrogen air-fuel cell or in a heat engine, or it may be burnt to generate heat. Therefore, according to the authors' anode materials may be provided by commercially pure Al, commercially produced Al alloys and secondary aluminium. These materials are cheaper and more readily available than special anode alloys and high purity aluminium. Their results showed that special Al-In alloy and commercial grade aluminium gave similar values of energy density in 4 M NaOH electrolyte.[47]

Finally as it has been stated by Adams and Andrukaitis, (2002) the Al-air cell technology has progressed to the point where it is a competitive power option for certain military applications such as unmanned vehicles for submarine and mine surveillance, long range torpedoes, swimmer delivery vehicles and submarine auxiliary

power.[5] Because some aluminium corrosion always occurs on open circuit (although much more slowly in NaCl than alkali), a general approach has been to store the battery dry and add electrolyte immediately before battery discharge.

Table 1.1 summarises the main points to be taken from the literature.

Table 1.1. *Simplistic summary from literature review on Al-air systems.*

Electrolyte	Alkaline	NaCl
Material	Pure Al	Special Alloys
O_2 cathode	Good performance	Poor performance
Power density	High possible	Only low

Despite the extensive literature, all the batteries described are far too heavy and none of the Al-air batteries approach the power density required for an UAV application, particularly when the electrolyte is NaCl. It should be emphasized that a successful battery would also require an O_2 cathode capable of delivering a current density of a fraction A cm^{-2} with a neutral brine electrolyte.

Regarding the oxygen electrode, the need for higher performance in air electrodes arises from the need to develop metal air batteries for applications which require higher specific energy and power.[48] Work has been done in the past on electrocatalysts such as perovskites[48-51] and transition metal macrocycles[52] in order to develop alternative catalysts to the expensive noble metals[53-55] and silver.[56] Air electrodes have been used in alkaline Zn-air cells since 1930s but they contained thick porous carbon electrodes where the rate of oxygen transport was limited by the thick structure.[48] In the 1950s, thinner plastic bonded, carbon structures were used as the air electrode in Zn-air cells improving their performance. The only major advances since the 1950s are the development of non-noble metal electrocatalysts and the development of thin PTFE-bonded electrode structures for air electrodes; most of this work was part of fuel cells related projects.[48] Research opened new opportunities for design and development of air electrodes with lower cost. However, until today, no better electrocatalyst has been developed than the long known and expensive platinum. Research today in metal air

power systems should really be focused on electrocatalysts development in order to design more efficient positive electrodes that would match the performance of metal electrodes in metal air systems.

1.9. Research on Gas diffusion Electrodes

Gas diffusion electrodes (GDEs) are becoming more familiar as they have been proved to be essential electrodes in fuel cells, metal-air batteries and certain electrolysers.[57-59] In a gas diffusion electrode, the contact zone where reactant, electrolyte and catalyst meet is called a three-phase zone.[8] The porous electrode structure consists of electrocatalyst (usually Pt) dispersed on high surface area carbon black, held together with binding agents such as polytetrafluoroethylene (PTFE). The hydrophobic polymer backbone wet-proofs the porous carbon black structure thereby reducing the propensity of electrode flooding and promoting gas permeable pathways in order to achieve rapid gas transport to catalytic sites.[48, 60]

Furthermore carbons are lightweight, have a large surface area and are suitable for the deposition of very active catalysts.[8] The porous carbon allows for the diffusion of gases and acts as local current collector to a wire screen, carbon paper or bipolar plate.[60]

Pt metals are the only possible electrocatalysts in acid solution because other catalysts undergo corrosion. In addition, platinum is known to be the best electrocatalyst for the ORR in an acidic fuel cell cathode.[48] Alkaline fuel cells (AFCs) are amongst the most mature fuel cell technologies. They were used in the 1960s by NASA in the Apollo and Space Shuttle programs.[61, 62] The fuel cells on these spacecrafts provided electrical power for onboard systems, as well as drinking water. Advanced alkaline fuel cells have the highest electrical efficiency (nearly 70%) in generating electricity and have shown excellent reliability when run at low current densities.[63] AFCs are also able to use non-noble catalysts, thereby significantly reducing the capital cost of the stack. AFCs can operate on air (with CO_2 removed) and they have fast oxygen kinetics under basic electrolyte conditions.

For cost reasons, non-platinum electrocatalysts have concerned the scientific community for a long time.[64] For instance, the first H_2/O_2 alkaline fuel cell, presented by Bacon[65] in 1933, used nickel oxide containing lithium ions on the cathode and nickel-based electrocatalysts on the anode. Throughout the years, in an effort to reduce the cost of oxygen reduction electrodes, several non-noble metals have been used. Rashkova et al., (2002), deposited mixed oxides of Co and Ni on a stationary substrate which in most of the cases was a gas-diffusion membrane (GDM).[66] The membrane consisted of teflonized carbon blacks hot pressed on a Ni screen. The system of the mixed oxides condensed on the GDM forms the GDE, the oxide being the active layer, while the membrane with Ni screen as current collector inside – the gas supplying layer of the electrode. The electrolyte was 20% KOH. By looking at the current voltage characteristics for the oxygen reduction, the best results were obtained for the GDE where the Co/Ni oxides ratio had the value of 4.5, (rich in cobalt versus nickel); current densities up to 50 mA cm^{-2} were achieved close to 0.5 V *vs* RHE (or -0.14 V *vs* Hg/Hg_2SO_4).[66]

GDE's with non-platinum cathode catalysts, i.e. iron tetramethoxyphenylporphyrin (FeTMPP), silver and nickel have been fabricated, tested and compared to traditional Pt catalysts in 1 M NaOH.[67] FeTMPP was found to have reasonable activity for oxygen reduction reaction (and low activity for a borohydride oxidation, making it a suitable candidate as a cathode catalyst for an undivided borohydride fuel cell). The FeTMPP cathode showed superior performances to those observed using the Ag and nickel cathodes. For instance FeTMPP gave a current density of 32 mA cm^{-2} at - 0.8 V *vs* Hg/HgO (or -0.512 V *vs* Hg_2SO_4).

Ag nanoparticles prototype electrodes were used at 80 ^oC in 30% NaOH and compared to Pt loaded electrodes and they proved to have superior performance.[68] Based on the polarization curves, the Ag-loaded electrode showed the highest performance for ORR reaching 100 mA/cm^2 at 0.8 V *vs* RHE. (C-Pt electrode at the same current density had a potential of 0.7 V *vs* RHE). The electrodes were also compared according to their impedance characteristics. The diameter of the semicircle of the Nyquist plots seemed to increase with the working time of the electrodes, faster with the C-Pt electrodes,

which implied that the charge transfer resistance R_{ct} increased with electrode degradation whereas the electrodes with the Ag catalyst showed higher durability. Moreover, SEM observations proved that the reaction layer of the GDEs became thinner with degradation. This was validated by XPS data that showed that as degradation progressed the peaks of carbon and fluorine (PTFE) decreased whereas the peaks of oxygen and adsorbed sodium ions increased.[68]

Furthermore work has been done on manganese oxide nanoparticles doped with Mg and Ni that exhibited ORR activity close to that of 10% wt Pt/C from E-TEK.[64] In addition a Zn-air battery with MnO_x-CoTMPP as a cathode gave an output current density of 216 mA cm^{-2} at 1 V in 1 M KOH and at 25^{o}C.[69] Moreover manganese oxide cathodes have been applied in a flowing alkaline electrolyte (3 M KOH), direct methanol and ethanol (1M) fuel cells achieving a maximum power density of 15 mW cm^{-2} at 34 mA cm^{-2} and 9 mW cm^{-2} at 28 mA cm^{-2} respectively.[70]

Also studies have been carried out on Ag-MnO_2/SWNT (Single Wall Carbon Nanotubes) and Ag-MnO_2 catalysts which were used as the air electrodes (on Acetylene black) in Zn-air batteries achieving a stable discharge potential plateau at approximately 1.2 and 1.1 V with discharge capacities 261 and 190 mAh/g respectively for the 2 different electrodes.[71] Additionally a decavanadium complex was used as the cathode material for ORR in a Zn-air battery which showed a stable discharge potential at approximately 1 V with discharge capacity of 80 mAh/g.[72]

It's worth mentioning here that there is no literature on catalysts for GDE's in NaCl solution. Again the reason is clear. As soon as the oxygen reduction reaction occurs, the solution around the catalyst will go alkaline. This leads to an unfavourable negative shift in the equilibrium potential. Also, a NaCl electrolyte is also significantly less conducting than 8 M KOH leading to a larger IR drop within the pores.

1.10. General description of applications of aluminium alloys

Aluminium alloys have been widely used as anode materials in power sources and are also the most widely used alloys for the cathodic protection of ships and other marine metallic structures. Considering the use of aluminium alloys in power sources applications it should be noted that Al-air batteries are the most widely tested power supplies as has been described in Section 1.7 of this introduction. Such power sources are mainly utilizing an alkaline or a saline electrolyte. Regarding the alkaline electrolytes, solutions of KOH and NaOH of concentrations 3-5 M have been shown to be best in terms of solubility of the reaction product, $Al(OH)_4^-$, from aluminium dissolution.[73] If mass production of Al-air batteries was considered NaOH is suggested as preferable electrolyte since KOH solution does not allow the retreatment via the industrial Hall Hėroult process, because potassium ions have harmful effects on the cathode of electrolysis cell.[7] Operating Al-air batteries with such electrolytes would give higher power/energy density compared to saline electrolytes (mainly 2 M sodium chloride); however in alkaline electrolytes hydrogen evolution and rapid aluminium corrosion limit the battery performance.[74] Alluminium anodes would be more stable to corrosion in brine media compared to caustic but would result in lower energy density power sources. If alkaline electrolytes or even saline media where, aluminium anodes are not stable to open circuit corrosion are to be used, the addition of the electrolyte immediately before the battery operation would be advised. In a battery application the Al anode must: (a) be stable to open circuit corrosion (b) give a low rate of hydrogen evolution during discharge (c) have a negative operating potential so that the battery has a high voltage (d) have a high rate of anodic dissolution.

Aluminium alloys have also been extensively used as sacrificial anodes for the cathodic protection of steel in seawater.[75] An alloyed anode material for an Al-air battery in brine electrolyte could also be used as a sacrificial anode material for cathodic protection of steel in seawater, since it would be more electronegative in the electrolytic environment than the cathode to be protected. The main requirements for a sacrificial anode material has been stated by Reding et al., (1966): a) a potential sufficiently electronegative to provide an adequate current flow, b) a high electrical output per gram of anode consumed and c) a low metal cost.[76]

While pure and commercial grade aluminium may be suitable for alkaline batteries, they never give the appropriate combination of properties in brine and hence each application has required the development of a specific range of alloys, see later.

1.11. Aluminium anode in battery

1.11.1. Al purity

The importance of aluminium as an anode was first realised when it was used in the Buff Cell in the late 19th century.[77] One of the vital characteristics of an anode to be used in alkaline Al-air battery system is the absence of impurities, such as iron and copper, which can lead to rapid corrosion on open circuit.[38] Doche et al., (1997) tested different grades of Al anodes and showed that iron impurities resulted in higher corrosion rate of the Al anode in 1 M NaOH.[7] As a result it is very important to use as pure Al as possible (preferably 5N Al-99.999%). However as has been stated by de Souza and Vielstich (2003), the high cost in energy of this grade of aluminium reduces the overall thermodynamic efficiency of the battery (taking into account the Faradaic efficiency of dissolution, aluminium extraction and aluminium refining) to about 10%. According to the same authors, to reduce considerably the cost of the battery, high purity smelter-grade metal (99.8%) anodes should be used instead of the super purity ones.[38]

1.11.2. Saline electrolytes: Metal ions and Al alloying

Pure Al always exhibits a very large overpotential for dissolution in NaCl based electrolytes. It can be used as negative electrode material in strong alkali although in such media corrosion on open circuit and high rates of hydrogen evolution during aluminium dissolution are always problems. The main approach to such issues is alloying the aluminium anode as it will be discussed further in the next section. Some aluminium alloys are more stable to corrosion in saline but it is also essential to use an alloy with a high dissolution rate.[5] However elements like Si and Fe accelerate corrosion and should be avoided as materials for battery anodes. Considerable efforts have been made to develop alloy anodes and electrolyte additives for Al-air batteries

with aqueous electrolytes.[78] During the 1990's, a group at Alcan developed a range of alloys containing Sn, Ga, In and/or Mg and described optimum compositions for both alkaline and brine electrolytes.[24, 79, 80] In saline electrolytes it has been shown that the addition of In^{3+} ions in the electrolyte revealed activation of pure Al which increases with increase of In^{3+} concentration.[24] In contrast to pure Al, deactivation was observed in the case of Al-Sn alloy on addition of In^{3+} because, according to the authors, Sn in the alloy retards the diffusion pathway of In ions to the bulk of the alloy matrix. El Shayeb et al., (2001) investigated the effect of Ga^{3+} ions in solution on the electrochemical behaviour of Al, Al-Sn, Al-Zn and Al-Zn-Sn alloys in chloride solutions.[24] According to the authors after cathodic polarization to – 2 V in Ga^{3+} containing electrolyte, deposition of Ga on the electrode surface occurs which gives rise to increased adsorption of Cl^- ions at more negative potential. In addition, they concluded that Ga^{3+} in solution with Al-Sn alloy causes big shift of potential in the negative direction and has a greater effect than with pure Al.[24]

Mathiyarasu et al., (2001) studied in detail the combined effects of In and Ga in 3% NaCl electrolyte.[81] They proposed a mechanism to explain the activation of minor alloying addition of elements in the Al anodes and concluded that for a given weight % there is a critical concentration of Ga which will have the positive and synergistic effect in alloy activation. In their view, 0.02% Ga was the critical concentration. Above or below this value, the efficiency and capacity of the anode decreases. Kliskic et al., (1998) presented their results in two Al-Sn alloy binary alloys (0.02 and 0.4 weight % Sn).[58] They concluded from a study of the time dependence of the open circuit potential on the low Sn content alloy that the open circuit potential shifted slightly in the negative direction (50 mV - which leads to crevice formation, that has been assumed to be due to tin hydride formation in the high cathodic potential region), while this value increases as high as 350 mV in the case of the alloy with the higher Sn content; these observations resulted from OCP monitoring of the two alloys for 35 hours. The phenomenon of superactivation (discussed in detail at Section 1.11.6 - suggested to be a consequence of a defilming process brought about by the retention and agglomeration of high mobile metallic species on electrode surface) and pit formation is characteristic for the alloy containing 0.4 weight % tin during changes of potential in the negative direction.

The alloys used for the current project typically contain Mg, Sn and Ga and they are very different in properties and structure to the Al alloys used as structural components. They are not always commercially available and have also been much less studied. Alcan and Alupower (a subsidiary of Alcan) carried out extensive studies of alloys containing Mg, Sn and Ga but almost all the published work relates to alkaline electrolytes.[24, 35, 41, 82] A conference presentation by Alupower indicates that an AlMgSnGa alloy (AB50V) was the preferred alloy for saline batteries and that Ga was unnecessary in alkaline electrolytes. They conclude that in alkaline solution the Mg reduces open circuit corrosion and the Sn led to a much lower overpotential during anodic dissolution. No experimental data was, however, reported for the properties or performance of AB50V in saline solutions. Alupower also supplied AB50V in the form of plates to Budevski et al., (1989).[14] The authors tested the aluminium alloy anode in 2 M NaCl and also applied it to an Al-air saline power system, (with air cathode fabricated as a double layer air electrode made of an active carbon catalyst and a special porous hydrophobic material pressed on a lead-plated metal net). As was mentioned previously, this battery with a power output of 24 W, was far too heavy (27 kg when empty) to be considered for any UAV applications. Furthermore, a similar alloy anode was supplied by Alcan to Shen et al., (1994), in order to test it in 3% NaCl and applied it as an anode in a sub-sea aluminium sea water power system, (cathodes were Teflon bonded Co_3O_4/C or Pr/C electrodes).[42] This battery design, although interesting, resulted in power output of 25 W with a dry weight 174 Kg and could not be considered for an ultra light power application of an Al-air system.

An AlMgSnGa alloy was also used by Tuck, (1992) to study the electrochemical activation and corrosion of the alloy in NaCl media. The author studied in situ the corrosion reaction of the AlMgSnGa alloy during voltage oscillations in order to comprehend the mechanism of pitting during galvanostatic polarisation.[35]

Since for this study NaCl electrolytes were largely used, only a brief discussion will follow on alkaline and acidic media.

1.11.3. Alkaline electrolyte systems

Tuck et al., (1987) suggested that the activation phenomenon of Al-Ga alloys, (0.026 - 2.6 atomic % Ga), in alkali solution took place at localised surface sites associated with gallium agglomerates at metal/oxide interface, a likely mechanism being rapid diffusion of aluminium through the gallium particles which seemed to prevent the normal, passive behaviour of aluminium. [83] Macdonald et al., (1988) reported that the alloying elements in Al anode in 4 M KOH inhibit hydrogen evolution partly by decreasing the exchange current density but also by modifying the Tafel slope.[84] In particular the same authors stated that in those alloys containing Ga, the oxidation of Ga to $Ga(OH)_4^-$ appears to determine the critical activation potential. Moreover, Macdonald et al., (1998) showed that addition of 2 or more alloying elements can result in a sharp reduction in the open circuit corrosion rate to well below of that of pure Al in 4 M KOH.[84] Furthermore El Abedin and Saleh (2004), evaluated and characterized Al (99.61%) and its alloys namely, Al-Ga-In, Al-Zn, Al-In, Al-Mn and Al-Mg as anodes in 4 M KOH.[85] Al-Ga-In is found to be the most promising since it exhibited a negative open circuit potential, minimum anodic polarization, good anode efficiency and minimum corrosion rates. In contrast Al-In and Al-Mn alloys showed higher corrosion rate compared with the other alloys. Finally these authors show a stoichiometric correlation between the corrosion rate obtained by weight loss and the hydrogen evolution rate.

1.11.4. Acidic electrolytes

Due to the belief that chloride ions effect the pitting of Al and its alloys, several studies have been made. A mechanism has been proposed by Abdel et al., (2006)[86] to explain the Cl^- ions effect on the Al in 1 M H_2SO_4, containing different chloride ion concentrations (0.01 - 0.06 M). These authors proposed a mechanism by which molecular oxygen is firstly chemisorbed onto the metal surface followed by chloride ion adsorption with a subsequent formation of oxide-chloride complex as a rate-determining step; the oxide - chloride complex exhibits fast dissolution in presence of hydrogen ion to give $AlCl_3$ and H_2O. In addition, in earlier years, Berzins et al., (1977), using a radiotracer technique (with ^{36}Cl as a radioactive tracer and pure Al (99.5% in NaCl solutions) showed that chloride is adsorbed by the corroding aluminium surface.[87]

1.11.5. Comparison of Aluminium behaviour in caustic and saline electrolytes

The behaviour of aluminium in saline electrolytes (usually 2 M NaCl) is quite different from that of aluminium in strongly alkaline media (i) the equilibrium potential of the Al/Al(III) is estimated as 1.66 V in neutral media and -2.33 V in alkaline solution (ii) the corrosion potentials are quite different and follow this trend[83] (iii) the product in alkaline media is the soluble species $Al(OH)_4^-$ but in chloride media largely ill defined insoluble species (see Section 1.3), (iv) on open circuit, H_2 evolution is rapid in alkaline media but difficult to observe in neutral chloride media[85, 88] (v) in alkali even high purity aluminium corrodes and dissolve anodically[35, 83, 88] (vi) in brine media, corrosion occurs at specific sites whereas general corrosion occurs in alkaline media (vii) in brine, the alloying elements are essential to rapid anodic dissolution while in alkaline media the main role of the alloying elements appears to be in minimising the parallel H_2 evolution. The roles of the alloying elements are clearly different and it is not necessarily helpful to seek uniform mechanisms.

1.11.6. Anode development- alloying elements

Aluminum is a thermodynamically reactive metal. However it owes its excellent corrosion resistance and its extensive commercial use to the oxide film formed to its surface in most environments.[17] The first extensive study of elements that could be added to aluminium and lead to higher rates of anodic dissolution[24] was carried out by Reding and Newport (1966), who tested more than 2500 alloys.[76] From this work it was shown that the addition of gallium, mercury, tin and indium caused aluminium to exhibit a potential from 0.3 to 0.9 V (potential difference *vs* a steel cathode) more negative than unalloyed aluminium. The authors concluded that the elements that made aluminium more active have a low melting point and except for zinc and magnesium, the solubilities of the addition elements in aluminium and of aluminium in the addition elements are low. The mechanism by which the low melting point elements including mercury, gallium, indium tin and thallium cause the so-called superactivation of the aluminium, i.e. activation above that of a normal aluminium electrode, was considered to be related to both their electrochemical and physical properties.[37, 76]

In the 1980's, extensive studies were carried out as part of Alcan's and its subsidiary Alupower program on aluminium anode developments. Pioneers in research on aluminium anode for Al-air batteries development program were Tuck, Hunter and Scamans although their published data mainly result from experiments in alkaline electrolyte.[24, 35, 83] These scientists studied the role of Sn and Ga on aluminium anodes behaviour. The enhanced behaviour of aluminium due to alloying that was firstly observed by Reding and Newport (1966),[76] was more recently referred as superactivity. Superactivity is, however, usually accompanied by high rates of hydrogen evolution.[24] Hunter et al., (1991) also stated that under certain conditions, aluminium anodes can exhibit a state which is considerably more active than the superactive state. In this 'hyperactive' state, anodes operate at potentials very close to the thermodynamic potential of aluminium and generate large amounts of hydrogen.[24] From the extensive anode studies initiated from Alcan International, ten elements were identified that induce superactive behaviour in aluminium when present in solid solution; Hg, Ga, In, Sn, Bi, Tl, Cd, Pb, Zn, and Sb. According to Hunter et al., (1991), solid solution elements exist in an aluminium matrix as discrete atoms. He further proposed that because of their low melting point, these metals must initially be retained on a reaction surface as highly mobile atoms. This accumulation of mobile species would occur beneath any 'protective' film.[24] Extensive studies by Tuck et al., (1987) on micro-cell system on Al-Ga alloys (with Ga weight percent content ranging between 2.6% and 0.026 %) showed that when this accumulation commences, activation of aluminium takes place at localised surface sites associated with gallium agglomerates at the metal oxide/interface and pitting of aluminium occurs. According to Tuck et al., (1987), the oxide above these particles is extremely thin and aluminium from the alloy diffuses rapidly through the gallium prior to its oxidation. Therefore, an electrode potential more electronegative than the one that is exhibited by pure aluminium was displayed. A critical concentration of gallium in the alloy is required for activation to occur. In addition the authors showed the effect on the open circuit potential (in 4 M NaOH at 60 ^{o}C) after the addition of a GaAl alloy to a liquid gallium electrode (amalgam). The latter caused shift of the open circuit potential to more negative values (from -1.5 V *vs* Hg/HgO to -1.7 V). Interestingly the authors demonstrated that by cooling below 20 ^{o}C during a reaction of an AlGa alloy in 4 M NaOH the voltage rapidly shifted to more positive values. The observation of this passivation by cooling of Al-Ga alloys, resulting in behaviour similar to that of pure aluminium, was made both in NaOH and

NaCl solutions. The latter strongly indicates that the gallium must be in the liquid state to be effective in its activation procedure; As the melting point of gallium is 28^{o}C and it very readily supercools below this temperature, it will be liquid in AlGa alloys reacting at room temperature.[83]

Coming back to the discussion on activators in aluminium alloys, Hunter et al., (1991), stated that for the hyperactive behaviour in aluminium alloys, at potentials more negative than -1.8 V *vs* Hg/HgO, fourteen elements could be considered: P, In, Se, Sn, Bi, Cd, Pb, Zn, Sb, As, Ge, and C.[24] With the exception of Zn, the similarity between all these metals is that thermodynamics predicts that they form gaseous hydrides at potentials above ~ -2.1 V *vs* Hg/HgO), where hyperactivity is exhibited. According to the authors, the starting point for hyperactivity to occur must be the release of discrete solute atoms onto the reaction surface from the dissolving solid solution. Even though these species would initially be in the elemental forms, they would be rapidly reduced to their equivalent hydride. It is believed by Hunter et al., (1991) that these hydride molecules must in some way cause defilming of the anodes.[24] Hyperactive anodes have been shown to dissolve in a homogeneous crystallographic way. Even though it has not been reported in aqueous media it is believed that solute metal hydrides could act as a reaction intermediates in the formation of aluminium hydride. In that case very small quantities of solute could have a dramatic effect upon aluminium corrosion and polarisation characteristics.[24] At potentials where aluminium dissolution occurs: (i) hydrogen evolutions is thermodynamically possible (ii) the amount produced depends on the mechanism and has been reported to be particularly high in the potential region for hyperactivity in alkaline media[74] (iii) the rate of hydrogen evolution also depends on the electrolyte medium. In alkali, hydrogen evolution is immediately obvious and an amount of 5-20 cm^3/min has been shown to be produced.[74, 83, 85]

Alupower's program on aluminium anode development during the late 1980's showed that AlMgSn alloys should be used in alkaline electrolytes but gallium addition is necessary to increase voltage at high current densities when high power torpedo and saline batteries are considered.

During this thesis, the anodic dissolution of aluminium potentials significantly negative to that for pure aluminium oxidation will be called activation. The term "superactivation" will not be used throughout this thesis for simplicity.

Anode development in saline electrolytes is based on specially designed aluminium alloys with a low content (up to 0.3%) of alloying elements.[14, 39, 76, 89] The alloying of aluminium with gallium, tin and indium enables high rates of anodic dissolution.[14] As has been mentioned earlier in this thesis studies of aluminium anodes containing gallium, tin and magnesium have proved that such materials give a high anode efficiency (80-89%) with high open circuit voltages during battery operation in NaCl.[14, 42]

For both alkaline and brine solutions, the role of the minor elements magnesium, tin and gallium, for the battery anode efficiency could be discussed in terms of the phase diagrams and solid solubilities of the elements (as mentioned earlier) since the activator species have been observed to accumulate on the alloy surface.[24] The anodic behaviour of the alloys may be strongly influenced by the extent that the alloying elements are present in solid solution in the aluminium phase or present as inclusions within the aluminium phase. The magnesium in such alloys is known to be mainly effecting the mechanical properties[17] of the anode (it used to avoid physical disintegration of the anode).

Gallium has a very low melting point, 303 K, and is therefore likely to be very mobile within the alloy structure even at room temperature. Moreover the Al–Ga phase diagram reveals no intermetallic compounds and very limited mutual solubilities. Hence only the Al-Sn binary phase diagram will be discussed here. From the Al-Sn phase diagram in Figure 1.7 it can be seen that from room temperatures to 220^{o}C Al solid matrix and a second phase of tin will exist. From the phase diagram it is clear that heat treatment of an alloy containing tin could affect the solid solubility and hence reactivity of the alloy. If heat treatments of temperatures above 220^{o}C were carried out, tin would be of liquid form (L) in an aluminium solid matrix. If heat treatments of Al-Sn alloys (equally of

AlMgSnGa) were to be carried out from low temperatures (e.g. room temperature) to 500 ^{o}C and then cooled quickly then aluminium solid would be the only phase (with Sn dissolved in it). Therefore if one would consider an aluminium alloy with 0.1% Sn that was heat treated to 600^{o}C and then quenched quickly into water, solid solubility of Sn on aluminium should be expected. However some βSn phases should also be expected to be seen on aluminium matrix even if really quick quenching takes place. At this stage just to enhance general understanding of the system it is worth noting that if another second phase was formed with Sn (e.g. MgSn would form if we had very high concentrations of magnesium in the alloy- greater than 17.1 wt% according to the aluminium-magnesium phase diagram[17]) then the solid solubility of Sn in aluminium would be decreased since some tin would be "used up" to form the magnesium-tin second phases.

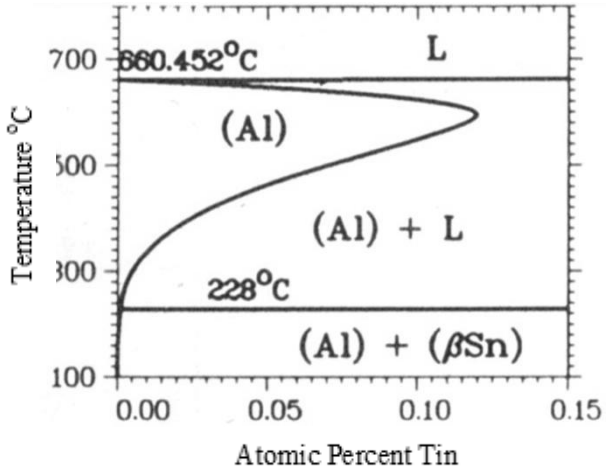

Figure 1.7: *Phase diagram for the Al-Sn binary system for low concentrations of tin, obtained from Aluminium and Aluminium Alloys Handbook, (1993).*[17]

Hence, for anode development for Al-air batteries, heat treatment would be probably beneficial since it would increase the solid solubility of Sn in aluminium and maybe more homogeneous utilization of the anode (oxidation/dissolution). It is also worth mentioning at that point while consideration is given to AlMgSnGa alloys with minor concentrations of Mg in aluminium, (e.g. 0.1% Mg), according to the aluminium magnesium binary phase diagram there should be only one phase, aluminium with magnesium dissolved in it.[90] So in an AlMgSnGa anode material the only second phases

could be βSn. It is important to note, however, that it is a simplification using binary alloys phase diagrams to interpret systems for alloys with more than one components.

The phase diagram leads to the concept of two limiting structures of potential interest for high rates of anodic dissolution: (a) a homogeneous Al/Sn phase and (b) a structure with many Sn centres of critical size within aluminium matrix.

It should be noted that since all the alloys are probably prepared in the molten state (> 700^{o}C), the critical factor in determining their structure is the cooling regime in their preparation; this is not known for the alloys used in this work.

1.12. UAVs applications

The US Department of Defence Dictionary defines a UAV as a powered, aerial vehicle that does not carry a human operator, uses aerodynamic forces to provide vehicle lift, can fly autonomously or be piloted remotely, can be expendable or recoverable, and can carry a lethal or non-lethal payload.[91, 92]

UAV's are presently emerging from development and beginning to make a real contribution to surveillance and other operations.[93] Unmanned air vehicles are not restrained by human limitations and requirements. They can gather information in dangerous environments without risk to flight crews. In addition, they can be more cost effective than manned aircraft operations. However, if they get damaged during flight, the repair costs could be very high. In the near future, UAVs are expected to be used for civilian missions as well. The United States Coast Guard plan to use UAVs for search, rescue, and patrol operations. UAVs could also be used for aerial surveys and to inspect pipelines and power lines, jobs done today by piloted airplanes! [58]

The performance of UAVs is largely determined by their weight and the battery currently contributes a large fraction of the total aircraft weight. Lighter batteries or other power supplies are essential to future high performance UAVs.

1.13. UAV's research objective

The anodes studied in this project are aimed to be used in an Al-air cell that would be used as a power source of a Micro Air Vehicle able to carry a sensor payload, has the processing capability to support both active control and autonomous behaviour and provides sufficient endurance and/ or range to make it truly useful in a military context. The UAV will be a small lightweight system that is designed to be carried by infantry into battle situations and perhaps launched from the ground by a catapult launch system.[94]

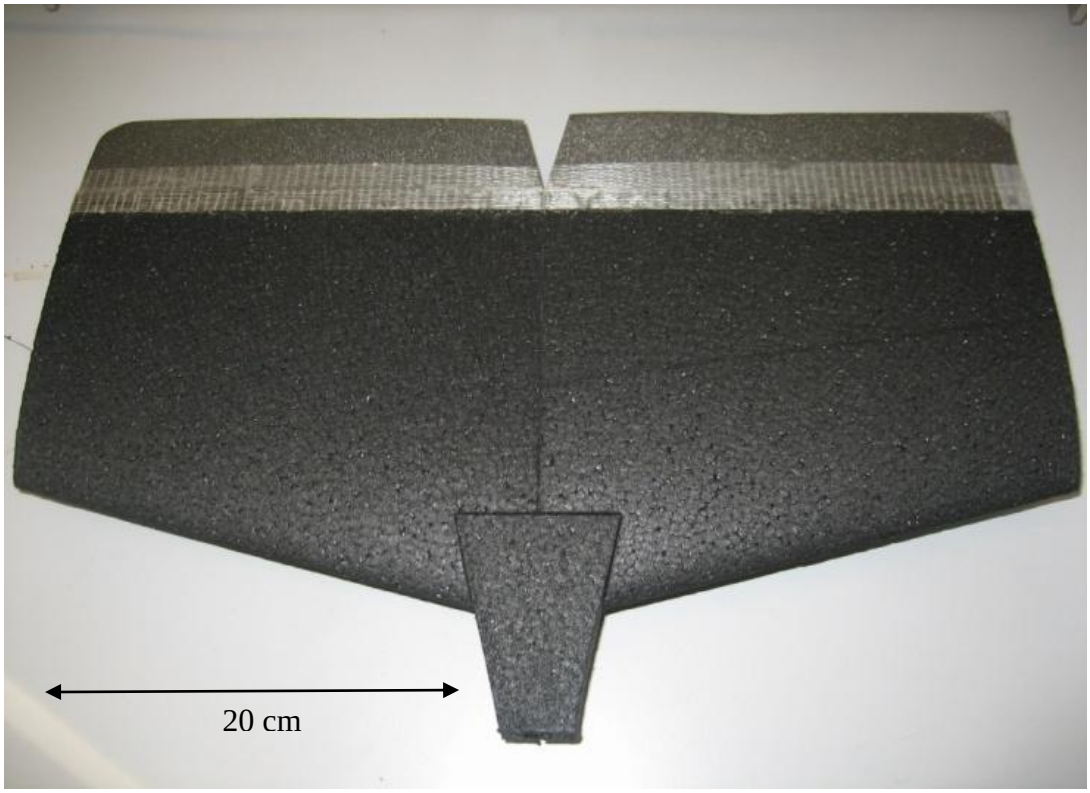

Figure 1.8: *A photograph of a possible UAV, for which the Al-air battery system is being designed, as has been proposed by Blue Bear Systems research Ltd.*

One possible microplane configuration has been proposed by Blue Bear Systems Research Ltd and is shown in Figure 1.8.[95] Ideally the flight time using the Al-air battery will reach 1 hour. The battery itself is required to give an average power of

20 W and a maximum power of 34 W. In Figure 1.9 such a mission profile is illustrated. The target for the battery weight is less than 50 g.

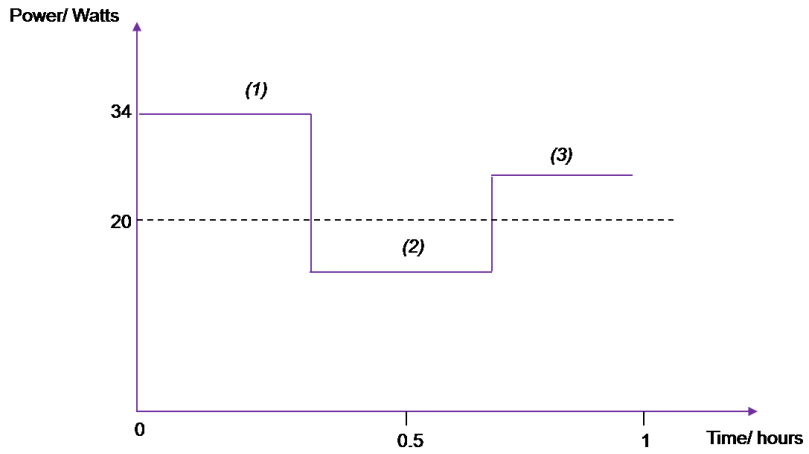

Figure 1.9: *An illustration of power requirements during the flight of the UAV using the designated Al-air battery where: (1) launch and climb, (2) level of flight, (3) surveillance/duty.*

It has to be mentioned at that point that the sponsors required the use of a saline electrolyte and therefore the work of this project is mainly carried out in NaCl. This requirement relates to issues upon restriction of acidic and alkaline solutions on the battlefield. Finally, if such a battery was employed is suggested that the electrolyte be always added immediately prior to flight to avoid any corrosion issues."

1.14. Al-air battery options

An aluminium air battery consists of the aluminium anode, the electrolyte and the air cathode. Since a battery for a UAV should be lightweight, the weight of all its components should be considered. The only part of such a battery that would have negligible weight is the air cathode since the air would come from the surroundings and the cathode can be very light. According to calculations the electrolyte would be the heaviest component of such a battery and hence its weight should be considered and

somehow minimised. Two possible battery configurations capable of the target power and meeting the weight limitation are shown in Table 1.2

There are a few important points that should be made. The battery weight is proportional to flight time and average power requirement because as the electrodes gets bigger the electrolyte volume goes up. Also the battery should always contain Al anode in excess to make electrical contact and for safety reasons, requirements that influence the overall battery weight.

Table 1.2. *Two possible Al-air battery systems along with their specifications.*

	Battery A	Battery B
Type	Single cell	6 cell stack
Voltage assumed	1.30V	6 x 1.30 V= 7.8 V
Max current to give 34 W	26 A	4.5 A
Current density assumed	250 mA cm^{-2}	250 mA cm^{-2}
Electrode area required	1 x 108 cm^2	6 x 18 cm^2
Al required for flight 1 hour with average power 20 W (based on Faraday's law)	4.9 g	4.9 g
Al in battery	10 g	10 g
Thickness of Al for the area given	0.4 mm	0.4 mm
Interelectrode gap	2 mm	2 mm
Electrolyte volume	22 cm^3	22 cm^3
Electrolyte weight	25 g	25 g
Concentration of product Al (III) if all product in solution	7.5 M	7.5 M
Weight of Al_2O_3 if all product solid	10 g	10 g
Battery weight (Al + electrolyte + cathode)	10 + 25 + 5 = 40 g	10 +25 + 5 = 40 g

Ultimately it has to be noted that a high battery voltage is advantageous since it reduces Al requirement and hence electrolyte requirement; the latter being the major weight of the battery system. The components of the battery should be designed in a way that

minimizes the electrolyte requirement. The Al (III) product of the discharge reaction should also be considered during the design of the components, so that it somehow does not clog the air cathode or interferes in any way with battery operation. The calculations in the Table 1.2 allow an estimate of the volume of electrolyte allowed in a successful battery; it is not clear that all the Al (III) can be contained within this small volume.

The above calculation does not consider any water consumed in the battery discharge chemistry. However if $Al(OH)_3$ is the product during the battery operation the reaction will be:

$$4Al + 3O_2 + 6H_2O \rightarrow 4Al(OH)_3 \quad \text{(R.9)}$$

If this is the reaction occurring during UAV operation then for every 27 g of Al oxidised 27 g of water will be consumed.

If the reaction product during the battery operation is Al_2O_3 then there will be no water consumption since the reaction will be:

$$4Al + 3O_2 \rightarrow 2Al_2O_3 \quad \text{(R.10)}$$

In addition, instead of including the battery in the components of the UAV, one different approach may be to design the battery so that it also forms part of the UAV body. For example, the electrodes could be the upper and lower surfaces of the wings or form the nose cone.

1.15. Summary of the current state of knowledge

Scientists from Alcan and Alupower identified AlMgSnGa alloys as the preferred anodes in Al-air batteries with brine electrolytes.[14, 39, 76, 89] They did, however, not publish extensively on the mechanism of the anodic dissolution in brine. More extensive studies in alkaline media were presented in several papers.[1, 24, 36, 41, 74, 83] Others have confirmed their conclusions[15, 40] in brine media but were satisfied with low rates of dissolution. The objective of this study was therefore to extend understanding of the mechanism and kinetics of such alloy dissolution and, particularly, to characterise their behaviour at high rates of dissolution.

CHAPTER 2 Experimental

2.1. Reagents, solutions and polishing materials

All reagents used in the present study are listed in Table 2.1. All aqueous solutions were prepared using deionised water from Whatman Analyst water purifier system (model 501.269 made by Whatman International Ltd, Maidstone,UK.

Table 2.1. *Reagents used during the current study.*

Name	Formula/Specifications	Supplier/ grade
DL-Lactic acid	$CH_3CH(OH)CO_2H$	Acros Organics/ 85%
Hydrochloric acid	HCl	Fisher Scientific/ ARISTAR
Hydrofluoric acid	HF	Fisher Scientific/ 48%
Kellers reagent	2 ml HF (48%), 3 ml HCl (conc), 5 ml HNO_3 (conc), 190 ml H_2O	All acids Fisher Scientific
Malonic acid	$HO_2CCH_2CO_2H$	Avocado Research Chemicals Ltd / 99%
Mercury	Hg	Aldrich/ 99.9+%
Mercury (I) chloride	Hg_2Cl_2	Aldrich/ 99.5+%
Nitric acid	HNO_3	Fisher Scientific/ 70%
Potassium chloride	KCl	Fisher Scientific/ analytical reagent
Potassium hydroxide	KOH	Fisher Scientific/ laboratory reagent
Sodium chloride	NaCl	Fisher Scientific/ Analytical reagent
Sodium hydroxide	NaOH	Fisher Scientific/ Laboratory reagent
Sulfuric acid	H_2SO_4	BDH/ ARISTAR
Tin chloride (II)	$SnCl_2$	Sigma-Aldrich/ 98%
1 μm diamond paste	MetaDi® II	Buehler
DP-mol cloth	DETMO - 40500221	Struers
SiC paper	600,1200 and 4000 grade	Struers
Epofix resin	EPOFI: 40200029	Struers

Pure aluminium (99.999 %) and eleven aluminium alloys were investigated. The pure aluminium and AlMg alloys were obtained from Goodfellow Metals. The SAFT and Chandlery anodes were supplied by the Defence Science and Technology Laboratory

(dstl) that informed us that Chandlery anode originated from M.E.Duff Ltd. The AB50V was a preferred alloy at the end of the Alcan programme in the 1980s, given to us in the form of a thin (1 mm thickness) 10 cm x 10 cm plate by Clive Tuck.[24] I0 is an alloy of similar composition prepared by Innoval Ltd and obtained in the form of a 5 kg cylindrical sample. B0 – B4 were a series of alloys prepared from 5N aluminium source in the Department of Metallurgy and Materials, University of Birmingham supplied in the form of small 5 g pellets. The compositions of all these alloys along with their suppliers are reported in Table 2.2.

Table 2.2. *Aluminium materials used for the project and their suppliers.*

Alloy Composition/ Supplier	Wt% Mg	Wt% Sn	Wt% Ga	Wt% Zn	Wt% Fe	Wt% Si	Supplier
99.999% Al	-	-	-	-	-	-	Goodfellow
AlMg3	3	-	-	-	-	-	Goddfellow
AlMg5	5	-	-	-	-	-	Goodfellow
SAFT anode	-	-	0.1	0.11	0.09	0.08	dstl
Chandlery anode	-	-	0.02	5.25	-	-	M.E.Duff
B0	0.5	0.1	0.05	-	-	-	Birmingham University
B1	0.4	0.1	-	-	-	-	Birmingham University
B2	0.4	0.4	0.03	-	-	-	Birmingham University
B3	0.4	-	0.03	-	-	-	Birmingham University
B4	-	0.1	0.03	-	-	-	Birmingham University
AB50V	0.6	0.1	0.05	-	-	-	Clive Tuck
I0	0.4	0.07	0.05	-	-	-	Innoval

2.2. Equipment in Electrochemistry

The voltammetry and chronopotentiometry experiments were controlled either with an

EG & G model 273 Potentiostat or a Bio-Logic model VMP2 Electrochemical Workstation run by Powersuite and EC-Lab V.512 softwares respectively. The data were analysed and presented in Origin. Open circuit potentials were always measured with a Fluke 83 Multimeter unless otherwise stated. Impedance measurements were taken by Gamry Instruments 600 potentiostat with operating software of Gamry Framework version 5.3. For all battery experiments, the PLZ164WA electronic load equipment by KIKUSUI was used where a constant current was applied to the battery and the voltage measurements were manually recorded to construct the battery I-V curves.

2.3. Electrochemical measurements

2.3.1. Electrochemical cells

All the electrochemical experiments where the aluminium material was not polished covered or mounted within an insulating medium (e.g. resin) were carried out in a three electrode, two compartment cell, (see Figure 2.1 a). The working electrodes were long strips of the aluminium/aluminium alloys immersed to a depth of 5 mm and having an active area of 0.25 cm^2; this simple electrode design allowed rapid removal of damaged alloy and replacement by a fresh sample for repeat experiments. For electrochemical experiments that were performed in this cell, the Al alloys were not polished or etched beforehand although experiments were carried out to confirm that surface preparation made little difference to the results. The counter electrode was a Pt mesh in the same solution and the reference electrode was a laboratory fabricated saturated calomel electrode (SCE) with a fine porous tip and separated from the working electrode by a Luggin capillary. The tip of the Luggin capillary was placed as close as possible to the surface of the working electrode. Experiments used 25 cm^3 of air-equilibrated, aqueous 2 M NaCl at room temperature (293 ± 2 K). When a polished working electrode was, however, required then a different cell with a flat horizontal electrodes moulded in resin was used, (see Figure 2.1 b). The latter cell was also used with a special holder (see Figure 2.1 c) for testing of GDEs; this set-up is described later in this section.

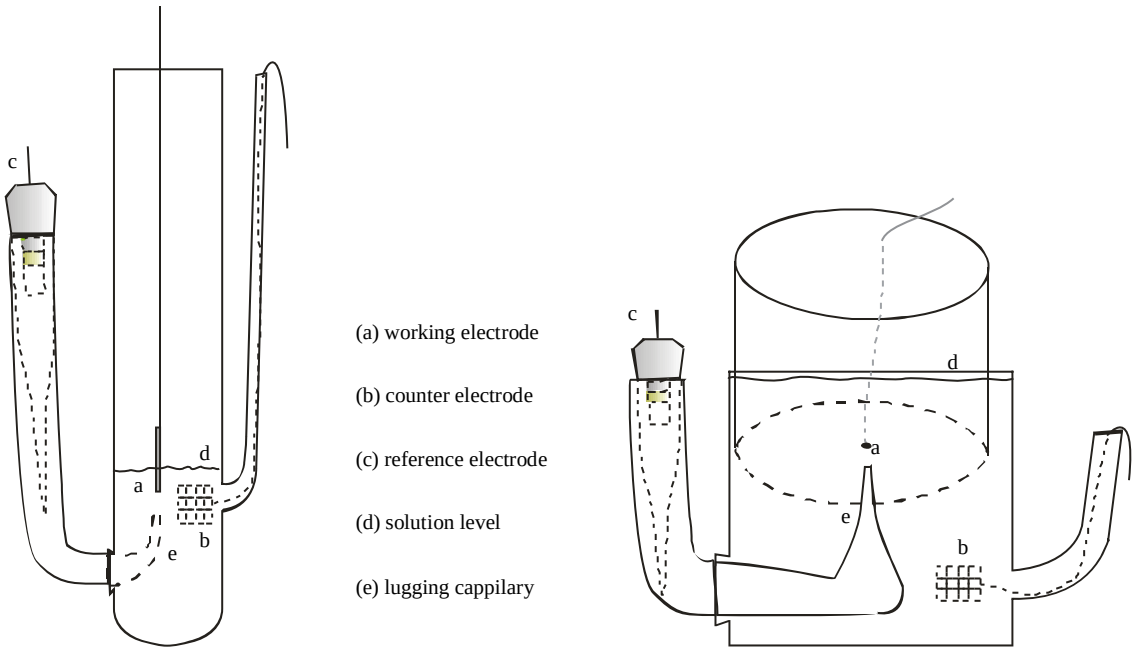

(a) **(b)**

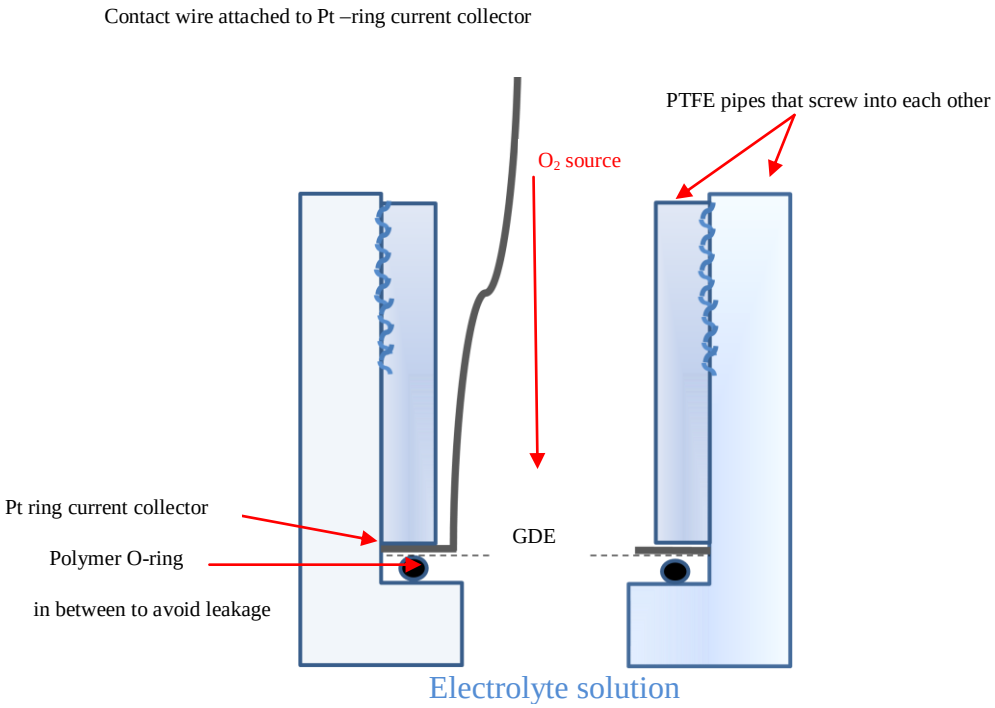

(c)

Figure 2.1: (a) *Cell used for voltammetry and potentiometry,* ***(b)*** *cell used for studies on polished materials and* ***(c)*** *GDE holder for cell (b).*

Electrochemistry experiments were also carried out in order to investigate the factors limiting aluminium dissolution; for the purposes of these experiments a small Perspex cell was used, (see Figure 2.2). The electrolyte was 2 M NaCl (6 ml) for each experiment. The anode was always an AlMgSnGa alloy, with an area 1.75 cm^2 exposed to the electrolyte. The cathode was stainless steel 904 L with the same area. A steel cathode had to be used since an air cathode able to deliver the current densities required has not been identified. At the steel electrode, hydrogen gas is formed by the following reaction:

$$2H_2O + 2e^- \rightarrow H_2 + 2OH^- \qquad \text{(R.8)}$$

It should be noted that this reaction leads to the formation of 1 OH^- / e^-, as at an oxygen cathode and hence the cathode's influence on solution pH is the same as in the Al-air cell.

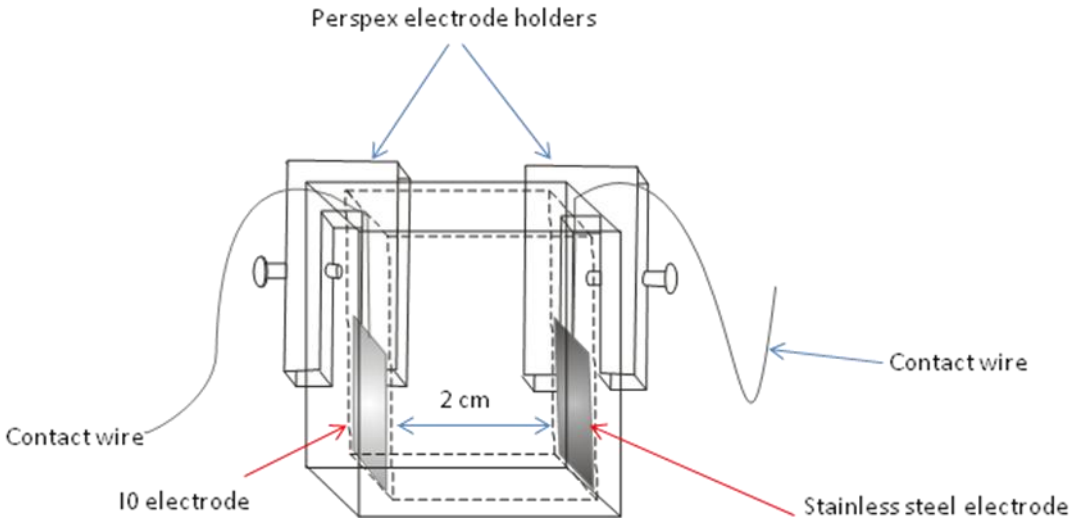

Figure 2.2: *Aluminium dissolution cell used for all electrochemistry experiments*

The experiments in the perspex cell involved the dissolution of the I0 alloy with a constant current at different current densities. In addition, some of them were performed in a heating or/and ultrasonic bath. In some experiments, the dissolution was interrupted at intervals and the impedance diagram obtained at open circuit. In addition, SEM

images of the alloy surface and cross sections were taken after different periods of dissolution. For cross sections, samples were mounted in epoxy resin and then mechanically polished. Impedance experiments were also carried out in this particular cell in various points between dissolution on OCP.

In experiments where a camera was used for visual and microscopic observations of aluminium alloys, one compartment, 3 electrode cell, (fabricated by the glassblowers at University of Southampton) was used with a flat optical window, (see Figure 2.3). The electrolyte used was 2 M NaCl (250 cm^3). The electrode fabrication process for the camera experiments is explained in detail later on in this chapter (see 2.13.1). The specially prepared electrodes were then ground and polished as will be reported later in Section 2.4.

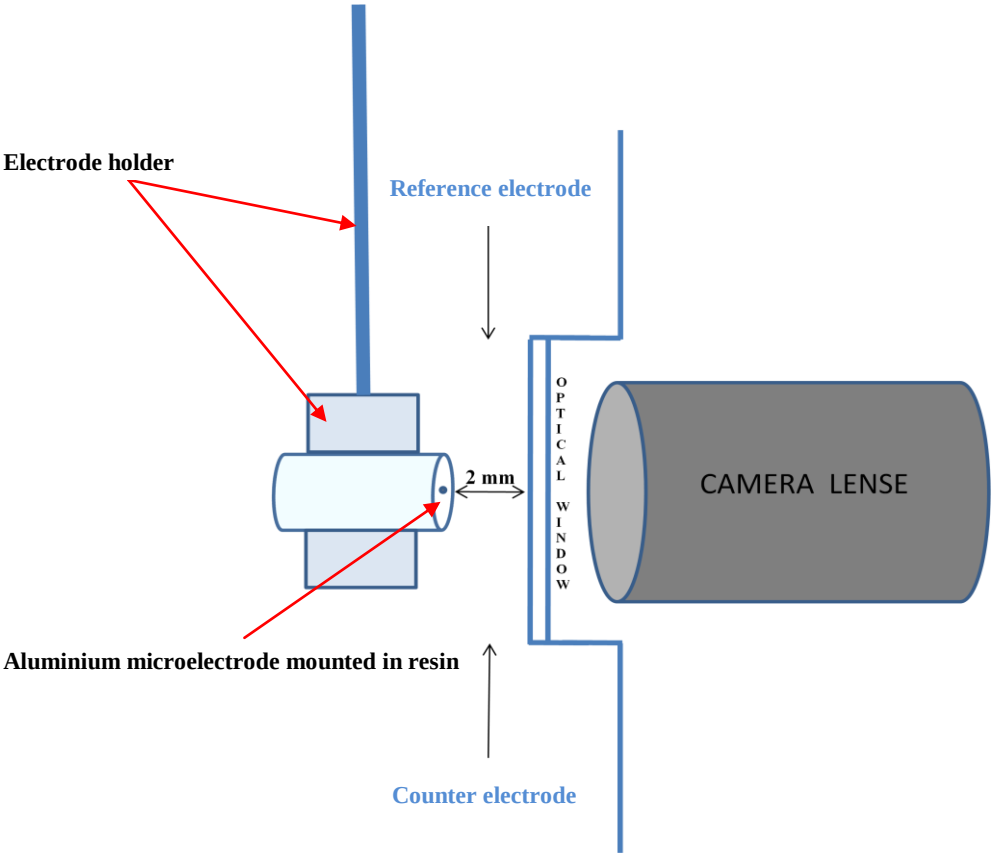

Figure 2.3: *Cell that used for camera experiments.*

2.3.2. Reference electrodes

A saturated calomel electrode (SCE) or a Hg/Hg_2SO_4 electrode were used as the reference electrodes in all experiments depending on the electrolyte being used at the time. The SCE electrode was used when the electrolyte contained Cl^- ions and the Hg/Hg_2SO_4 reference electrode would be normally used with electrolytes that would contain SO_4^{2-} ions.

The fabrication of both electrodes was very similar. Both reference electrodes were made from two glass bodies; a glass tube with one closed end through which a platinum wire was sealed, and a pipette with a sinter at the tip.

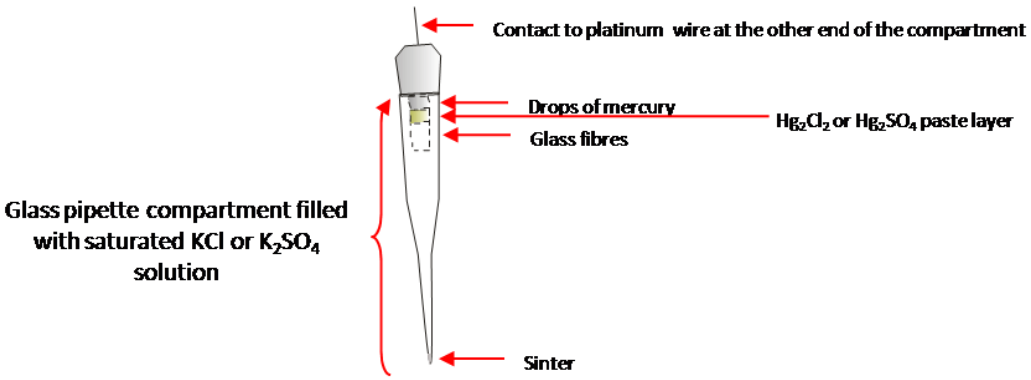

Figure 2.4: *Illustration of homemade reference electrodes used in this project.*

Drops of mercury were placed into the glass tube until the platinum wire was covered. A Hg_2Cl_2 and a Hg_2SO_4 paste layer was put on the top for the SCE and Hg/Hg_2SO_4 electrodes respectively. Glass fibres were then put into the tube to ensure that mercury and paste will stay in place. The glass tube was then inserted in the glass pipette filled with saturated KCl (for the SCE) and K_2SO_4 (for the Hg/Hg_2SO_4) solutions. The SCE and Hg/Hg_2SO_4 reference electrodes were stored in saturated KCl and K_2SO_4 solutions respectively and rinsed with purified water before and after use. In Chapter 5, potentials were converted to the Reversible Hydrogen Electrode (RHE) to allow comparison with the literature. The potentials were converted for three solutions of different pH by taking into account that the potentials of the RHE shifts – 60 mV per pH unit increase in pH.[12]

2.4. Sample preparation: Mechanical polishing

For electron microscopy, the strips of the Al/Al alloys were mounted in epoxy resin (Struers Epofix Resin) so that only the end was exposed. The exposed surface was then (i) mechanically ground successively with 600, 1200 and 4000 grade emery paper, each for one minute until examination of the surface by optical microscopy (the optical microscope model was Moticam 1000) showed only fine scratches in the same direction (ii) mechanically polished with 6 μm diamond paste on a DP-mol cloth for 3 minutes (iii) repeatedly polished with 1 μm diamond paste on a DP-mol cloth for 3 minutes until scratches could not be seen with the optical microscope. Between each stage, the surface was washed with soap solution and then water before being dried. Unlike Al alloys used in structural applications, the alloys used in this project are soft, e.g. AB50V has a hardness of 52, they scratch easily and therefore they are labour intensive to polish.

At the end of the preparation, the sample was cleaned with water in an ultrasonic bath. Scanning electron images were obtained with either a Jeol JSM 5910 or a Jeol FEG 6500F microscope; both allowed imaging by secondary electrons and backscattered electrons and were fitted with an Oxford Inca 300 EDX for elemental analysis.

For the transmission electron microscopy analysis disks of 3 mm in diameter were punched out from thin slices of the alloys, ground to around 0.25 mm in thickness and then electropolished using a solution of HNO_3 and methanol (1:3 in volume). TEM foils were examined using a JEOL 3010 microscope operating at 300kV.

2.5. Methods used in Electrochemistry

2.5.1. Voltammetry and chronopotentiometry

Linear sweep voltammograms were recorded using a scan from the OCP of the materials to more positive potentials when aluminium oxidation was examined or to

more negative when H_2 evolution was considered. The scan rate used for all the experiments in this project was 20 mV/s.

In some experiments a constant anodic current was applied in the electrolyte solution under study for 10 minutes in order to investigate 'activation' of the respective material used as working electrode. A large set of experiments included this activation process followed by constant current pulses of different current densities, where the potential was monitored continuously.

2.5.2. Impedance measurements

The principle of this technique was to apply a small sine wave (where ω is the frequency) to the working electrode so the voltage is $E(\omega)$ and measure the response through the resulting current ($I(\omega)$). This allowed the frequency dependant impedance to be calculated ($Z(\omega) = E(\omega) / I(\omega)$). In this work impedance measurements were carried out in order to quantitatively obtain the solution and charge transfer resistances before and during aluminium dissolution. In Figure 2.5 the equivalent circuit model that was considered as the simplest representation of an electrochemical interface.[96]

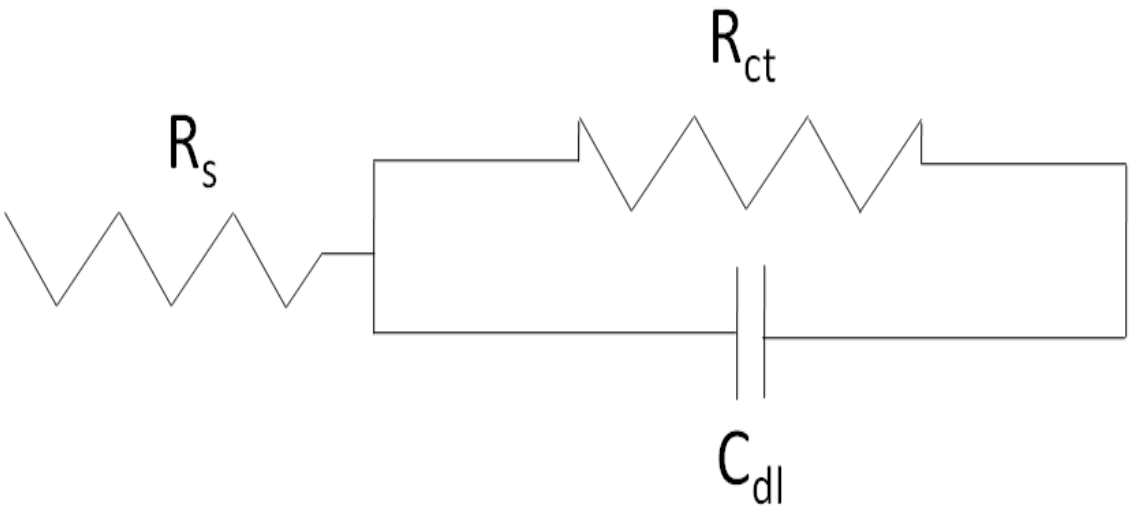

Figure 2.5: *Equivalent circuit model considered in impedance measurements as the simplest representation of an electrochemical interface.*

2.6. Chemical and electrochemical etching

In order to characterise the structure of the aluminium alloys (mainly that of AB50V) etching was undertaken after mechanical polishing of the sample. The sample was immersed for 10 or 30 seconds in an etchant. Etching was followed by washing in a stream of water and air blow drying of the sample. The prepared sample was kept in a desiccator to avoid Al/H_2O chemistry during storage until the analysis with Scanning Electron Microscopy could take place. Chemical etching was carried out using several etching solutions and electrochemical etching using different current densities, both of which are shown in Table 2.3.

Table 2.3. *Etchants used at different times for AB50V alloy*

Etchant solution used	Etching time/ s
Kellers reagent	**10 and 30**
Kellers reagent without HF	**10**
Kellers with HF diluted x 4	**10**
HF as in Kellers in H_2O	**10**
HF concentrated	**10**
Anodic etching 1 mA cm^{-2} in 2 M NaCl	**10,60, 125**
Anodic etching 50 mA cm^{-2} in 2 M NaCl	**1,10,60**

2.7. Scanning electron microscopy

The resolution of the SEM is closely related to the sampling volume of the signal used. Secondary electrons, having the smallest sampling volume, are therefore capable of giving a better spatial resolution than the other signals, while backscattered electrons which have a broad energy spread.[97]

However the backscatter electron detector, especially that of the JSM 5910 SEM, has been widely used for the current project when the dissolution of AB50V mainly was investigated. Particles of Sn, Mg and Ga were to be imaged, since the backscatter electrons emitted from the specimen for each incident electron, (known as backscatter

electron coefficient (η)), are strongly dependent on the atomic number of the specimen. This implies that particles brighter that Al matrix on the sample surface should have higher atomic weight, so by imaging them and them analyse them with EDX the existence of particles of the alloying elements was verified. For the current project three different scanning electron microscopes were used, listed in Table 2.4.

Table 2.4. *The SEM instruments used for the current project.*

Characteristics	XL30 ESEM, Philips	JSM 6500F, JEOL	JSM 5910, JEOL
accelerating voltage	0.2 to 30 KV	0.5 to 30 kV	0.3 to 30 kV
Secondary electron and backscatter electron imaging	✓	✓	✓
Electron backscatter diffraction	-	✓	✓
Energy dispersive X-Ray microanalysis	EDAX X130	Oxford Inca 300	Oxford Inca 300

For some preliminary experiments, where images of non-polished alloy strips were obtained before and after voltammetry and potentiometry experiments, an environmental scanning electron microscope ESEM (Philips) was used. The ESEM differs from a conventional SEM (CSEM) by not requiring a high vacuum sample environment. It retains all of performance advantages of a CSEM, but at sample chamber pressures as high as 50 Torr (760 Torr=1 Atmosphere), temperatures as high as 1500 ^{o}C and practically any gas composition.

For the purposes of experiments where the dissolution of AB50V was investigated, JSM 6500F and JSM5910 SEMs from JEOL were used due to their higher resolution and in general due to their better performance.

2.8. Transmission Electron Microscopy

Transmission electron microscopy analysis was carried out in order to detect the possible existence of small particles on aluminium surface that would not be detected by SEM. Ga was the main element wished to be imaged or detected by EDX since it was not detectable by SEM. A JEOL 3010 microscope operating at 300kV was used along with elemental analysis that was carried out using Oxford Inca 100 energy-dispersive X-ray system.

2.9. Heat treatments

Heat treatments of aluminium alloys, when used, employed from 100 - 600 ^{o}C in a CFS-1100 Carbolite furnace for 2 hours in air. The sizes of the samples ranged from strips of 1 cm^2 when samples were to be used in electrochemistry experiments to 2 cm^2 rectangles when samples were to be used in other analysis. The sample was immediately quenched in cold water and kept in a clean box until they were used.

2.10. Electron Backscatter Diffraction Analysis

2.10.1. Definition and Principle

Electron backscatter diffraction (EBSD) is a technique which allows crystallographic information to be obtained from samples in the SEM.[98] In EBSD, a stationary electron beam strikes a tilted crystalline sample and the diffracted electrons form a pattern on a fluorescent screen.[98] This pattern is characteristic of the crystal structure and orientation of the sample region from which it was generated. The patterns obtained from all EBSD results were analysed by a by the computer software HKL Channel 5 on a JEOL JSM-6500F FEG-SEM where a step size of 3 and 13 μm was used. EBSD was used in this work in order used to measure the grain boundary misorientations and measure grain sizes of different alloys. In addition the effect of heat treatment in grain size was investigated by EBSD. In the last ten years EBSD is rapidly developing into an important analytical tool.[97, 98]

2.10.2. Preparation of metal sample for EBSD analysis

Because diffracted electrons escape from within only a few tens of nanometers of the specimen surface, specimen preparation is critical for EBSD analysis in order to gain satisfactory results. For this project where the grain analysis of aluminium alloys was sought, the samples for electron backscatter diffraction analysis were ground with 600, 1200 and 4000 grade Si/C paper, each for one minute until examination of the surface by optical microscopy showed only fine scratches in the same direction. When the aluminium samples were to be heat treated, heat treatment in a Carbolite CSF 1100 furnace for 2 hours, (that was followed by water quenching), was always done before the grinding step. The final step of sample preparation was its electropolishing in 20 % HNO_3 in methanol at 243 K. Liquid nitrogen was used to cool the solution used for electropolishing. Safety precautions should be undertaken when the above procedure is carried out since if the temperature is not low enough, combustion could occur.

2.11. Gas Diffusion Electrodes

All the commercial gas diffusion electrodes (GDEs) used in this project are listed in Table 2.5.

Table 2.5. *Gas-diffusion electrodes used in the current study are listed along with their characteristics.*

Model	Pt loading/ mg cm^{-2}	supplier
catalyst printed on Toray substrate with Pt Black ink	4.66	Johnson Matthey
A2 STD ESNS, Silver Plated Nickel Screen Electrode, standard 0.6 mg/cm^2 TM loading using 10% Pt on Vulcan XC-72	0.6	E-TEK

All voltammetry experiments with the gas diffusion electrodes were carried out in the 3 electrode, two compartment glass cell, showed earlier in this section in Figure 2.1 c. The working electrode (WE) was always a circular gas diffusion electrode of a 0.8 cm^2 area that was held by a PTFE holder (see Figure 2.1 c) that was designed specifically for

that purpose. Oxygen gas was fed to the back of the GDE at a flow rate of 200 cm^3/min. The counter electrode was a platinum mesh and the reference electrode was a saturated calomel electrode (SCE) or a Hg/Hg_2SO_4 depending on the electrolyte medium. The cell was connected to an EG&G potentiostat/galvanostat model 263A controlled by a PC running "Electrochemistry Power suite" software by Princeton Research. A standard volume of 200 ml air-equilibrated electrolyte solution was used at variable temperatures depending on the experiment. Steady state experiments were also performed for all the gas diffusion electrodes (GDEs) using the older HiTek potentiostat type DT2101 equipment where a constant potential was applied and the respective current values where manually recorded.

2.12. Preliminary battery experiments

Preliminary battery experiments were carried out using a model battery (see Figure 2.6) where the interelectrode gap was 2 mm and the electrolyte volume was 3 ml. As anode, a disc of an AlMgSnGa alloy was employed and an air cathode from Table 2.5 was used. The surface areas of both electrodes were the same since both electrodes were circular and had a radius of 1 cm (so an area of 3.14 cm^2). Finally it has to be mentioned that during all battery and the gas diffusion electrodes experiments, oxygen was fed at the back of the electrode at a flow rate of 200 cm^3/min. The Scanning Electron Microscopy (SEM) equipment JSM-5910 from JEOL was used to obtain images of two of the air cathodes used for the battery discharge experiments.

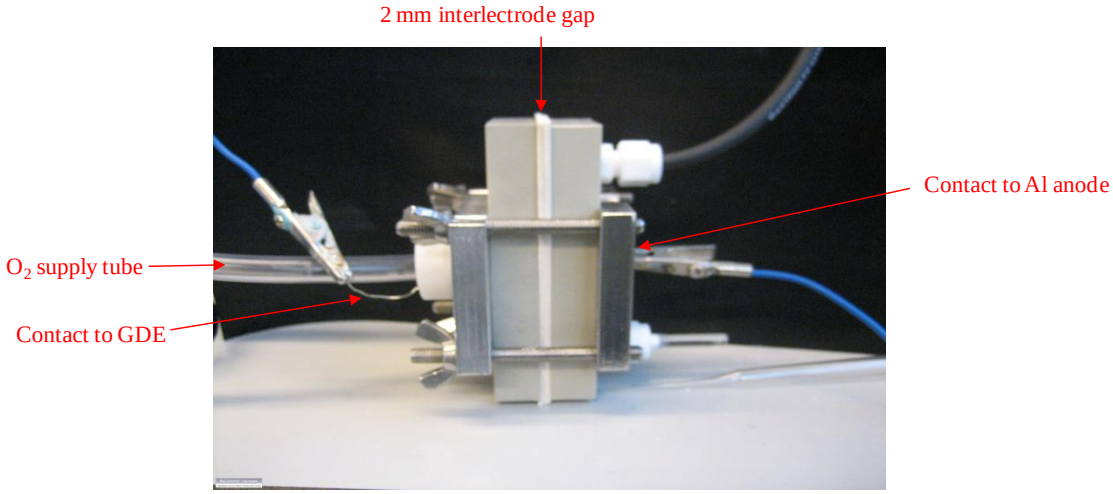

Figure 2.6: *Model Al-air battery*

2.13. Visual and microscopic observation experiments

2.13.1. Electrode preparation

A schematic illustration of the electrode making process is shown in Figure 2.7. A 15 cm length of coaxial cable was cut and the ends stripped to reveal shielding and core. The shielding was twisted into a wire at both ends and trimmed at one end. The core was stripped and twisted in a similar manner at both ends.

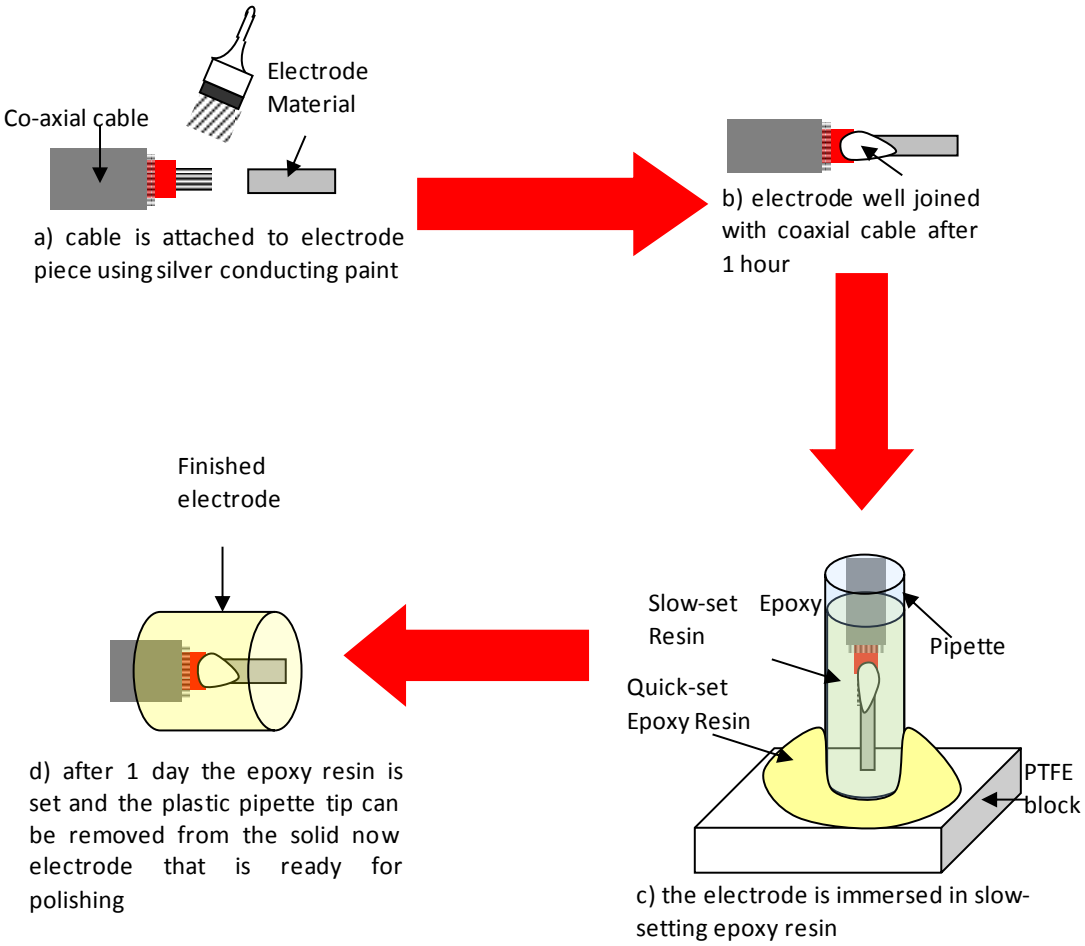

Figure 2.7: *Schematic of preparation procedure of the aluminium electrodes used for the camera experiments.*

A piece of electrode material (3 cm strip of an AlMgSnGa alloy) was attached to the core wire, at the end where the shielding was trimmed, using silver conducting paint *(RS Components)* and allowed to dry. The electrode material-core wire connection was coated with nail varnish and allowed to dry. The pointed end of a 5 cm^3 plastic pipette

was cut and discarded. The remainder of the pipette was cut in half and the bottom piece attached to a PTFE block using quick-setting epoxy resin *(RS Components)* and allowed to dry. The pipette half was ¾ filled with slow setting epoxy-resin *(Struers Epofix)*. The electrode end of the cable was immersed into the pipette. Care was taken to ensure the electrode material did not touch the sides of the pipette and to ensure the join between the material and the wire was also submerged.

The wire was held in place with respect to the pipette using blue-tac and the epoxy resin was left to set overnight. When set the plastic pipette part was cut and removed. The epoxy-resin set electrode was then ground and polished as mentioned earlier in Section 2.4.

2.13.2. Camera experiment and equipment

The experiments were carried out in a special electrochemical cell (see Figure 2.3) with an optical window to allow the camera to image the surface of interest of an (e.g. of an AlMgSnGa alloy) which was always the working electrode. The counter electrode was a Pt mesh placed in the same solution and the reference electrode was a laboratory fabricated saturated calomel electrode. The tip of the reference electrode was placed as close as possible to the surface of the working electrode. The experiments were controlled with an EG & G model 273 Potentiostat and data were analysed using Power Suite software. Open circuit potentials were measured with a Fluke 83 Multimeter. Experiments used 250 cm^3 of air-equilibrated, aqueous 2 M NaCl at room temperature (293 ± 2 K).

A Photron APX-RS high speed camera fitted with a Navitar 12x lens with a x2 extension tube and x2 lens adaptor was employed to image the surface of the electrode at a variety of frame rates. The camera had solid state memory (6 Gb) which allows considerable time periods (e.g. 240 seconds at 50 frames per second and 768 x 672 pixels) to be acquired. The data was then transferred to a PC through a fire wire connection. These images were then processed/analysed to elucidate mechanisms

occurring on the electrode surface. Lighting of the sample was critical and a 150 W cold light source proved adequate (SCHOTT – KL 1500).

Setting up the camera and adjusting the lighting took several minutes (up to 30 minutes). During this time the Al alloy surfaces were in contact with the NaCl electrolyte and corrosion inevitably commenced. Hence, experiments were limited to alloy surfaces that already had a history.

CHAPTER 3 Preliminary Experiments

3.1. Introduction

The overall objective of the project was to design a high power Al-air battery that could be stored before use. This would require:

a) an aluminium material that:

- was stable to corrosion on open circuit
- dissolved anodically at a high rate at a potential that would lead to a voltage of ~ 1.5 V for an Al-air battery i.e. a potential in the range - 1.5 to - 2.0 V *vs* SCE.

b) a medium where:

- Al (III) is highly soluble or
- the Al (III) precipitate does not interfere with further dissolution.

In this chapter, a number of Al materials and aqueous media were examined to see whether they could meet these challenges.

3.2. Pure Al in various electrolytes

3.2.1. Corrosion on open circuit

Several candidate electrolyte solutions (see Table 3.1) were used to test the stability to corrosion of pure Al on open circuit. NaCl and NaOH solutions were used because they are common electrolytes used for Al-air battery systems. In addition the use of NaOH seemed interesting since the Al (III) product of aluminium oxidation is known to have a higher solubility compared to other media.[99]

Furthermore, 2 M NaCl + 0.1 M HCl was used since the acid addition would help to keep any Al (III) product in solution and could be superior than a saline electrolyte for the operation of the air cathode (this electrolyte is much more conductive) as will be discussed later in this thesis. Moreover, due to suggestions in the literature that the Al dissolution is catalysed by Sn (II) in solution, in chloride media, three electrolytes of 2 M NaCl + 0.1 M HCl with three different concentrations of $SnCl_2$ were used, the acid

being used to prevent hydrolysis of the Sn (II).[100] Other acidic electrolytes including 3M H_2SO_4 and 3M H_2SO_4 + 40 mM HCl were also studied because of the high solubility of the Al (III) salts formed. Furthermore, experiments with malonate were carried out to see whether a complexing agent for Al (III) would shift the open circuit potential to more negative values and also whether it would increase the solubility of Al (III) in the neutral chloride media.

Table 3.1. *Summary of observations from experiments with pure Al in different electrolytes.*

Electrolyte	H_2 on open circuit potential	Open circuit potential *vs* SCE / V
2 M NaCl	none	- 0.79
2 M NaCl + 0.1 M HCl	none	- 0.79
2 M NaCl + 0.1 M HCl +10 mM $SnCl_2$	obvious	- 0.78
2 M NaCl + 0.1 M HCl +20 mM $SnCl_2$	obvious	- 0.79
2 M NaCl + 0.1 M HCl +100 mM $SnCl_2$	obvious	- 0.8
3M H_2SO_4	none	- 0.73
3 M H_2SO_4 + 40 mM HCl	none	- 0.65
1 M sodium malonate + 2 M NaCl	obvious	- 0.76
2 M NaOH	vigorous	- 2.05

So for the corrosion tests, a wire of pure Al (99.999%) was dipped into each electrolyte solution along with a SCE. The open circuit potential was measured and the Al sample was monitored for 5 minutes for signs of corrosion i.e. H_2 evolution and/or formation of

aluminium oxide/hydroxide. The experiment was carried out with the nine solutions listed in Table 3.1.

In 2 M NaCl there was no evidence of corrosion on open circuit but the open circuit potential of pure Al was always insufficiently negative (~ - 0.80 V *vs* SCE). In contrast, in 2 M NaOH, the open circuit potential was significantly more negative (- 2.05 V *vs* SCE). However, the H_2 evolution from the corrosion of Al was instantaneous and very rapid. Such an electrolyte could be an interesting candidate for use in an Al-air battery provided the electrolyte was only to be added to the battery immediately prior to use and not stored in it. The acidification of 2 M NaCl with 0.1 M HCl did not affect the corrosion potential or increase the corrosion rate on a short timescale; no improvement compared to NaCl was observed. For the experiments where $SnCl_2$ was added in acidic NaCl the observations on open circuit were (a) rapid hydrogen evolution for all three solutions and (b) tin dendrites formed rapidly onto the Al surface for the media with 20 and 100 mM of $SnCl_2$ added. In Figure 3.1 a) a photograph and b) the EDX analysis of such a dendrite are shown.

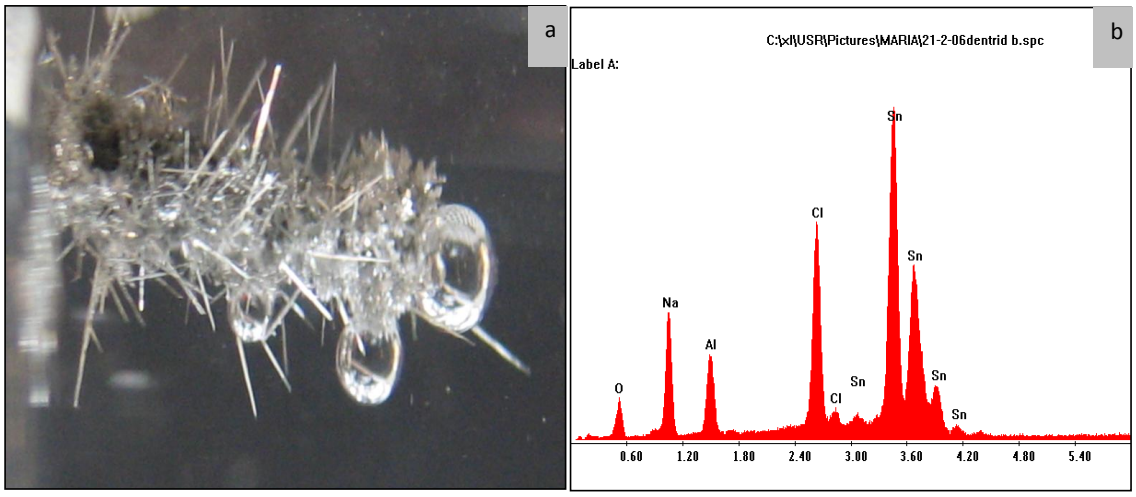

Figure 3.1: ***(a)*** *Photograph and* ***(b)*** *EDX analysis of Al-Sn dentrite.*

The formation of such massive dendrites indicates that in these solutions the rate of reaction (R.9) is high as reported by Holzer et al., (1993).[101]

$$2Al + 3Sn^{2+} \rightarrow 2Al(III) \quad + 3Sn \qquad \text{(R.9)}$$

In all the experiments where the acidic electrolytes, 3M H_2SO_4 and 3 M H_2SO_4 with 40 mM HCl, were used, no corrosion was observed on open circuit. The open circuit potential was, however, even more positive than that in the 2 M NaCl, which makes these electrolytes inappropriate for use in an Al-air battery. Finally the addition of malonate to NaCl led to corrosion and hydrogen evolution on open circuit without significantly improving other characteristics.

3.2.2. Electrochemistry of pure Al

Voltammograms for pure Al were run in 2 M NaCl scanning from the open circuit potential (- 0.8 V *vs* SCE) to more positive values. It can be seen from the voltammogram in Figure 3.2 that Al is only dissolving at potentials well positive to its open circuit potential. A current of ~ 100 mA cm^{-2} occurred only at ~ - 200 mV, a very high overpotential and a value which would lead to a very low battery voltage for an Al-air battery.

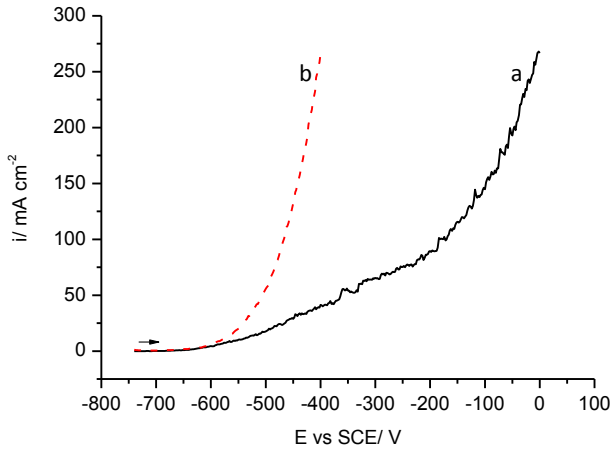

Figure 3.2: *Voltammetry of pure Aluminium in 2 M NaCl a) before and b) after a 50 mA cm^{-2} current was applied for 600 seconds.*

It will be shown later in this thesis that with some Al materials, passing an anodic current density of 50 mA cm^{-2} for 600 seconds led to an Al surface where rapid dissolution at low overpotential was possible i.e. 'activation' had occurred. Hence, such

an anodic current was applied to pure Al before a voltammogram was run. The resulting voltammogram is shown in Figure 3.2 b. The Al oxidation here occurs in slightly more negative potentials but still well positive to the open circuit potential. These results show only a small and hence not significant activation of pure aluminium in the 2 M NaCl electrolyte since there is not a noteworthy decrease of overpotential in pure aluminium oxidation after applying a current in 2 M NaCl.

In Figure 3.3 the voltammetry of pure Al is shown for 2 M NaOH (see Figure 3.3 a) and 2 M NaCl (see Figure 3.3 b) scanning from the OCP (- 2.0 V in NaOH and - 0.8 V in NaCl) value towards positive direction, after a 50 mA cm^{-2} current density was applied.

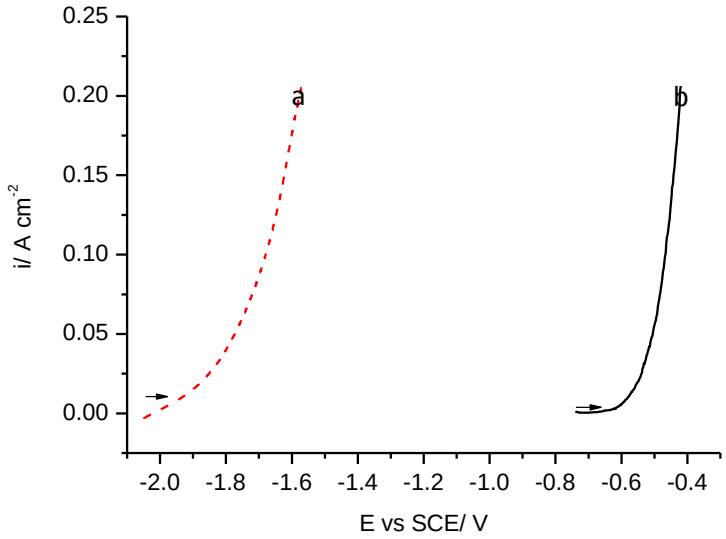

Figure 3.3: *Voltammetry of pure Aluminium in a) NaOH and b) NaCl after a 50 mA cm^{-2} current was applied in both media for 600 seconds.*

The anodic dissolution of pure Al in NaOH occurs in a much more negative potential range compared to NaCl. An important feature to notice from the voltammetric curves in Figure 3.3 is that, for example, the current density of 50 mA cm^{-2} occurs at about - 1.8 V in 2 M NaOH and at - 0.5 V *vs* SCE in 2 M NaCl. So the difference in voltage for the same current density values between the two electrolytes is really significant, more than 1 V. The behaviour of pure Al in 2 M NaOH is promising i.e. the pure Al is

dissolving at a higher rate in the alkaline solution. From these results it is concluded that 2 M NaOH is the electrolyte that has the best electrochemistry for an Al-air battery but corrosion is a problem. Certainly the battery could not be stored containing the 2 M NaOH electrolyte and the electrolyte would have to be added immediately prior to battery applications.

It should be noted that in all voltammograms, the current density continued to increase to more than 1 A cm^{-2} at high overpotential but the voltammograms were then certainly distorted by IR drop and for this reason data above 200 mA cm^{-2} are not reported here.

3.3. Comparison of Al and Al alloys in several electrolytes

A set of corrosion tests at open circuit potential (as in 3.2.1) and electrochemistry experiments (as in 3.2.2) were carried out for some other commercial Al alloys in 2 M NaCl, 2 M NaCl + 0.1 M HCl and 2 M NaCl + 0.1 M HCl + 10 mM $SnCl_2$. The materials that were used along with their composition and characteristics at open circuit potential are given in the Table 3.2. It is obvious from the results in Table 3.2 that for all the Al materials the open circuit potentials were very similar in all three media. The open circuit potentials for most of the alloys are close to that of pure Al in all solutions. The exceptions were AB50V and the SAFT alloy that gave OCP of - 1.5 V and - 1.0 V *vs* SCE respectively. However, the rate of corrosion at open circuit (as seen by H_2 evolution) differs between the three media. There is no H_2 evolution visible by eye at open circuit potentials in the 2 M NaCl solution, there is some at 2 M NaCl + 0.1 M HCl solution and significantly more at the 2M NaCl + 0.1 M HCl + 10 mM $SnCl_2$ for most of the Al materials. By adding only 10 mM $SnCl_2$ in the acidified NaCl solution, dendrite formation was avoided (in contrast with higher concentration of the salt as it was shown for pure Al in Section 3.2.1). Since H_2 evolution was clearly increased by Sn^{2+} in solution, it appears that Sn is deposited on the Al but too slowly to give dendrites. However, the addition of the Sn salt did not have any positive effect and such a medium is inappropriate for an electrolyte solution.

Table 3.2. *Aluminium materials that were used along with their characteristics on open circuit potential.*

Media		2 M NaCl		2M NaCl + 0.1 M HCl		2M NaCl + 0.1 M HCl + 10 mM $SnCl_2$	
Aluminium type	**Composition**	**H_2 evolution at OCP**	**Open Circuit Potential *vs* SCE/ V**	**H_2 evolution at OCP**	**Open Circuit Potential *vs* SCE/ V**	**H_2 evolution at OCP**	**Open Circuit Potential *vs* SCE / V**
Pure Al	Al 99.9%	none	- 0.79	none	- 0.79	obvious	- 0.78
AB50V	Al 98.30%, Mg 0.39, Sn 0.10%, Ga 0.05%	none	- 1.51	obvious	- 1.50	vigorous	- 1.48
SAFT anode	Al 97.9%, Zn 0.11%, Ga 0.10%, Fe 0.09%, Si 0.08%	none	- 1.05	obvious	- 1.10	obvious	- 1.065
Chandlery anode	Al 94.47%, Zn 5.25%, Ga 0.02%	none	- 0.85	obvious	- 0.9	obvious	- 0.85
3% Mg	Al 97%, Mg 3%	none	- 0.82	none	- 0.9	obvious	- 0.82
5% Mg	Al 95%, Mg 5%	none	- 0.89	none	- 0.82	fast	- 0.80

With the materials in Table 3.2 where fast H_2 evolution occurred, alumina product tend to be formed and the Al would lose its reflective surface and would adopt a more grey tinge.

The electrochemistry experiments were carried out by recording voltammograms for a series of aluminium materials (shown in Table 3.2) in the three electrolytes that were used for the corrosion tests mentioned above, by scanning from their open circuit potentials to more positive values. None of these materials showed oxidation close to - 1.50 V *vs* SCE.

With AB50V alloy, an experiment was carried out where an anodic current of 50 mA cm^{-2} was passed and then voltammograms were recorded. Figure 3.4 shows voltammograms (a) before and (b) after the anodic current (activation) was applied. It is obvious that curve (b) occurs at about ~ 200 mV more negative than the voltammogram (a), was recorded before applying the anodic current. Curve (b) occurs at a potential close to - 1.5 V *vs* SCE which is the open circuit potential for AB50V alloy. The behaviour of the alloy in 2 M NaCl is promising since, after the activation, the same current density occurs at a more negative potential, i.e. the Al alloy is dissolving at a higher rate. This shift in potential is considerable. This experiment was repeated for the other materials listed in Table 3.2. for all three media. The sponsors favored a battery with a NaCl electrolyte and since it gave promising results, this is the medium emphasized throughout this thesis. The voltammograms that were recorded in 2 M NaCl for each of the materials after a 50 mA cm^{-2} anodic current density was applied are shown in Figure 3.5. The curve for pure Al is also shown for comparison. Only AB50V showed any shift in potential after activation The next best alloy is the SAFT anode, however, its dissolution occurs well positive to AB50V and it is more prone to corrosion. According to literature the presence of Fe and Si is known to accelerate corrosion. As it has been stated by de Souza and Vielstich, (2003), impurities such as iron and copper can distinctly affect the electrochemistry of the anode and Si and Fe are bad for corrosion and should be avoided as materials for battery anodes.[38, 78]

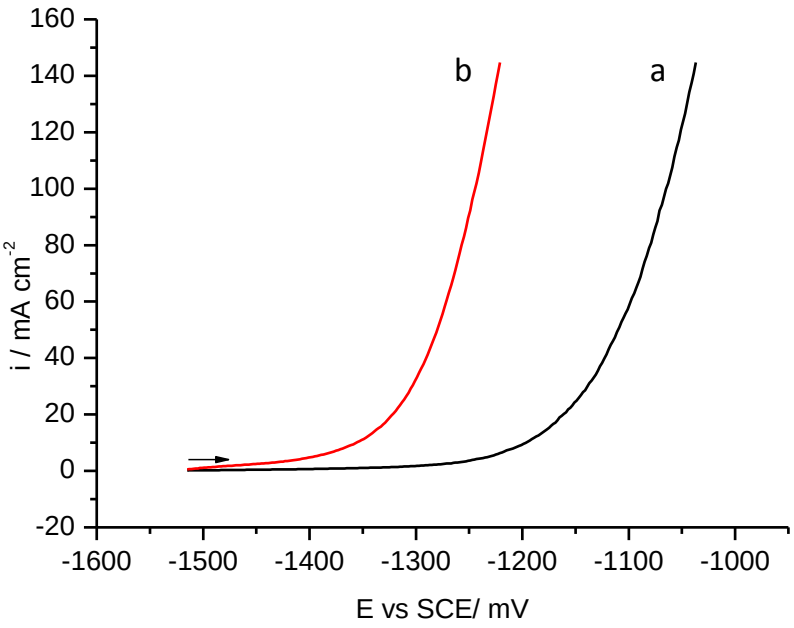

Figure 3.4: *Voltammograms of AB50V alloy in 2 M NaCl a) before and b) after an anodic current of 50 mA cm^{-2} was passed for 600 seconds.*

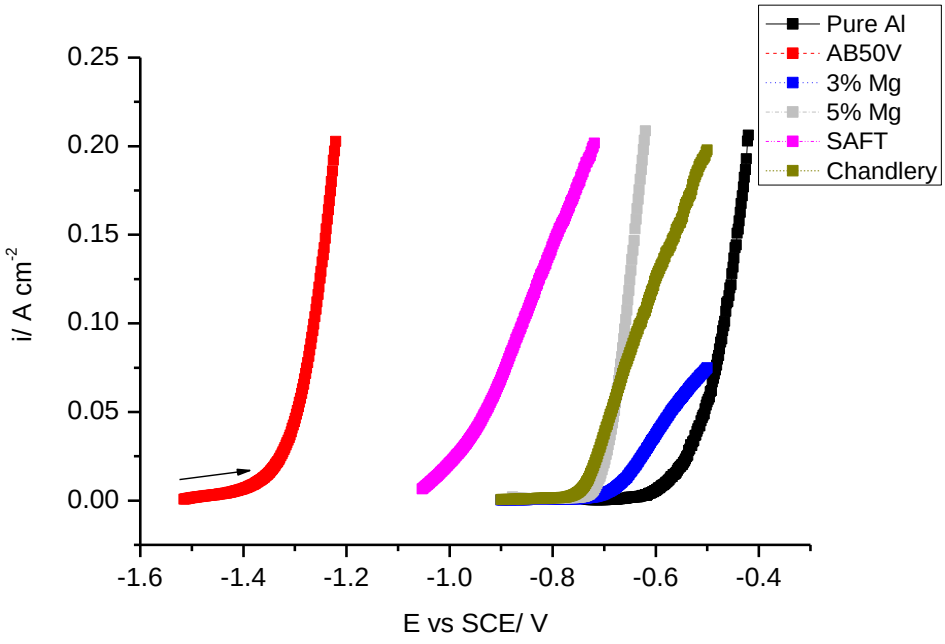

Figure 3.5: *Linear sweep voltammetry scans from open circuit potential to more positive values of some Al alloys after a 50 mA cm^{-2} constant anodic current density was applied for 600 seconds in an aerated 2 M NaCl solution, using a scan rate of 20 mV/sec.*

The rest of the alloys dissolved at more positive potentials, very close to that of pure Al, results that establish that they are inappropriate to use with a 2 M NaCl electrolyte for a battery system. Nevertheless AB50V gave an open circuit potential around -1.5 V and dissolved at 50 mA cm^{-2} close to -1.3 V *vs* SCE after activation. These results in addition to the lack of open circuit corrosion in 2 M NaCl establish AB50V as the preferable alloy for further examination. The reason for the good open circuit potential corrosion and electrochemistry characteristics of the AB50V alloy will be examined and discussed later in this thesis.

3.4. Conclusions

It is clear that the alloy AB50V had very superior characteristics for the anode in an Al-air battery in brine media. This is perhaps not surprising since it was the alloy developed by Alcan for this application.[14] The extent of its superiority is, however, interesting. In contrast to the literature[102] however, the addition of Sn^{2+} to the electrolyte appeared to lead to disastrous results; the reason for the differences is not clear. More detailed conclusions are:

- These results show only a small and hence not significant activation of pure aluminium in the 2 M NaCl electrolyte since there is not a noteworthy decrease of overpotential in pure aluminium oxidation after applying a current in 2 M NaCl.

- In 2 M NaCl there was no evidence of corrosion on open circuit but the open circuit potential of pure Al was always insufficiently negative (~ - 0.80 V *vs* SCE). In contrast, in 2 M NaOH, the open circuit potential was significantly more negative (- 2.05 V *vs* SCE). However, since the H_2 evolution from the corrosion of Al was instantaneous and very rapid such electrolyte would be inappropriate for an aluminium air battery unless it was stored dry.

- The addition in 2 M NaCl of solutions like HCl, H_2SO_4 and $SnCl_2$ and sodium malonate did not have any benefit in terms of dissolution potential of pure Al or open circuit corrosion stability.

- In NaCl media only some aluminium materials have appropriate properties for application in Al-air batteries with the AlMgSnGa alloy, AB50V, being the best investigated.

- Overall no advantages to acidifying the brine or adding complexing agent have been identified.

CHAPTER 4 Study of Al alloys dissolution and the influence of minor elements

From the preliminary experiments, AB50V was confirmed as an alloy with the properties that make it a candidate for the anode in an Al-air battery with a brine electrolyte. For this reason corrosion tests and anodic dissolution experiments were carried out with this alloy in several other electrolyte solutions to examine the possibility for an even better performance in a medium other than NaCl. The main part of this chapter, however, will concern the investigation of the reasons for the low open circuit potential corrosion and good electrochemical characteristics of the AB50V alloy in 2 M NaCl. The properties of alloys, with similar elemental compositions will be discussed.

4.1. Corrosion on open circuit

4.1.1. Short time corrosion of AB50V alloy

Several media (see Table 4.1) were used to test the stability to corrosion of AB50V alloy at open circuit. These included the electrolytes that were used earlier for pure aluminium in Section 3.2.1, as well as some others. The corrosion tests were carried out in exactly the same way as with pure aluminium described in Section 3.2.1. Rapid corrosion was concluded from the formation of H_2 gas as observed by eye and/or a gelatinous white precipitate over a short period of 5 minutes.

In 2 M NaCl, corrosion at open circuit was negligible and the open circuit potential of AB50V alloy had the rather negative value of - 1.5 V *vs* SCE. In the 2 M NaCl + 0.1 M HCl and 2 M NaCl + 0.1 M HCl + 10 mM $SnCl_2$ electrolytes a similar open circuit potential value was obtained but more vigorous H_2 evolution on open circuit was also observed. With the higher pH solution, 2 M NaCl + 0.01 M HCl, the H_2 evolution rate seemed to decrease with the increase of pH value but it was still visible. There was not any significant change in the OCP. Tin dendrite formation was not observed on open circuit potential with the AB50V alloy in the media that contained 10 mM $SnCl_2$ but the high H_2 evolution rate

implies that Sn deposition was occurring. In 3M H_2SO_4 electrolyte, passivation of AB50V alloy occurred since its open circuit potential was well positive ~ - 0.35 V *vs* SCE. Due to suggestions in the literature that chloride ions in the electrolyte would induce shift of the potential to more negative values,[86, 103] HCl was added to the H_2SO_4. Indeed, the open circuit potential was more negative by 1 V *vs* SCE, however the addition of HCl increased significantly the corrosion on open circuit since rapid hydrogen evolution was observed. Also a more concentrated H_2SO_4 solution was tested (5 M), but it was inappropriate due to the rapid corrosion of AB50V and the positive open circuit potential. In the 1 M sodium malonate + 2 M NaCl solution the open circuit potential of AB50V was similar to the brine solution with additional corrosion on open circuit, showing that the addition of such a complexing agent does not have any positive effect for the alloy. In KOH electrolyte, AB50V alloy had the best open circuit potential value; however the open circuit corrosion rate was very high. Finally HNO_3 and lactic acid were tested. In both acids no corrosion on open circuit was observed, but the open circuit potential was too positive for an Al-air battery system.

Table 4.1. *Short time corrosion characteristics of AB50V alloy in different electrolytes.*

Electrolyte	Visible H_2 on open circuit potential	Open circuit potential *vs* SCE / V
2 M NaCl	none	- 1.51
2 M NaCl + 0.1 M HCl	vigorous	- 1.53
2 M NaCl + 0.01 M HCl	obvious	- 1.50
2 M NaCl +0.001 M HCl	tiny	- 1.51
2 M NaCl + 0.1 M HCl + 10mM $SnCl_2$	vigorous	- 1.48
3M H_2SO_4	none	- 0.35
3 M H_2SO_4 + 40 mM HCl	vigorous	- 1.32
1 M sodium malonate + 2 M NaCl	obvious	- 1.51
5 M KOH	vigorous	- 2.1
5M H_2SO_4	vigorous	- 0.93
3M HNO_3	none	- 0.67
1M Lactic Acid	none	- 1.30

From these corrosion tests, it was concluded that considering both the corrosion and the open circuit potential the most appropriate electrolyte for the AB50V alloy would be the 2 M NaCl solution. Hence, the rest of experimental results from electrochemical experiments will be in this electrolyte.

4.1.2. Long term corrosion tests of other alloys in NaCl

Several alloys with similar compositions to AB50V and with compositions selected to probe the role of each minor element were obtained. These alloys and pure Al were tested for longer time periods in 2 M NaCl. Table 4.2 reports the results for nine materials, along with their elemental compositions. The alloys AB50V, I0 and B0 had similar elemental compositions while B1-B4 were prepared in order to probe the influence of each alloying element.

For these corrosion tests, each of the Al materials (samples with a surface area ~ 0.2 cm^2) in Table 4.2 were placed in a closed phial containing 10 ml of 2 M NaCl at 293 K and then observed by eye until signs of corrosion appeared. The latter included the formation of small bubbles of hydrogen on the surface of the metal. This was followed by the observation of a gelatinous cloud of a white precipitate, alumina and/or aluminium hydroxide, on and around the surface of the alloy sample. The alloys surfaces were damaged and lost their shine with continuous corrosion, as were noted by visual observations and verified by scanning electron microscopy, (SEM). The pure Al and the alloys AlMg3 and AlMg5, (containing additions of Mg to pure Al), when immersed in NaCl had a stable open circuit potential of - 0.8 V. Moreover, these alloys could stay in the electrolyte for weeks showing indefinite resistance to open circuit corrosion (by eye) and retaining their shiny surfaces.

The alloys B1 (containing Sn but not Ga) and B3 (containing Ga but not Sn) had an open circuit potential of - 0.8V in 2 M NaCl and corrosion started after 1 day. The behaviour of the two alloys, however, differed in the period needed to establish a stable open circuit potential.

Table 4.2. *Compositions of alloys investigated together with open circuit potentials and observations of corrosion by eye in 2 M NaCl at 293 K.*

Alloy	Wt% Mg	Wt% Sn	Wt% Ga	Open Circuit Potential / V *vs* SCE	Observations
99.999% Al	-	-	-	- 0.80	No evidence of corrosion over weeks.
AlMg3	3	-	-	- 0.82	No evidence of corrosion over weeks.
AlMg5	5	-	-	- 0.89	No evidence of corrosion over weeks.
B0	0.5	0.1	0.05	- 1.53	Corrosion evident after ~ 1 hour.
B1	0.4	0.1	-	- 0.85	Corrosion evident after ~ 1 day.
B2	0.4	0.4	0.03	- 1.51	Corrosion evident after ~ 1 hour.
B3	0.4	-	0.03	- 0.80	Corrosion evident after ~ 1 day.
B4	-	0.1	0.03	- 1.50	Corrosion evident after ~ 1 hour.
AB50V	0.6	0.1	0.05	- 1.53	No evidence of corrosion over weeks.
I0	0.4	0.07	0.05	- 1.53	Corrosion evident after~ 1 hour

More specifically, the alloy B1 initially had an open circuit potential of - 1.3 V which drifted to - 0.85 after the period of one hour. In contrast B3 alloy had a stable open circuit potential at - 0.8 V from the first seconds of immersion in NaCl. The rest of the alloys, containing both Sn and Ga had an open circuit potential ~ - 1.5 V *vs* SCE, including B4 that did not include Mg.

These observations suggest that the presence of tin in the alloy is critical to the initiation of the corrosion mechanism whereas Ga may be important to the prevention of passivation when corrosion has started. In addition to the elemental composition of the alloys, other factors like their sources seemed to play an important role in the stability to corrosion. For example, the alloys AB50V, B0 and I0, had almost identical elemental composition but they had different corrosion characteristics on open circuit.

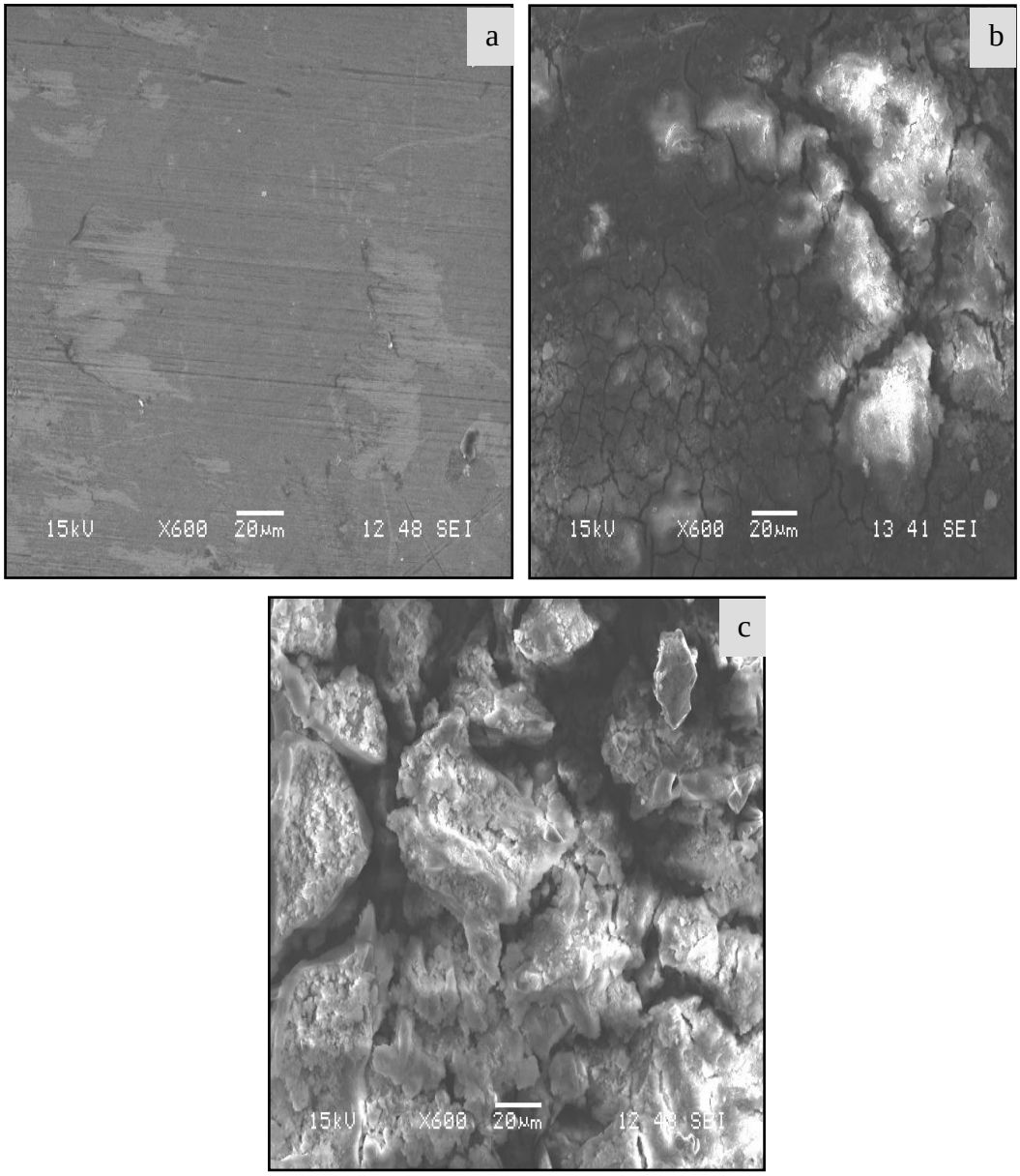

Figure 4.1: *a) AB50V, b) B0, c) I0 under secondary electron detector at the SEM after 24 hours in 2 M NaCl.*

This could be attributed to the fact that these alloys come from different sources and may have been subjected to different cooling regimes, heat treatments and mechanical working. To confirm the results from the qualitative experiments, these three materials were immersed in 2 M NaCl for 24 hours at 293 K and then examined by SEM. In Figure 4.1 a, the presence of a very thin oxide film on the surface of AB50V alloy can be observed. In contrast in Figure 4.1 c a thick and porous film of alumina is shown on the surface of I0 alloy. In Figure 4.1 b, the surface of B0 alloy with an intermediate appearance is shown.

The different properties of the series of alloys containing both Sn and Ga and having very similar elemental compositions imply that stability to corrosion may depends on the history of the alloys including heat treatments and mechanical working. Hence, the alloys AB50V, B0 and I0 were heated at 873 K for 2 hours and then quenched in distilled water. No variations of open circuit potential values were observed but significant changes of stability on open circuit occurred. By significant changes, it is meant that all the alloys exhibited signs of corrosion by eye after ~ 1 day, a substantial increase in corrosion resistance for B0 and I0 but a decrease for AB50V. This may implies that AB50V had already been heat treated at a lower temperature and 873 K is above that optimum temperature. Definitely, the distribution of minor alloying elements and their structure seems to be critical in determining their properties on open circuit, which are very important in terms of corrosion in a battery that would be stored with electrolyte before use.

In order to further investigate the effect of heat treatment on the corrosion stability of AlMgSnGa alloys, samples of I0 alloy were heat treated at 373 K, 473 K, 573 K, 673 K, 773 K and 873 K for 2 hours and quenched in water before being immersed in 2 M NaCl to test their corrosion resistance on open circuit. The samples heated at 373 – 673 K all formed a fine alumina deposit within 1 hour of placing them in 2 M NaCl at room temperature and the film continued to form with time, (see Table 4.3). In contrast, the samples heated at higher temperature showed little sign of corrosion after 1 day and the most stable appeared to be the sample heated at 773 K which showed no change in visual appearance even after several days.

Table 4.3. *Corrosion characteristics of I0 alloys in 2 M NaCl heat treated at different temperatures for 2 hours.*

	After 1 hour		After 24 hours	
Heat treatment temperature/ K	**Visible H_2 evolution**	**Al (III) deposit on I0**	**Visible H_2 evolution**	**Al (III) deposit on I0**
373	Vigorous	Yes	Vigorous	Yes
473	Vigorous	Yes	Vigorous	Yes
573	Vigorous	Yes	Vigorous	Yes
673	Obvious	Yes	Vigorous	Yes
773	Tiny	No	tiny	No
873	tiny	No	tiny	Yes

4.1.3. Corrosion tests of I0 in several electrolytes

The corrosion stability of I0 alloy was tested by eye in several solutions, shown in Table 4.4. with short term and long term corrosion tests as in Sections 4.1.1. and 4.1.2.

In alkaline solutions, H_2 evolution increased with increasing molarity of NaOH although the time passed before solid Al (III) was observed was the same for all concentrations of NaOH added.

As the rate of H_2 evolution increases, the rate of formation of Al (III) must follow but Al (III) is more soluble in the more concentrated NaOH. In acidic solutions the visible H_2 evolution rate increased with increasing concentration of HCl but Al (III) solid was formed more rapidly in more concentrated acid.

From these corrosion tests, it was concluded that considering both the corrosion and the open circuit potential the most appropriate electrolytes for the I0 alloy would be the alkaline solution 2 M NaCl + 0.01 M NaOH and the acidic 2 M NaCl + 0.0001 M HCl (at pH 4). Neither medium, however, had an obvious advantage over the neutral 2 M NaCl.

Table 4.4. *Results from corrosion tests of I0 alloy in various solutions*

Solution	pH	Open circuit potential *vs* SCE/ V	H_2 evolution visible after immersion in solution	Time passed before Al (III) formed
2 M NaCl + 0.01 M NaOH	11.97	- 1.67	tiny	2 hours
2 M NaCl + 0.1 M NaOH	12.80	- 1.80	obvious	2 hours
2 M NaCl + 1 M NaOH	13.56	- 1.86	vigorous	2 hours
2 M NaCl + 0.1 M HCl	1	- 1.50	vigorous	40 minutes
2 M NaCl + 0.01 M HCl	2	- 1.50	obvious	40 minutes
2 M NaCl + 0.001M HCl	3	- 1.50	tiny	40 minutes
2 M NaCl + 0.0001 M HCl	4	- 1.52	tiny	2 hours

4.2. Electrochemistry

4.2.1.1. AB50V alloy in NaCl

Samples of AB50V alloy (area ~ 0.21 cm^2) were placed in a 3 electrode electrochemical cell with an SCE in aerated NaCl solution and voltammograms were run scanning from the open circuit potential (- 1.50 V *vs* SCE) to more positive values. It can be seen from Figure 4.2 that AB50V alloy is dissolving at potentials quite close to its open circuit potential. However, as it was mentioned earlier in this thesis, activation of the alloy is feasible by subjecting the material to a constant anodic current of 50 mA cm^{-2} for 600 seconds. So in Figure 4.2 b it can be seen that the AB50V dissolution occurs at even more negative values after this activation period. Replicate experiments before and after activation were reproducible to ± 5 mV. So, for example, before the activation a current

density of 50 mA cm^{-2} occurred at - 1.10 V *vs* SCE, (see Figure 4.2 a). After the activation the same current density occurred at - 1.30 V *vs* SCE, (see Figure 4.2 b). So a shift of 200 mV in voltammetry shows that by passing the anodic current density for 600 seconds somehow led to an Al surface where more rapid dissolution of AB50V at lower overpotential was possible. In Figure 4.3 the SEM images of the surface of AB50V alloy are shown (a) before and (b) after a 50 $mAcm^{-2}$ current was applied to the alloy.

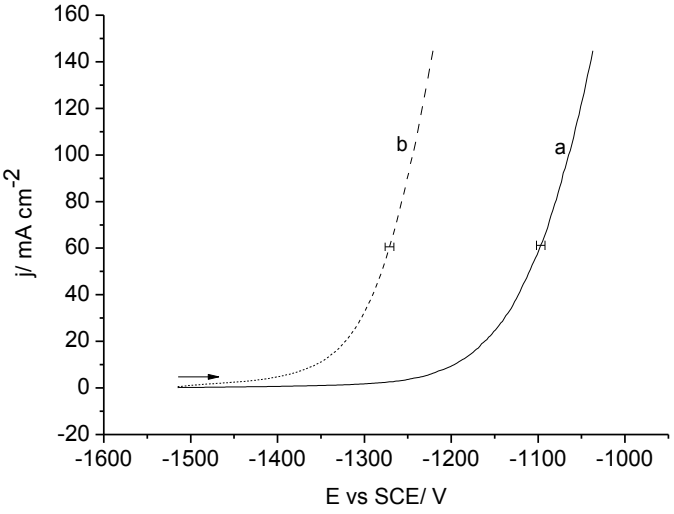

Figure 4.2: *Voltammograms for the alloy AB50V in 2 M NaCl (a) before and (b) after activation by the imposition of an anodic current density of 50 mA* cm^{-2} *for 600 seconds. Three replicate experiments showed reproducibility to ± 5 mV.*

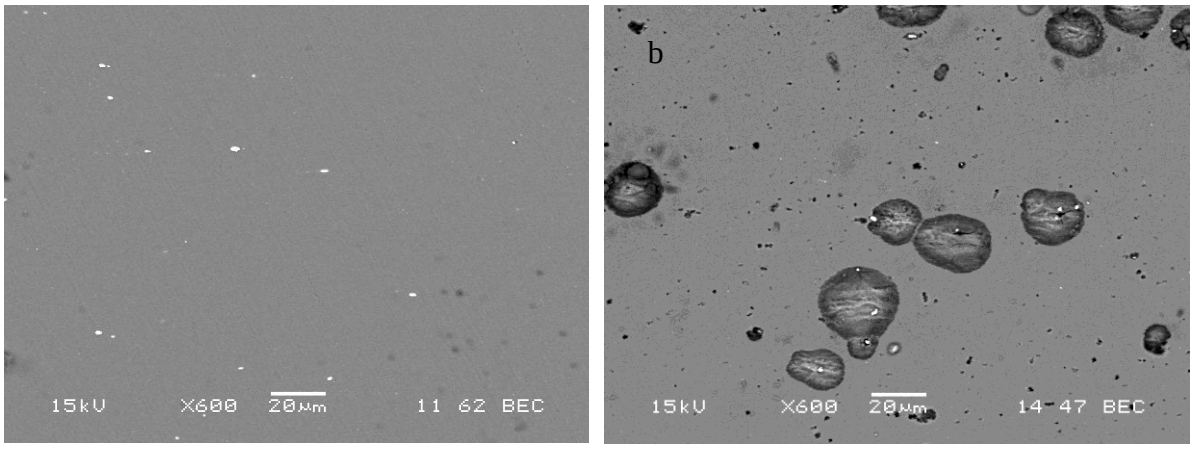

Figure 4.3: *The surface of samples of AB50V alloy under the backscatter detector of the SEM* ***a)*** *before and* ***b)*** *after 50 mA* cm^{-2} *were applied for 10 seconds at the alloy.*

It can be seen that pits of various sizes have been formed at the surface of the alloy even after the first 10 seconds of the current imposition. The pits were observed to be formed around the Sn or MgSn centers (white particles in the images of the backscatter electron detector).

Since the NaCl was the preferred electrolyte, the influence of its concentration on the activation was examined. Three different concentrations of NaCl were used; 0.2 M, 2 M and saturated (~ 6 M) solutions and a 50 mA cm^{-2} constant anodic current was applied to AB50V for 600 seconds in the three solutions. The chronopotentiograms are shown in Figure 4.4 a, b and c and the key observations summarized in Table 4.5.

Table 4.5. *Key observations with AB50V alloy on chronopotentiograms of Figure 4.4.*

NaCl Concentration/ M	Time to steady state potential/ s	Steady state potential/ V *vs* SCE
0.2	100	- 1.45
2	150	- 1.50
saturated	Almost instantaneous	- 1.50

It can be seen from these chronopotentiometric responses that for the electrolytes of 0.2 and 2 M NaCl, initially the potential goes to very positive values and then recovers to a steady state close to - 1.50 V *vs* SCE after 100 and 150 seconds respectively. The activation time for the saturated solution was much less, < 25 seconds, and the steady state potential - 1.51 V *vs* SCE. Furthermore it can be observed that the steady state voltage of the 0.2 M is more positive (- 1.44 V *vs* SCE) than the other two solutions. Overall it can be noted at that point that the alloy can dissolve at a high rate close to the open circuit potential in all three electrolytes. For most of the following experiments 2 M NaCl was used.

Throughout the program, the activation of AB50V in this way was carried out more than 20 times. The "steady state" potential at – 50 mA cm^{-2} was reproducible to ± 5 mV.

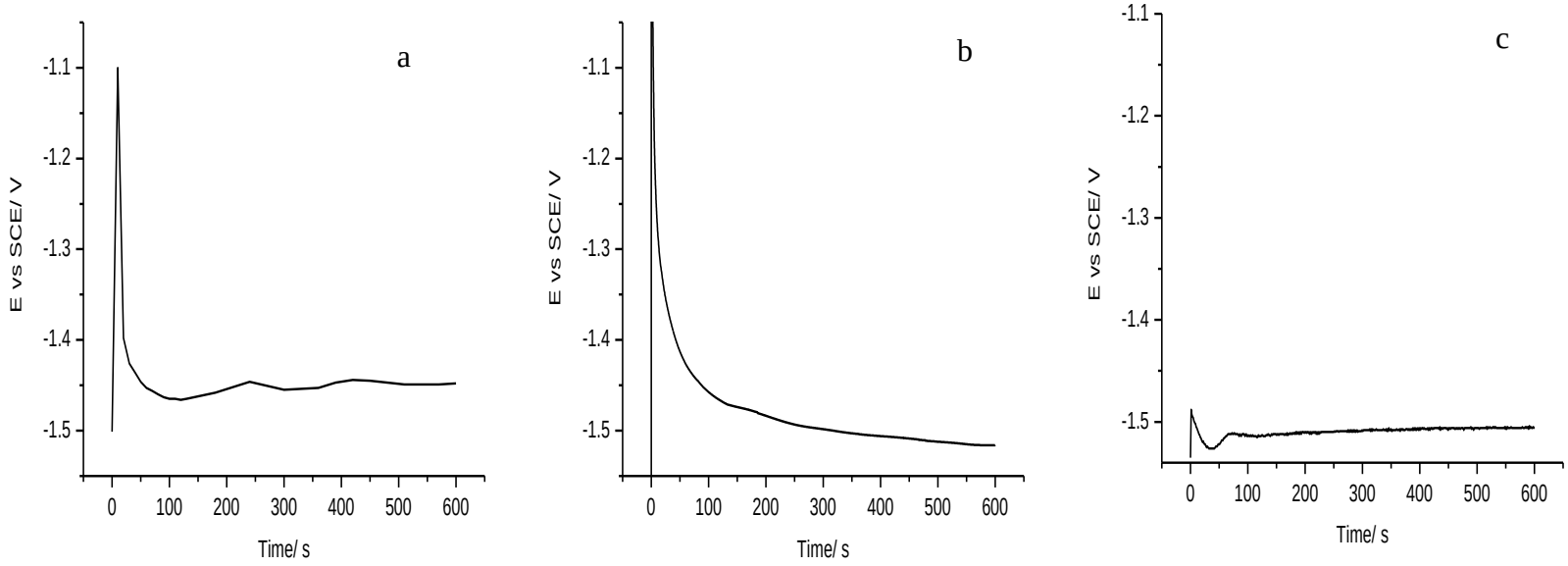

Figure 4.4: *Applying a constant anodic current of 50 mA cm^{-2} at AB50V alloy for 10 minutes in a) 0.2 M NaCl, b) 2 M NaCl and c) saturated NaCl. The experiments were repeated more than twenty times and the "steady state" potential was reproducible to ± 5 mV.*

It should also be noted that the relationship between current density and potential seems to depend significantly on the exact experiment. For example, in Figure 4.4 b the steady state potential for 50 mA cm^{-2} is – 1.50 V *vs* SCE. In contrast, in the voltammogram of Figure 4.2 this current density was not reached until - 1.30 V. Such differences would suggest that the rate of dissolution depends critically on the precise state of the surface and this depends on the exact experimental procedure.

4.2.1.2. AB50V alloy in NaCl

The current/potential characteristics were determined for the rest of the alloys and AB50V in a different way. A current density of 50 mA cm^{-2} was applied for 600 seconds to activate the alloy and then the alloy was subjected to current densities of 1, 2, 10, 50, 100, 200 and 500 mA cm^{-2} at 600 seconds intervals. At each current density the potential was monitored. Figure 4.5 shows a typical example of the results for AB50V. The inset shows the relevant current density *vs* potential characteristics. It can be seen that a current density of 100 mA cm^{-2} can be achieved at a potential (~ - 1.49 V) slightly positive to the open circuit potential of the alloy. It was also found that the open circuit potential after activation had shifted negative to ~ -1.55 V *vs* SCE. Also, it can be seen that the potential changes little over the 600 s where each current density is applied. Even higher current densities than 0.2 A cm^{-2} could be passed, however the potentials measured are not presented here since, due to uncorrected IR drop and dramatic changes to the alloy surface, due to the considerable loss of Al, they become significantly unreliable. At all current densities below 100 mA cm^{-2} the potentials are reproducible to ± 10 mV.

According to Faraday's law calculations and visual observations during the experiments a substantial part of the alloy was dissolved during the imposition of the different current densities, especially above 50 mA cm^{-2}. In addition a significant amount of alumina was formed for 50 mA cm^{-2} or higher current densities on the surface of the alloy and subsequently in the electrolyte solution around it. As a result the surface of the alloy will have dramatically changed towards the higher current densities near the end of the experiment. Hence, fresh samples of alloy were used for each of the higher current densities for some of the results that will follow. Overall it was shown that AB50V alloy could be

successfully dissolved at very high rates such as 200 mA cm^{-2} at about - 1.46 V which is very close to its open circuit potential.

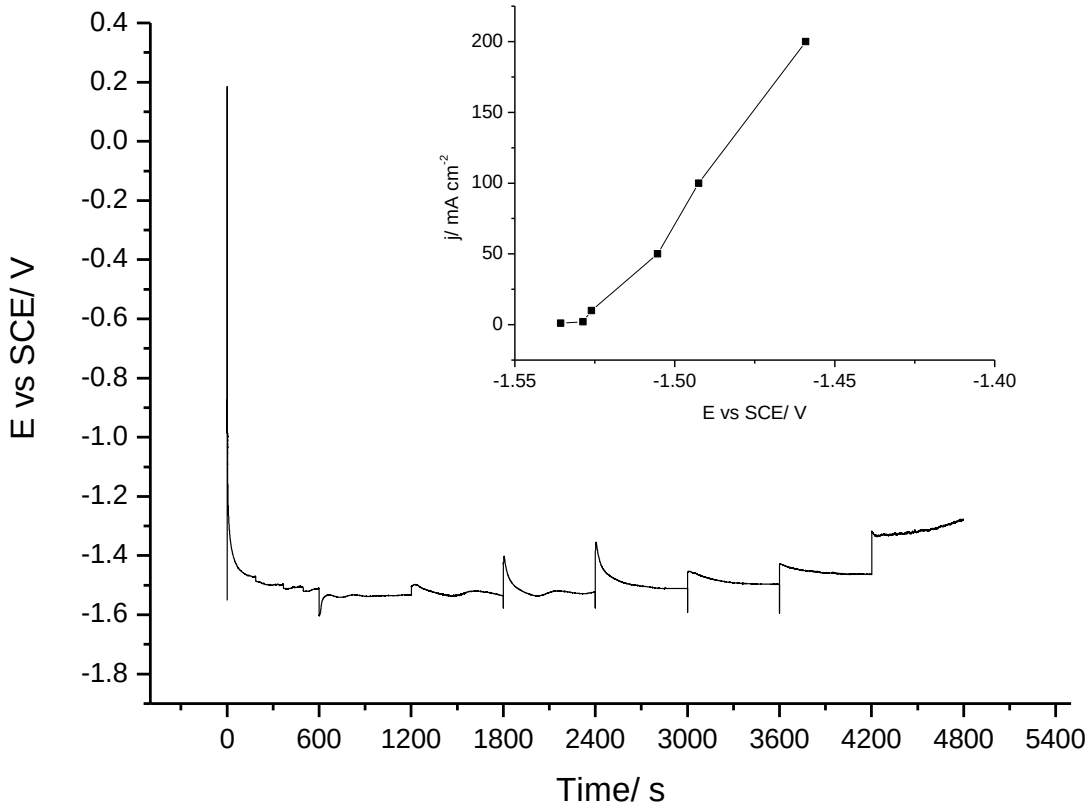

Figure 4.5: *Potential vs time response for the alloy AB50V in 2 M NaCl in an experiment where the alloy surface was initially activated by passing a current density of 50 mA cm^{-2} for 600 seconds and then current densities of 1, 2, 10, 50, 100, 200 and 500 mA cm^{-2} at 600 seconds intervals were imposed. The inset shows the steady state current density potential relationship. At all current densities below 100 mA cm^{-2} the potentials are reproducible to ± 10 mV. At higher current densities, IR drop, hydrogen evolution and loss of material led to poorer reproducibility and current oscillation*.

4.2.1.3. The influence of activation current density on the voltammetry of AB50V

The influence of activation current on voltammetry was examined for the AB50V alloy in 2 M NaCl.

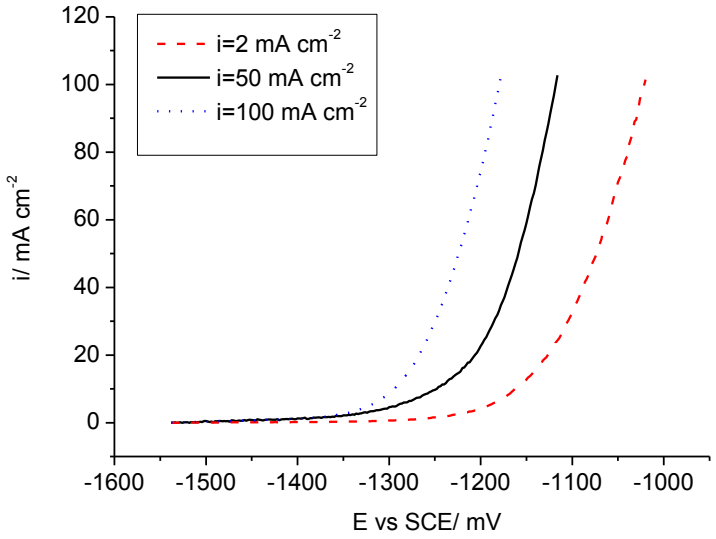

Figure 4.6: *The influence of the current density during the activation period (600 seconds) on the voltammetry for the anodic dissolution of Al.*

The AB50V alloy was subjected to current densities of 2, 50 and 100 mA cm^{-2} for 600 s and then voltammograms were run from the OCP to more positive values. As can be seen in Figure 4.6 the bigger the activation current, the greater the shift in voltammogram to more negative potentials. This trend was expected since the charge density with an activation current of 100 mA cm^{-2} is 50 times that of an activation current of 2 mA cm^{-2}; hence much more Al will have dissolved creating a rougher, more highly pitted surface. The middle value of 50 mA cm^{-2} was the one chosen for all the activation experiments later in this project.

4.2.2. Anodic dissolution of AlMgSnGa alloys

The current density/potential characteristics for a series of the aluminium alloys with similar elemental composition to AB50V (see Table 2.2, page 39) were determined in 2 M

NaCl in an experiment where the alloy surface was initially activated with a current density of 50 mA cm^{-2} for 600 seconds and then subjected to current densities of 1, 2, 10, 50, 100, 200, 500 and 1000 mA cm^{-2} at 600 seconds intervals. The data from these experiments are given in Table 4.6. It can be seen that pure Al and the alloys that do not contain Ga (B1) or Sn (B3) had a very positive open circuit potential at ~ - 0.8 V and did not show any shift to more negative ones after the 600 seconds of attempted activation. Consequently, they require a large overpotential for their dissolution. The rest of the alloys exhibited much more negative potentials (- 1.5 V) when the 50 mA cm^{-2} were applied to them for 600 seconds and large current densities could be sustained at these negative potentials. Presumably, these alloys could oxidize by a mechanism not available to alloys without both Ga and Sn. AB50V, B0 and I0 alloys with similar elemental compositions had very analogous current density/potential characteristics. In order to represent and compare the current density/potential characteristics of the three alloys some extra current densities to those reported in Table 4.6 were applied to the alloys and plotted in Figure 4.7. It can be observed that there is some trend; at higher current densities AB50V seems to perform slightly better than B0 and I0. There is also significantly more scatter in the data for B0 and I0, partly because the experiment with these alloys was carried out only once. Coming back to Table 4.6, the alloy B2, the one with the highest Sn content seem to have the worst performance at higher current densities compared to the other AlMgSnGa alloys. The alloy B4, the one that did not contain Mg showed good performance and dissolved at rates similar to the other AlMgSnGa alloys but it clearly disintegrated faster when higher current densities were imposed. For example, at high current densities the alloy sample could for instance break in two pieces and therefore half of the anode would fall into the solution. This suggests that Mg plays a crucial role in the mechanical properties of the alloy and hence is beneficial for an Al anode.

In Table 4.6 the current density/potential characteristics for the AB50V, B0 and I0 alloys that were heat treated at 873 K for 2 hours are also shown. Dissolution rates are achieved slightly closer to the open circuit potentials (even at 200 mA cm^{-2}) compared to the non heat treated alloys. So, even if the effect of heat treatments is not dramatic, it seemed to improve the performance of the alloys.

Table 4.6. *Current/potential characteristics for the alloys in 2 M NaCl at 293 K. Data obtained potentiometrically (current varied at 600 seconds intervals) following activation at 50 mA cm^{-2} for 600 seconds. Potentials were reproducible to ±10 mV below 100 mA cm^{-2} Above this current density IR drop caused additional variation.*

j/mA cm^{-2} / Alloys	Potential *vs* SCE/ V					
	1	**4**	**10**	**50**	**100**	**200**
99.999 % Al	- 0.775	- 0.770	- 0.750	- 0.660	- 0.530	- 0.230
B0	- 1.540	- 1.520	- 1.480	- 1.450	- 1.440	- 1.390
B1	- 0.860	- 0.800	- 0.790	- 0.770	- 0.740	- 0.680
B2	- 1.530	- 1.490	- 1.440	- 1.380	- 1.260	- 1.120
B3	- 0.810	- 0.790	- 0.760	- 0.720	- 0.700	- 0.620
B4	- 1.530	- 1.520	- 1.510	- 1.500	- 1.490	- 1.460
AB50V	- 1.540	- 1.530	- 1.510	- 1.470	- 1.440	- 1.380
I0	- 1.540	- 1.530	- 1.500	- 1.490	- 1.480	- 1.450
Heated to 873 K for 2 hours						
B0	- 1.530	- 1.520	- 1.490	- 1.480	- 1.460	- 1.390
AB50V	- 1.530	- 1.520	- 1.500	- 1.490	- 1.470	- 1.400
I0	- 1.550	- 1.530	- 1.500	- 1.490	- 1.480	- 1.450

To examine the latter further, I0 alloy was heat treated at a temperature range between 373 and 873 K for two hours and the same controlled-current experiments as above were carried out in 2 M NaCl. The results are shown in Figure 4.8. In addition, the potentials for the middle 300 seconds for the 120 mA cm^{-2} step were averaged and plotted against the temperature for heat treatments of the I0 alloy in Figure 4.9. Heat treatment seems to improve slightly the electrochemistry of I0 alloy. In addition, heat treated I0 alloys perform better than the AB50V as it can be seen from Table 4.6. Heat treatment at 573 K seems to give the best alloy but differences are small. On the other hand, repetition of the heat treatment at 573 K lead to the same potential value within an error of ±10 mV.

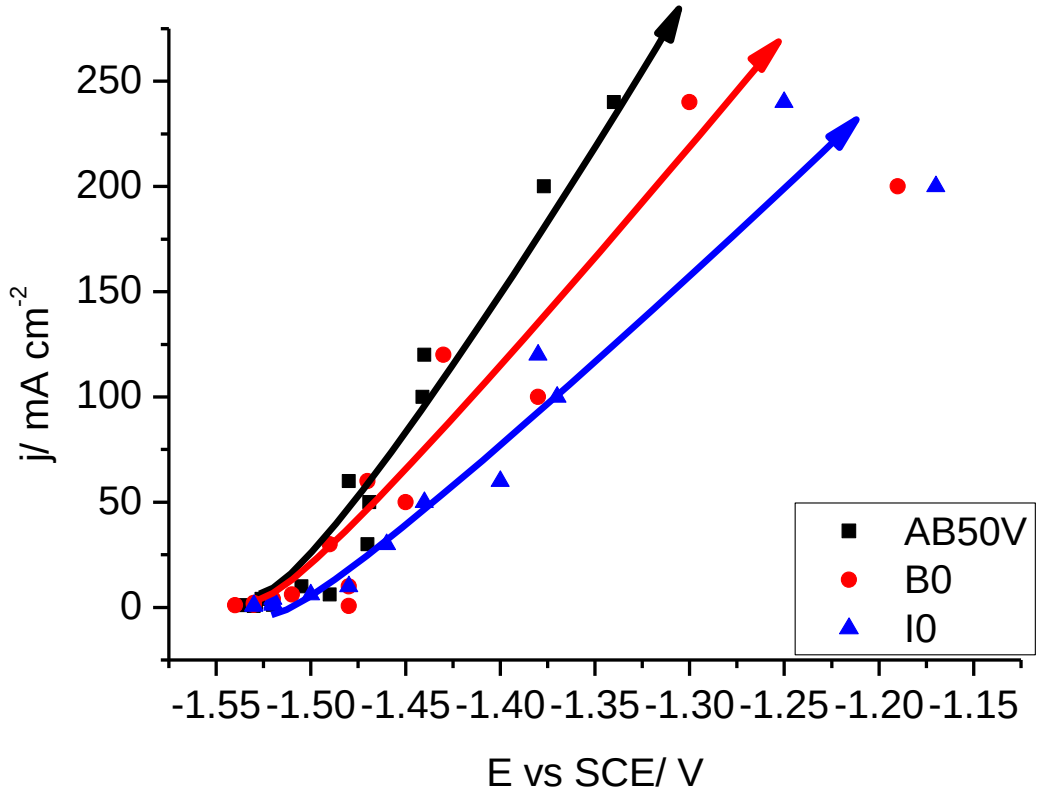

Figure 4.7: *Current/potential characteristics for the alloys AB50V, B0 and I0 of the control-current experiments where current density was progressively increased after activation at 50 mA cm^{-2} in 2 M NaCl.*

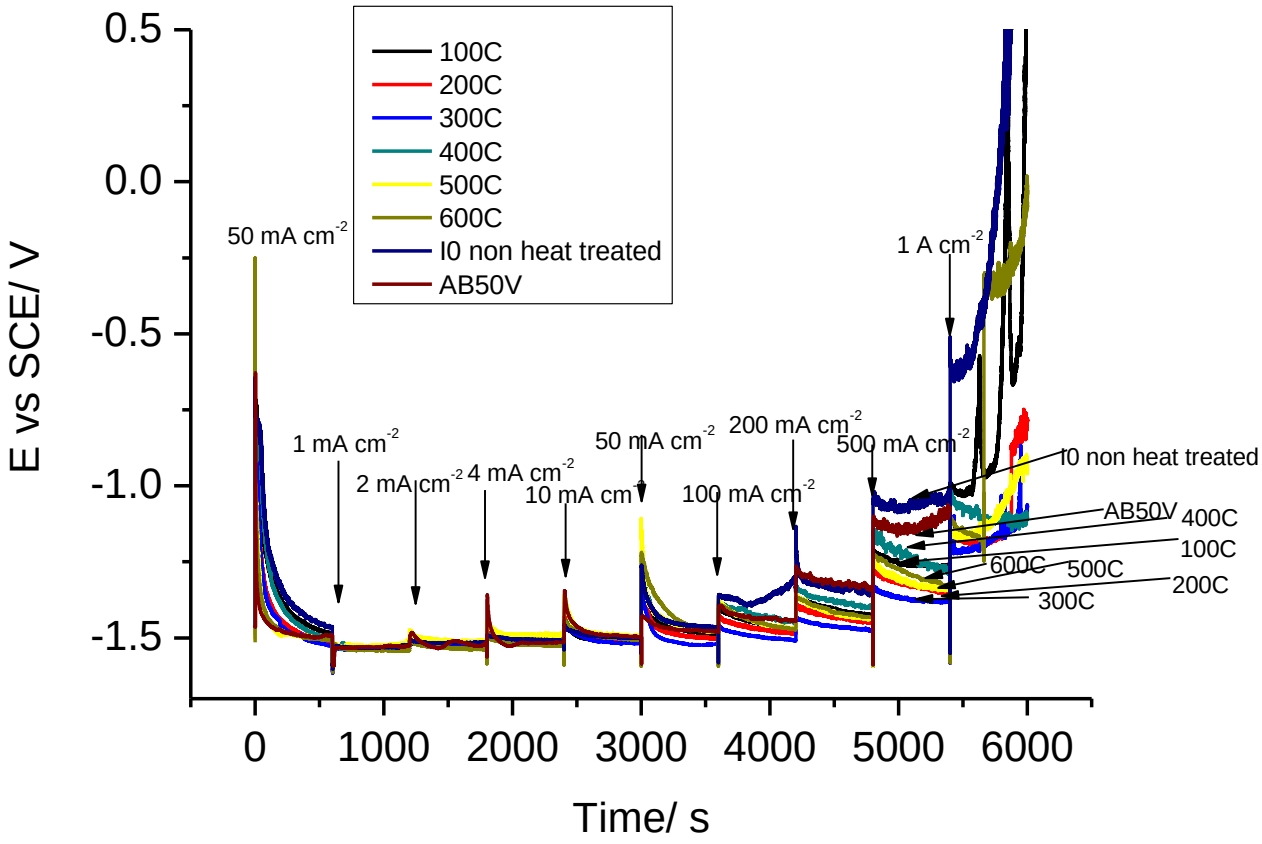

Figure 4.8: *Experiment where different current densities where applied for 600 seconds in untreated I0 and AB50V alloys and I0 alloy heat treated at various temperatures for 2 hours in 2 M NaCl. Below 100 mA cm^{-2}, the reproducibility was ±10 mV. At higher current densities, IR drop, hydrogen evolution and loss of material led to poorer reproducibility and current oscillation.*

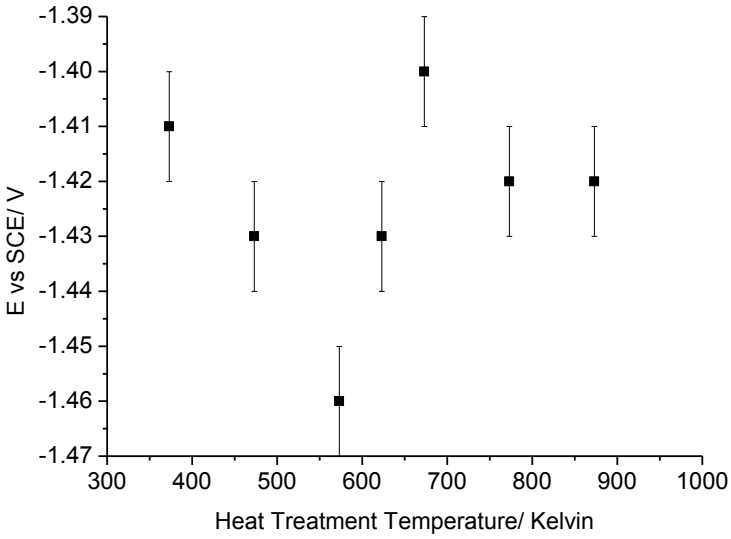

Figure 4.9: *Potential for 120 mA cm^{-2}vs heat treatment temperature from control current experiments with heat treated I0 alloys in 2 M NaCl. Replicate experiments were reproducible to ± 10 mV as indicated by error bars.*

4.2.3. Anodic dissolution of I0 alloy in different electrolytes

The current density/potential characteristics for the I0 alloy (with similar elemental composition to AB50V) were determined as in Section 4.2.2. in the solutions 2 M NaCl + 0.01 M NaOH, 2 M NaCl + 0.1 M NaOH, 2 M NaCl + 1 M NaOH and 2 M NaCl + 0.001 M HCl. In these solutions, the stability to open circuit corrosion was tested and the results were given in Section 4.1.3. The results from these experiments are shown in Figure 4.10 and summarized in Table 4.7. The dissolution potential (~ - 1. 5 V *vs* SCE) of I0 alloy in 2 M NaCl + 0.01 M NaOH, 2 M NaCl + 0.1 M NaOH and 2 M NaCl + 0.001 M HCl solutions is similar to that in 2 M NaCl presented earlier in this thesis therefore considering the corrosion characteristics of the alloy in these solutions the most appropriate electrolyte between them for an Al –air battery would still be 2 M NaCl. However there is a marked improvement in dissolution potential in 2 M NaCl + 1 M NaOH solution where I0 dissolves close to -1.7 V *vs* SCE at 100 mA cm^{-2} compared to the dissolution potential (~ -.1.5 V *vs* SCE) of the same alloy in NaCl where the alkali has not been added. The most alkaline 2 M NaCl would therefore be a good candidate electrolyte in an Al-air battery. Again, however

it exhibits some corrosion on open circuit and this electrolyte could only be used if added immediately prior to battery discharge. Hence, considering all parameters, 2 M NaCl would still be the most appropriate electrolyte in an Al – air battery where the anode would be an AlMgSnGa alloy like I0.

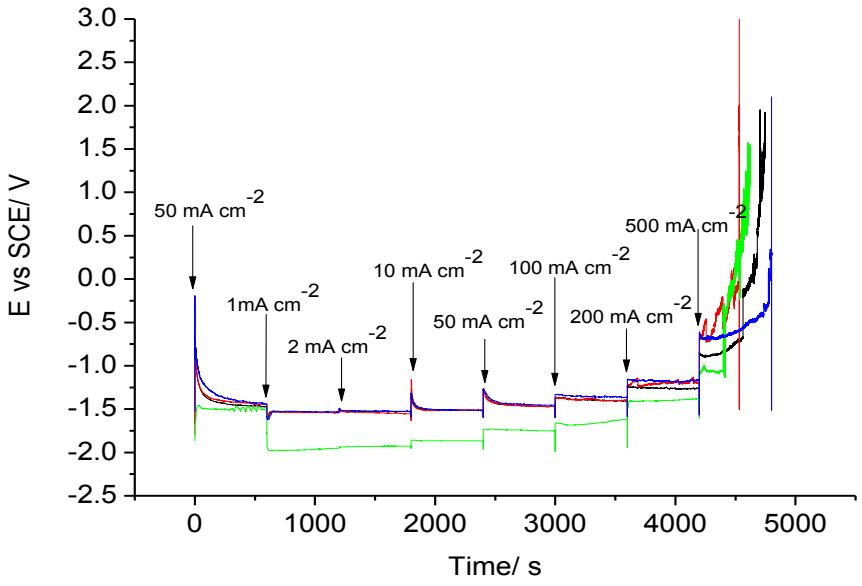

Figure 4.10: *Experiment where different current densities where applied for 600 seconds to untreated I0 alloy in various solutions. These were 2 M NaCl + 0.01 M NaOH (black line), 2 M NaCl + 0.1 M NaOH (red line), 2 M NaCl + 1 M NaOH (green line) and 2 M NaCl + 0.001 M HCl (blue line). Below 100 mA cm^{-2}, the reproducibility was ±10 mV. At higher current densities, IR drop, hydrogen evolution and loss of material led to poorer reproducibility and current oscillation.*

Table 4.7. *Key observations on chronopotentiograms of Figure 4.10.*

	E/ V *vs* SCE		
Solution	**At j = 2 mA cm^{-2}**	**At j = 50 mA cm^{-2}**	**At j = 200 mA cm^{-2}**
2 M NaCl + 0.01 M NaOH	- 1.50	- 1.45	- 1.25
2 M NaCl + 0.1 M NaOH	- 1.50	- 1.45	- 1.20
2 M NaCl + 1 M NaOH	- 1.90	- 1.74	- 1.40
2 M NaCl + 0.001M HCl	- 1.50	- 1.45	- 1.15

4.3. Structural Studies

In Section 4.2 it was shown that all the alloys containing both Sn and Ga tended to dissolve at high rates at a low overpotential. The main difference between the AlMgSnGa alloys was their stability to corrosion on open circuit as was shown in Section 4.1 of this thesis. Microstructural studies using chemical etching and electrochemical dissolution followed by scanning electron microscopy (SEM) imaging and elemental analysis (EDX), were carried out in order to investigate the role of Sn and Ga combination in rapid anodic dissolution of the AlMgSnGa alloys and variations on stability at open circuit depending on the history and working of the alloys.

4.3.1. Polished AlMgSnGa alloys and chemical etching

Samples of the three AlMgSnGa alloys with similar nominal composition were mechanically polished and observed under the backscatter detector of the SEM in order to define the distribution of the minor elements with higher atomic number than the aluminium matrix in the alloy. In Figure 4.11 the polished SEM images of the alloys AB50V, B0 and I0 are shown. The tin precipitates than can be observed as white spots in the figure. The Sn particles are sometimes associated with Mg, as was shown by EDX analysis. Sn occurs as a second phase in the aluminium matrix as predicted by the phase diagrams due to its poor solubility in aluminium. The typical size of Sn inclusions over the aluminium surface is ~ 1 μm for both the AB50V and B0 alloys. In contrast, in I0 alloy the second phases of Sn were observed to be somewhat fewer and larger (~10 μm). In Figure 4.12 TEM images of the three alloys show that Sn precipitates on the surface of these AlMgSnGa alloys can be as small as 0.2 μm. In order to further examine and establish the results found by the examination of the polished samples, chemical etching of the three alloys using Kellers reagent for 10 seconds was carried out. This resulted in a significant corrosion of the surface as expressed by rounded pits all over the surface, (see Figure 4.13). At higher sensitivity it can be observed that the pits occurred around Sn or SnMg inclusions, (see Figure 4.14). As expected, the pits distribution and sizes seem to be time dependent in chemical etching. In Figure 4.15 an obvious increase can be noted in size and frequency of pits on AB50V alloy when etched for 30 seconds with Kellers reagent

(a) (b) (c)

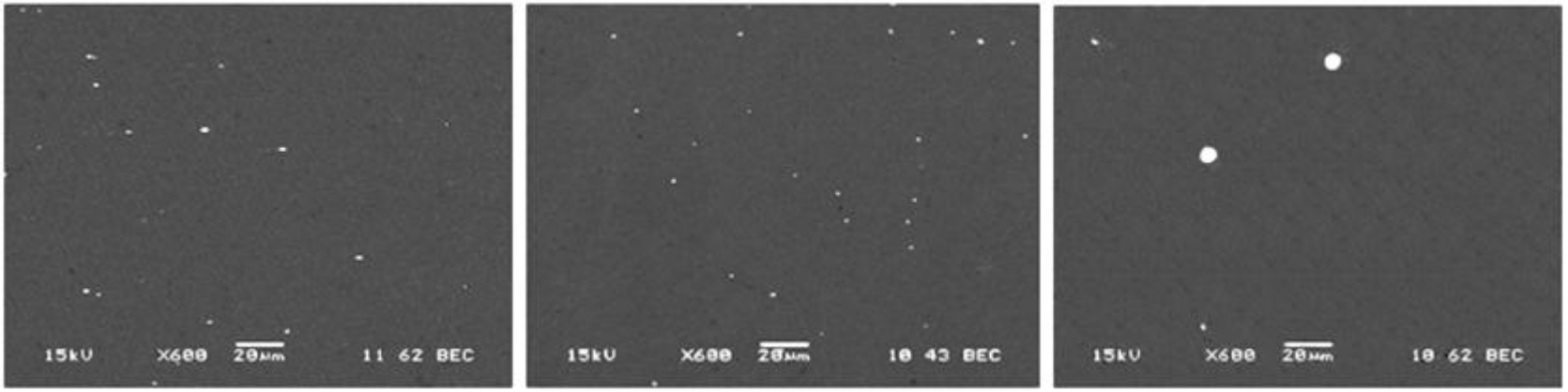

Figure 4.11: *SEM images of the alloys (a) AB50V, (b) B0 and (c) I0 under the backscatter detector of the SEM.*

(a) (b) (c)

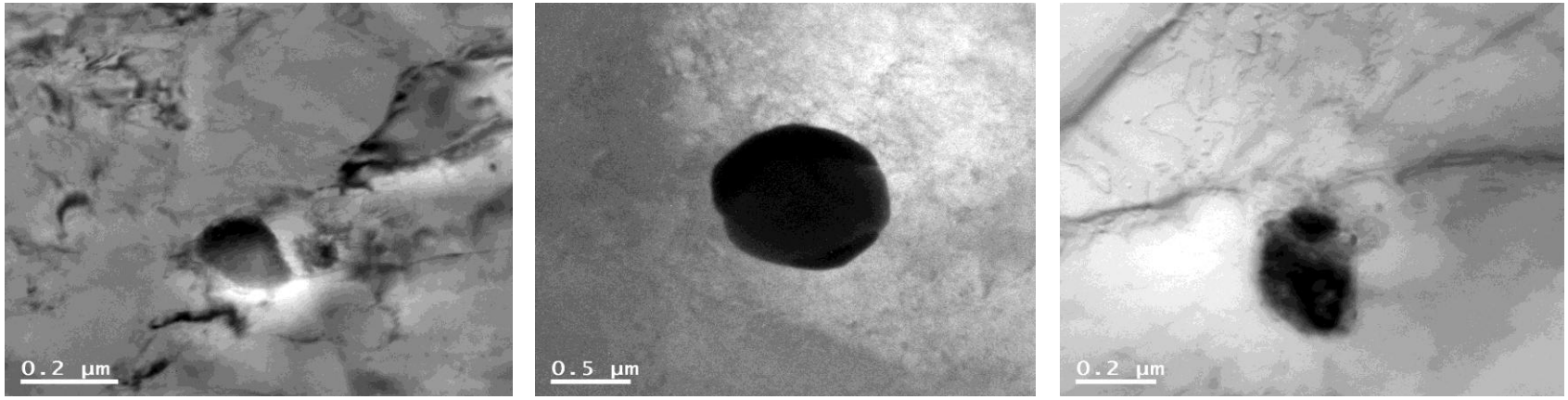

Figure 4.12: *TEM images of the alloys (a) AB50V, (b) B0 and (c) I0*

.

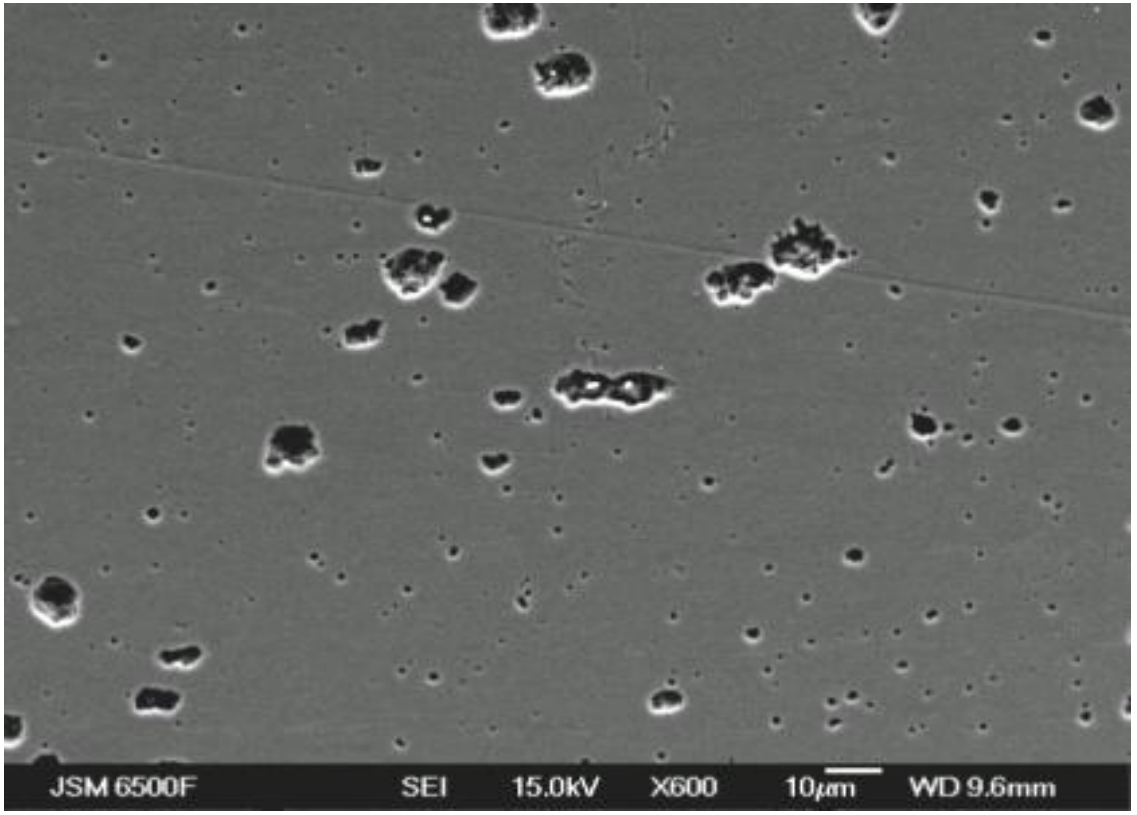

Figure 4.13: *Surface of the AB50V alloy, after 10 seconds chemical etching in Kellers reagent, observed under the secondary electron detector of the SEM.*

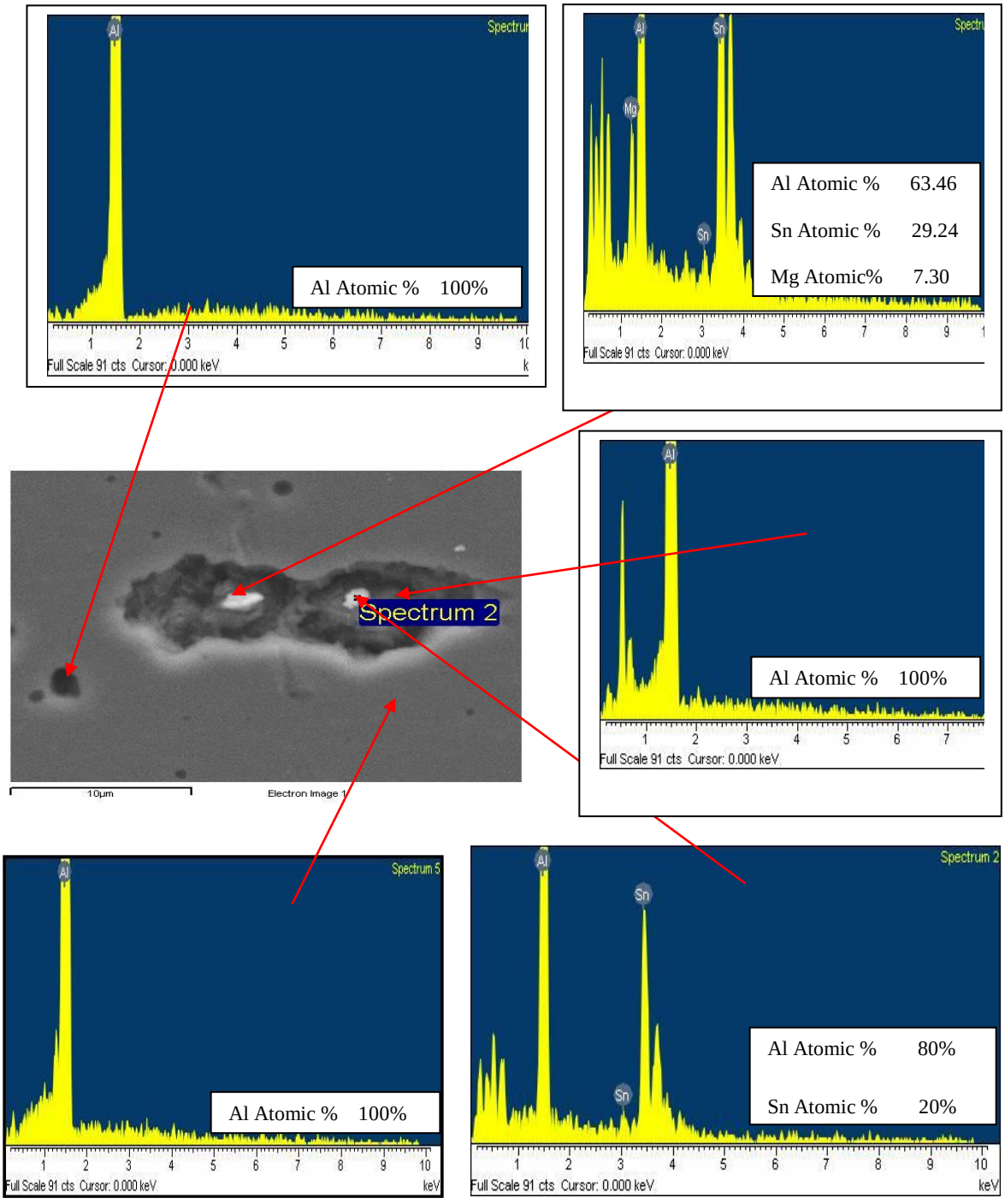

Figure 4.14: *SEM and EDX analysis of AB50V alloy after a chemical etching for 10 seconds in Kellers reagent; rounded pits around Sn and SnMg inclusions can be observed.*

compared with the image when it was etched for 10 seconds. In strong contrast, the lack of any sort of pitting and surface damage in general can be observed in Figure 4.16 from the SEM image of 99.999% pure Al after 10 seconds chemical etching in Kellers reagent. Comparable pitting to AB50V alloy was observed with I0 and B0 with similar compositions to AB50V, when chemical etching was carried out. In Figure 4.17 the images of etched a) B0 and b) I0 alloys are shown. These experiments confirm the conclusion that fewer and larger Sn and/or SnMg inclusions occur in I0 alloy, compared to the other two alloys. It has to be mentioned here that primarily Kellers reagent was used in an attempt to identify the grain boundaries of the alloys and their grain size. In this regard, the experiments were unsuccessful and a different approach will be described later in this chapter.

Chemical etching of AB50V alloy for 10 seconds was also carried out using other etching solutions. These included Kellers reagent without HF (so only HNO_3, HCl, H_2O), Kellers where HF was diluted times 4 and 0.24 M HF (same concentration that it has in Kellers reagent) in water. Images of the AB50V alloy surface after the three chemical etchings are shown in Figure 4.18. Kellers reagent was the strongest of the chemical etchants, together with HF in H_2O solution and it gave the most medium (1-2 μm) and small (0-1 μm) size pits. HF in H_2O was used together with the other milder than Kellers etching solutions in order to achieve a less aggressive chemical etching of AB50V alloy and see how it relates to the pits size and distribution, as is shown in Table 4.8.

In order to understand further the role of minor elements in the aluminium alloys, chemical etching with Kellers reagent was carried out for the B1 alloy (no Ga) for 10 seconds. SEM analysis showed that a different type of pitting occurred in the AlMgSn alloy (B1) compared to the AlMgSnGa (AB50V, B0, I0) ones. As it can be seen in Figure 4.19 a and b more angular pits that were not always associated with Sn seconds phases were located. At this point it has to be mentioned that unlike Sn and Mg, Ga was not detected in any of the analysis; such an outcome is not surprising given the very low atomic % of Ga in the alloys as well as its relatively low atomic number.

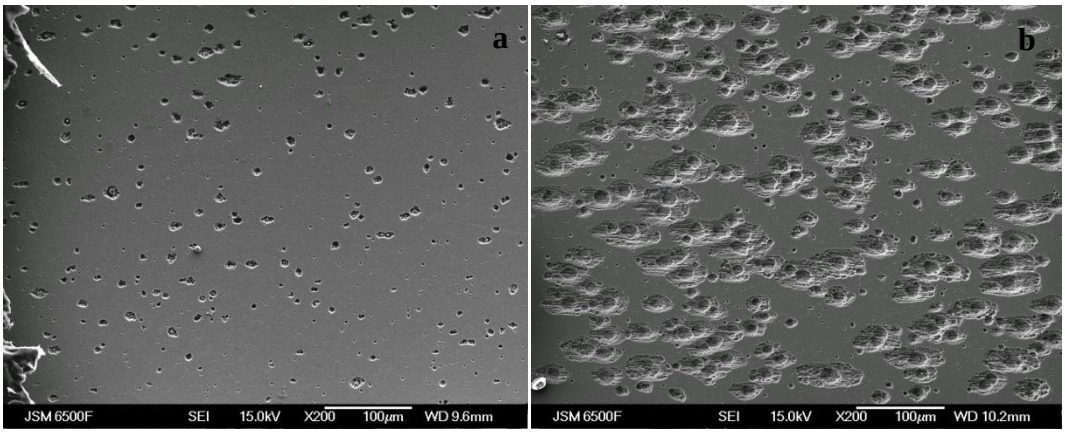

Figure 4.15: *SEM analysis of AB50V after a) 10 s and b) 30 s etching with Keller's reagent.*

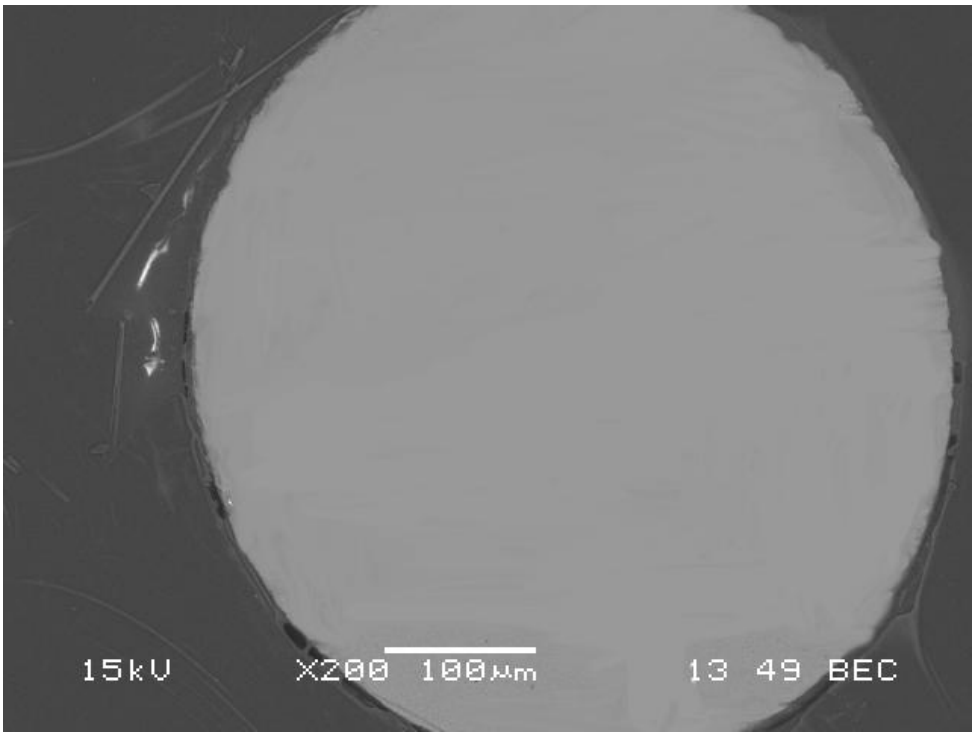

Figure 4.16: *SEM image of 99.999% pure Al after 10 seconds chemical etching in Kellers reagent. Pits or any other surface damage cannot be observed.*

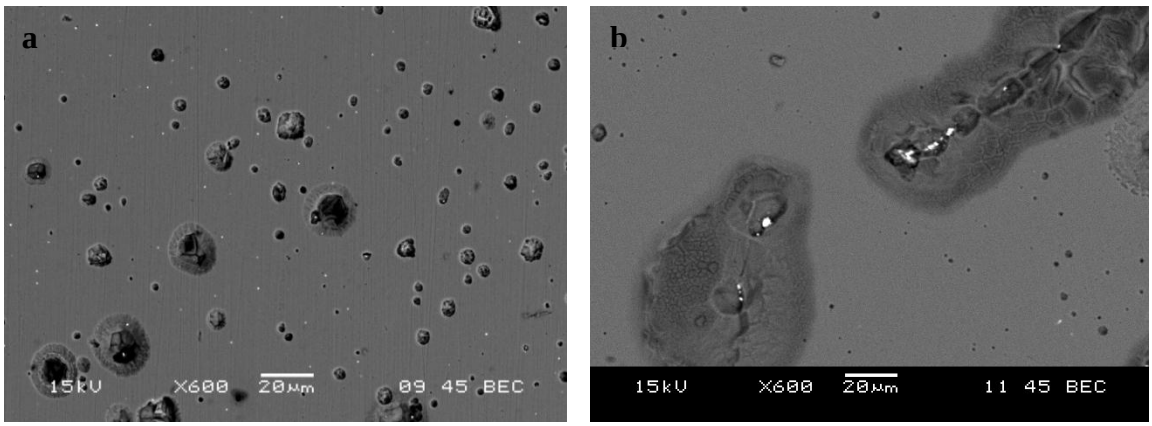

Figure 4.17: *SEM images of a) B0 and b) I0 alloys after 10 seconds etching in Kellers reagent under the backscatter electron detector. Pitting occurs around Sn and SnMg inclusions.*

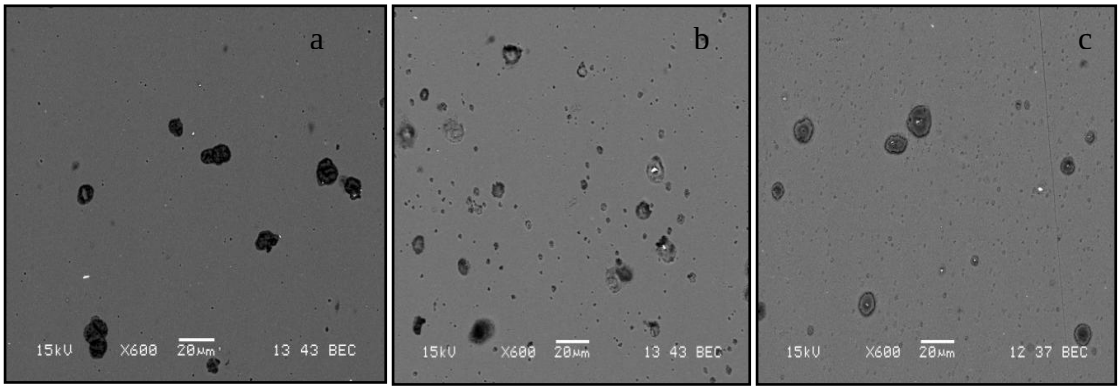

Figure 4.18: ***a)*** *AB50V etched with Kellers reagent that does not include HF (only HNO_3, HCl, H_2O),* ***b)*** *Kellers where HF was diluted times 4 and* ***c)*** *HF in H_2O with the same concentration (0.24 M) as in Kellers.*

Table 4.8. *Sizes of pits and distribution after chemical etching for 10 seconds with the different solutions listed.*

Size characterization of pits / 293.4 μm^2				
Etchant solution used for AB50V alloy	**10-40 μm Very big**	**2-9 μm Big**	**1-2 μm Medium**	**0-1 μm Small**
Keller's reagent	2	2	37	42
Keller's reagent without HF	1	6	9	19
Keller's with HF diluted x 4	3	4	12	20
HF as in Keller's in H_2O	2	1	59	40

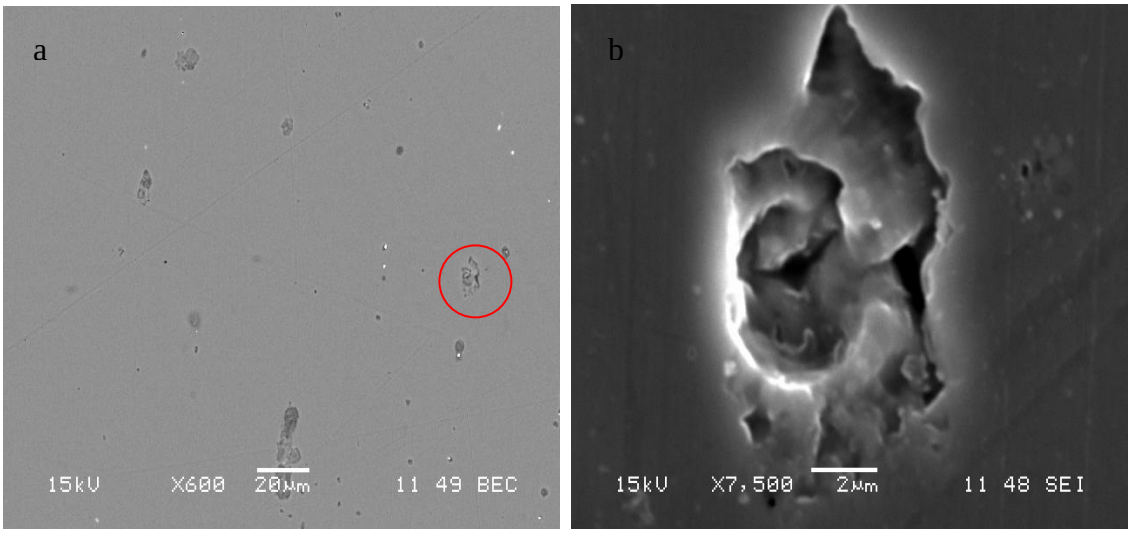

Figure 4.19: *SEM images of B1 alloy after 10 seconds etching in Kellers reagent showing* ***a)*** *the alloy surface under the backscatter electron detector at low resolution and* ***b)*** *the selected area in the red circle of Figure 4.19 a) under the secondary electron detector at high resolution.*

4.3.2. Electrochemical dissolution and structural studies

In order to enhance the knowledge of the role of minor elements in leading to pit formation and distribution in relation to the high dissolution rates of AlMgSnGa alloys, experiments

were carried out during which a constant anodic current was applied to a mechanically polished alloy surface that would be later observed under the SEM and analysed by EDX. In Figure 4.20 an SEM image of the AB50V alloy surface, after it had been subjected to an anodic current density of 50 mA cm^{-2} for 10 seconds is shown. The low magnification image 4.20 a shows that the passage of such a relatively high current density even for a short time has caused extensive pitting to the surface. Figures 4.20 b and c show higher magnification images along with EDX analysis at selected points of the surface. The pits are again rounded as with the Kellers etching of the same alloy. In addition as EDX analysis verified most of the pits are associated with Sn or MgSn inclusions throughout the alloy surface. The pits that are not obviously associated with a tin inclusion are large enough to postulate that during the increase in their size the second phases were lost to the solution. The distribution of the pits certainly reflects that of the Sn inclusions.

From these results, it was shown that the facile dissolution of AlMgSnGa alloys at potentials close to their open circuit potential close to - 1.5 V, directly relates to the formation of these rounded pits which in turn is determined by the Sn or MgSn inclusions. In Figure 4.20 c a typical 'dissolution centre' is shown which is large enough to be consist of overlapping pits which occur around the Sn inclusion. Of course, the tin inclusions will be distributed throughout the Al matrix and as a pit grows, more Sn inclusions will become exposed to the electrolyte. Furthermore, different current densities and dissolution times were applied to AB50V alloy to examine the relevance of these factors to the size and number of the pits. Current densities of 1 mA cm^{-2} were applied for 10, 60 and 125 seconds and 50 mA cm^{-2} were applied for 1, 10 and 60 seconds to the AB50V alloy and images afterwards were captured in SEM. Examining the correlation of the pits size with time (Figures 4.21 a to 4.21 c and 4.21 d to 4.21 e) it can be observed that they become bigger with longer periods of time and current density. Charge density determines the size and number of pits since according to Faraday's law (q = mnF), fifty times more dissolution will be involved in the dissolution of Al matrix around the Sn centres when a 50 mA cm^{-2} current density is applied compared to 1 mA cm^{-2}.

a) b) c)

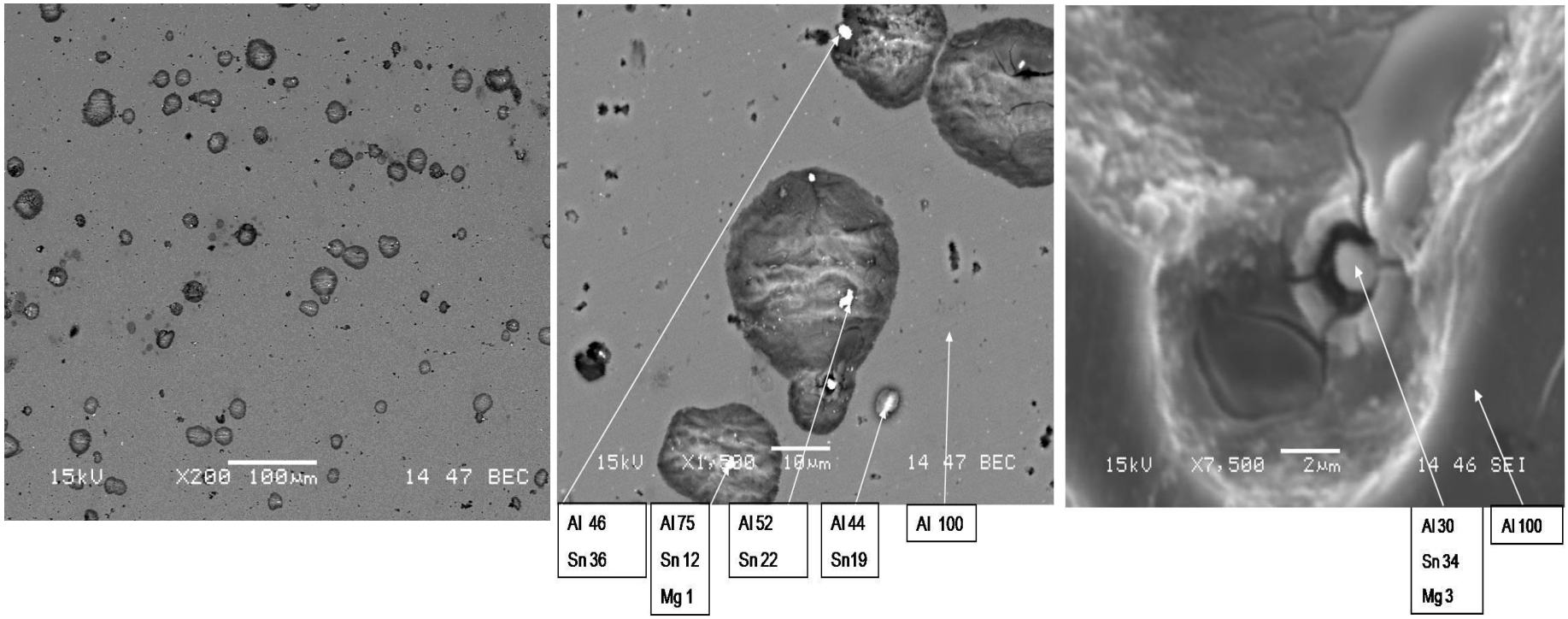

Figure 4.20: *SEM images of the surface of the alloy AB50V after a passage of a current density of 50 mA cm^{-2} for 10 seconds. a) low magnification image, b) medium magnification image, c) high magnification image with EDX analysis at various points. The EDX analyses are shown as atomic % reporting only the metal components.*

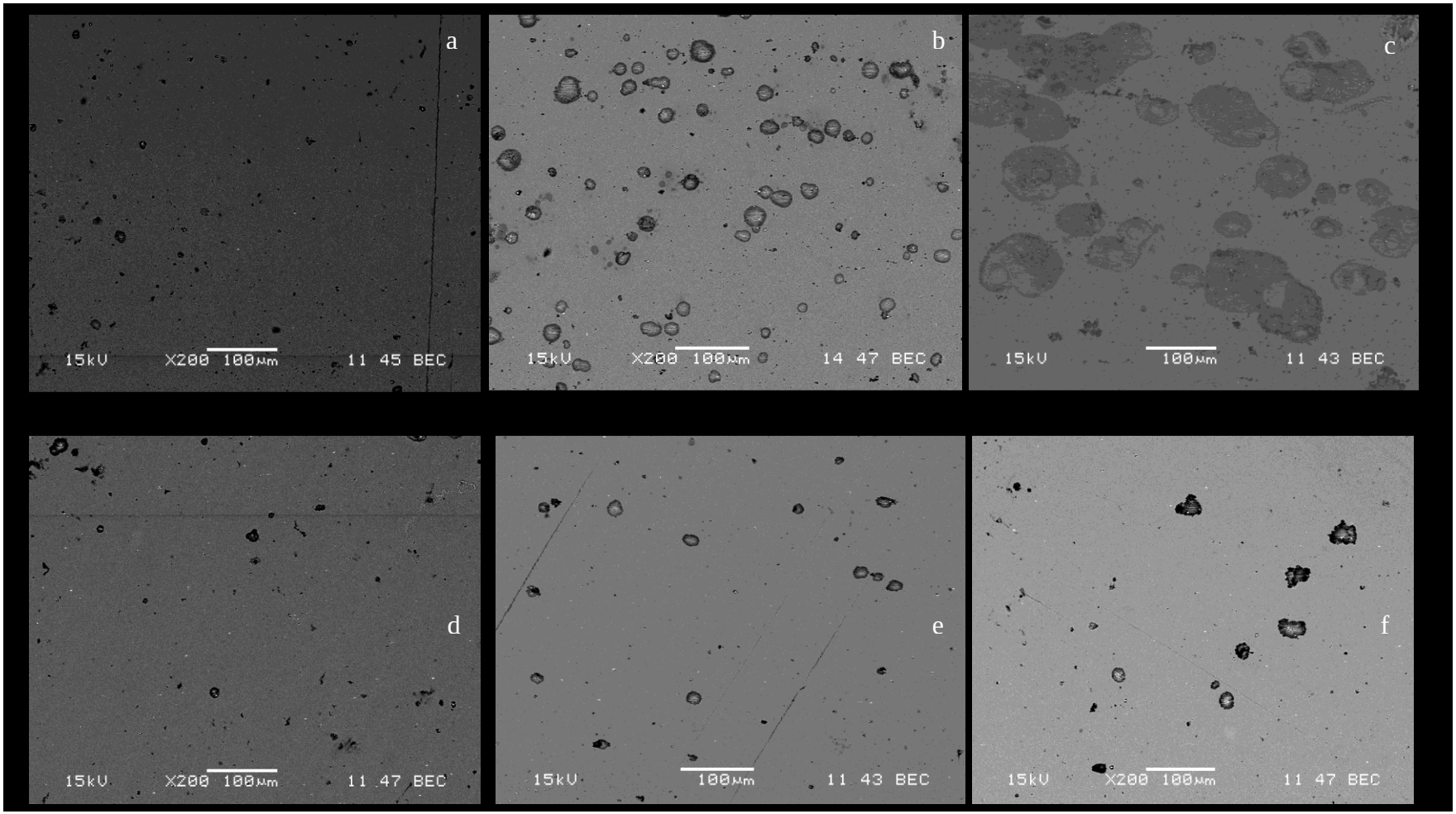

Figure 4.21: *AB50V anodically etched by 50 mA cm^{-2} in 2 M NaCl for* ***a)*** *1,* ***b)*** *10 and* ***c)*** *60 seconds \and AB50V anodically etched by 1 mA cm^{-2} in 2 M NaCl for* ***d)*** *10,* ***e)*** *60 and* ***f)*** *125 seconds respectively.*

As in the chemical etching experiments, the Ga could not be detected by the EDX analysis and hence direct evidence for its role could not therefore be obtained. Hence, an indirect approach was employed. The B1 alloy (the AlMgSn with no Ga) was subjected to the passage of 50 mA cm^{-2} for 10 seconds. Since the amount of Al dissolution is proportional to charge passed, substantial damage to the surface was expected to the AlMgSn alloy when 50 mA cm^{-2} where applied to it. However, the potential with the B1 alloy remained at - 0.8 V during oxidation, having a much higher overpotential compared to the AlMgSnGa alloys that dissolved at ~ - 1.5 V at a similar rate. Figure 4.22 shows images of the B1 alloy after the anodic dissolution. It can be seen that the pits are not rounded as with the AlMgSnGa alloys but angular. The pit morphology seems to be crystallographic in nature and there are many linked cavities. This pattern is very similar to what has been recently been reported for AlFe alloys.[29] A similar oxidation charge with pure aluminium also led to less but angular pits suggesting that the oxide film formation is a more important reaction in the absence of alloying elements.

By the latter statement it is implied that other mechanisms are responsible for pitting of aluminium in chloride media, in the absence of the reported intermetallics, related to the oxide film. The effect of chloride incorporation in the passive film of pure aluminium is the mechanism that should be considered in such a case;[104] such chloride penetration could be determined by X-ray fluorescence.[105] It has been reported in the literature that an increasing amount of chloride in the passive film can be related to the decreasing conductivity of the passive film at potentials more negative than the pitting potential.[106, 107] It has also be shown that oxygen vacancies in the passive film of aluminium are responsible for charge transfer in the passive film.[104] This chloride incorporation into oxygen vacancies it is believed to impede the motion of these vacancies though the film.[108] The mechanism of chloride incorporation in the oxide film of pure aluminium will not be discussed further in this thesis since, this study was focused on aluminium alloys containing intermetallics where different mechanisms of corrosion and dissolution are occurring.

A higher magnification image of a pit in B1, Figure 4.22 a shows that the alumina product has a more crusty appearance than at the AlMgSnGa alloys. Furthermore as is shown in Figure 4.22 b there is no evidence that the pits are associated with Sn phases (as in the chemical etching) and that many Sn centres remain unattacked in the Al surface.

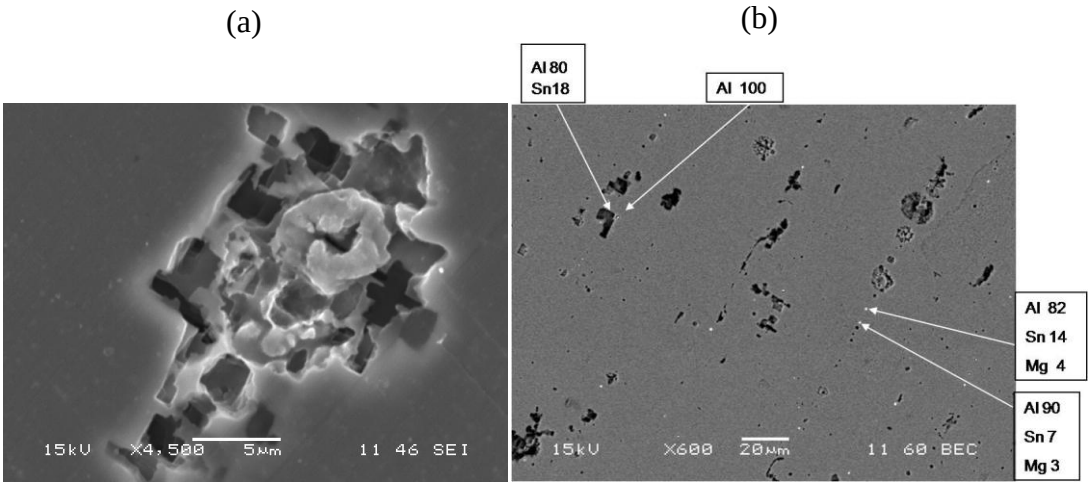

Figure 4.22: *SEM images of the surface of the alloy B1 (Sn no Ga) after it has been imposed to 50 mA cm^{-2} for 10 seconds using* ***a)*** *secondary electron detector and* ***b)*** *backscatter detector and EDX analysis at selected points. The EDX analyses are shown as atomic % in which only the metal components are included.*

These differences with the AlMgSnGa alloys certainly imply that the gallium somehow plays a key role in activating the Sn inclusions for a pit formation. The gallium also may plays a role in preventing passivation by alumina that terminates further pit growth.

4.4. Electron Backscatter Diffraction Analysis analysis and correlation between grain size at open circuit potential

Electron Backscatter Diffraction (EBSD) analysis is a powerful tool to obtain diffraction data. The orientations of particular features of the microstructure such as recrystallized grains can be correlated with the microstructure and by measuring the orientations of adjacent grains, grain boundary crystallography may be determined.[97]

For this project EBSD analysis was carried out for the 3 similar AlMgSnGa alloys, AB50V, B0 and I0, in order to determine their grain size and to investigate if the differences in stability to open circuit corrosion between the three alloys are related to differences in grain size. In Figure 4.23 the grain boundary (Figure 4.23 a, b and c) and the orientation maps (Figure 4.23 d, e and f) for the three alloys are shown respectively. The colours in the orientation boundary maps represent different orientations (showing the individual crystal direction of grains). The dark and grey lines at the grain boundary maps represent misorientation angles i.e. > 15º High Angle Grain Boundaries-(HAGB) and 2-15º Low Angle Grain Boundaries (LAGBs), respectively.

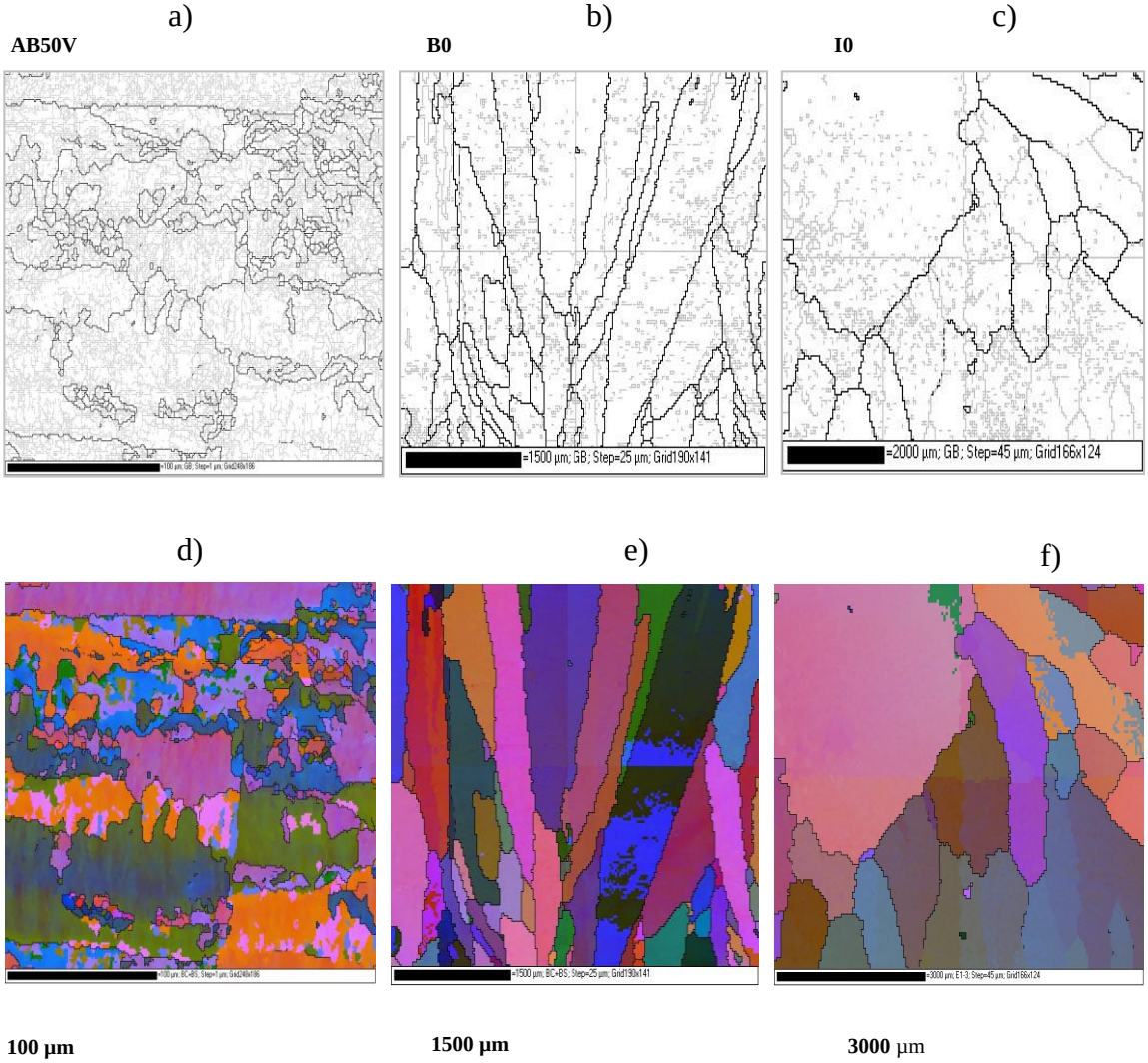

Figure 4.23: *EBSD analysis results including:* ***a)***, ***b)*** *and* ***c)*** *Grain boundary maps for AB50V, B0 and I0 alloys and* ***d)***, ***e)*** *and* ***f)*** *orientation maps of AB50V, B0 and I0 alloys respectively – note different scales.*

The results showed that the misorientations between two neighbour grains are larger than 15°. Within the grains, there exist some misorientations between 2-15°, represented by silver lines. They are the so-called low angle grain boundaries that are formed by deformation such as rolling or extrusion. As it can be seen in the figure the grain sizes in the three alloys (with the same elemental composition) are significantly different. This could have resulted from different processing parameters such as the melting temperature and cooling rate.

Deformations of the grains shown in Figure 4.23 a and 4.23 d imply that dislocations due to working (probably rolling) have occurred in AB50V alloy. In contrast, since B0 has been prepared by arc melting and it is thus in as-cast condition it has a band size ~500 μm which is ~ 10 times wider than AB50Vs'. The I0 alloy (Figure 4.23 c) shows an even larger one ~ 1000 μm. From the above results it is clear that the AB50V alloy is substantially different from the other two alloys. The AB50V alloy has band like grains (high angle grain boundaries) and plenty of low angle grain boundaries. In contrast both B0 and I0 have much less low angle grain boundaries and are not deformed, as would be expected for as-cast alloys. From these experiments, AB50V appears to have been subjected to cold rolling.

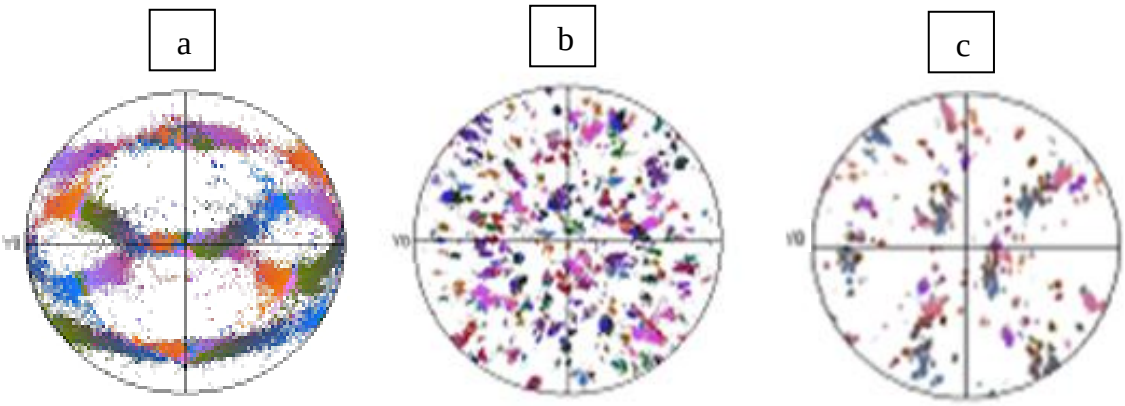

Figure 4.24: *Pole figures {110} from the stereographic analysis software corresponding to grain maps (Figure 4.21).*

Furthermore, the respective {110} pole figures (see Figure 4.24) of the three alloys along with their grain maps were obtained. The pole figure of AB50V (Figure 4.24 a) shows a typical rolled structure with mixtures of three textures: {112}<111>,

{123}<634>, and {011}<211> as was expected. In contrast, a random distribution of the grain and their orientations characterize both Figures 4.24 b and c. The only difference between Figure 4.24 b and 4.24 c is that in Figure 4.24 b the grains are more dense, which is reasonable since B0 alloy has much smaller grain size that I0 alloy as it was shown from their grain maps.

4.5. Heat treatment of AlMgSnGa alloys and subsequent grain size changes

In Section 4.2.2 of this thesis, it was shown that the as cast alloy I0 gave the best electrochemical performance after it was heated at 573 K compared to a range of other heat treatment temperatures. It was also shown that after heat treatment of the same alloy at 873 K the corrosion resistance (by eye observations) at open circuit increased significantly from 1 and ½ hours (without heat treatment) to 16 hours. Because of this difference and improved performance of the alloy after heat treatment, both in electrochemistry and corrosion resistance, a change in grain size after the heat treatments was suspected.

In order to examine the latter, EBSD analysis of I0 alloy was carried out for the same area of the alloy (the location was marked when looked under the FEG SEM in order to be observed again after the heat treatment) before and after heat treatment at 573 K.

In Figure 4.25 the orientation map of the I0 alloy before and after the heat treatment is given. From these results it is concluded that the heat treatment at 573 K did not cause any changes in the grain size or texture. The latter agrees with the literature that supports that there is some critical degree of cold work (between 2% and 20% cold work) below which recrystallization cannot be made to occur;[109] since the I0 alloy has not been worked in any way, such an outcome should be expected.

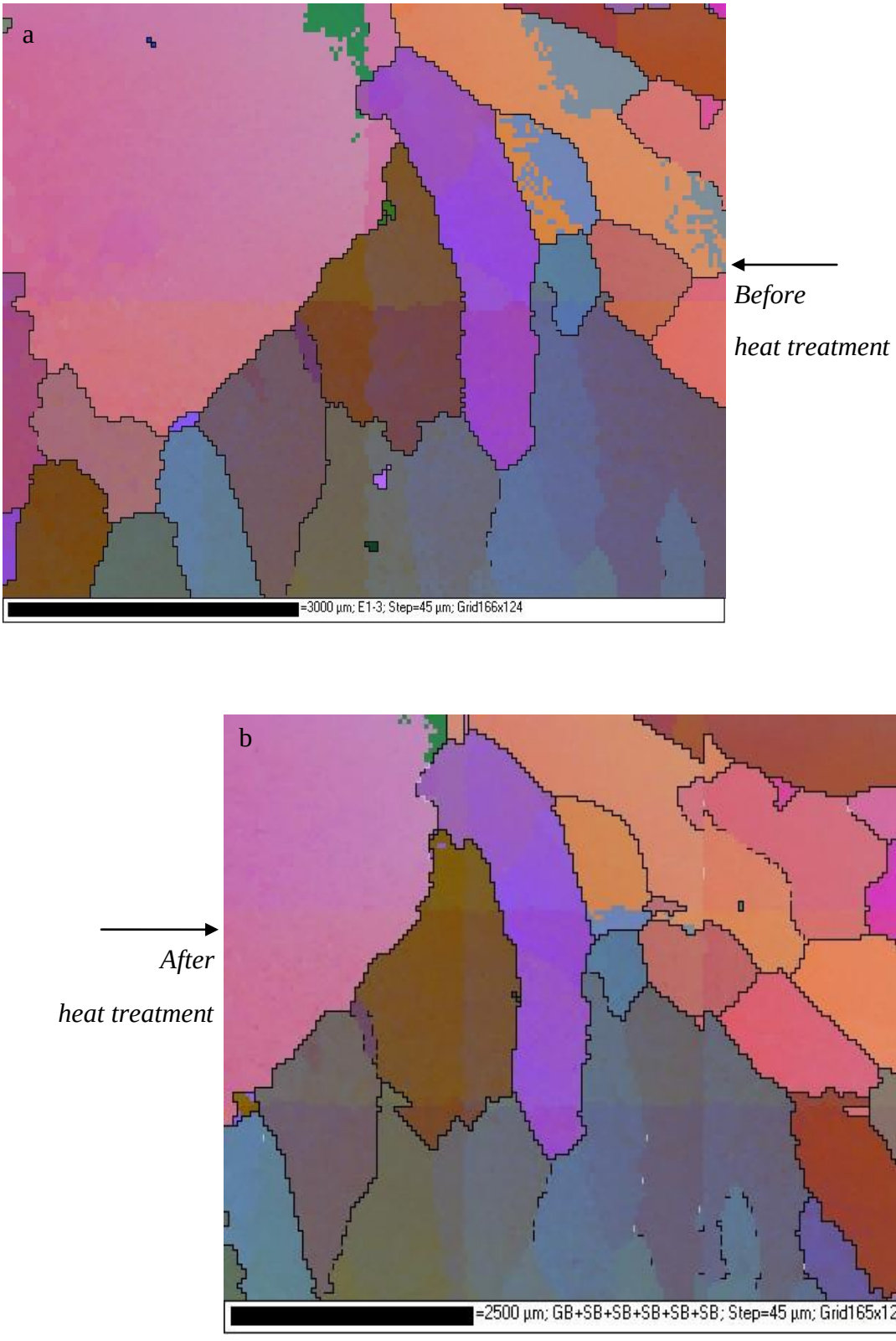

Figure 4.25: *EBSD maps of the I0 alloy a) electropolished and b) electropolished and heat treated at 573 K for 2 hours.*

Earlier it was reported that the cold worked alloy AB50V corroded more rapidly after heat treatment at 873 K. Hence, further experiments including heat treatments of AB50V alloy were undertaken. The heat treatments were carried out at 573 K and 873 K and EBSD analysis followed in both cases in order to examine any possible changes of the grain. The typical orientation and grain boundary maps of this analysis are shown in Figure 4.26. In the {100} and {111} pole figures (see Figure 4.27) of the AB50V alloy heat treated at 573 K the rolling textures still remain (comparing pole Figure 4.27 a) with 4.24 a)). In contrast, the {100} and {111} pole figures of the AB50V alloy heat treated at 873 K (Figure 4.27 b)) shows cubic texture of {100}<001> (scattered).

From the orientation and grain boundary maps, it is clear that, at 573 K, the grains become equal axis and the grain size is much larger than as received (the latter shown in Figure 4.24). The majority of grains are high angle grain boundaries. When heated further at 873 K for 2 hours, the orientation map shows that all the grains have the similar colour, which means that the area has only one high angle grain boundary consisting of a lot low angle grain boundaries (misorientation less than 15°). So the grain size after heat treatment at 873 K is much larger that shown previously for the non heat treated alloy (see Figure 4.23 a). In Figure 4.26 d it can be observed that the colour contrast is small. This is because the misorientation is small after heat treatment at 873 K which results in the lower colour contrast. That also implies that at 873 K there is essentially only one grain.

In addition, as it was predicted from the theory, when the rolled alloy AB50V was heated at 573 K recrystallisation occurred and grains have kept most of orientation of rolling texture (see Figure 4.27 a). When further heat treatment was carried out, some grains will disappear and some grains will grow, eventually only one grain left at 873 K as it is shown in maps 4.26 c and d. So from the pole Figures 4.27 a and b it can be seen that there are plenty of recrystallisaton grains in Figure 4.26 b (after heat treatment at 573 K), but only one grain in Figure 4.26 d (after heat treatment at 873 K) because of grain growth.

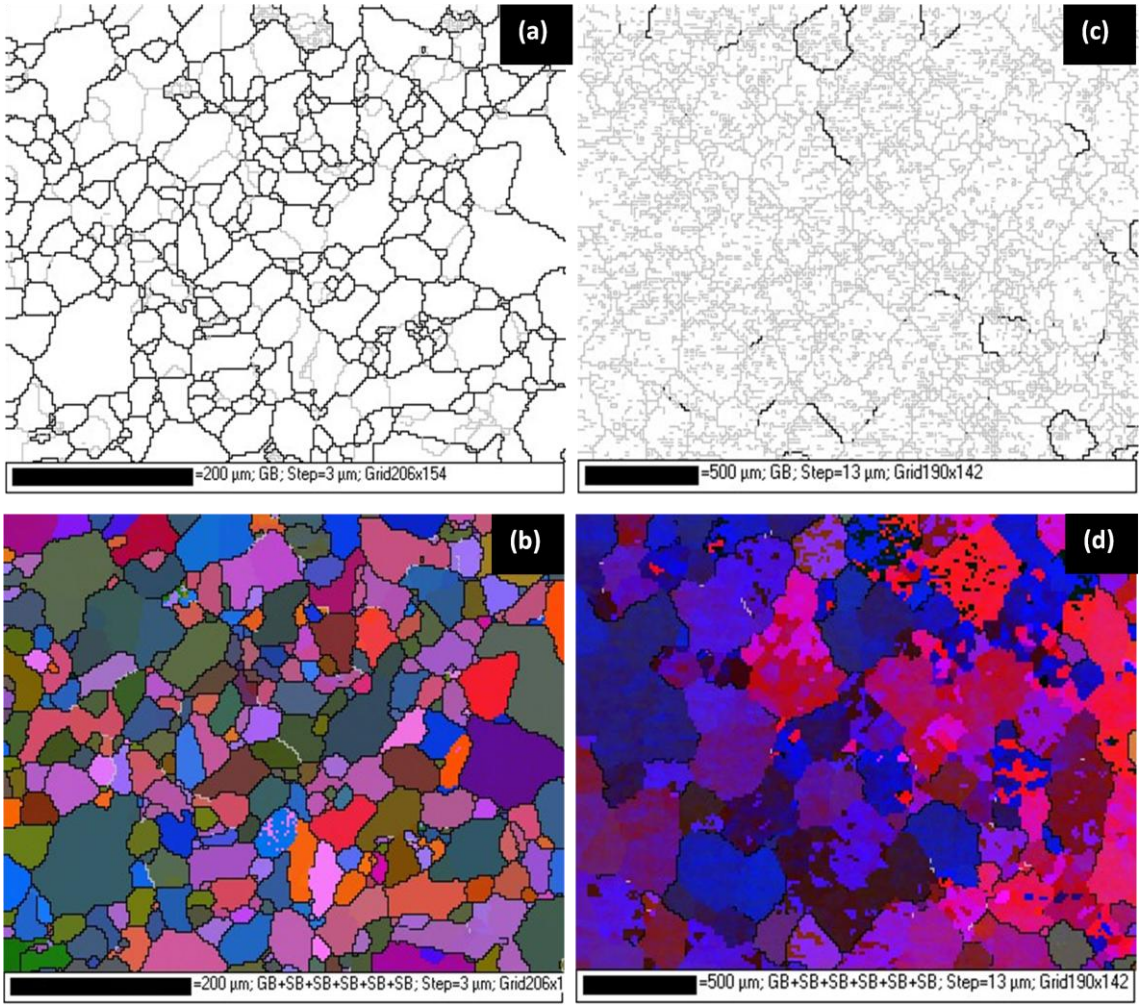

Figure 4.26: *EBSD orientation boundary maps (in black and white) and grain boundary maps (colour) for AB50V alloy heat treated at 573, a) and b), and 873 K c) and d), respectively.*

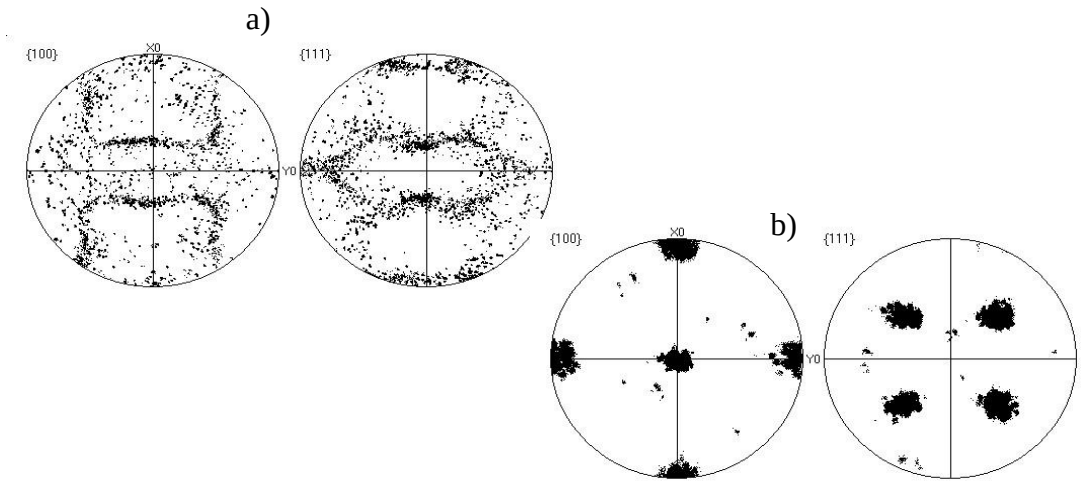

Figure 4.27: *Pole figures of AB50V alloy after heat treatment at a) 573 K and b) 873K.*

4.6. Conclusions from Corrosion, electrochemistry and structural studies of AlMgSnGa alloys

The Alcan alloy AB50V,[14, 110] as expected, performed very well and certainly could be dissolved anodically at high rates up to 500 mA cm^{-2} in 2 M NaCl. Alloys with a very similar composition and produced especially for this project, showed similar electrochemistry but somewhat different stabilities to corrosion. It was confirmed that both Sn and Ga are essential to high rate anodic dissolution close to – 1.5 V *vs* SCE and their presence to the alloy leads to a different dissolution mechanism where dissolution occurs around Sn centres. The three AlMgSnGa alloys were shown to have different structures, both in terms of grain size and dimensions of the Sn inclusions. These could be associated with different histories with respect to mechanical working and heat treatments. More detailed conclusion follow:

- It has been clearly shown from this work that Sn and Ga facilitate a new mechanism for the dissolution of aluminium alloys in NaCl at room temperature, with a shift of dissolution potential from - 0.8 for pure Al to - 1.5 V when both elements are present.

- Chemical etching of the AlMgSnGa alloys showed that aluminium tends to dissolve around Sn centres, implying that Sn acts as a cathodic centre, with aluminium matrix dissolving anodically around it.

- The Mg in AlMgSnGa alloys does not influence the electrochemical dissolution rate but may be helpful in a battery electrode to delay physical disintegration.

- Ga even if it was not detected by EDX analysis, as it was expected since the Al-Ga phase diagram reveals no intermetallic compounds and very limited mutual solubilities[17, 111] and due to the low concentration of the element in the alloy, has been indirectly shown to play a key role in the activation of aluminium.

- Sn and Ga could possibly activate the alloys to anodic dissolution via their influence to the properties of the alumina film, either by permitting the pitting of the native alumina layer present before the initiation of dissolution or they could

prevent locally the repassivation of the aluminium by the oxide film once the dissolution has started.

- It has also been demonstrated that alloys with the same elemental composition have very different properties, in particular with regard to stability at open circuit. This results from their history, including their sources, preparation and cooling rates, and any sort of working.

- It was shown from EBSD analysis that the AB50V alloy was cold worked and for this reason recrystallisation was feasible at 573 K. At 873 K grain growth was demonstrated.

- In contrast, with the similar as cast alloys, B0 and I0, heat treatment at 873 K, seems to influence positively both the electrochemistry and stability to open circuit corrosion properties.

- EBSD analysis of I0 alloy before and after heat treatment at 573 K showed that the grain does not undergo any change; this implies that the improvement in electrochemistry after heat treatment at this temperature is related to some other factor. One possibility could be the nature of the oxide layer on aluminium surface.

- Since after chemical etching experiments filliform corrosion was not observed in any of the three AlMgSnGa alloys along the grain boundaries, the change in grain size after heat treatments does not imply correlation to stability to corrosion at open circuit. According to the Al-Sn phase diagram discussed in the introduction of this thesis, heat treatments would affect solid solubilities in the alloys. Therefore the positive effect of heat treatment to B0 and I0 alloys could be due to increased solid solubility of tin in aluminium and therefore higher stability to corrosion.

- One cannot rule out that trace contaminants (i.e. other minor elements) not identified in this programme could have affected the results. Common contaminants in aluminium, e.g. iron, has been clearly probed.[112] Indeed, there is

possibility of contamination by unknown minor elements that should be recognised in all the literature related to Al alloys.

- Ultimately, the results of the current work are significant in aiding the selection of a good anode for an aluminium-air battery system. Factors that influence directly and indirectly the electrochemistry and behaviour on open circuit in aluminium alloys were clearly established.

CHAPTER 5 Battery, cathode and factors limiting Al dissolution

Preliminary battery experiments were carried out using the AlMgSnGa alloy I0 as the anode and, as cathode, two different commercial gas diffusion electrodes were used. The Johnson Matthey Pt/C with 4.66 mg cm^{-2} of Pt catalyst printed on a Toray paper substrate (in this thesis it will be called GDE 1 for convenience) and the E-TEK A2 STD ESNS, Silver Plated Nickel Screen Electrode, with 0.6 mg cm^{-2} loading using 10% Pt on Vulcan XC-72 (or GDE 2 for convenience).

5.1. Battery preliminary results

Batteries were constructed using the cell shown in Figure 2.6. The I0 Al anode and GDE cathode (each 3.14 cm^2) were parallel and spaced by a 2 mm gap filled with 2 M NaCl electrolyte. In Figure 5.1 the discharge curve of the battery at 20 mA cm^{-2} in 2 M NaCl using GDE 1 cathode and the I0 alloy as the anode, shows that the battery operated at 20 mA cm^{-2} giving a voltage close to 1.2 V for 3 hours.

The charge passed of 700 C cm^{-3} of electrolyte was equivalent to the formation of an "Al (III) concentration in solution" of approximately 1 M although in fact some solids were formed. By lowering the current in stages it is even possible to continue operating at 1 V for 8 hours when 1000 C cm^{-3} had been passed. The charge before a rapid drop of cell voltage also corresponded to 900 C cm^{-2} of anode area.

In Figure 5.2 the discharge curve at 50 mA cm^{-2} using the GDE 2 cathode from E-TEK is illustrated. It shows that the battery can be discharged at a higher current density and give greater than 0.8V for the first 30 min. Nevertheless the performance seems to decay with time since the voltage goes down to zero after 55 minutes of operation.

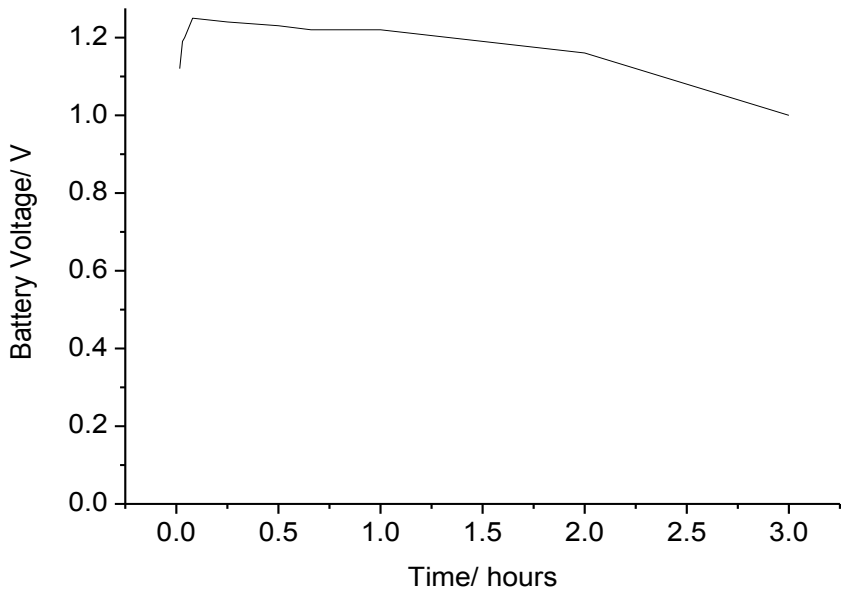

Figure 5.1: *Discharge at 20 mA cm^{-2} using the GDE 1 cathode and the I0 alloy as the battery anode.*

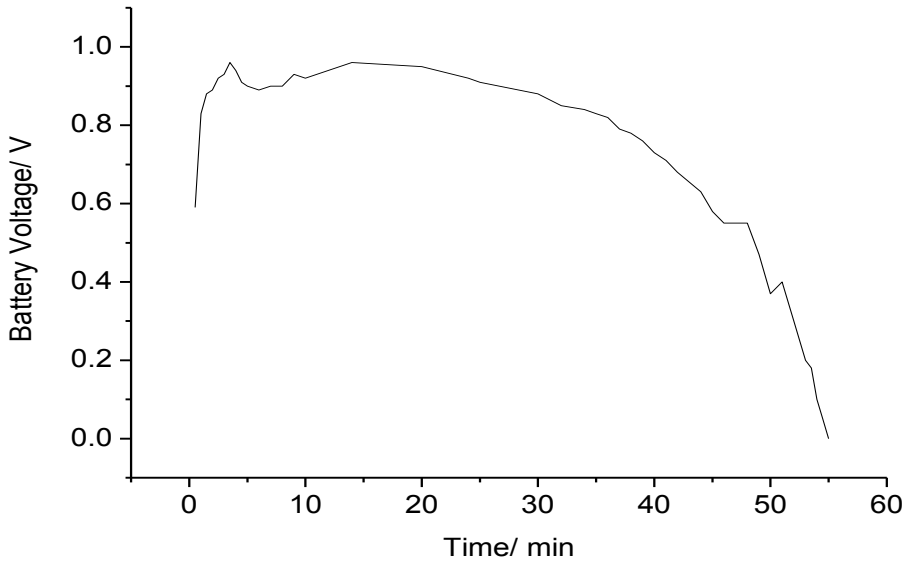

Figure 5.2: *Discharge at 50 mA cm^{-2} using GDE 2 cathode and the I0 alloy as the battery anode in 2 M NaCl.*

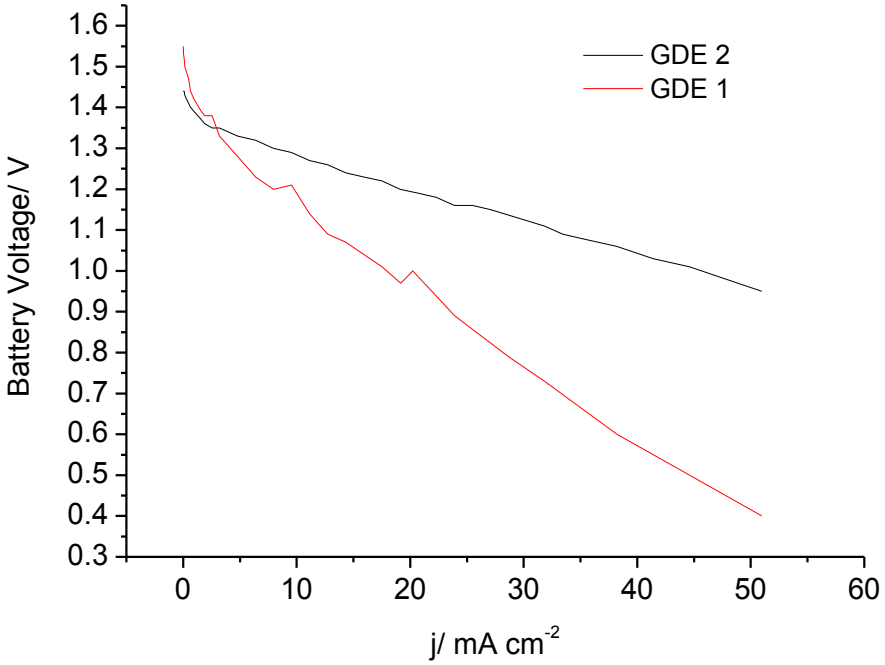

Figure 5.3: *I-V curves for the Al-air battery with the GDE 1 and GDE 2 cathodes in 2M NaCl.*

Figure 5.3 shows the relationship between current density and battery voltage for batteries with the two air cathodes. The battery voltages obtained in these experiments were unexpectedly low and certainly not those expected on the basis of the experiments of Figure 5.1 and 5.2. The curves are also quite different implying limitation by the GDE. GDE 2 seems to give superior results. It should be noted, however, that all the battery experiments should be regarded as preliminary. They were carried out with limited supplies of both Al anodes and air cathodes and components were often reused without a detailed log of their history. From these preliminary battery experiments it was concluded that the battery performance was promising but needed improvement to higher current densities and longer discharge times. The cell voltage is, however low compared to the expected value approaching 2 V based on earlier experiments with the Al alloy confirming limitations by the oxygen cathode. Moreover, the factors limiting the extent of Al consumption need further investigation.

5.2. Factors limiting battery discharge

In Figure 5.2 the discharge at 50 mA cm^{-2} using GDEp 2 cathode and I0 anode alloy in 2 M NaCl was shown; it was seen that the battery voltage reached zero after approximately 55 minutes. In a trial to investigate the reason for that rapid drop in voltage another experiment was carried out. After the experiment reported in Figure 5.2, the electrolyte of the battery was replaced with fresh solution and the Al (III) formed on aluminium surface was washed away with water. Then a discharge curve was run again, (see Figure 5.4).

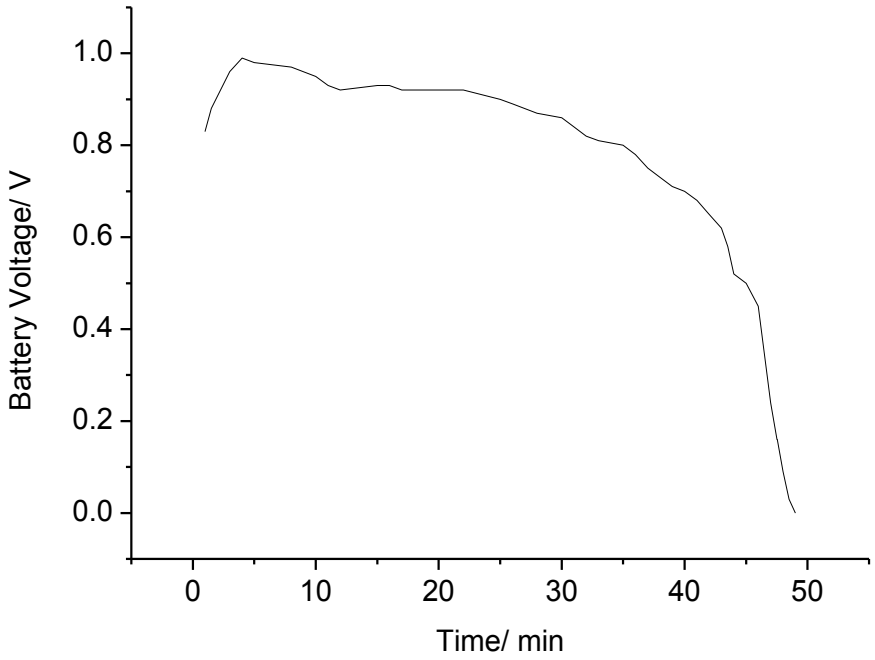

Figure 5.4: *Discharge at 50 mA cm^{-2} using the used GDE 2 cathode and I0 alloy with fresh 2 M NaCl electrolyte after a previous discharge..*

The discharge curve in Figure 5.4 is very similar to the one in Figure 5.2. After the electrolyte was replaced with fresh, the battery ran for 49 minutes, while in the first experiment (see Figure 5.2) where the fresh electrodes were used the battery ran at similar voltage for 55 minutes. These results imply that the limiting factor for further aluminium dissolution was either the Al (III) formed in the electrolyte or the loosely bound $Al_2O_3/Al(OH)_3$ on the Al surface. It is not a passivation layer on the Al surface

since the only material that was different in the battery experiments was the air cathode, the GDEs were examined by SEM. The SEM images of the two electrodes are given in Figure 5.5.

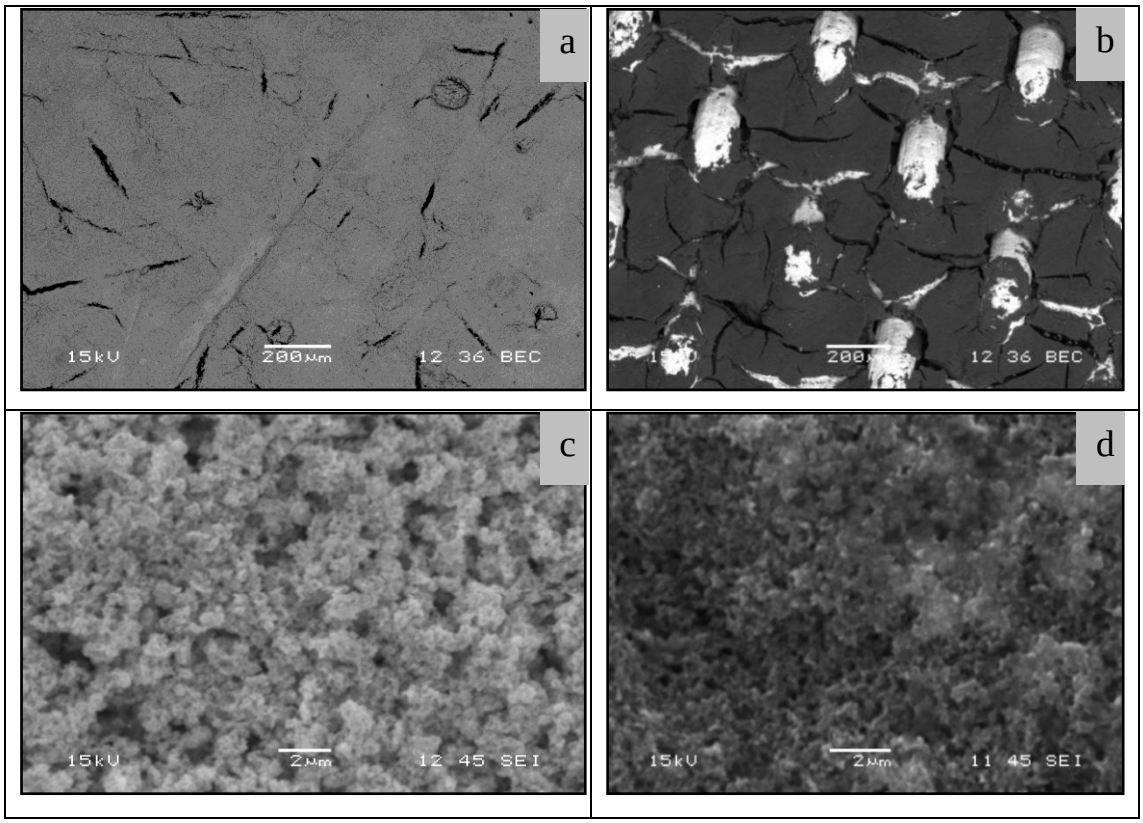

Figure 5.5: *SEM images of GDE 1 cathode at **(a)** low and **(c)** high resolution and GDE 2 cathode at **(b)** low and **(d)** high resolution.*

From Figure 5.5 a and 5.5 b lower resolution images it can be seen that the main difference between the two electrodes is the Ag-coated Ni grid of the GDE 2 electrode. The higher resolution images (Figure 5.5 c and 5.5 d) indicate that their matrix is quite similar and is composed by carbon particles of similar size (~1 μm).

Overall, the battery performance was acceptable but not as good as was required. Therefore, the performance of the positive gas diffusion electrodes was investigated. While the performance of GDEs in acid is well described in the literature and some data is available in alkali, there are no reported data in neutral NaCl. It should be emphasized that we sought current densities higher than 100 mA cm^{-2}.

5.3. Voltammetry of gas diffusion electrodes

5.3.1. Pt/ C 4.66

The voltammetry of the GDE 1 cathode was run in acid, base and neutral media at 353 K. In all experiments oxygen was supplied to the gas diffusion electrodes at a flow rate of 200 cm^3/ min. In Figures 5.6 (a) the results from these experiments can be seen where the potentials are plotted *vs* Hg/Hg_2SO_4 and in Figure 5.6 (b) the results are replotted *vs* the RHE.

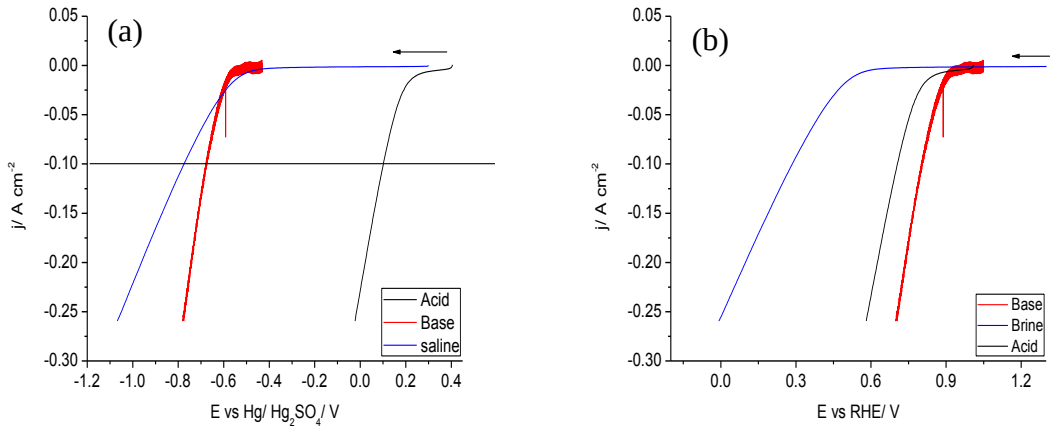

Figure 5.6: *Voltammetry of* GDE *1 electrode from OCP in 2 M H_2SO_4, 2 M NaOH and 2 M NaCl at 353 K (a) vs the Hg/Hg_2SO_4 and (b) vs the RHE.*

In Table 5.1 the conversion of potentials between the difference reference electrodes is shown for a specific current density in the three solutions.

Table 5.1. *Conversion of potentials of GDE 1 electrode in 2 M H_2SO_4, 2 M NaOH and 2 M NaCl from Hg/Hg_2SO_4 reference electrode to RHE.*

Solutions (2M)	E at 100 mA cm^{-2} *vs* Hg/Hg_2SO_4 / mV	E at 100 mA cm^{-2} *vs* RHE / mV
H_2SO_4	102	706
NaOH	-673	825
NaCl	*-773*	*287*

It has to be noted at this point that the voltammetry of the GDEs was carried out at elevated temperature as this is necessary to reach their optimum performance and also to be able to compare with results from the fuel cell industry. It can be seen from Figure 5.6 b that the performance of GDE 1 in acid is similar to that reported in the literature and that the performance in base is slightly better.[78] The performance of the electrode in NaCl is much poorer as can be seen from Figure 5.6 and Table 5.1. It can be noted that the voltages observed in brine explain the low battery voltage; the expected potential of the Al anode is ~ -2.1 V *vs* Hg/Hg_2SO_4 and the observed O_2 cathode potential of -0.8 V would give a battery voltage of ~ 1.3 V. Such a performance for the GDE might be expected mainly due to poor O_2 reduction kinetics and lower conductivity in brine compared to the acid and alkali. Moreover, in brine solution, the pores of the GDE go alkaline as the oxygen reduction proceeds producing OH^- in the pores and it is probably more appropriate to think of the electrolyte as alkaline. Furthermore the steepness of all the curves presented in Figure 5.6 it is believed that are related more to IR drop than kinetics.

Since the Al battery was to be operated at ambient temperature, voltammograms of GDE 1 were also ran in acid, base and brine in 293, 333 and 353 K. The respective results are shown in Figures 5.7, 5.8 and 5.9.

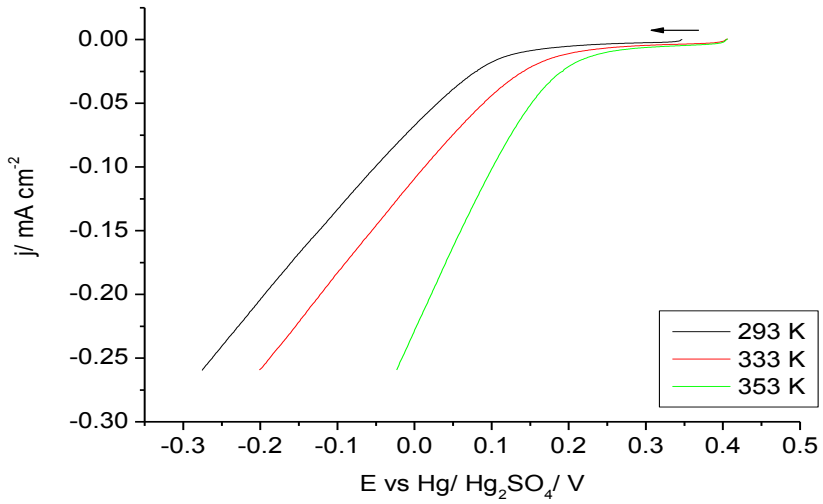

Figure 5.7: *Linear voltammetry of* GDE *1 cathode electrode from OCP in 2 M* H_2SO_4 *at various temperatures.*

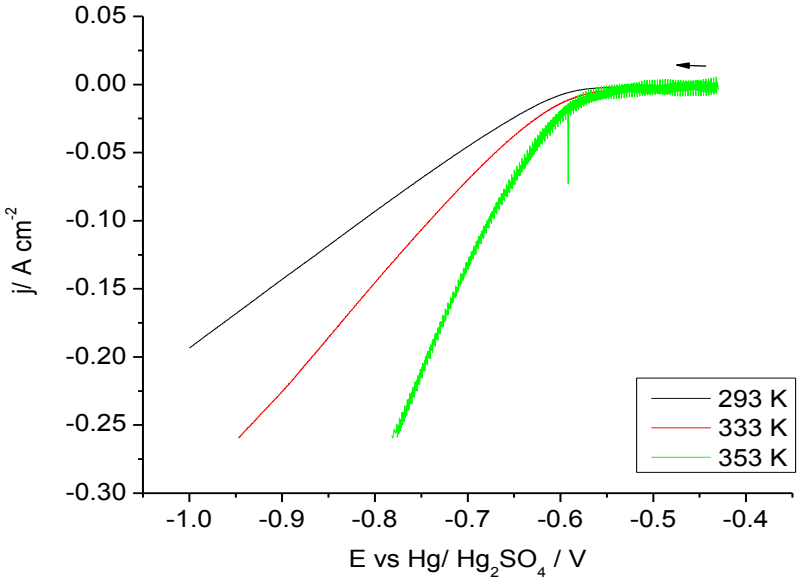

Figure 5.8: *Linear voltammetry of* GDE *1 cathode electrode from OCP in 2 M NaOH at various temperatures.*

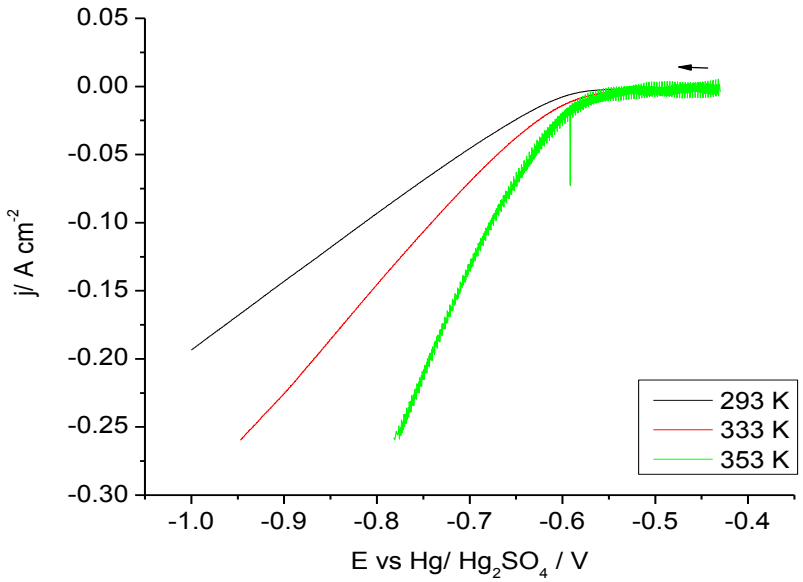

Figure 5.9: *Linear voltammetry of GDE 1 cathode electrode from OCP in 2 M NaCl at various temperatures.*

From the curves in Figures 5.7, 5.8 and 5.9 it is clear that the temperature has an impact in the performance of GDE 1. In all media the performance of the GDE for oxygen reduction improves with increasing temperature. This results both from an enhancement of the O_2 kinetics and an increase in conductivity of the solutions.

5.3.2. Behaviour of GDE 1 with time in H_2SO_4

Oxygen reduction reaction experiments were carried out at 333 K for 4.5 hours. The results of those experiments are plotted in Figure 5.10. The performance of the GDE 1 electrode as it can be seen improved with time. Between experiments time was given for the OCP to stabilize (~ 0.37 V *vs* Hg/Hg_2SO_4).

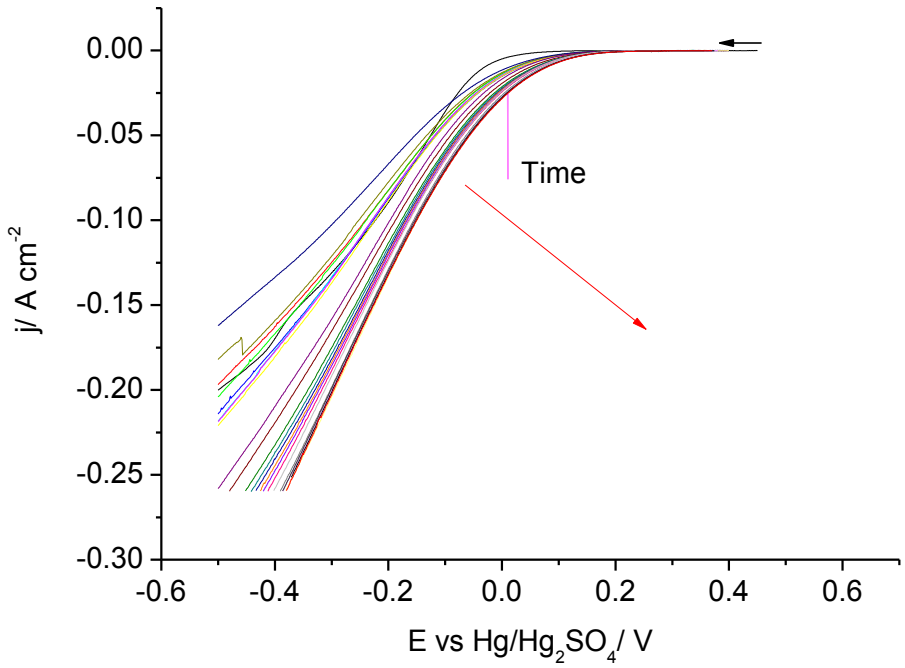

Figure 5.10: *Replicate Linear sweep voltammetry curves in 2 M H_2SO_4 of GDE 1.*

After the experiments that are illustrated in Figure 5.10, the used electrode was kept in electrolyte overnight and the next day it was noted that its OCP had increased by approximately 0.3 V. Moreover, voltammetry curves of the used GDE 1 electrode were run again in 2 M H_2SO_4. In Figure 5.11 the results of these second day experiments are shown and compared with the last curve obtained from the experiments with the GDE 1

electrode of the previous day. As it can be seen in Figure 5.11 the replicate voltammetry curves during the second day, show that the performance of the GDE kept improving slightly when repeated voltammetry curves were ran.

Overall it was concluded that Pt/C electrodes (GDE 1) in acid improve their performance with time and ideally they should be left for 12 hours in electrolyte before use in order to get the best possible performance.

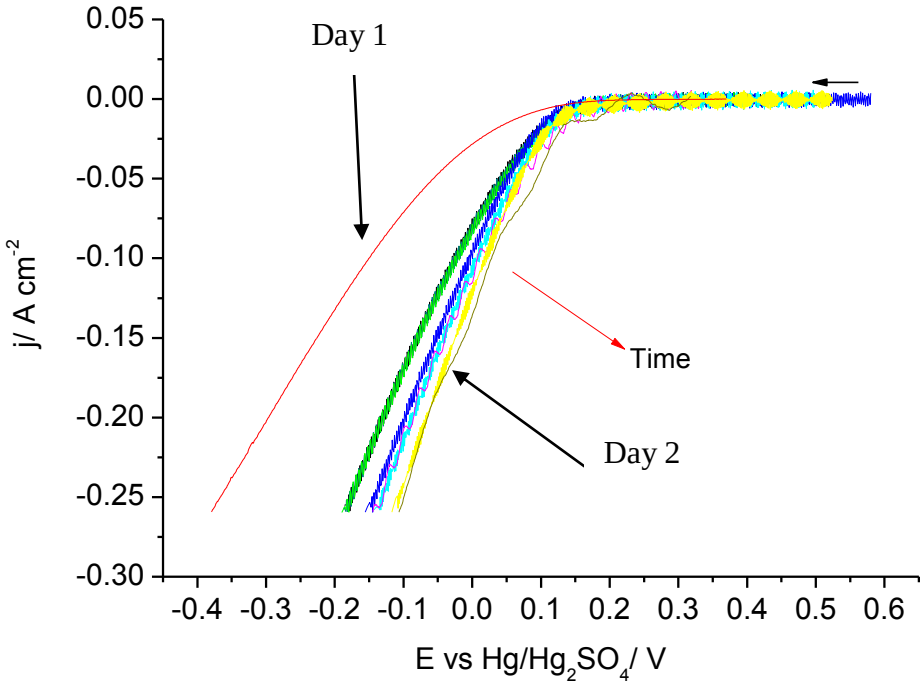

Figure 5.11: *Replicate Linear sweep voltammetry curves in 2 M H_2SO_4 at 293 K of a used GDE 1 that was also left overnight in electrolyte.*

5.4. Factors limiting the dissolution of aluminium

Experiments were carried out to define the factors ultimately limiting the extent of the anodic alloy dissolution reaction.

- Does the reaction continue until all the alloy has dissolved?
- Is the dissolution limited by the volume of electrolyte?

- Does a passivating layer eventually form on the alloy surface?
- Was the reaction limited by alumina formation or by a partially soluble Al (III) in solution?

In order to address these questions, a cell with a large ratio of Al alloy area to electrolyte volume was designed. All of the experiments involved the dissolution of the I0 alloy (unless otherwise stated) with a constant current in the small Perspex cell, (see Figure 2.2 of Section 2.3.1 in the thesis) containing 6 ml of NaCl electrolyte. The anode was always an AlMgSnGa alloy, with a weight of approximately 1.0 g and an area of 2.5 cm^2 exposed to the electrolyte. If all the anode dissolved, the equivalent Al (III) concentration 'in solution' would be approximately 6 M. The cathode was stainless steel 904 L with the same area. A steel cathode had to be used since an air cathode able to deliver the current densities required has not been identified. At the steel electrode, hydrogen gas is formed by the following reaction:

$$2H_2O + 2e^- \rightarrow H_2 + 2OH^- \quad \text{(R.8)}$$

As has been mentioned earlier in this thesis, this reaction leads to the formation of 1 OH^- / e^-, as at an oxygen cathode and hence the cathode influence on solution pH should be same as in the Al-air cell.

From the viewpoint of a battery operation the important question is whether the energy density is limited by:

- the amount of aluminium in the cell
- changes to the aluminium surface
- volume of electrolyte
- changes to electrolyte composition, e.g. change in pH, depletion of Cl^-, increase in $Al\ (III)$
- simply filling the interelectrode gap with solids.

In some experiments in this section, the dissolution was interrupted at intervals and the impedance diagram obtained at open circuit. In addition, SEM images of the I0 alloy surface and cross sections were taken after different periods of dissolution. For cross sections, samples were mounted in epoxy resin and then mechanically polished. All the experiments were carried out at room temperature unless stated otherwise.

5.5. Dissolution dependence on current density

The AlMgSnGa alloy, I0, was dissolved anodically at a series of current densities - 50, - 170 and - 200 mA cm^{-2} in 2 M NaCl. The cell voltage *vs* time responses can be seen in Figure 5.12.

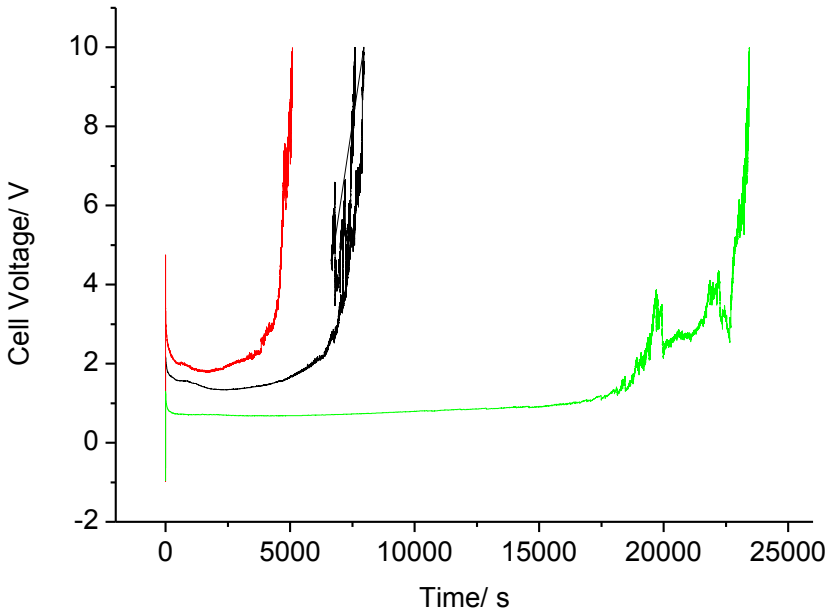

Figure 5.12: *Cell voltage vs time response to the imposition of anodic current densities of 50 (green line), 170 (black line) and 200 mA cm^{-2}(red line), to the anode Al alloy I0 vs stainless steel 904L.*

It can be seen that for a period of time, the electrolysis occurs with a constant cell voltage. The overall chemical change is:

$$Al + H_2O \rightarrow Al(III) + H_2 \qquad \text{(R.5)}$$

Thermodynamics predict that this reaction should proceed spontaneously. In practice, it was necessary to apply a small voltage because of overpotentials at the electrodes and IR drop through the electrolyte.

Table 5.2. *Charge density passed during the experiment illustrated in Figure 5.1.*

Current density applied / mA cm^{-2}	Time/ s	Q/ C cm^{-2}
50	17900	890
170	6400	1090
200	3800	760

When the experiment started, rapid H_2 evolution could be observed from the steel electrode. Some slight gas evolution could also be observed from I0 and it was increased at higher current densities. The solution was not clear due to the gas evolution but some Al (III) solid was observed after the first 300 s. After 3000 seconds the precipitation of Al (III) was heavy and a more compact layer (here termed the "shroud") of an Al (III) precipitate was attaching itself to the Al alloy surface. It can be seen from Figure 5.12 that the cell voltage increases with current density but this is largely due to IR drop through the electrolyte in the interelectrode gap in the cell. Eventually at all current densities there was a sharp increase in cell voltage.

Table 5.2 reports the time before the steep increase in cell voltage (a voltage of ~ 3 V was selected for comparison) and also the charge passed at that time. It can be seen that the charge passed is almost independent of the current density used for dissolution. The charge density is also similar to that passed in the battery experiment before the voltage dropped to a low value. This charge is equivalent to the formation of an Al (III) solution with a concentration of 0.5 M.

5.6. Dissolution factors

A further series of experiments was carried out using a constant current density of 170 mA cm^{-2} applied to the I0 alloy in 2 M NaCl where several other parameters were varied. The experiments and the observations are reported in Table 5.3.

Table 5.3. *Observations for a series of anodic dissolution reactions in 2 M NaCl with the alloy I0 carried out at 170 mA cm^{-2}.*

Experiment	Charge passed / C cm^{-2}	Comment
Fresh electrode Fresh electrolyte	1090	Al_2O_3 in electrolyte at end of electrolysis
Fresh electrode Reused electrolyte	935	Despite Al_2O_3 in electrolyte, Electrolyte does not determine performance
Reused electrode But Al_2O_3 shroud dispersed Fresh electrolyte	1070	Cleaned electrode still capable of further dissolution
Reused electrode Care not to remove Al_2O_3 shroud Fresh electrolyte	120	Thick Al_2O_3 deposit on Al stops dissolution
Fresh electrode Fresh electrolyte at T= 38 ^{o}C	1090	High temperature has minor effect
Fresh electrode Fresh electrolyte In ultrasonic bath	1585	Ultrasonic breaking up the Al_2O_3 shroud, allows greater dissolution

As reported above, when a fresh alloy electrode and fresh electrolyte were used, the aluminium dissolution proceeded smoothly for approximately the first 6000 seconds during which 1090 C/cm^2 were passed and then the cell voltage increased up to 10 V at ~ 8000 seconds when the experiment was stopped. At the end of the experiment the product formed can be easily observed at the surface of the I0 alloy electrode, (see Figure 5.13). Next to the aluminium metal a grey gel (probably some aluminium hydroxide) was kept in place due to a ‘shroud’ of more solid white crystalline form of aluminium oxide. Only a tiny amount of Al (III) could be seen in the electrolyte independently of this layer.

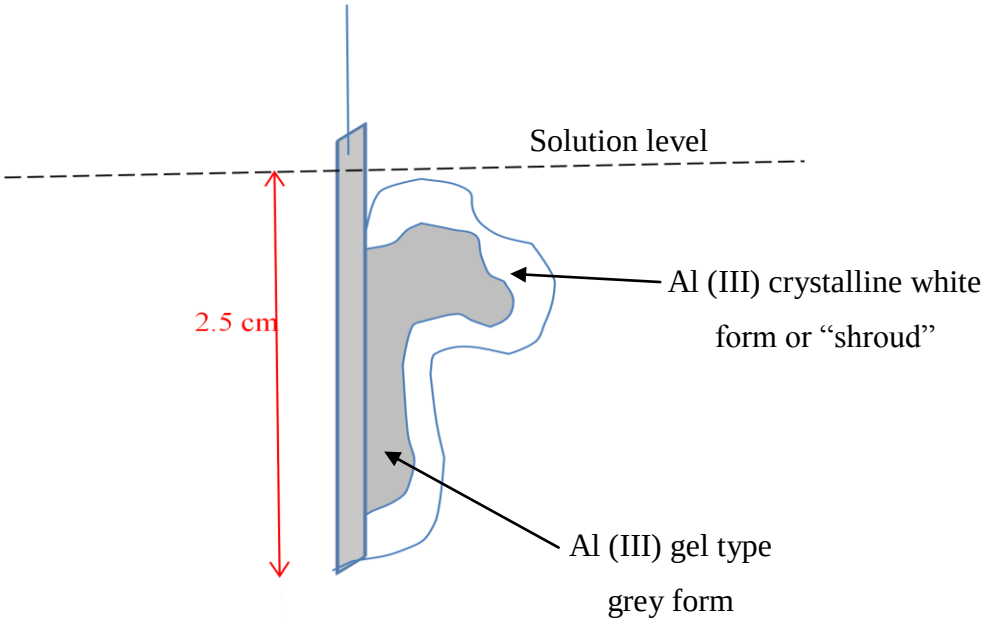

Figure 5.13: *I0 electrode and Al oxide / hydroxide on it at the end of the experiment.*

When a fresh electrode was used along with a reused electrolyte effectively the same charge could be passed for the same experiment. So despite some Al_2O_3 in the electrolyte, it did not decrease the electrolysis period. Similarly, when the alloy anode was washed with water and then tested in a fresh electrolyte, a very similar charge could be passed. There is no passivating film immediately on the alloy surface. Furthermore using an elevated temperature did not have any effect on the aluminium dissolution since a similar charge was passed, 1090 C/ cm^2, (see Table 5.3). When a reused electrode was used along with a fresh electrolyte but care was taken not to remove the Al (III) products attached on aluminium metal surface the electrolysis continued only to 120 C/ cm^2. The thick Al (III) 'shroud' on the alloy surface seems to limit the extent of Al dissolution. This conclusion is supported by an experiment where the dissolution was carried out in an ultra sonic bath. Using a fresh alloy anode and fresh electrolyte, the electrolysis continued until the charge passed was 1585 C/ cm^2. The ultrasound breaks up the 'shroud' to some extent.

These results show that neither the electrolyte nor the actual alloy surface pose any limitation for further aluminium dissolution. It appears that the formation of the 'shroud', the thick alumina deposit over the surface stopped aluminium dissolution. The

charge of ~ 1000 C cm^{-2} corresponds to the dissolution of ~ 0.1 g Al per cm^{-2} or Al (III) oxide/hydroxide equivalent to ~ 0.5 M Al (III) in solution. The former is the critical factor as the electrolyte can be reused until the cell is almost full of alumina/hydroxide crystals with only a slight increase in cell resistance.

5.7. The Al (III) product and impedance characteristics

In order to further understand the above results, an anodic dissolution reaction carried out at 170 mA cm^{-2} was stopped at intervals and the impedance determined on open circuit. The results from these experiments are shown in Figure 5.14. The charge transfer and the solution resistance were extracted from the all the bode plots shown in Figure 5.14 as is indicated on the bode plot before electrolysis. The terms could be related to the equivalent circuit in Figure 2.5 presented in the experimental section.

Before electrolysis the charge transfer impedance is approximately 100 ohms. Initially, after the first 300 seconds of the electrolysis the impedance of the alloy/electrolyte interface decreases to approximately 30 ohms (corresponding to activation and the formation of pits and perhaps the breakdown of the native alumina layer). After 3000 seconds the I0 alloy seems to have the best electrochemical performance since it dissolves with a cell voltage of ~1.6 V at 170 mA cm^{-2} and at the same time it has an impedance value of less than 6 ohms. At 6500 seconds the dissolution of aluminium still occurs smoothly but the voltage of dissolution along with the impedance seem to have slightly increased to ~ 9 ohms, implying that a surface layer has somehow evolved or developed. After the 8000 seconds of the experiment the charge transfer impedance value was enormous reaching values greater than 10^5 ohms and the layer formed on aluminium surface is illustrated in a schematic in Figure 5.13. Clearly, the increase in cell voltage results from the IR drop through this ‘shroud’.

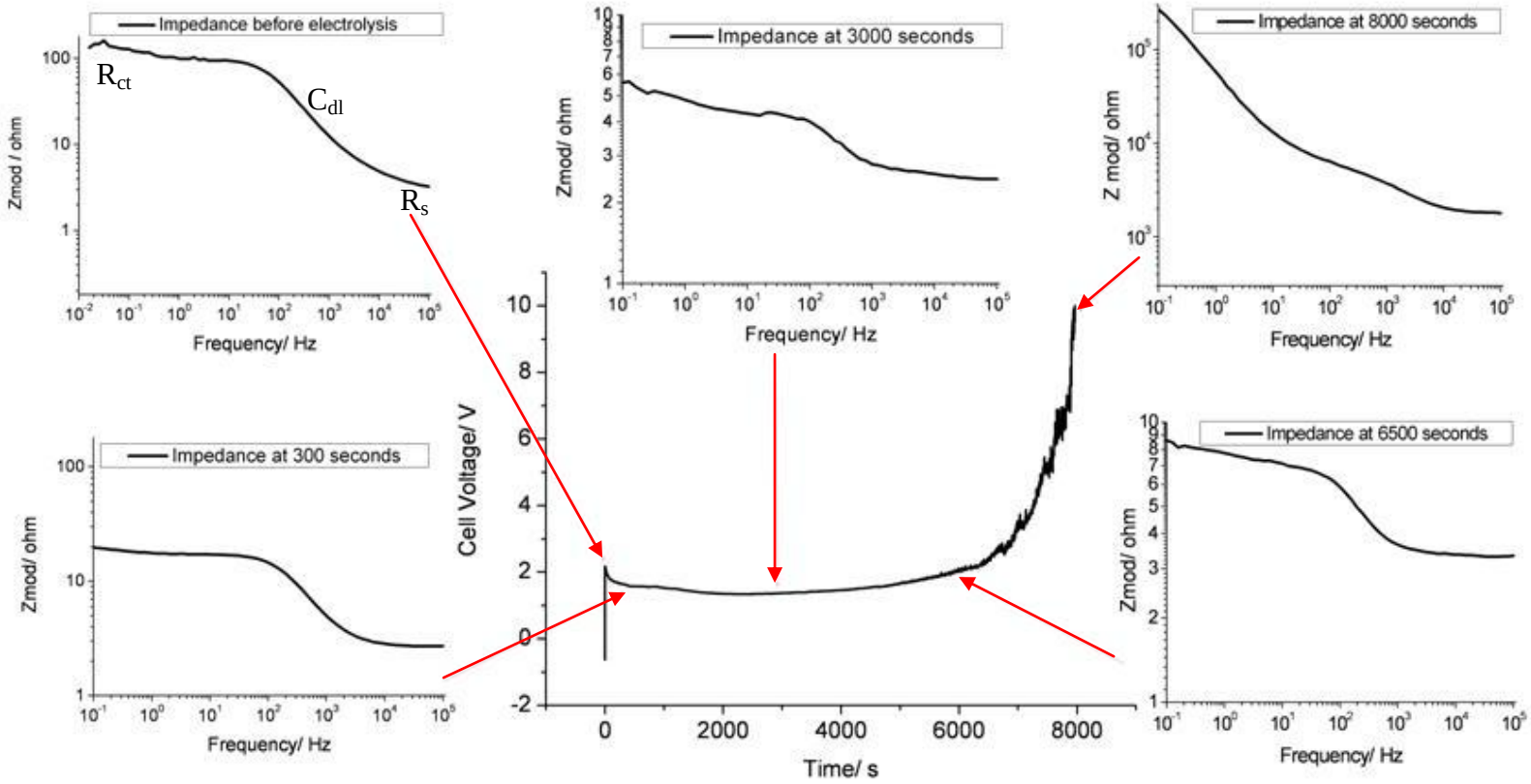

Figure 5.14: *Impedance measurements at several stages before during and after a chronopotentiometric experiment where 170 mA cm^{-2} were applied to I0 in 2 M NaCl at room temperature. The parameters R_{ct}, C_{dl} and R_s have been noted in one of the Bode plots.*

5.8. Structural characterisation of I0 during its dissolution in 2 M NaCl

The experiment was repeated with the same current density of 170 mA cm^{-2}. Cell voltage and electrolyte pH were monitored and the surface I0 alloy was observed under the SEM at 300, 3000 and 6500 seconds of the chronopotentiometry experiment in 2 M NaCl in order to try and correlate the SEM images to the electrochemistry. The backscatter detector, BEC, was used when Sn was to be located (though this was not always possible at small scales) and secondary electron detector, SEI, when features like the oxide layer or surface morphology were of interest.

5.8.1. The surface after 300 seconds of dissolution

During the first 300 seconds of the dissolution of aluminium at a current density of 170 mA cm^{-2} in the Perspex cell (see E-t transient in Figure 5.15), the cell voltage shifts to a lower value with time mirroring the activation noted in earlier chronopotentiometric experiment. The pH also shows a very slight increase from pH 7 to pH 9.2 during the 300 seconds.

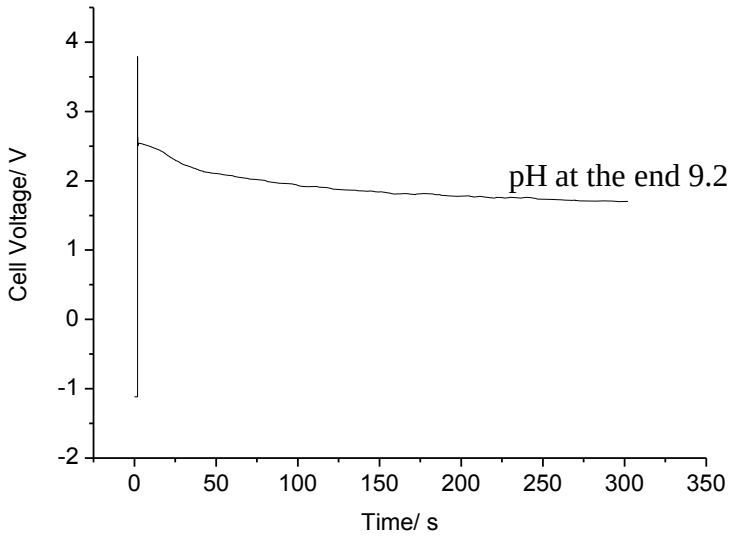

Figure 5.15: *The first 300 seconds chronopotentiometric response where a current density of 170 mA cm^{-2} was applied to I0 alloy in 2 M NaCl when stainless steel 904 L is used as the counter electrode.*

In Figure 5.16, SEM images of the surface of the I0 alloy at this point of the experiment are shown and big round pits can be seen. The images in the figure show the pit diameters are really large; >200 μm, for most of the pits but not many overlap so that there are areas on the Al alloy surface not yet corroded. In addition it seems like the pits are covered by a thin crust that starts "breaking" at several points where the pit surface looks deformed and "wavy". In Figure 5.16 c and d SEM images with the backscatter electron detector (BEC) have been obtained in order to ensure that the white parts of the surface are not Sn particles but oxide layer of the surface.

It has to be mentioned here that one cannot rule out that the breaking of the thin crust mentioned could be a result of dehydration of the corrosion product in the SEM vacuum. An attempt to characterize the anatomy of a pit was made. For that purpose the pit shown in Figure 5.16 d was used. In Figure 5.17 higher resolution images were used to characterise the pit and learn more about its morphology. In fact, this feature appears to be a complex collection of pits with evidence for the formation of new, smaller pits within the larger pit.

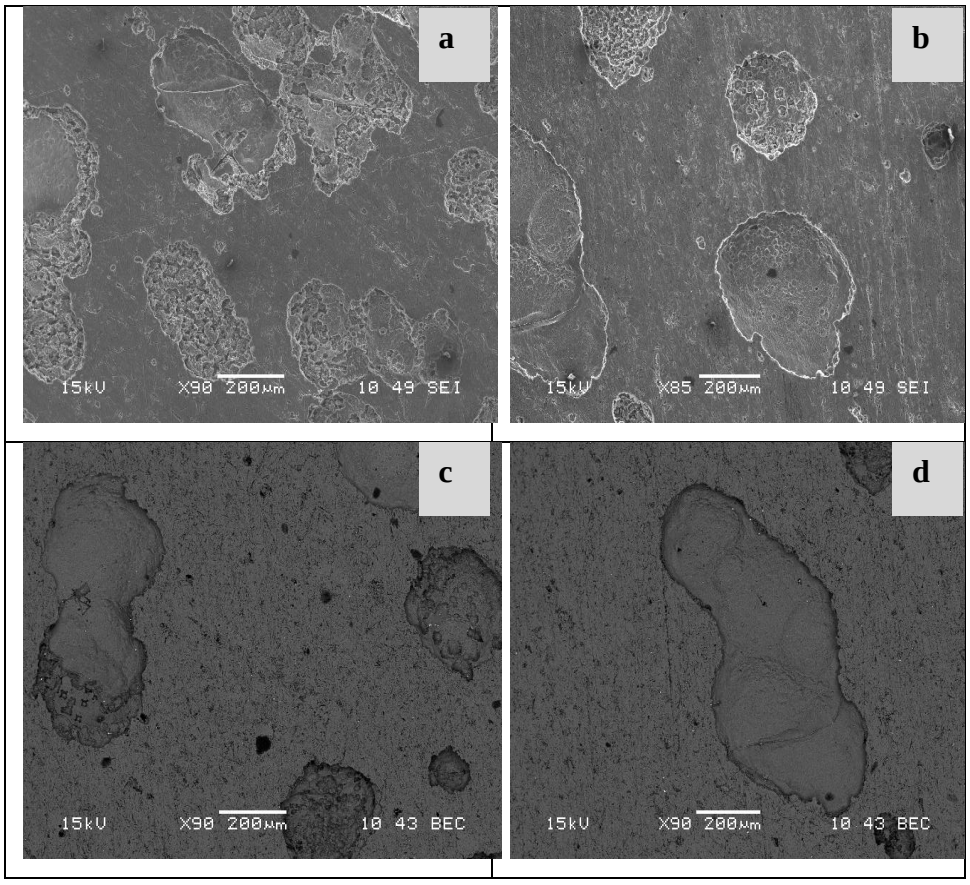

Figure 5.16: *SEM images captured from different parts of the surface of I0 alloy after 300 seconds of a chronopotentiometric experiment where a current density of 170 mA cm^{-2} was applied to it in 2 M NaCl:* ***(a)*** *and* ***(b)*** *are SEI images and* ***(c)*** *and* ***(d)*** *are BEC images.*

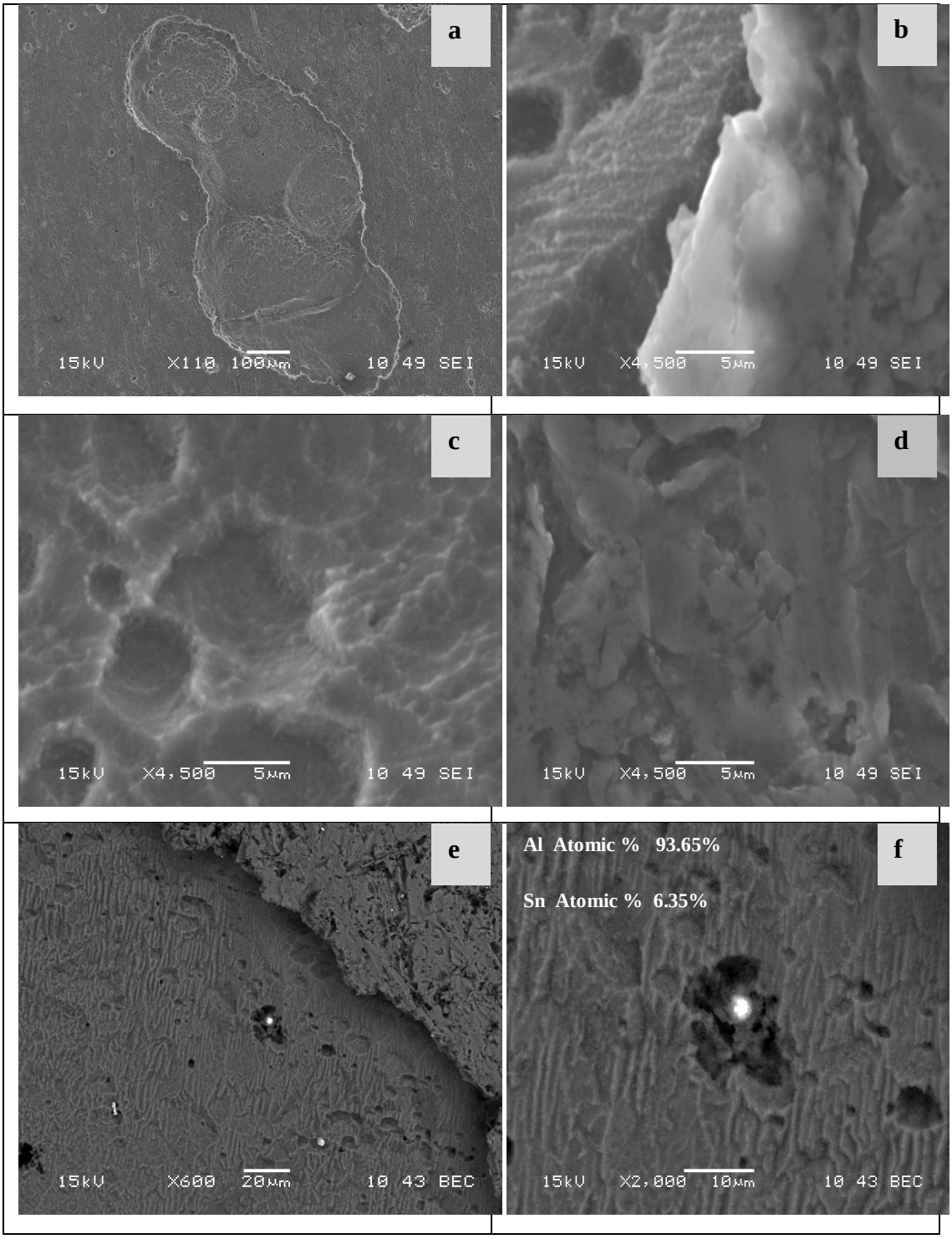

Figure 5.17: *SEM images to investigate pit **(a)** formed after 300 s of applying 170 mA cm^{-2} to I0 in 2 M NaCl: **(b)** High resolution image from an edge of the pit showing the white thick oxide layer surrounding the pit; **(c)** and **(d)** are images from different areas of the inside part of the pit showing that Al surface is "muddy" and "wavy". Image **(e)** shows the formation of a small pit of 20 µm diameter inside the big pit of ~ 200 µm diameter; higher resolution image **(f)** with the BEC detector and EDX analysis it was clearly showed that the pit is formed around a Sn centre.*

In Figure 5.17 the secondary electron image of the 'pit' investigated is shown. It can be clearly seen that there is a white "mark" around the pit. With the detector used, this results from charging of an oxide layer. To verify this conclusion, a higher resolution image of the edge of the pit was taken (see Figure 5.17 b). It can be clearly seen that at the edges of the pit a thick well formed oxide layer exists. Figure 5.17 c and d show areas inside the pit 5.17 where aluminium looks "muddy" and rough. In BEC images of Figures 5.17 e and f a small pit inside the big pit analysed is shown. Inside this small pit with approximately 20 μm diameter, a Sn centre of 2 μm diameter is spotted and analysed by EDX. Due to the size of the Sn inclusions, their presence can only be detected with the high resolution images.

5.8.2. The surface after 3000 seconds of dissolution

In Figure 5.18 the chronopotentiometric response for the first 3000 seconds of I0 dissolution at a current density of 170 mA cm^{-2} in the Perspex cell in 2 M NaCl is shown. After the initial change, the cell voltage remains constant but the electrolyte pH again shows a small increase. In Figure 5.19 representative collective series of SEM images of the surface of I0 alloy at that point of the experiment are shown.

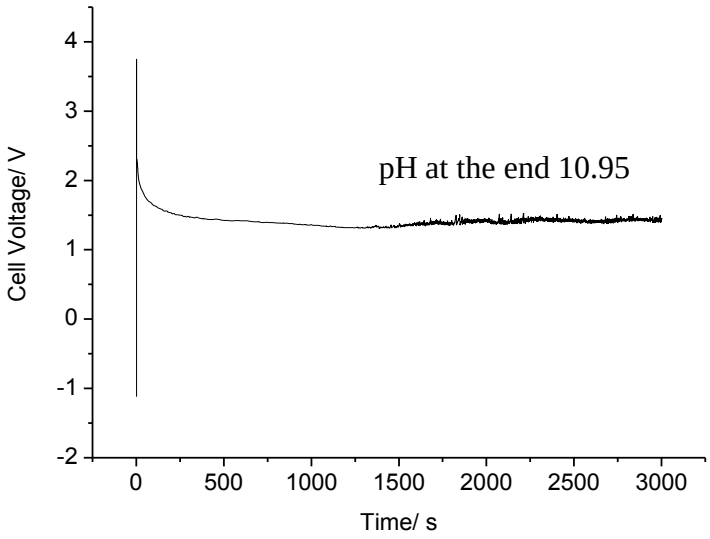

Figure 5.18: *Chronopotentiometric response of I0 alloy in 2 M NaCl when stainless steel 904 L is used as the counter electrode for the first 3000 seconds.*

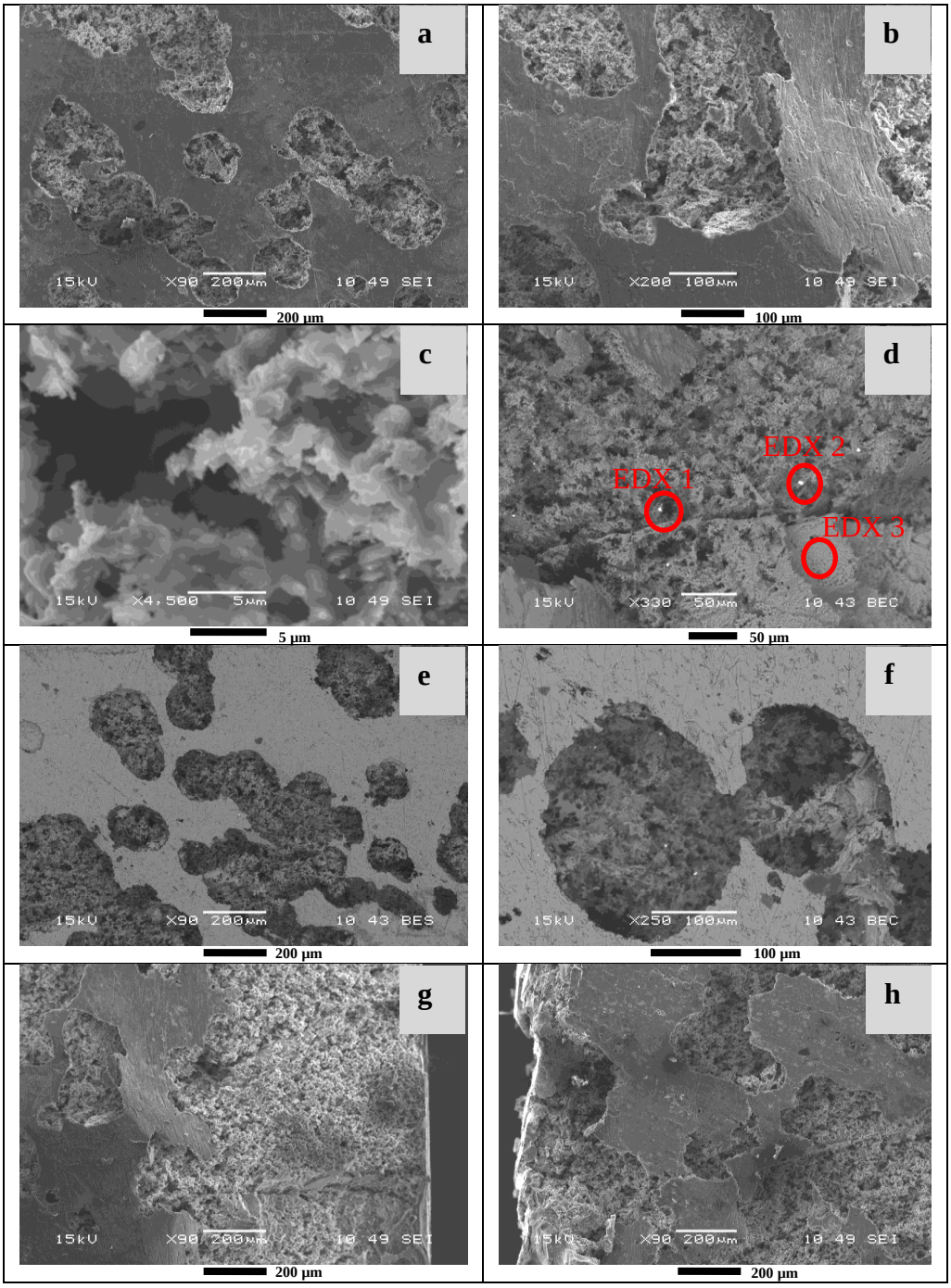

Figure 5.19: *SEM images captured from different parts of the surface of I0 alloy after a current density of 170 mA cm^{-2} was applied to it for 3000 seconds in 2 M NaCl. Images* ***(a)*** *and* ***(b)*** *are low resolution SEI image of different parts of the surface, showing big pits (~200 µm diameter).Image* ***(c)*** *shows the inside part of one of those pits that is consisted of a solid form of Al (III) oxide. Image* ***(d)*** *shows Sn particles inside a pit that is accompanied by the EDX analysis presented in Figure 5.23. Images* ***(e)*** *and* ***(f)*** *are BEC images of the surface captured to show the surface without the charging of the any oxide. Images* ***(g)*** *and* ***(h)*** *show the "edge effect" of the current where the alloy seems to dissolve more at the edges of the sample.*

From the images in Figure 5.19 a, e and f it can be observed that now the pits have become bigger and some overlap with each other. In addition the layer of Al (III) inside the pits looks thicker and more crystalline now than earlier in the experiment. In Figure 5.19 d an area of the I0 surface where it was uniformly deformed from dissolution is shown. The backscatter electron detector was used to capture the particular image and Sn particles were detected inside the "muddy" aluminium surface with EDX. In Figure 5.20 the EDX analysis of the two Sn particles and the crusty aluminium surface inside the red circles in Figure 5.19 are given.

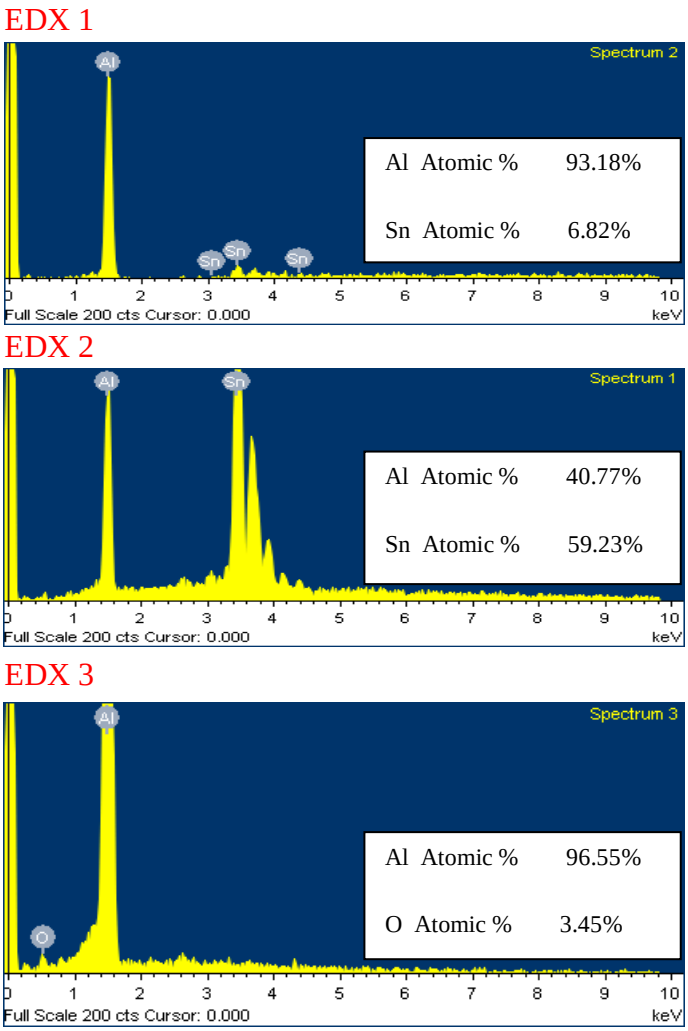

Figure 5.20: *EDX analyses for red spotted areas of Figure 5.19 d.*

From EDX analyses (see Figure 5.20) it is proved that the particles 1 and 2 in Figure 5.19 d are Sn. In addition EDX 3 shows that there is an oxide layer on the surface of alloy I0.In Figures 5.19 g and h it is shown that an edge effect exists since big part of the Al surface has been extensively dissolved at the edges of the sample.

5.8.3. The surface after 6500 seconds of dissolution

In Figure 5.21 the E-t transient when a current density of 170 mA cm^{-2} was applied to I0 in NaCl where stainless steel 904 L was used as the cathode is shown.

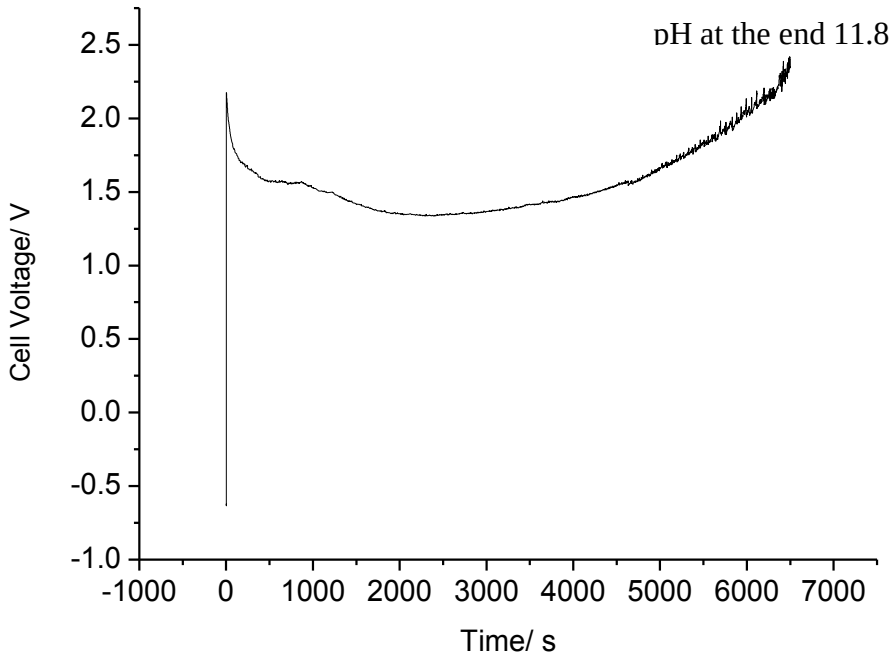

Figure 5.21: *Chronopotentiometric response of I0 alloy in 2 M NaCl when an anodic current of 170 mA cm^{-2} was applied for 6500 seconds.*

The cell voltage starts to increase after approximately 4000 seconds and the pH of the electrolyte shows a significant increase reaching pH 11.8 after 6500 seconds. The simple cell reaction:

$$2Al + 6H_2O \rightarrow 2Al(OH)_3 + 3H_2 \qquad \text{(R.9)}$$

does not fully represent the chemistry; the generation of OH^- at the steel cathode is exceeding the consumption of OH^- at the anode. This is a small effect but the pH change could have a major impact on the details of the Al (III) chemistry (e.g. the ratio of $Al(OH)_3/Al_2O_3$ or particle size). SEM and EDX analyses of the I0 surface were also carried out at that point of the dissolution.

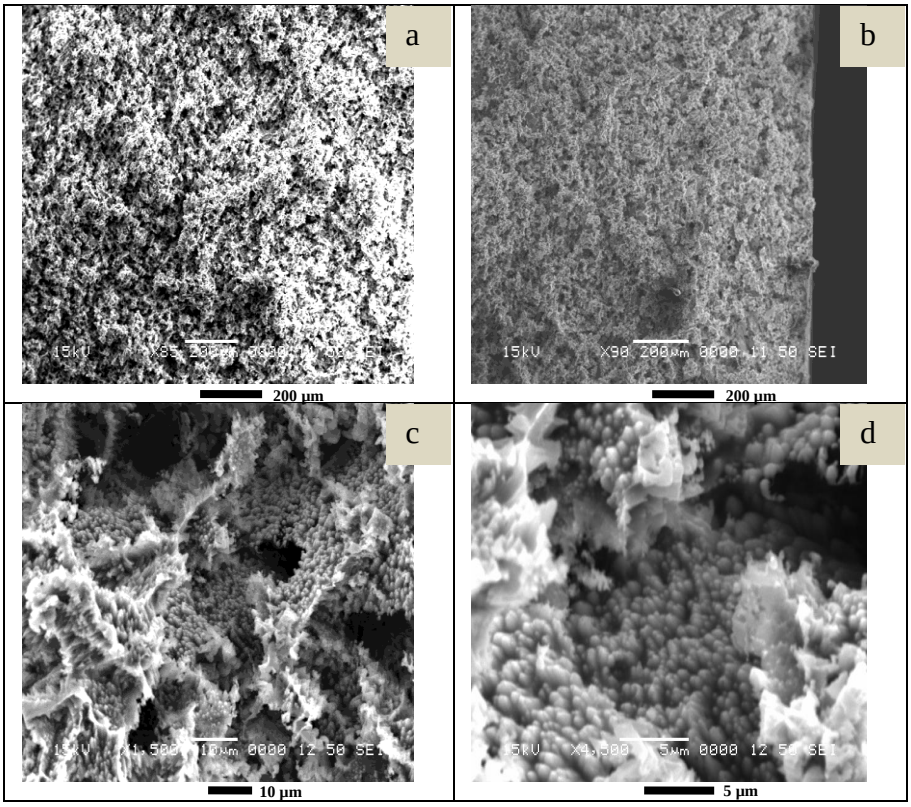

Figure 5.22: *SEM images captured from different parts of the surface of I0 alloy after a current density of 170 mA cm^{-2} was applied to it for 6500 seconds. Image* ***(a)*** *is a low resolution image showing the appearance of the surface after this experiment. Image* ***(b)*** *shows the edge of the sample. Image* ***(c)*** *is a high resolution image of the surface .Image* ***(d)*** *is a higher resolution image of image* ***(c).***

As it can be seen in the SEM images of Figure 5.22 a and b the surface after the first 6500 seconds of the experiment seems to be totally deformed due to the quantity of aluminium dissolved. Images 5.22 c and d show a closer version of the surface of aluminium after 6500 seconds of the experiment. Looking at the SEM pictures, the electrochemistry, the high pH (11.8) value of the solution after the 6500 seconds of the experiment and impedance characteristics it could be concluded that some form of the solid oxide layer had been formed on the surface of the alloy I0 (since the shroud and gelly Al (III) were removed and the electrode was rinsed and dried before the SEM session). EDX analysis was carried out on a high resolution image to investigate the composition of that surface. In Figure 5.23 the enlarged image of Figure 5.22 d is shown. From the EDX analysis it is shown that the oxide seems to include Mg. It must be remembered, however that once the shroud is removed, a further discharge is possible, see Table 5.3. Hence the surfaces pictured in Figure 5.22 remain active for further dissolution.

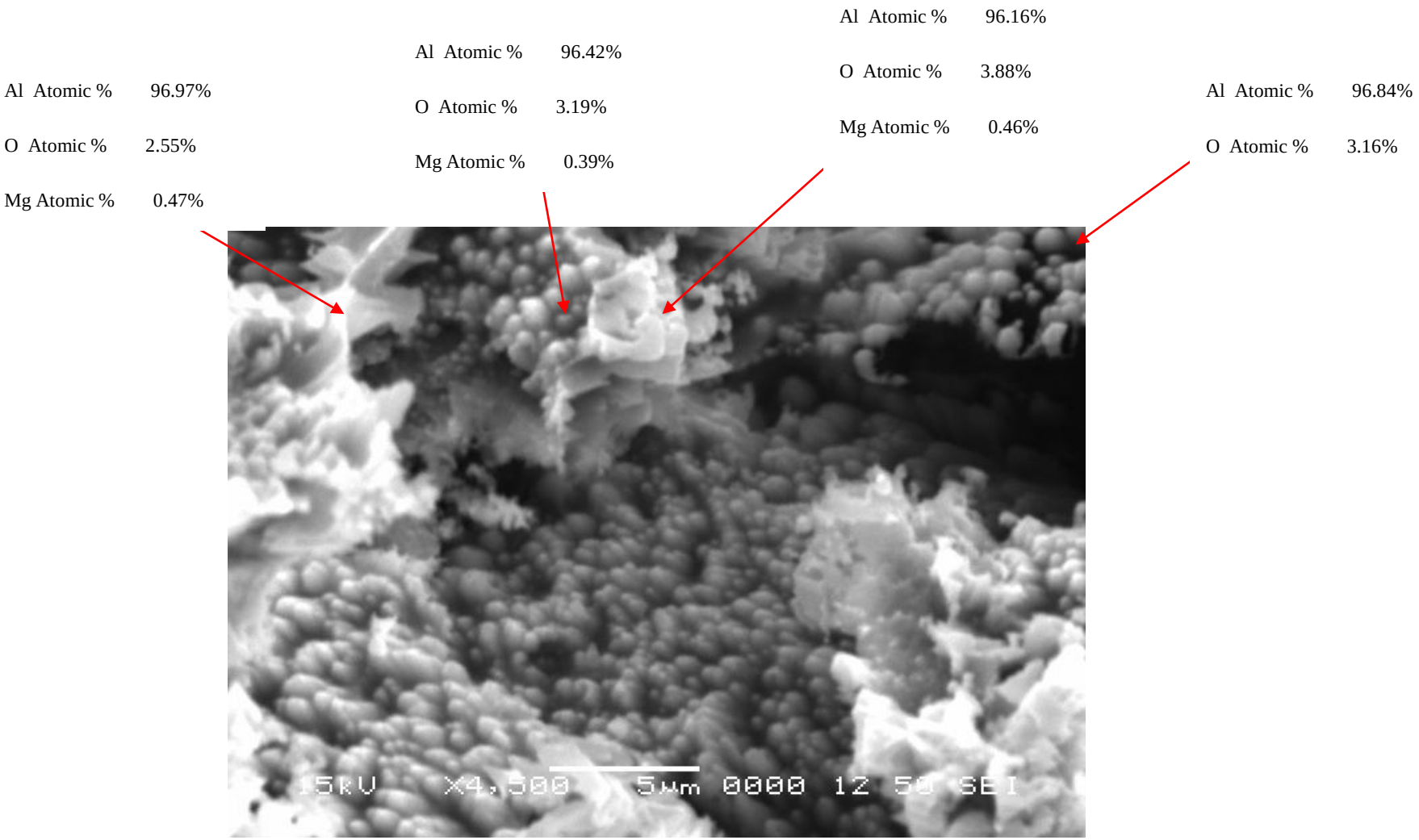

Figure 5.23: *High magnification (x 4500- scale bar 5µm-enlargement of Figure 5.11 (h)) image of a surface of I0 after the alloy had been imposed at a current density of 170mA cm^{-2} for 6500 seconds in 2 M NaCl.*

5.9. Cross sections of I0 and EDX mapping of the pits

Crossectional SEM images were taken for the same samples after the shroud had been removed, (see Figure 5.24). The cross sections show that less than 20 μm of the aluminium have been lost over a limited fraction of the surface after the first 300 seconds. At 3000 s when the aluminium was dissolving with the lowest voltage,(as it was shown earlier in this thesis) and the pits on the surface had fully evolved and started overlapping as it was shown earlier, it was shown from crossections that some of them are as deep as 200 μm. At 6500s when it was shown from surface SEM images that the surface seems was highly porous and had a rough structure, the cross section showed that the pits overlapped and cover the whole surface.

Crossections at: 300s 3000s 6500s

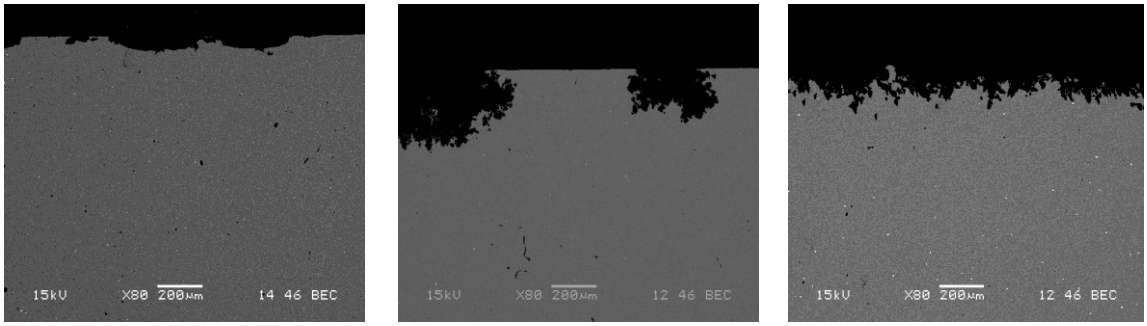

Figure 5.24: *Crossection SEM images of I0 alloy at different times after the imposition of 170 mA cm^{-2} in 2 M NaCl.*

EDX mapping was carried out at these cross sections for Al (pink colour) and oxygen (yellow colour). All three images in Figure 5.25 show the presence of aluminium and oxygen over much of the alloy surfaces at each of the three stages of dissolution. The intense pink colouration areas shown in Figure 5.25 at the bottom and the edges of the pits seemed to have the highest concentration of the Al (III) oxide/ hydroxide product.

EDX Mapping at: 300s 3000s 6500s

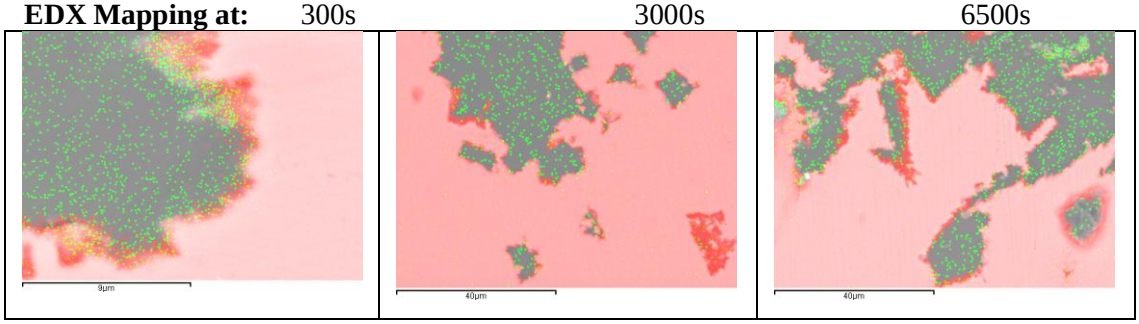

Figure 5.25: *EDX mapping for oxygen (yellow colour) and aluminium (pink colour) of crossections of I0 alloy at different times after the imposition of 170 mA cm^{-2} in 2 M NaCl.*

5.10. Dissolution of I0 alloy in various electrolytes

The AlMgSnGa alloy, I0, was dissolved anodically at a current density of 170 mA cm^{-2} in 2 M NaCl, 2 M NaCl + 0.01 M NaOH, 2 M NaCl + 0.1 M NaOH, 2 M NaCl + 1 M NaOH and 2 M NaCl + 0.001 M HCl in the small Perspex cell using always steel 904L as the counter electrode for the reaction. The charge density passed in these experiments and the dissolution time for each solution for the alloy I0 are given in Table 5.4.

Table 5.4. *Results from dissolution of I0 alloy in different solutions. The times reported are those when the cell voltage reached 3 V.*

Solution	Time/ s	Q/ C cm^{-2}
2 M NaCl	6200	1090
2 M NaCl + 0.01 M NaOH	2160	367
2 M NaCl + 0.1 M NaOH	2600	442
2 M NaCl + 1 M NaOH	2700	460
2 M NaCl + 0.001 M HCl	4400	748

From the results in Table 5.5 it can be seen that the highest charge density was passed in the NaCl solution. In all the alkaline solutions the charge densities passed were increasing with increasing concentration of NaOH. At very high NaOH concentrations (8M), the Al (III) is soluble as $Al(OH)_4^-$ but at low OH^-, especially where $\frac{[Al(III)]}{[OH^-]} \ll 1$

$Al(OH)_4^-$ formation is unlikely and the OH^- may lead to a more passivating layer on the Al surface. Such a conclusion is consistent with results in the Section 5.8.

By looking at the data of Table 5.4 it is clear that the addition of acid or alkali does not have any benefit for aluminium dissolution. I0 when dissolved in 2 M NaCl passed a charge density of 1090 C cm^{-2} which is higher than in all other solutions presented in Table 5.4. The Al alloy is also more stable to corrosion in 2 M NaCl, see Chapter 4.

5.11. Effect of electrolyte volume in I0 dissolution

During the earlier experiments with small electrodes and large electrolyte volumes (Chapter 4), all the alloys appeared to dissolve anodically. This contrasts totally with the observations in the small volume cell. Hence, it was interesting to see whether larger alloy electrodes would dissolve more in "unbound" larger electrolyte volumes. The experiment was carried out in a usual 100 ml beaker. The electrodes were however not touching the bottom of the beaker and had a distance of 5 cm between them. In contrast to the Perspex cell where the electrodes had a 2 cm interelectrode gap between them and were touching the bottom of the cell. In Figure 5.26 the chronopotentiometric response of I0 in 2 M NaCl, when dissolved at a current density of 170 mA cm^{-2}, in the two different cells, (Perspex and beaker), is shown.

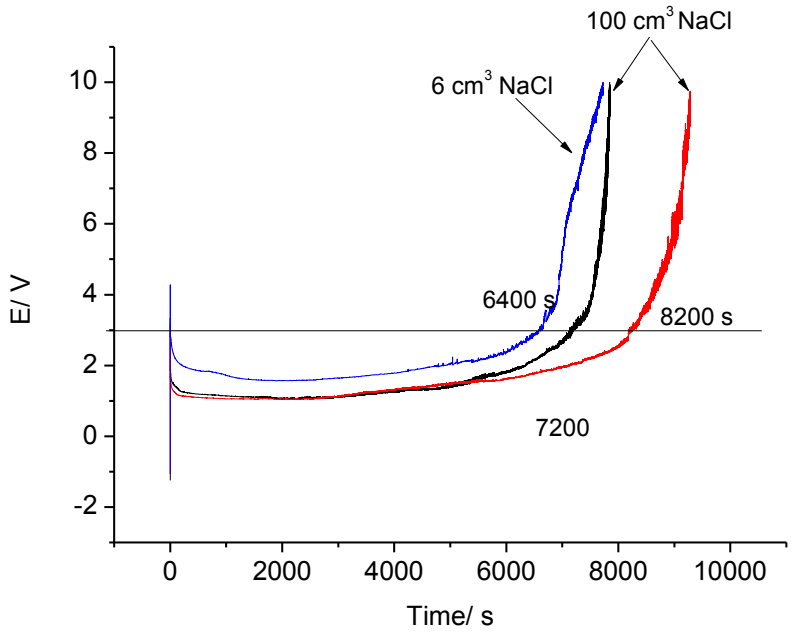

Figure 5.26: *Chronopotentiometric response of I0 alloy when it was subjected to a current density of 170 mA cm^{-2} in 2 M NaCl. The blue curve shows the response in a small perspex cell; the black and red curves are replicate experiments carried out in a 100 ml beaker.*

It was noted that because the Al sample was not touching the bottom of the beaker, much of the insoluble Al (III) material fell to the base of the cell. There was, however a heavy deposit again attached to the surface of the Al alloy.

From the Figure 5.26 it can be seen that the two curves resulting from the two replicate experiments in the beaker are very similar. The slight difference of the curves for the repeat experiments is believed to be due to the difficulty in encapsulating the Al electrode.

In the Perspex cell, the back of the electrode and the edges were insulated but they were also attached to the walls of the cell. That was not the case in the beaker where the electrodes were exposed to the electrolyte from all the sides. The minor dissimilarity in the two beaker experiments might mean that somehow electrolyte had penetrated the insulation layer and more Al was dissolved in one experiment than the other.

The extent of dissolution of aluminium does not change significantly with the volume of electrolyte and it is concluded that the electrolyte volume does not limit the extent of aluminium dissolution.

5.12. Dissolution of AB50V in different temperatures

A series of preliminary experiments were carried out where 170 mA cm^{-2} was applied but where the anode electrode was AB50V, the cathode was stainless steel 904 L and the electrolyte was 2M NaCl (6 cm^3). The experiments were conducted in different temperatures of 333, 313, 333 and 353 K. In Figure 5.27 the results from these experiments are shown.

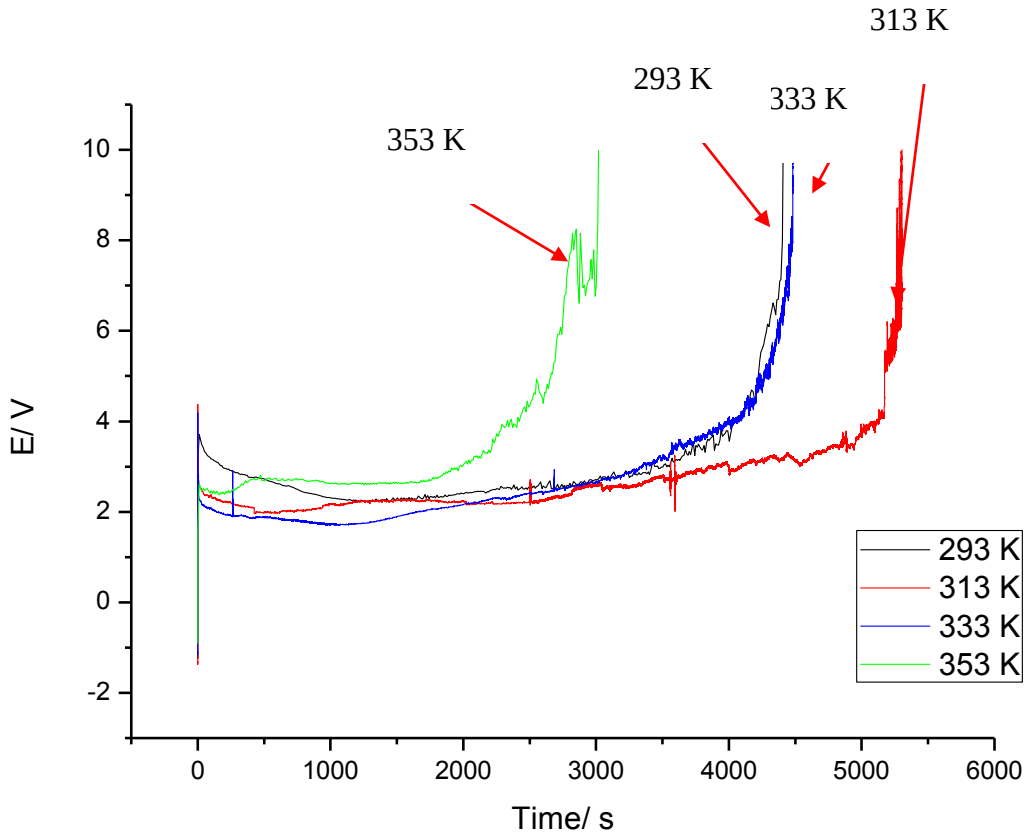

Figure 5.27: *Chronopotentiometric response of AB50V alloy when it was subjected at a current density of 170 mA cm^{-2} in 2 M NaCl at various temperatures.*

It has to be mentioned here that the AB50V electrode was much thinner than the I0 electrode (~ 0.5 mm) which made it much more difficult to make sure that the edges of the electrode was insulated. In additional the experiments were not repeated so the results are provisional. In Figure 5.27 it is shown that the response in all temperatures is quite similar with the exception of the experiment at 353 K that terminates over a lower charge density compared to lower temperatures. There is clearly no trend with temperature but it is possible that the Al (III) chemistry undergoes complex changes with temperature.

5.13. Al – air battery application

It was concluded from Chapter 4 that superior anode materials were AlMgSnGa alloys. They were the most stable to corrosion on open circuit but dissolve anodically at a high

rate in a NaCl based electrolyte. Considering the operation of an Al-air battery using such anode materials the factors that limit the dissolution of aluminium were investigated by using a model laboratory battery (as presented earlier in this chapter) and doing experiments in a Perspex cell mimicking the situation in a battery employing though as a cathode a stainless steel electrode. The Al (III) product of the discharge reaction was considered and correlated to the performance of the electrolysis cell mimicking a power source. The commercial Pt/C oxygen air electrodes presented earlier in this section were used for preliminary battery experiments. In Figures 5.28 a and b voltammetry curves are shown for oxygen reduction on Pt/ C electrodes with 4.6 mg/cm^2 Pt loading along with the voltammetry of pure aluminium in 2 M NaOH and AB50V alloy in 2 M NaCl.

In Table 5.5 the potentials of the Al oxidation and oxygen reduction reactions are given along with the voltage of the cell if the respective electrodes and electrolytes were to be used in a battery. The performance of the oxygen cathode in 2 M NaCl is poor and decays strongly with increasing current density. This is clearly reflected in the cell voltages calculated in Table 5.5.

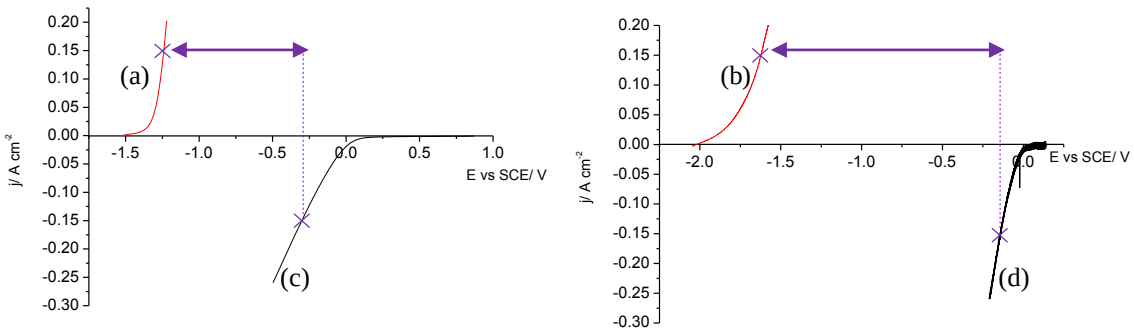

Figure 5.28: *Voltammetry of oxidation of* ***(a)*** *AB50V in 2 M NaCl and* ***(b)*** *pure Al in 2 M NaOH at room temperature and oxygen reduction on Pt/C gas diffusion air electrodes in* ***(c)*** *2 M NaCl and* ***(d)*** *2 M NaOH at 353 K. Oxygen flow rate was 200 cm^3/min. By the purple arrows on the graphs the voltage of a battery in the respective medium is shown at a current density of 150 mA cm^{-2}.*

Table 5.5. *Potential values for Aluminium oxidation and oxygen reduction obtained from voltammetry curves and battery voltage calculated according to the individual potential values for a basic and an acidic Al-air battery.*

j/ A cm^{-2}	Al oxidation E *vs* SCE/ V		O_2 reduction on Pt/C E *vs* SCE/ V		$*E_{Cell}$ / V	$*E_{Cell}$ / V
	Pure Al in NaOH	AB50V in NaCl	NaOH	NaCl	NaOH	NaCl
0.01	-1.95	-1.34	-0.01	0.037	1.94	1.377
0.1	-1.67	-1.24	-0.11	-0.205	1.56	1.035
0.15	-1.60	-1.2	-0.18	-0.298	1.42	0.902
0.4	-1.41	-1.15	-0.29	-0.75	1.12	0.4

* The IR drop in the battery is not included in the voltage calculation

From the discharge curve (see Figure 5.1) of a model aluminium battery at 20 mA cm^{-2} in 2 M NaCl using Pt/C (with 4.66 mg cm^{-2} of Pt catalyst printed) cathode and the I0 alloy as the anode, it was shown that the battery operated at 20 mA cm^{-2} giving a voltage close to 1.2 V for 3 hours.

The charge passed of 700 C cm^{-3} of electrolyte was equivalent to the formation of an "Al (III) concentration in solution" of approximately 1 M although in fact some solids were formed. By lowering the current in stages it was even possible to continue operating at 1 V for 8 hours when 1000 C cm^{-3} had been passed. The cell voltage was, however low compared to the expected value approaching 2 V based on earlier experiments with the Al alloy confirming limitations by the oxygen cathode.

5.14. Conclusions

Despite the identification of an Al alloy capable of dissolution at very high current densities (> 250 mA cm^{-2}), a high power and energy density Al-air battery with a brine electrolyte remains beyond present technology. The performance of the air cathode in neutral sodium chloride is way below that required especially at ambient temperature. In addition, it remains necessary to find a way to prevent the Al alloy anode from ceasing

to perform after a charge density of 1000 C cm^{-2} without increasing the weight of electrolyte in the battery. More detailed conclusions follow;

- The performance of Al-air model battery in 2 M NaCl is limited both by the O_2 cathode and the extent of dissolution of Al alloy.

- In brine, the ORR occurs with large overpotential and a large current density could not be achieved. Reasonable cathode performance was limited to $<$ 10 mA cm^{-2}.

- The charge that can be passed for the anodic dissolution of I0 is independent of the current density and is typically 1000 C cm^{-2} and is independent of the electrolyte volume and immediate aluminium metal surface.

- Impedance results before dissolution show that there is a film, most probably very thin, on aluminium surface which has broken down at the 300 s.

- The best electrochemistry of the aluminium was obtained at ~ 3000 s, where the impedance had the lowest value and the cell voltage was also lowest. At this time, a large number of pits cover the whole surface.

- After 6500 s the impedance and cell voltage seem to increase along with the oxide/hydroxide layer on Al surface that by that time is easily observable by eye.

- From the depth of the pits crossections images showed that by 300 s ~20 μm of Al surface were lost, by 3000 s ~ 100-200 μm and by 6500s a whole layer of the surface seems to have dissolved.

- There is no benefit in terms of charge density obtained from I0 dissolution from the addition of acid or base to NaCl.

CHAPTER 6 Optical microscopic observations

The corrosion and anodic dissolution of the AlMgSnGa alloys were observed by optical microscopy using the equipment sketched in Figure 6.1. The cell is more fully described in the experimental section. A Photron APX-RS high speed camera fitted with a Navitar 12x lens with a x2 extension tube and x2 lens adaptor was employed to image the surface of the electrode at a variety of frame rates. The camera had solid state memory (6 Gb) which allows considerable time periods (e.g. 240 seconds at 50 frames per second and 768 x 672 pixels) to be acquired. The data was then transferred to a PC through a fire wire connection. These images were then processed/analysed to elucidate mechanisms occurring on the electrode surface. Lighting of the sample was critical and a 150 W cold light source proved adequate (SCHOTT – KL 1500).

The areas of the Al alloy samples used ranged from 0.008 mm^2 to 0.1 mm^2 and these were exposed to the 2M NaCl electrolyte. This size of the working electrode was a compromise between (a) the resolution of the microscope that would not allow observation on a 1-10 μm scale and (b) the desire to employ samples with only a few Sn centres and to define precisely the position of the Sn centres on the surfaces before and after the experiments; from the SEM images reported in Figure 4.11 it is to be expected that the electrodes fabricated from the alloy I0 would have ~ 10 Sn inclusions with dimensions ~ 5 - 10 μm (c) the form of the materials available for fabrication of the electrodes. In reality, not all the Sn centres in the surface (typically 1 – 2 μm, see Chapter 4) could be identified because of scale of the observation. Also on the timescale of these experiments, Sn centres might be exposed and/or lost into solution by dissolution of surrounding aluminium.

The equipment required that the Al alloy surface was pushed right up to the optical window. This led to the difficulty that gas bubbles were easily trapped in the gap. While on the video it was easy to distinguish stationary bubbles and a stream of bubbles, this is not easy to show in a series of single frames. Indeed other features are more clearly seen on the video and, here, are reported in words. It should also be noted that the focusing of the camera and arranging the illumination took approximately half an hour while the

Al electrode was in solution on open circuit. In consequence, all the experiments are for a surface already changed by corrosion for this period of time. It may well be that this period of open circuit corrosion determines the site of dissolution during the chronopotentiometry experiments.

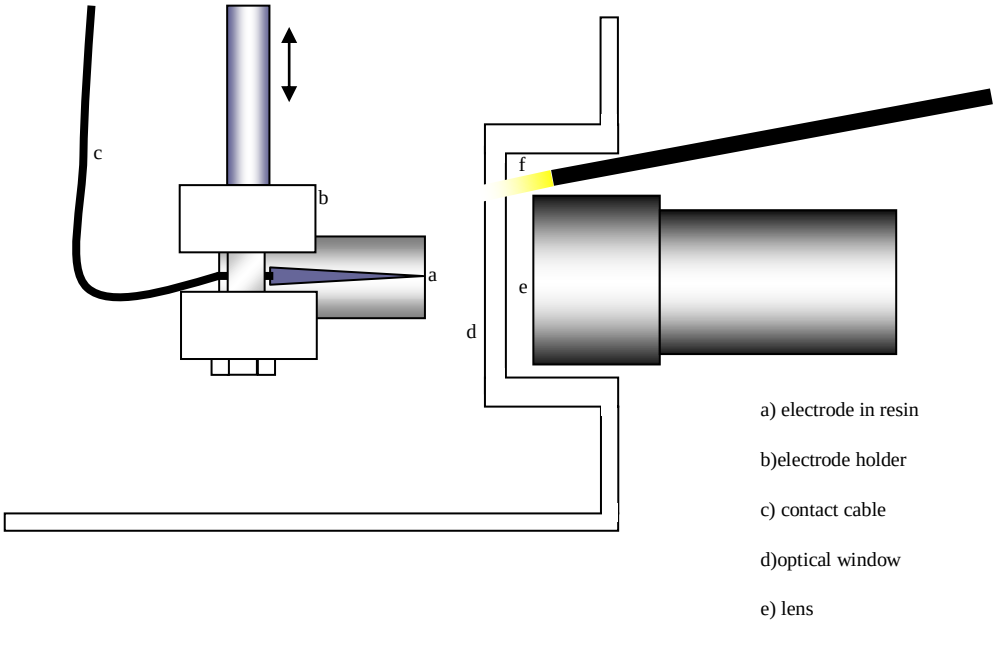

Figure 6.1: *Configuration of Al electrode, cell optical window and lens during camera experiments.*

6.1. Corrosion at open circuit potential

During the corrosion tests presented in Chapters 3 and 4 of this thesis, no H_2 evolution from the AlMgSnGa alloys was observed by eye within the first hour of the experiments. The optical microscope allows in situ observation at a much higher resolution.

The first experiment used a sample of the alloy AB50V with area 0.057 mm^2. Firstly an SEM picture was taken before the experiment in an attempt to locate the Sn centres on the surface by EDX. In Figure 6.2 a, an SEM image of a lightly polished sample of AB50V alloy is shown; the red circles show the areas where Sn particles have been

located. Then a camera picture of the dry alloy was taken before the electrolyte was poured in the cell, (see Figure 6.2 b).The picture of the dry alloy with the optical microscope confirms that there are no pits on the surface of the alloy. Afterwards the 2 M NaCl solution was poured in the cell, the camera was focused and then the electrode behaviour was monitored on open circuit. Some frames of this video taken on open circuit for AB50V alloy are shown in Figures 6.2 c and d.

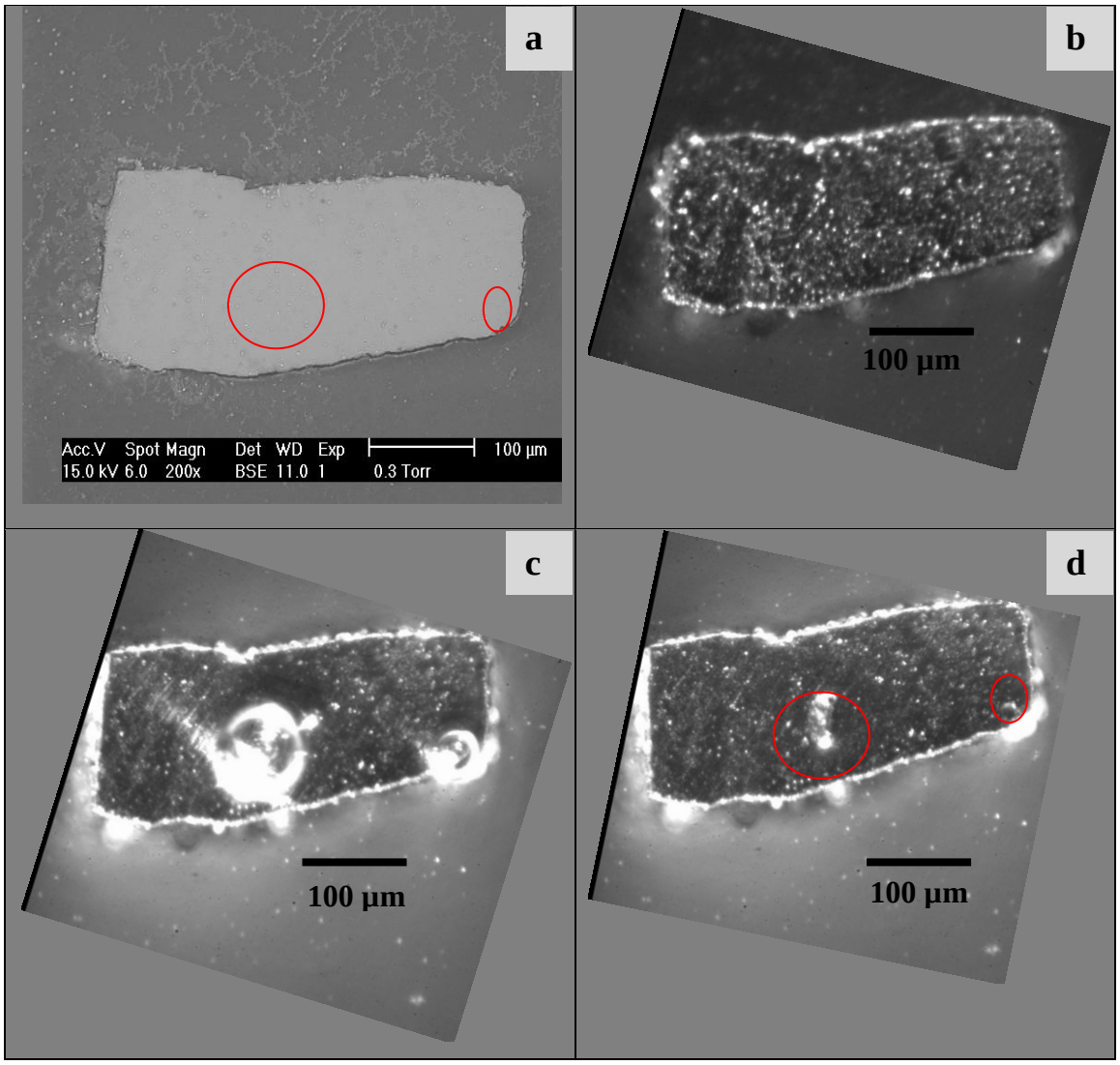

Figure 6.2: ***(a)*** *SEM image of a polished AB50V sample before the experiment showing in the red circles the two areas of the alloy where Sn centres were located by EDX,* ***(b)*** *Camera picture of the AB50V dry sample before the experiment,* ***(c)*** *bubbles on two spots only from the surface of AB50V alloy being at OCP in 2 M NaCl,* ***(d)*** *AB50V alloy after a few minutes on OCP showing two pits (inside the red circles) on the areas of the surfaces where from the bubbles where evolved.*

It can be seen that two hydrogen bubbles formed and grew on aluminium surface on open circuit and when the hydrogen gas was dislodged after about an hour on open circuit two pits were formed, (Figure 6.2 d). By looking at the images in Figure 6.2 it can be seen that the hydrogen bubbles and the pits were formed where the Sn centres where located before the experiment.

A similar experiment on open circuit was carried out with a sample of I0 alloy with an area of 0.01 mm^2.The SEM picture was taken before the experiment and the Sn centres on the surface were located by EDX. In Figure 6.3 a, an SEM image of a slightly polished sample of I0 alloy is shown; only a single Sn inclusion could be located in the red circle. Then a camera picture of the dry alloy was taken before the electrolyte was poured in the cell, (see Figure 6.3 b), confirming that there were no pits on the surface before the experiment started. Afterwards the NaCl solution was poured in the cell, the camera was focused and then the electrode behaviour was monitored on open circuit. Some frames of this video taken on open circuit for I0 alloy are shown in Figures 6.3 c and d. In Figure 6.3 c, a camera picture of the I0 on open circuit in 2 M NaCl is shown where some hydrogen has formed on the surface. However it is important to mention here that the alloy has been in the electrolyte already for 40 minutes when this picture was taken and this is the reason that a pit has already formed in the middle of the alloy. After dislodging the hydrogen bubbles, two other pits are visible where the hydrogen bubbles were formed. It is worth noting that there was hydrogen formation originating from the middle part of the surface where a pit formed after about 30 minutes; however this pit stopped evolving hydrogen for some reason for the rest of the experiment (passivation) and hydrogen was formed only from the other two pits shown in Figure 6.3 d. By looking at the images in Figure 6.3 a and d it can be seen that at the location where the middle pit was formed on I0 surface a Sn centre where located before the experiment by EDX. Sn centres were not located before the experiment where the other two pits were formed, however as it was shown by SEM and TEM in Chapter 4, Sn centres can be smaller than 1 μm in which case would not be visible by the SEM used here. It has been proved from the work in this project (Chapter 4 mainly) that pits in the AlMgSnGa alloys form around Sn centres. For that reason it is strongly believed that Sn centres exist in all the areas of the alloy where pits formed during the experiment.

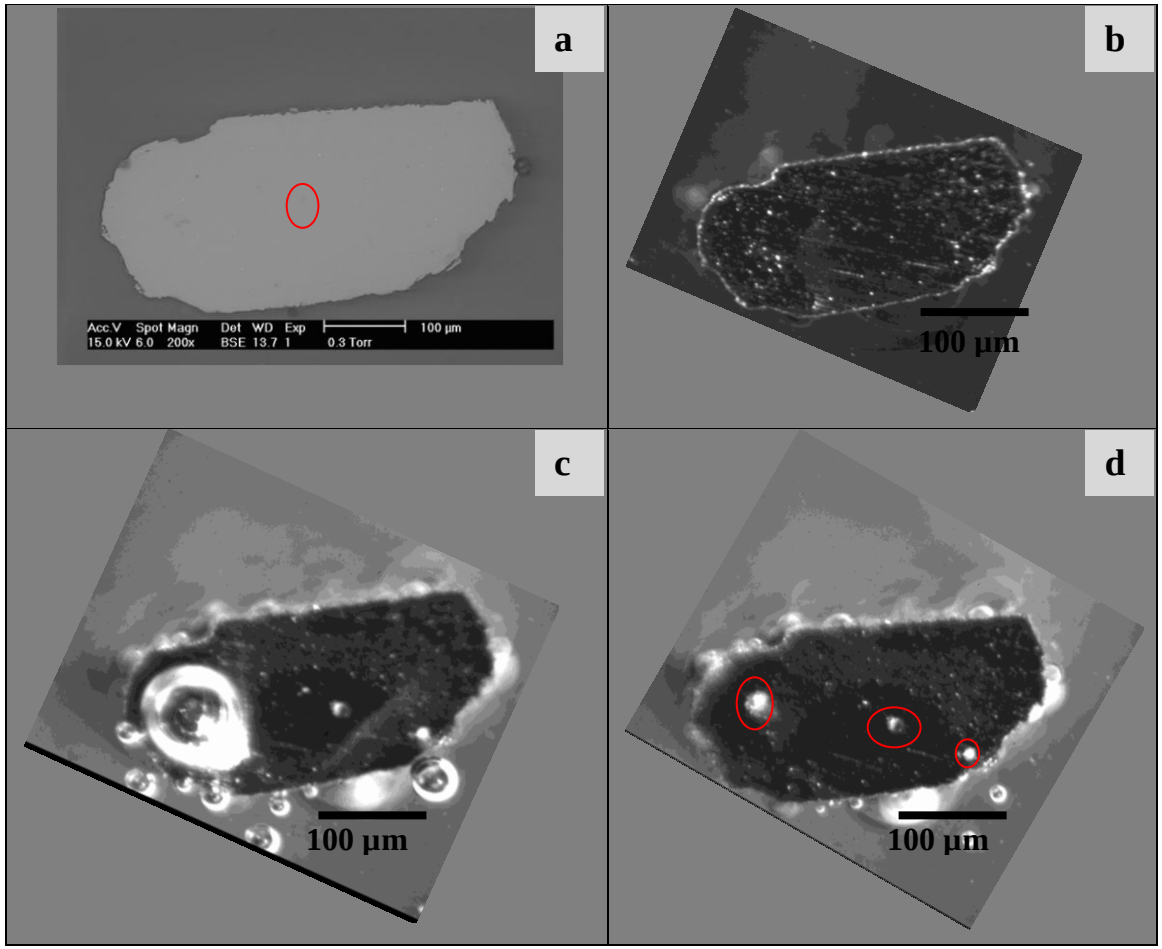

Figure 6.3: ***(a)*** *SEM image of a polished I0 sample before the experiment showing in a red circle where a Sn centre was located by EDX,* ***(b)*** *Camera picture of the I0 dry sample before the experiment,* ***(c)*** *bubbles on a few spots only from the surface of I0 alloy being at OCP in 2 M NaCl,* ***(d)*** *Camera picture of I0 alloy after a few minutes on OCP showing few pits (inside the red circles) on the areas of the surfaces where from the bubbles where evolved.*

Overall from the results of open circuit corrosion tests of the alloys AB50V and I0 it is concluded that Sn centres are acting as cathodic centres catalysing the reaction:

$$2H^+ + 2e^- \rightarrow H_2 \quad \text{(R.7)}$$

The Al dissolution then occurs around the Sn centre to minimize IR drop between anodic and cathodic sites:

$$Al \rightarrow Al(III) + 3e^- \quad \text{(R.1)}$$

6.2. High current densities

An I0 electrode of 0.04 mm^2 area was polished and then viewed under the backscatter detector of the SEM. In Figure 6.4 the resulting SEM image is shown and the Sn centres with size ranging from 1.45 to 5 μm are emphasized with red circles. An experiment where a current density of 50 mA cm^{-2} was applied to this I0 sample in 2 M NaCl followed.

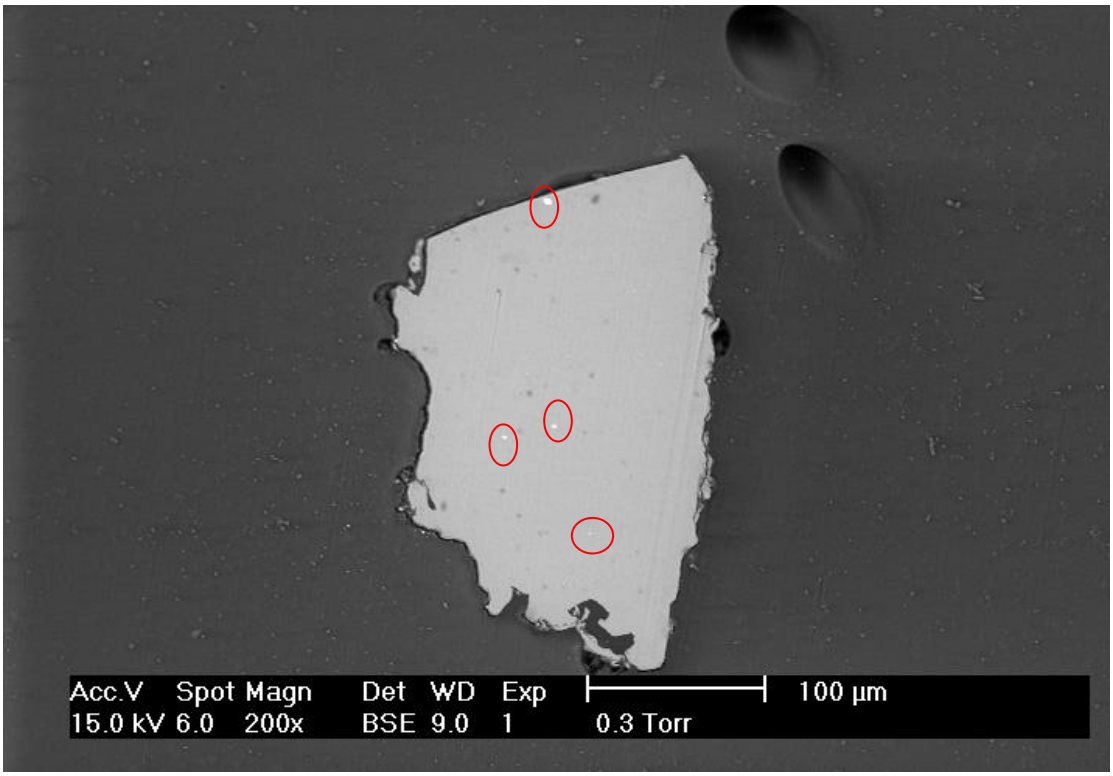

Figure 6.4: *SEM image of a polished sample of I0 alloy. Sn centres have been detected by EDX and marked in the red circles of the image.*

In Figure 6.5 a series of camera pictures showing the surface of the I0 alloy when such a current density was applied to it are shown. In Figure 6.5 a, a picture of the I0 alloy in the 2 M NaCl solution is shown just before the experiment was started.

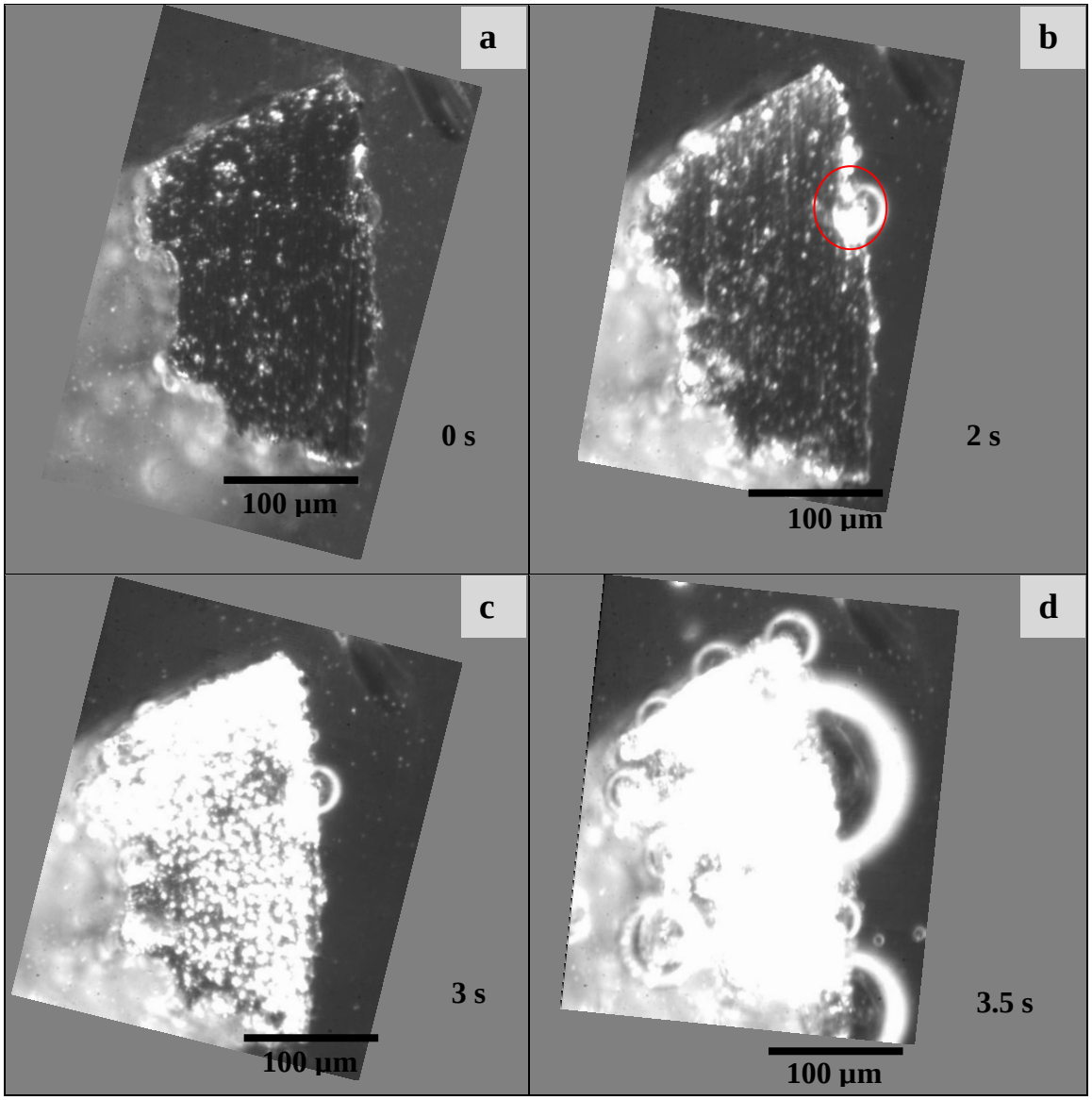

Figure 6.5: ***(a)*** *Camera picture of I0 in 2 M NaCl just before the experiment started. Camera pictures at the* ***(b)*** *1st second of the experiment;* ***(c)*** *2nd second of the experiment* ***(d)*** *3rd second of the experiment where 50 mA cm-2 were applied to I0 in 2 M NaCl*

It can be observed that there are no pits on the surface which is expected since tests on open circuit had not preceded this experiment and the sample was a fresh polished one. In Figure 6.5 b a camera picture after the first two seconds of the experiment is shown. One bubble has formed, emphasized with a red circle. In Figure 6.5 c, a camera picture

after the first 3 seconds of the experiment can be seen, showing that tiny bubbles have formed all over the surface of the alloy. In Figure 6.5 d, a camera picture after only 3.5 seconds of the experiment is showing that bubbles have grown that much and more have formed obstructing the view of the alloy surface.

In all pictures of Figure 6.5 it can be seen that the left part of the image, which is actually the resin, is different in colour from the right part of pictures. This is probably due to some roughness in the left part of the resin that reflects the light. The current density was chosen to be 50 mA cm^{-2} in this experiment in order to be consistent with previous chronopotentiometric experiments in Chapter 4. However, a stream of bubbles was observed from several points on the surface and the image became obscured by many hydrogen bubbles. After the experiment the surface was full of pits, in agreement with previous experiments with the current alloy at similar current densities.

Due to the difficulty to view clearly the surface because of the extremely vigorous hydrogen evolution and the trapping of the bubbles between the flat window of the cell and the electrode, lower current densities were used for the rest of the experiments in this section.

6.3. Optical observations at lower current densities

The sample of I0 alloy used for the experiment on open circuit in Section 6.1 (see Figure 6.3) was used for a chronopotentiometry experiment. A current density of 1 mA cm^{-2} was applied to the I0 alloy for 120 seconds immediately after the experiment on open circuit was conducted. The E-t transient is shown in Figure 6.6.

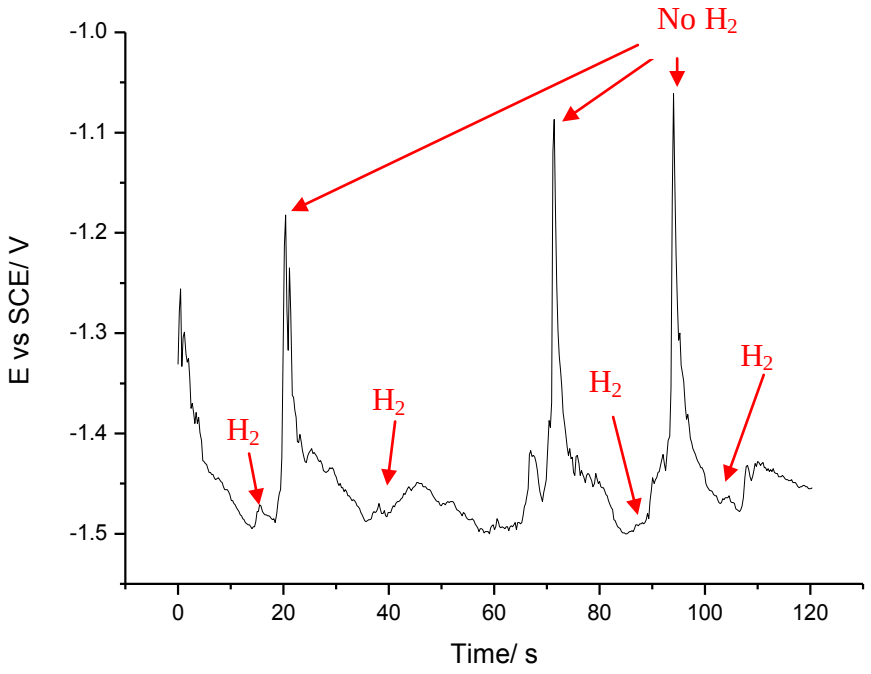

Figure 6.6: *Chronopotentiometric response of I0 alloy (area ~ 0.1 mm^2) when a current density of 1 mA cm^{-2} was applied to it in 2 M NaCl.*

The video recorded during this experiment clearly showed pulses of hydrogen originating from the pits formed earlier on open circuit. A collective series of frames from this video are presented in Figure 6.7. Red circles indicate the origin of hydrogen bubbles. The SEM picture after the end of the experiment is also shown in Figure 6.7 h. In Figure 6.7 c it can be clearly seen that vigorous hydrogen evolution originates from only one of the three pits on the right hand side of the sample. After some tens of seconds that pit passivated, as it can be seen in Figure 6.7 d, (no hydrogen evolution observed) and later as it can be seen in Figure 6.7 e the pit is active again showing rapid hydrogen evolution and at the same time another pit activates and starts evolving hydrogen, (see red circle in Figure 6.7 e). In Figure 6.7 h the SEM image of the I0 sample after the experiment shows that the pits formed on open circuit after a current density of 1 mA cm^{-2} was applied for 120 seconds where larger and that a few new smaller ones were formed. Earlier in this section it was concluded that pits are formed on Al surface due to Sn cathodic centres on open circuit. It can clearly be concluded that hydrogen evolution occurs locally from these pits.

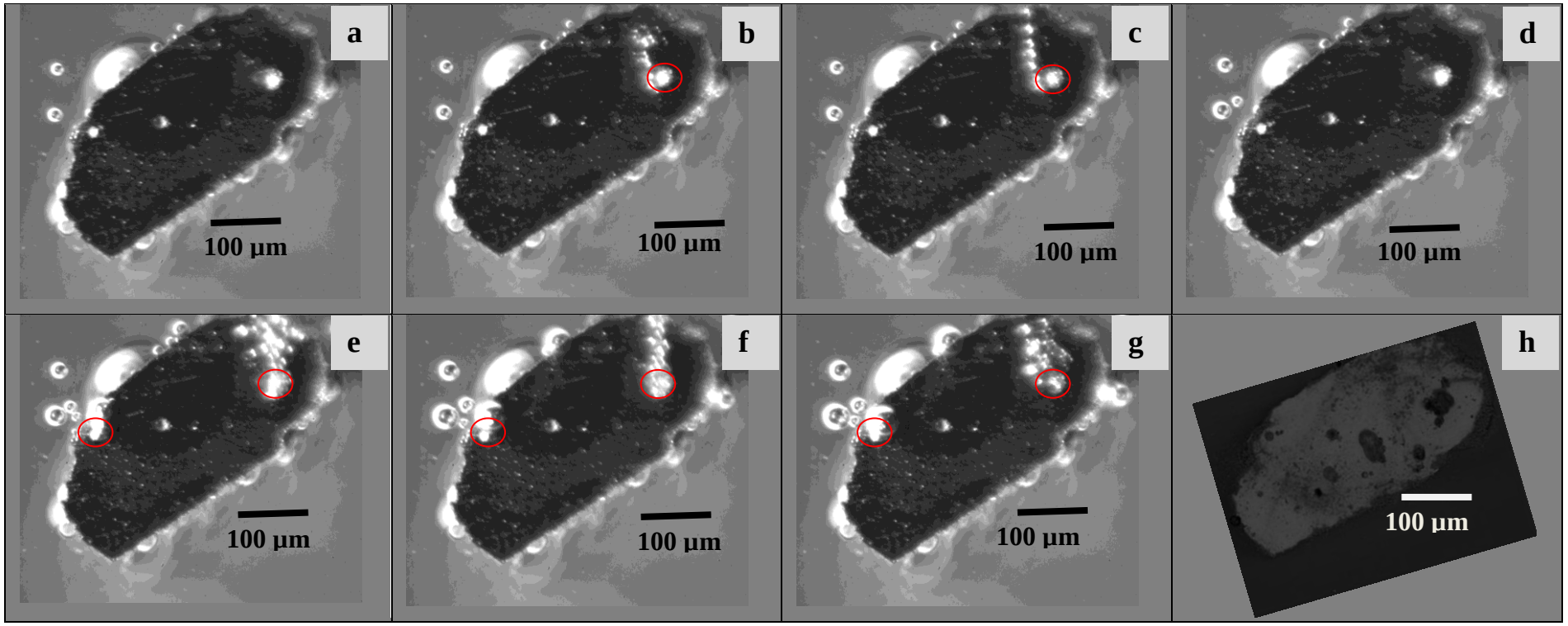

Figure 6.7: ***(a)*** *Camera picture of the I0 alloy in 2 M NaCl while on OCP where some pits have already formed on the surface.* ***(b)*** *to* ***(g)*** *Camera pictures of the I0 alloy when a current density of 1 mA cm^{-2} was applied to it. Hydrogen evolution occurs from the pits that were formed during the OCP time.* ***(h)*** *SEM image of the alloy I0 after the experiment. Red circles indicate the origin of hydrogen bubbles.*

By observing the video, looking at the chronopotentiometric response and using the aid of a sound channel, it was observed that the hydrogen evolution was directly related to the most negative potentials in the E-t transients; when hydrogen was evolved from the surface I0 had a potential of approximately -1.5 V *vs* SCE and when hydrogen evolution would periodically stop the potential would take up a more positive value (see Figure 6.6). Of course the evolution of hydrogen at the Sn centres will cause the electrolyte within the pit to go strongly alkaline. Hence, it is likely that precipitation of $Al(OH)_3/Al_2O_3$ causes passivation of the Sn centre and the passivating material is broken by build up of the hydrogen pressure and on fracturing the potential returns to - 1.5 V *vs* SCE.

Similar behaviour to I0 was observed for AB50V alloy when 1 mA cm^{-2} were applied to it in 2 M NaCl In Figure 6.8 the E-t transient for AB50V alloy is shown and in Figure 6.9 the SEM image of the alloy surface after the experiment is shown.

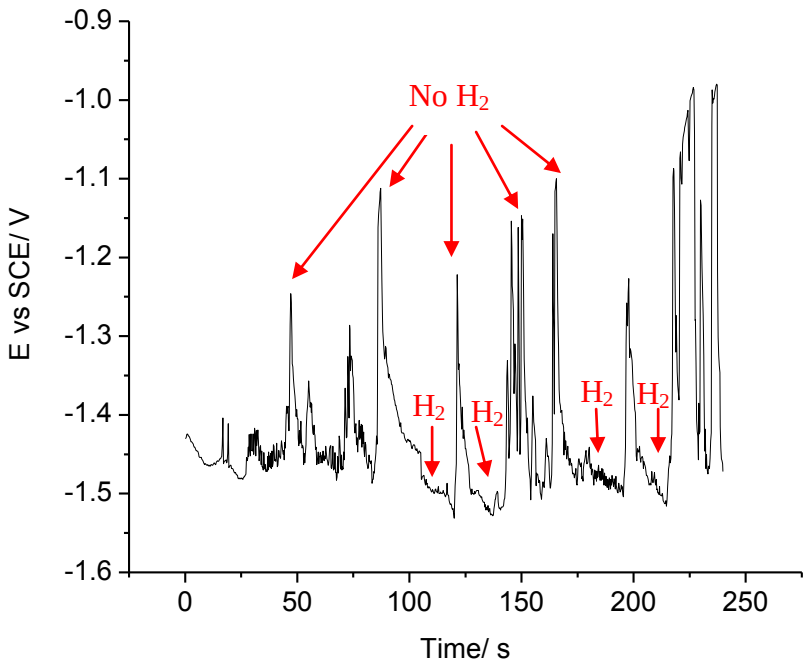

Figure 6.8: *Chronopotentiometric response of AB50V alloy (area ~ 0.0086 mm^2) when a current density of 1 mA cm^{-2} was applied to it in 2 M NaCl.*

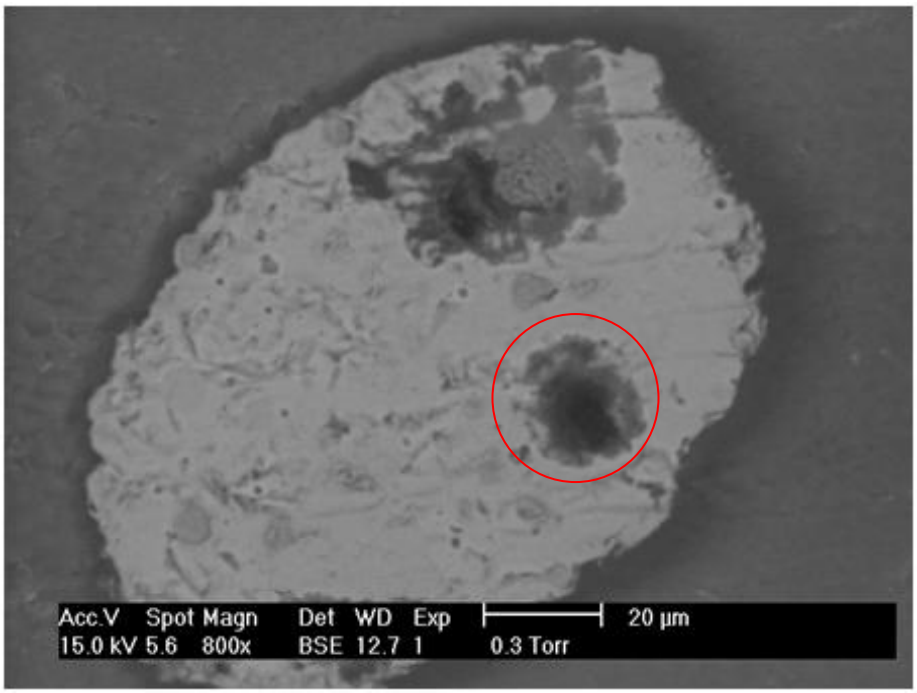

Figure 6.9: *SEM image of AB50V alloy after 1 mA cm^{-2} current density was applied to it in 2 M NaCl for 240 seconds. In the red circle a pit is marked where Sn particles were located with EDX before the experiment.*

The hydrogen pulses were mainly occurring periodically from the pit marked in the red circle in Figure 6.9 where Sn centres were detected before the experiment by EDX.

Overall from the optical observations with the aid of the high speed camera it is concluded that the Sn centres on AlMgSnGa alloys surface fix the site for anodic dissolution. Pits are formed on OCP on sites were Sn centres exist. Hydrogen gas is evolved from the Sn cathodic centres and the Al is dissolving around them forming the pits. Spikes in chronopotentiometric experiment in Figure 6.6 and 6.8 were correlated to hydrogen (bubble) evolution from the camera optical observations. Overall from the open circuit corrosion tests and chronopotentiometric experiments it is concluded that some local corrosion process between Sn and aluminium occurs as a precursor of a local anodic dissolution of I0 surface around Sn (or MgSn) particles.

6.4. Voltammetry and hydrogen evolution

Previously, the focus of voltammetric studies has been for the anodic dissolution of aluminium and its alloys and the influence of 'activation' on the rate of this process. It was recognised that aluminium corrosion could also take place as a parallel reaction during Al dissolution as well as on open circuit and for this reason the cathodic behaviour was examined in this section. Figure 6.10 reports voltammograms for the alloy AB50V in 2 M NaCl (a) without any pre-treatment and (b) after the surface had been activated with an anodic current density of 50 mA cm^{-2} for 600 seconds, (i.e. the standard procedure for the studies of anodic dissolution). The experiment without activation was commenced from the open circuit potential and scanned towards negative potentials. The voltammogram with the activated surface was commenced from -1.4 V to demonstrate that Al dissolution was indeed taking place. After activation it can be seen that there is a significant increase in the cathodic current immediately negative to the open circuit potential but it then plateaus before a further increase at more negative potentials.

It is believed that the cathodic current just negative to – 1.5 V at the activated surface represents hydrogen evolution at the tin centres as shown from the optical observations. Tin is a good catalyst for H_2 evolution and this reaction might be expected at all potentials negative to ~ - 0.8 V *vs* SCE. It is not unreasonable to conclude that H_2 evolution at Al does not commences until ~ - 1.8 V *vs* SCE. Then the limitation of the hydrogen evolution current density at ~ - 2 mA cm^{-2} around -1.6 V would result from the very low surface area of tin exposed to solution. In fact, based on the surface area of Sn exposed this is a huge current density ($>$5 A cm^{-2}). It should then be recognised that the experimental current for Al alloy dissolution in the range negative to – 1.0 V is then the sum of two components

$$I_{exp} = I_{Al}\ oxidation + I_{H_2}\ evolution$$

and it is likely that if the same number of Sn centres were involved the H_2 evolution rate is constant (at - 2 mA cm^{-2}) over all this range. This would effectively give an estimate of the importance of the Al corrosion rate compared to anodic dissolution at the surface created by the activation procedure. In reality, the number of Sn centres exposed to

solution will increase with the current density for Al dissolution and time and as this happens, the hydrogen evolution current will also increase.

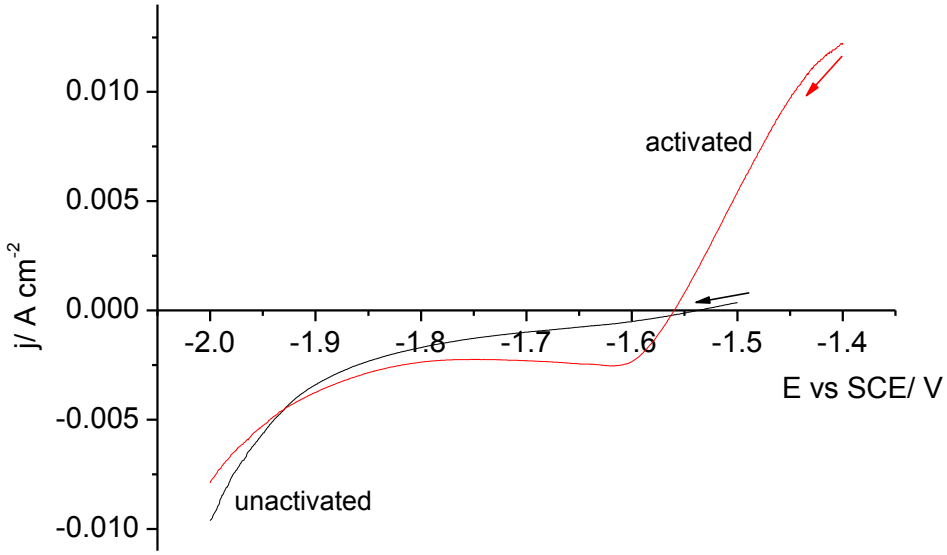

Figure 6.10. *Voltammograms for AB50V in 2 M NaCl, before and after activation, with an anodic current density of 50 mA cm^{-2} for 600 s.*

6.5. Conclusion

In this chapter optical microscopy was used to observe, in situ, the surface of AlMgSnGa alloys on open circuit and during their anodic dissolution. Video techniques have been used in the past to study corrosion of AlMgSnGa alloys but the samples were far bigger than those in this study.[35] Electrodes of 176 mm^2 area were used for this past study. So this work sought to look at much higher resolution at the aluminium surfaces. The pits observed by Tuck (1992), had a diameter of ca 120 μm whereas in this study smaller pits of around 20 μm could be observed while forming and evolving hydrogen. Moreover, we know from studies in Chapter 4 that pits of 120 μm diameter are "aged" and probably many overlapping pits. The authors related the pit with the hydrogen evolution but they did not show any evidence of correlation with Sn intermetallics as was achieved in this project. Other scientists did in situ video observations of the

corrosion on open circuit of Al-Sn alloys (1 wt % Sn) in sodium sulphate. [30] However these authors also used very big electrodes of 1 cm^2 working surface. In fact the authors presented SEM picture of a Sn inclusion with an very big area ca 0.047 mm^2 and they reported that the cathodic reduction of hydrogen is concentrated only on these inclusions, while the anodic dissolution of aluminium proceeds through its oxide film on the remaining surface.[30] The work in this project is in disagreement with the latter statement since it was proven that the Al dissolution occurs specifically around the Sn cathodic inclusions and not through its oxide film on the remaining surface. From this project it is also concluded that H_2 evolution originates from Sn inclusions in agreement with these authors. Another interesting work including in situ observation of the corrosion process of AlZnCuMg alloys was carried out by Zhao and Frankel (2007), for which though very big samples 4 cm^2 were used.[31] Even though their work gave very significant information on the breakdown of a surface layer on aluminium alloys in correlation to potentiodynamic polarization of the alloys, it would not relate intermetallics to hydrogen evolution and corrosion due to low resolution and big sample sizes.

Finally Ambat et al., (2004) concluded that cathodic reactivity of AlFeSiMn alloys increases due to an increased number of Fe and Mn-rich precipitates. In situ analysis of corrosion for those alloys showed a large number of cathodic reaction sites for the surface compared with the bulk by observing Al alloys surface at different depths of the alloy. The area observed was circular with a diameter 4 mm so the area of their samples were 12.56 mm^2.[29] The work in this project is in agreement with the conclusion of these authors that since the intermetallics are sites for cathodic activity, hydrogen evolution would occur proportionally to their density and locally. However due to the smaller size of samples used in this project it was possible to prove that corrosion of AlMgSnGa alloys on OCP occurs from very specific local sites on surface 1-3sites/ 1000 μm^2 where most of the times Sn is present there; such a conclusion agrees to the fact that tin is far superior to aluminium as a catalyst for hydrogen evolution[113] Moreover from the work presented in this chapter it was shown that aluminium dissolution occurs where hydrogen is evolved and confirms that Al dissolution is fixed by Sn sites. Furthermore it has to be addressed that the precise mechanism by which Sn fixes the Al dissolution is not known. Finally when low current densities are applied to the alloy, periodic

hydrogen evolution and passivation was observed with the microscope and could be correlated with changes to the sample potential.

CHAPTER 7 Final conclusions

Each of the chapters has a set of conclusions and this final chapter is intended only to highlight the overall conclusions of this programme. It should again be noted that the programme sought to determine whether a high energy and power density Al-air battery employing a brine electrolyte, suitable to power an unmanned aircraft, was a possibility.

7.1. Selection of alloys for battery anodes in brine electrolytes

A successful anode for the desired battery must combine the properties of (a) a low rate of corrosion in the battery electrolyte, on open circuit and on load and (b) a high rate of anodic dissolution at a rather negative potential (c) continued anodic dissolution over an extended period of time.

Unlike alkaline media, pure aluminium, although stable to corrosion, requires a very large overpotential to drive its anodic dissolution at a significant rate in the brine media. Indeed, of the materials tested, only alloys containing both tin and gallium showed the ability to dissolve at current densities > 0.5 A cm^{-2} at potentials close to the open circuit potential of ~ -1.50 V *vs* SCE. A similar conclusion was reached by a group working at Alcan in the 1990s[35] who recommended the alloy AB50V containing additions of Mg, Sn and Ga for the anode in Al-air batteries with brine electrolytes. Moreover, the alloy was employed in batteries[13, 42] but their performance was limited to lower current densities. In this thesis, dissolution at high rates of AB50V has been demonstrated and it was shown that two other AlMgSnGa alloys had similar electrochemical activity. In contrast to alloys with additions of many other elements, e.g. Fe and Si,[17, 19, 79] all three AlMgSnGa alloys were relatively stable to corrosion in brine. There were, however, differences in the rates of corrosion. The three alloys were shown to have differences in structure – different sizes of Al grains and different sizes of tin inclusions. AB50V with a structure resulting from mechanical working and a moderate heat treatment after fabrication was shown to have the lowest corrosion rate. The Alcan alloy therefore remains the material of choice for a high energy/power density Al-air battery.

7.2. The mechanism for the anodic dissolution of AlMgSnGa alloys in NaCl electrolytes

The aluminium alloys containing both Sn and Ga appear to undergo anodic oxidation by a mechanism quite different to pure aluminium and most other alloys. The dissolution occurs at very high current densities at low overpotentials whereas other materials only oxidise with a potential 800 mV more positive. The dissolution can also be seen to occur by a local mechanism around the Sn inclusions and the pits are rounded rather than crystallographic as found for other aluminium alloys.[112] The distribution of the gallium in the AlMgSnGa alloys could not be determined but it clearly has a key role in supporting this local dissolution mechanism. It is attractive to postulate that Ga is to be found close to the tin inclusions and results in a liquid film through which the aluminium can diffuse and oxidise[83] – experience at mercury electrodes provides compelling evidence that electrode reactions at liquid surfaces are more facile than at solid surfaces. During corrosion on open circuit, it is straightforward to imagine that the tin inclusions act as local cathodes and that the Al dissolves around the tin because this minimises IR drop through the metal and surrounding electrolyte. During high rate anodic dissolution it is less clear why the dissolution is limited to the close proximity of the tin. It cannot be ruled out that corrosion before the commencement of anodic oxidation fixes the site of dissolution or that the presence of Sn and Ga modifies the native alumina film to concentrate dissolution in these localities.

The experiments with the high speed camera provide further information about the growth of the pits. It is clear that H_2 is evolved from particular points within the pits (presumably the tin inclusions) and not from the bulk, surrounding aluminium surface. Also at low current density where few pits are growing, the evolution of H_2 from any one Sn inclusion can be seen to be intermittent. It appears that passivation by a solid Al (III) species periodically results from the local increase in pH associated with the water reduction within the pit and renewed gas evolution requires a crust to be broken, Indeed, in some video sequences the 'explosive' breakdown of such a crust could be monitored. But again, it is not clear whether this H_2 evolution is a critical process to the Al dissolution or simply arises because tin centres are in electrical contact with the aluminium surface at a potential in the range -1.40 V to -1.50 V *vs* SCE.

While these observations are interesting, in other respects the experiments with the high speed camera are disappointing. At the present time, the resolution is limited to 10 – 20 μm. Also there is a time period to focus the camera and optimise the lighting before high resolution observation can be commenced. Both limitations make it impossible to use the technique to study the initial formation of pits.

A practical battery must maintain the ability to give the desired current and voltage performance over the required lifetime of the battery. In the battery for an unmanned aircraft, the high rate dissolution must continue for a substantial period and the battery can only contain a limited volume of electrolyte (both because of a weight limitation and the need to minimise the interelectrode gap to optimise the battery voltage). While high rate dissolution of the AlMgSnGa alloys was possible initially and for some time, the dissolution was shown to terminate because of a thick white crystalline deposit that eventually forms a compact 'shroud' over the Al alloy surface. In the early stages of dissolution, the Al (III) product largely stays in solution as supersaturated oxide/hydroxide or a chlorocomplex[114] but precipitation occurs after a period. Perhaps surprisingly, the Al alloy never passivates in the conventional sense since gentle removal of the 'shroud' allows dissolution to recommence. In the experiments carried out here, the charge before dissolution terminates was independent of current density and was typically 1000 C cm^{-2} of Al surface. The value probably defends on cell dimensions and geometry.

7.3. Is a high energy/power density Al-air battery possible?

Clearly, not at the present stage of the technology! While the AB50V alloy developed by Alcan[24, 79, 80] is an excellent material for high current density dissolution in certain situations, there are two major problems preventing the design of such a battery.

Firstly, there is not an air cathode able to deliver a realistic current density with a brine electrolyte. The performance degrades from that obtained in acid and alkaline fuel cells for three reasons (a) the Al-air battery is required to operate close to ambient temperature while the fuel cells typically operate at temperatures of 333 - 353 K (b) the reduction of oxygen itself causes an increase of pH at the catalyst centres and this leads to a negative shift in cathode potential and decrease in battery voltage (c) the

conductivity of brine is a factor of ten less than acid electrolytes and this leads to IR drop within the pores of the GDE. The latter two factors lead to drawn out j *vs* E responses. In a laboratory battery, it was only possible to achieve a voltage of 1.0 V even with a low current density of 20 mA cm^{-2}.

Secondly, it is difficult to see how dissolution of the aluminium alloy could be continued to the desired operational lifetime of the battery in a limited volume (weight) of electrolyte. In both the laboratory battery and the small volume cell, discharge terminated after a charge of 1000 C cm^{-2} of Al surface. If this restriction cannot be eliminated, the necessary area of aluminium could only be contacted by an electrolyte volume in considerable excess of the target 40 cm^3 (see, Chapter 1). There may also be a limitation to the amount of Al (III) product that can be 'contained' within unit volume of brine. Again, the experimental evidence is that to obtain the required energy output, the volume of electrolyte would need to >> 40 cm^3, maybe as high as 500 cm^3.

It would also be essential for the battery design to handle the significant H_2 gas evolved. The formation of H_2 at the anode and reduction of O_2 at the anode both certainly consume water. In addition if $Al(OH)_3$ is the product of Al dissolution this also consumes water. All these reactions add to the water that must be present in the battery and hence to its weight.

REFERENCES

1. S. Zaromb, *Journal of the Electrochemical Society*, 1962, **109**, 1125-1130.
2. M. Ritschel and W. Vielstich, *Electrochimica Acta*, 1979, **24**, 885-886.
3. M. Rota, C. Comninellis, S. Muller, F. Holzer and O. Haas, *Journal of Applied Electrochemistry*, 1995, **25**, 114-121.
4. D. Linden, *Handbook of Batteries*, 2nd edn., McGraw-Hill, New York, 1995.
5. M. Adams and W. Halliop, *Proceedings of the Power Sources Conference*, 2002, **40th**, 359-362.
6. R. P. Hamlen, in *Handbook of Batteries*, ed. D. Linden, McGraw-Hill, New York, 3rd edn., 2002.
7. M. L. Doche, F. Novel-Cattin, R. Durand and J. J. Rameau, *Journal of Power Sources*, 1997, **65**, 197-205.
8. K. Kordesch and V. Hacker, in *Handbook of Fuel Cells*, John Wiley & Sons, Chichester, UK, 2003, vol. 4, pp. 765-773.
9. C. C. Chang and T. C. Wen, *Materials Chemistry and Physics*, 1997, **47**, 203-210.
10. E. Yeager, *Electrochimica Acta*, 1984, **29**, 1527-1537.
11. D. Pletcher and F. C. Walsh, *Industrial Electrochemistry*, 2nd edn., Chapman and Hall, London, 1990.
12. D. Pletcher, *A First Course in Electrode Processes*, The Electrochemical Consultancy, Romsey, UK, 1991.
13. B. M. L. Rao, R. Cook, W. Kobasz and G. D. Deuchars, *Proceedings of the International Power Sources Symposium*, 1992, **35th**, 34-37.
14. E. Budevski, I. Ilien, A. Kaisheva, A. Despic and K. Krsmanovic, *Journal of Applied Electrochemistry*, 1989, **19**, 323-330.
15. M. Pourbaix, *Atlas of Electrochemical Equilibria in Aqueous Solutions*, Houston, 1974.
16. K. Shimizu, R. C. Furneaux, G. E. Thompson, G. C. Wood, A. Gotoh and K. Kobayashi, *Oxidation of Metals*, 1991, **35**, 427-439.
17. J. R. Davis, *Aluminium and Aluminium Alloys*, 9th edn., ASM International, Ohio, 1993.
18. H. Ezuber, A. El-Houd and F. El-Shawesh, *Materials & Design*, 2008, **29**, 801-805.
19. Z. Szklarska-Smialowska, *Corrosion Science*, 1999, **41**, 1743-1767.
20. P. M. Natishan, W. E. O'Grady, E. McCafferty, D. E. Ramaker, K. Pandya and A. Russell, *Journal of the Electrochemical Society*, 1999, **146**, 1737-1740.
21. E. McCafferty, *Corrosion Science*, 2003, **45**, 1421-1438.
22. O. Saevik, Y. D. Yu, J. H. Nordlien and K. Nisancioglu, *Journal of the Electrochemical Society*, 2005, **152**, B334-B341.
23. A. Barbucci, G. Cerisola, G. Bruzzone and A. Saccone, *Electrochimica Acta*, 1997, **42**, 2369-2380.
24. J. Hunter, G. Scamans and J. Sykes, *Power Sources, The 17th International Power Sources Symposium*, 1991, **13**, 193-211.
25. K. Nisancioglu, Proceedings of ICAA3, Trondheim, 1992.
26. G. Svenningsen, in *Department of Materials Technology, 7491 Trondheim, Norway*.
27. C. B. Bargeron and R. B. Givens, *Journal of the Electrochemical Society*, 1977, **124**, 1230-1232.

28. A. V. Volkov, P. K. Datta, J. S. Burnell-Gray and R. Couper, *Corrosion Science*, 2004, **46**, 2613-2619.
29. R. Ambat, A. J. Davenport, A. Afseth and G. Scamans, *Journal of the Electrochemical Society*, 2004, **151**, B53-B58.
30. A. V. Goncharov and Y. Y. Andreev, *Protection of Metals*, 2006, **42**, 507-509.
31. Z. Zhao and G. S. Frankel, *Corrosion Science*, 2007, **49**, 3064-3088.
32. G. S. Frankel, *Corrosion Science*, 1990, **30**, 1203-1218.
33. R. M. Pidaparti, E. B. Neblett, S. A. Miller and J. C. Alvarez, *Smart Materials & Structures*, 2008, **17**, 1-6.
34. D. E. Bryant and D. Greenfield, *Progress in Organic Coatings*, 2006, **57**, 416-420.
35. C. D. S. Tuck, *Faraday Discussions*, 1992, 171-182.
36. L. Trevethan, D. Bockstiem and S. Zaromb, *Journal of Electrochemical Society*, 1963, **110**, 267.
37. C. D. S. Tuck, *Modern Batteries*, Ellis Horwood Limited, 1991.
38. J. P. Souza and W. Vielstich, *Seawater Aluminium / Air cells.* , Wiley and Sons, New York, 2003.
39. A. R. Despic, D. M. Drazic, M. M. Purenovic and N. Cikovic, *Journal of Applied Electrochemistry*, 1976, **6**, 527-542.
40. *Uk Pat.*, 5,004,654, 1991.
41. D. K. Creber, W. B. O'Callaghan and G. M. Scamans, *Power Sources*, 1993, **14**, 217-226.
42. P. K. Shen, A. C. C. Tseung and C. Kuo, *Journal of Power Sources*, 1994, **47**, 119-127.
43. E. J. Rudd and D. W. Gibbons, *Journal of Power Sources*, 1994, **47**, 329-340.
44. S. Yang and H. Knickle, *Journal of Power Sources*, 2002, **112**, 162-173.
45. S. H. Yang and H. Knickle, *Journal of Power Sources*, 2003, **124**, 572-585.
46. X. Zhang, S. H. Yang and H. Knickle, *Journal of Power Sources*, 2004, **128**, 331-342.
47. A. Z. Zhuk, A. E. Sheindlin, B. V. Kleymenov, E. I. Shkolnikov and M. Y. Lopatin, *Journal of Power Sources*, 2006, **157**, 921-926.
48. K. Kinoshita, *Electrochemical Oxygen Technology*, 1st edn., , New York, 1992.
49. Y. Shimizu, K. Uemura, H. Matsuda, N. Miura and N. Yamazoe, *Journal of the Electrochemical Society*, 1990, **137**, 3430-3433.
50. R. Manoharan and A. K. Shukla, *Electrochimica Acta*, 1985, **30**, 205-209.
51. G. Karlsson, *Electrochimica Acta*, 1985, **30**, 1555-1561.
52. M. J. Niksa and D. J. Wheeler, *Journal of Power Sources*, 1988, **22**, 261-267.
53. R. Thacker, *Energy Conversion*, 1972, **12**, 17-&.
54. F. Zaragoza-Martin, D. Sopena-Escario, E. Morallon and C. S. M. de Lecea, *Journal of Power Sources*, 2007, **171**, 302-309.
55. H. Gharibi, R. A. Mirzaie, E. Shams, M. Zhiani and M. Khairmand, *Journal of Power Sources*, 2005, **139**, 61-66.
56. H. Meng and P. K. Shen, *Electrochemistry Communications*, 2006, **8**, 588-594.
57. Z. Siroma, T. Sasakura, K. Yasuda, M. Azuma and Y. Miyazaki, *Journal of Electroanalytical Chemistry*, 2003, **546**, 73-78.
58. M. Kliskic, J. Radosevic, S. Gudic and M. Smith, *Electrochimica Acta*, 1998, **43**, 3241-3255.
59. M. Shibata and N. Furuya, *Electrochimica Acta*, 2003, **48**, 3953-3958.
60. J. C. Huang, R. K. Sen and E. Yeager, *Journal of the Electrochemical Society*, 1979, **126**, 786-792.

61. M. L. Perry and T. F. Fuller, *Journal of the Electrochemical Society*, 2002, **149**, S59-S67.
62. K. Kordesch and G. Simader, *Fuel Cells and their Applications*, VCH, New York, 1996.
63. B. Y. S. Lin, D. W. Kirk and S. J. Thorpe, *Journal of Power Sources*, 2006, **161**, 474-483.
64. I. Roche, E. Chainet, M. Chatenet and J. Vondrak, *Journal of Physical Chemistry C*, 2007, **111**, 1434-1443.
65. F. T. Bacon, *BEAMA Journal*, 1954, **61**, 6.
66. V. Rashkova, S. Kitova, I. Konstantinov and T. Vitanov, *Electrochimica Acta*, 2002, **47**, 1555-1560.
67. H. Cheng and K. Scott, *Journal of Electroanalytical Chemistry*, 2006, **596**, 117-123.
68. K. Okajima, K. Nabekura, T. Kondoh and M. Sudoh, *Journal of the Electrochemical Society*, 2005, **152**, D117-D120.
69. X. Y. Xie, Z. F. Ma, X. X. Ma, Q. Z. Ren, V. M. Schmidt and L. Huang, *Journal of the Electrochemical Society*, 2007, **154**, B733-B738.
70. A. Verma, A. K. Jha and S. Basu, *Journal of Power Sources*, 2005, **141**, 30-34.
71. F. P. Hu, X. G. Zhang, F. Xiao and J. L. Zhang, *Carbon*, 2005, **43**, 2931-2936.
72. E. L. Dewi, K. Oyaizu, H. Nishide and E. Tsuchida, *Journal of Power Sources*, 2004, **130**, 286-290.
73. Q. Li and N. J. Bjerrum, *Journal of Power Sources*, 2002, **110**, 1-10.
74. D. D. Macdonald, S. Real and M. Urquidi-Macdonald, *Journal of the Electrochemical Society*, 1988, **135**, 2397-2409.
75. J. T. Reding, R. L. Riley and W. C. Jordan, *Power Engineering*, 1976, **80**, 46-49.
76. J. T. Reding and J. J. Newport, *Materials Protection*, 1966, **12**, 15-18.
77. D. Tommasi, *Traite des Piles Electriques*, Paris 1889.
78. G. J. May, *Electronics and Power*, 1984, **30**, 885.
79. G. Scamans, J. Hunter, C. Tuck, R. Hamlen and N. Fitzpatrick, *Electric Vehicle Developments*, 1989, **8**, 28-29.
80. T. A. Dougherty, A. P. Karpinski, J. H. Stannard, W. Halliop and S. Warner, *Iecec 96 - Proceedings of the 31st Intersociety Energy Conversion Engineering Conference*, 1996, **1-4**, 1176-1180.
81. J. Mathiyarasu, L. C. Nehru, P. Subramanian, N. Palaniswamy and N. S. Rengaswamy, *Anti-Corrosion Methods and Materials*, 2001, **48**, 324-329.
82. W. B. O'Callaghan, 7th Department Of Energy Contractors Conference, Washington, 1985.
83. C. D. S. Tuck, J. Hunter and G. M. Scamans, *Journal of the Electrochemical Society*, 1987, **134**, 2970-2981.
84. D. D. Macdonald, K. H. Lee, A. Moccari and D. Harrington, *Corrosion (Houston, TX, United States)*, 1988, **44**, 652-657.
85. S. Z. El Abedin and A. O. Saleh, *Journal of Applied Electrochemistry*, 2004, **34**, 331-335.
86. A. M. Abdel-Gaber, B. A. Abd-El-Nabey, I. M. Sidahmed, A. M. El-Zayady and M. Saadawy, *Materials Chemistry and Physics*, 2006, **98**, 291-297.
87. A. Berzins, R. T. Lowson and K. J. Mirams, *Australian Journal of Chemistry*, 1977, **30**, 1891-1903.
88. M. Nestoridi, D. Pletcher, R. J. K. Wood, S. Wang, R. L. Jones, K. R. Stokes and I. Wilcock, *Journal of Power Sources*, 2008, **178**, 445-455.

89. N. Fitzpatrick and G. Scamans, *New Scientist*, 1986, **111**, 34-37.
90. L. F. Mondolfo, *Aluminium Alloys: Structure and Properties*, 1st edn., Butterworth & Co, London, 1976.
91. United States Department of Defense, Dictionary of Military and Associated Terms - JP 1-02, Joint Doctrine Division, J-7, Joint Staff, 2008.
92. L. R. Newcome, *Unmanned Aviation: A Brief History of Unmanned Aerial Vehicles*, American Institute of Aeronautics and Astronautics Reston, VA., 2004.
93. R. Jones and J. Morris, *Journal of Defense Science*, 2000, **5**, 227-234.
94. D. A. Heley, *A Flight Control Design Methodology For Micro Air Vehicles*, Blue Bear Systems Ltd, 2003.
95. S. Willcox, *Milestone Report, Systems Integration and Flight Test, Blue Bear Systems Research Ltd*, 2004, 27.
96. R. S. Scully, D. C. Silverman and M. W. Kendig, *Electrochemical Impedance: Analysis and Interpretation*, 1st edn., ASTM, Fredericksburg, 1993.
97. P. J. Goodhew, J. Humphreys and R. Beanland, *Electron Microscopy and Analysis*, 3rd edn., Taylor & Francis, London, 2001.
98. Oxford Instruments Plc, *Electron Backscatter Diffraction*, http://www.ebsd.com/ebsdexplained.htm, Accessed 30-08-2008.
99. K. C. Emregul and A. A. Aksut, *Corrosion Science*, 2000, **42**, 2051-2067.
100. H. A. El Shayeb, F. M. Abd El Wahab and S. Zein El Abedin, *Journal of Applied Electrochemistry*, 1999, **29**, 473-480.
101. F. Holzer, S. Müller, J. Desilvestro and O. Haas, *Journal of Applied Electrochemistry*, 1993, **23**, 125-134.
102. H. A. El Shayeb, F. M. Abd El Wahab and S. Z. El Abedin, *Corrosion Science*, 2001, **43**, 655-669.
103. A. A. Elawady, B. A. Abdelnabey and S. G. Aziz, *Journal of the Chemical Society-Faraday Transactions*, 1993, **89**, 795-802.
104. F. J. Martin, G. T. Cheek, W. E. O'Grady and P. M. Natishan, *Corrosion Science*, 2005, **47**, 3187-3201.
105. S. Y. Yu, W. E. O'Grady, D. E. Ramaker and P. M. Natishan, *Journal of the Electrochemical Society*, 2000, **147**, 2952-2958.
106. W. J. Lee and S. I. Pyun, *Electrochimica Acta*, 1999, **44**, 4041-4049.
107. S. I. Pyun, S. M. Moon, S. H. Ahn and S. S. Kim, *Corrosion Science*, 1999, **41**, 653-667.
108. E. McCafferty, *Corrosion Science*, 1995, **37**, 481-492.
109. W. D. Callister, *Materials Science And Engineering*, 7th edn., Wiley New York, 2007.
110. G. M. Scamans, D. K. Creber, J. H. Stannard and J. E. Tregenza, 1994 Symposium on Autonomous Underwater Vehicle Technology (AUV 94), Cambridge, Ma, 1994.
111. R. C. Hugo and R. G. Hoagland, *Scripta Materialia*, 1999, **41**, 1341-1346.
112. R. Ambat, A. J. Davenport, G. M. Scamans and A. Afseth, *Corrosion Science*, 2006, **48**, 3455-3471.
113. S. Trasatti, *Journal of Electroanalytical Chemistry*, 1972, **39**, 163.
114. D. M. Drazic, Z. V. Ledinski and S. K. Zecevic, *Journal of Applied Electrochemistry*, 1983, **13**, 337-340.